The Extraction of Bitumen From Western Tar Sands

Annual Report

A.G. Oblad
J.W. Bunger
M.D. Deo
F.V. Hanson
J.D. Miller
J.D. Seader

July 1990

Work Performed Under Contract No.: DE-FC21-89MC26268

DISCLAIMER

The Extraction of Bitumen From Western Tar Sands

Annual Report

A.G. Oblad
J.W. Bunger
M.D. Deo
F.V. Hanson
J.D. Miller
J.D. Seader

TABLE OF CONTENTS

LIST OF FIGURES

LIST OF TABLES

EXECUTIVE SUMMARY

Principal Investigator: Alex G. Oblad

A large amount of physical property data has been obtained on the Whiterocks oil sand deposit. This was obtained on mined ore and on core samples drilled on the deposit. Details of the locat ͌n of the mining and coring are given in the report along with sample preparation and analytical procedures. Core number 1 was discontinued at 260 feet during the drilling as a tar filled fracture was encountered. Core #2 was completed at 425 feet. Several gallons of bitumen were bailed from Core 1 and will be analyzed in the near future. The data obtained on the mined samples show that there is little lateral variation in the bitumen content across the deposit south-north and west-east. Likewise for the most part there is little vertical variation in bitumen content in the two cores obtained. Extensive physical and chemical property data were obtained for the bitumen on many of the samples. All of this information was obtained for Post Petroleum Company and funded by them. Post Petroleum has consented to making this extensive information on the Whiterocks deposit available in this report.

This information indicates that the physical and chemical properties were quite uniform. A significant finding was a substantiation of the low asphaltene content of the Whiterocks bitumen. The molecular composition of the bitumen appears to be mainly polycyclic alkyated naphthenes with small amounts of aromatic content interspersed in the naphthenic structures.

Determination of the mineral make-up in the Whiterocks oil sands indicated it was mainly quartz, dolomite and kaolin. The minerals present in the water extracted bitumen concentrate were determined to be mainly kaolin and carbonates. The accumulation of these minerals in the bitumen concentrate are believed to be related to their particle size and the presence of chemisorbed organic compounds presumably compounds which contain carboxylic acid groups.

Studies of the viscosity of Whiterocks bitumen showed the bitumen behaved as a Newtonian fluid in the temperature range of 40°-90°C. This result was attributed to the low asphaltene content of the bitumen.

Since routine analysis of oil sand involves bitumen extraction using toluene and considering the importance of being able to determine the true viscosity of the bitumen, studies were conducted to investigate the effect of small amounts of toluene on the viscosity of the bitumen. The influence of residual toluene appeared to be balanced by the loss of light ends during the extended evaporation procedure. Knowing this, correlation of the effect of residual toluene on bitumen viscosity has been derived so that reliable estimates of the true bitumen viscosity can be made using toluene extracted bitumen.

The electrophoretic mobility of bitumen droplets and fine mineral particles have been determined for Asphalt Ridge and Sunnyside oil sands. Negative surface charges were observed for all mineral particles and bitumen droplets of the two oil sands.

2

The Zeta potentials obtained via electrophoretic mobilities varied from -65 to -10 mV for bitumen droplets and from -55 to -25 mV for the mineral particles depending on the pH of the medium. These results indicate that gravity separation of bitumen from the digested slurry is feasible.

The effect of oil sand slurry viscosity in the digestion step during the water extraction process has been investigated. Using literature reported data and correlating these, the viscosity of the slurries have now been determined. Experiments were conducted to determine the separation efficiency of bitumen from the sand in the water extraction process as a function of slurry viscosity. The efficiency was highest with slurries in the 40-75 wt% solids range. The bitumen recovery and the concentrate grade from the gravity separation cell were significantly influenced by the slurry viscosity while the floatation kinetics remained nearly unchanged.

The slurry viscosity is believed to influence the shear rate in the disengagement reactor whether it is a CSTR, a rotating device or a pipeline reactor.

A considerable effort has been made to improve the University of Utah water extraction process during this year's program. As a result of this effort additional features have been added to the separation process concept such as the procedure for diluent addition, holding time for diluent effectiveness, and use of an additional electrolyte as a dispersant, sodium tripolyphosphate, in the extraction slurry. Optimization of the process variables: temperature, mechanical energy input, slurry viscosity and reaction

time have led to a new process definition for the extraction of Utah's tar sand bitumens. A flow sheet of this new concept is included in this report. The new process concept has led to improved extraction efficiencies for recovering the bitumen from Utah's oil sands. A much better understanding of the chemical factors in the recovery process has been achieved.

The results of a study of the use of electrostatic coalescence as a means of bitumen concentrate clean-up have been investigated. Bitumen emulsions containing amounts from 9.08% to 0.2 wt% of dispersed water with droplet diameters below 20 μm have been separated at an efficiency exceeding 80% at a residence time of 25 seconds. A pronounced improvement in the process efficiency was apparent when the voltage was raised to 140 ku/m. A separation optimum was observed for pulsation frequencies between 8 and 11 Hz.

In the extraction of a bitumen-derived hydrocarbon liquid from oil sands by the energy-coupled thermal method, an in-depth mathematical model for the combustion portion of the reactor that incorporated the information on the hydrodynamics, transport and kinetics was completed. The results of a number of simulations predicting the concentration profiles and the mean conversions of oxygen and coke are presented in this report. Through these simulations, it was recognized that excessively high residence times ($\approx$7000 s) were required to effect complete (>99%) conversion. A residence time of 2000 s resulted in a conversion of about 96%. Based on this observation, it is recommended that a third "after-burner" bed be added to the original two-bed configuration.

4

Preliminary calculations showed this to be the better overall configuration. Considerable progress has been made in the modification and automation of the existing equipment. Design of the apparatus to study heat-pipe conversion is also complete.

The problems associated with feeding tar sand into fluidized-bed pyrolysis reactors were solved by the use of a double-screw feeder acquired from Acrison, Inc. In prior studies with small-diameter reactors, the quality of fluidization was a constant source of concern. A detailed study of the fluidization of Group B sands was undertaken in order to understand fluidization of these sands. This led to the development of new correlations for the minimum fluidization velocity (U_{mf}) of group B sands. A relationship between U_{mf} and temperature was developed for predicting U_{mf} at elevated temperatures. Key parameters for the design of laboratory-scale fluidized bed reactors were also identified.

The successful completion of the preliminary rotary kiln pyrolysis reactor test at the Harper Electric Furnace Corporation led to the purchase of a rotary kiln. Experiments were conducted to define the operating procedures, to establish the material balance capabilities and to determine the reproducibility of the product distribution data. With the help of a product recovery system designed and fabricated at the University, a material balance of 90-95% with respect to the bitumen fed to the reactor was obtained. The experimental reproducibility was determined to be excellent.

A feasibility study of a riser reactor for the combustion of the carbonaceous residue produced during tar sand pyrolysis indicated that both the dilute-phase and the dense-phase transport reactors would be suitable. Design parameters of these reactors were determined and a mathematical analysis was conducted.

A solvent extraction program was initiated to understand solvent extraction as it pertains to tar sands led to an understanding that it would beneficial to study the extraction of tar sand at both the super and subcritical conditions in a reactor that would insure good contacting between the extract and the residual phases and an effective separation of the phases. It was decided that a turn-key supercritical fluid extraction system be purchased from Autocalve Engineer, Inc.

Catalytic upgrading of bitumen and bitumen-derived liquids was undertaken to determine the kinetic parameters and process operating conditions necessary for hydrotreating of Uinta basin bitumens and bitumen-derived liquids. A high-pressure, high-temperature reactor system was constructed which will be used to determine the process variables necessary to effect denitrogenation and desulfurization of bitumen. Ebullieted-bed hydrocracking emerged as one of the most promising processes when bitumen upgrading processes were considered. In this context, the H-oil process, developed for the upgrading of coal liquids and petroleum resids was reviewed and design considerations of the pilot and laboratory scale ebullieted-bed hydrocracking units were identified.

Process data from hydropyrolysis was reduced to a mathematical model. The reaction model was then used for the reactor block in a process simulation model. Process simulation was performed to optimize the heat exchange network for a conceptual commercial design. An economic trade-off existed between maximizing the heat utilization and minimizing the equipment costs.

The optimized heat exchange network was used in the process configuration to optimize the H_2 split ratio. Optimum reactor conditions depend strongly on the feedstock/product value assumptions. The results suggested an economic optimum exists at 500°C, 20 seconds residence time and 1800 psig H_2 pressure. At these conditions process yields are 2% gas, 60% distillate and 38% residue.

Acquisition and Characterization of the Bitumen Impregnated Sandstone from the Whiterocks Tar Sand Deposit

Principal Investigator: F.V. Hanson

Post Graduate Fellow: C.H. Tsai
Research Associate: R.C. White

The magnitude of the University of Utah mining/surface recovery tar sands research and development program requires frequent acquisition of drum quantity samples of the tar sand ore from the Uinta Basin tar sand deposits. The work conducted during the period covered by this report focused on the Whiterocks tar sand deposit and made use of the mined ore from that deposit in much of the experimental work.

ACQUISITION OF MINED ORE AND CORE SAMPLES FROM THE WHITEROCKS TAR SAND DEPOSIT

The mined ore sample sites and the core locations are indicated on the map of the Whiterocks tar sand deposit (Figure 1).

Whiterocks Mined Ore Samples

The mined ore from the Whiterocks tar sand deposit used in various projects was obtained from the Fausett pit on the outcrop on the western flank of the Whiterocks River. Two to three feet of tar sand on the surface of the floor of the pit were removed to expose fresh material in three designated locations: West Central, West North and West South regions of the pit. A backhoe was then used to mine barrel quantities of the freshly exposed ore. The barrels were lined with polyethylene bags and sealed for transportation to the University of Utah. Six to eight barrels of ore were obtained

8

LOCATION OF SAMPLE SITES ON THE
WHITEROCKS TAR SAND DEPOSIT
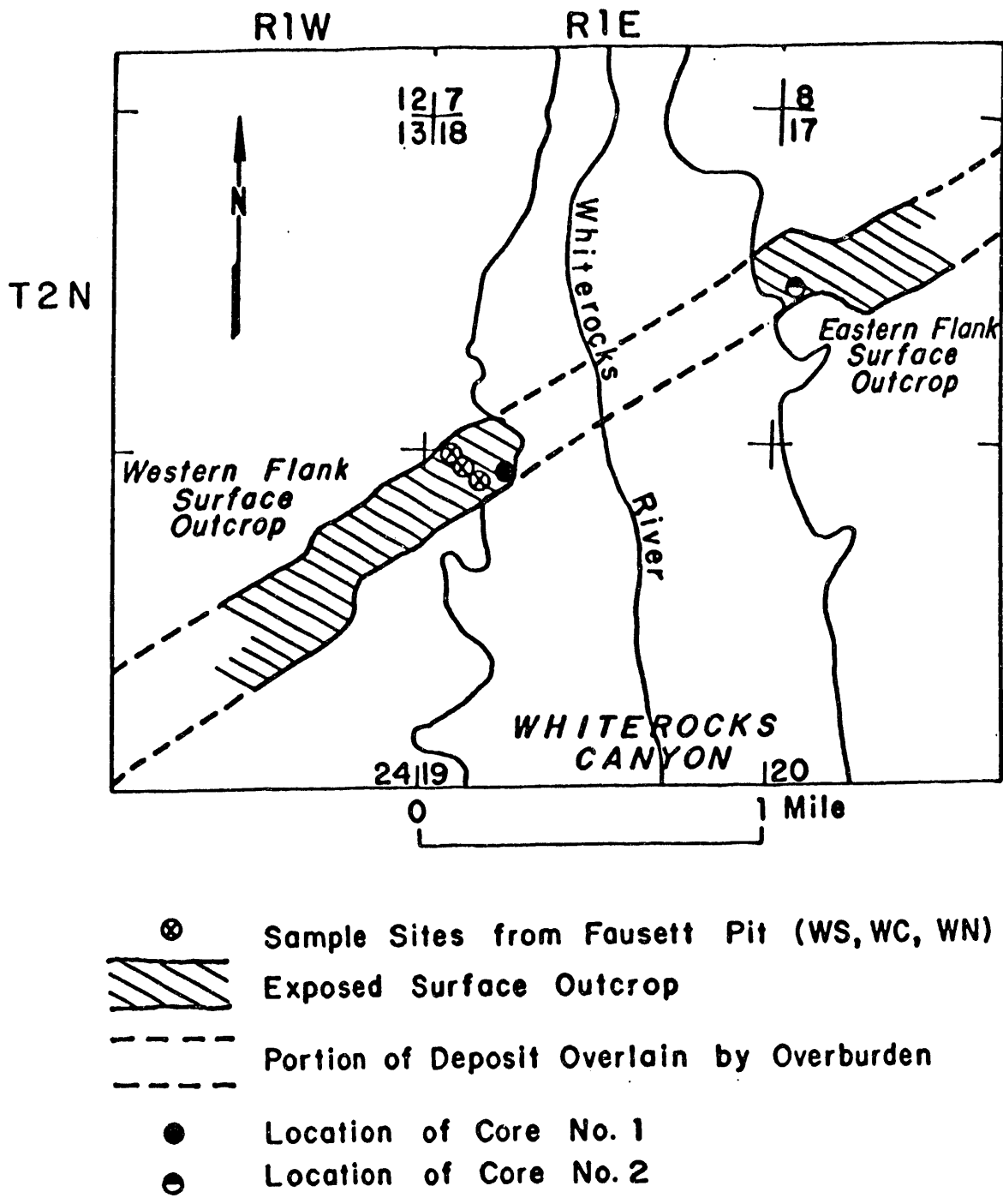
Figure 1   Whiterocks Tar Sand Deposit Sample Locations

9

from each of the three sites in the pit. At the time these samples were obtained the pit was approximately 800-1000 feet wide and 50 feet below the top of the saturated zone. An attempt to obtain freshly mined ore from the outcrop on the eastern flank of the Whiterocks River was not successful. The explosive charge merely lifted the saturated cap rock in the vertical plane and it immediately settled back in-place so that no fresh, accessible ore was exposed.

The ore in the barrels was crushed to minus 0.5 inches after being transported to the University and the crushed ore from each specific location was mixed and blended prior to storage in lined and sealed barrels. The composite tar sand sample from each location was prepared as follows. Equal portions from each of four barrels of the crushed ore from a specific location were placed in separate ends of two polyethylene mixing boxes (6 feet X 4 feet X 2 feet) forming four conical piles of the crushed ore. The ore in each pile was mechanically mixed and equal portions of the mixed ore from each pile were placed in a rotary cement mixer and mixed for 5 minutes at the maximum rpm. The well mixed composite tar sand ore from each location was placed in lined barrels and stored in a cool place. This procedure was used to insure that repre-sentative, composite samples were used in all subsequent experiments.

Eighteen samples from each location were extracted with toluene to determine the bitumen saturation and water content. The average bitumen saturations were 9.65 wt%, 5.96 wt% and 7.29 wt%, for the west north, west central, and west south samples,

10

respectively. The average water saturations were 0.37 wt%, 1.89 wt%, and 0.41 wt% for the west north, west central, and west south samples, respectively. The west central location was the low point in the pit and thus was throught to contain additional gravitational water relative to the west north and west sourth sample locations. The bitumen and water saturation data are presented in Table 1 and the statistical analysis of the data is presented in Table 2.

The chemical and physical properties of the crushed and composited ore samples from the West Central, West North and West South sections of the pit are reported in Tables 3 through 5. The properties of the bitumens extracted from the original outcrop sample provided by Mr. Fausett and from a composite sample of the mined ore obtained from the Fausett pit in 1988 are included in Tables 3 through 5 for comparison.

Whiterocks Core Samples

Waterford Resources Ltd., supplied the Laboratory of Coal Science, Synthetic Fuels and Catalysis with two cores which were drilled on the Whiterocks deposit. Core number 1 (11.0' - 259.7') was drilled on the western flank of the deposit near the Fausett pit in the NW 1/4 of the NW 1/4 of Section 19, Township 2 North, Range 1 East. The core bit bound-up in a tar filled fracture at 259-260 feet and the coring operation was terminated. Several gallons of tar were bailed from the hole and the bitumen will be analyzed in the next phase of the program. The second core (80.0' - 425.0') was obtained from the east flank of the deposit.

11

Table 1
Bitumen and Water Saturation Analyses for Mined Ore Samples
from the Whiterocks Tar Sand Deposit
Western Flank Outcrop

Location	Run	Bitumen Saturation (wt%)			Water Content (wt%)		
		Extraction 1	Extraction 2	Extraction 3	Extraction 1	Extraction 2	Extraction 3
West North	1	7.9	7.9	7.7	0.2	0.2	0.3
	2	7.5	7.5	7.8	0.4	0.4	0.4
	3	7.8	7.7	7.8	0.4	0.4	0.4
	4	7.8	7.8	7.9	0.4	0.4	0.4
	5	5.2[1)	7.8	7.8	0.4	0.4	0.5
	6	8.0	7.8	8.0	0.3	0.3	0.5
West Central	1	5.8	5.8	5.8	0.4	1.0	1.7
	2	5.6	5.9	6.0	2.3	2.1	2.2
	3	6.4	6.2	6.2[2)	1.9	1.6	1.1
	4	5.7	5.8	_[2)	2.7	2.5	
	5	5.8	5.7	6.0	2.5	2.3	1.9
	6	6.4	5.8	6.4	1.8	2.3	1.8
West South	1	7.4	7.3	7.3	0.2	0.4	0.5
	2	7.2	7.0	7.2	0.4	0.3	0.4
	3	7.3	7.2	7.4	0.4	0.4	0.3
	4	7.3	7.6	7.4	0.4	0.7	0.5
	5	_[3)	7.3	7.2	_[3)	0.5	0.4
	6	7.3	7.3	7.2	0.3	0.4	0.4

1) Not completely extracted.
2) Lost solvent; coked bitumen.
3) No extraction was made.

Table 2

Statistical Analysis of Bitumen and Water Saturation Determinations
for the Mined Ore Samples from the Whiterocks Tar Sand Deposit
Western Flank Outcrop

Sample Location	N	Mean	Standard Deviation	Standard Error of the Mean	90% Confidence Interval
West North					
Bitumen	18	7.65	0.626	0.15	7.39-7.91
Water	18	0.37	0.083	0.019	0.34-0.41
West Central					
Bitumen	17	5.96	0.265	0.064	5.85-6.07
Water	17	1.89	0.603	0.15	1.63-2.14
West South					
Bitumen	17	7.29	0.127	0.031	7.23-7.34
Water	17	0.41	0.109	0.026	0.36-0.45

Table 3

Average Bitumen Properties for the Mined Ore Samples
from the Whiterocks Tar Sand Deposit

	Fausett[1] Outcrop Sample (West Pit)	Fausett[2] Mine Sample (West Pit)	Fausett[3] Mine Sample (West North)	Fausett[3] Mine Sample (West Central)	Fausett[3] Mine Sample (West South)
Bitumen Saturation, wt.%	11.2	7.2	7.6	6.0	7.3
Water Saturation, wt.%			0.4	1.9	0.4
Gravity, °API	11.9	11.9	12.7	13.5	11.4
Specific Gravity (60°F/60°F)	0.987	0.987	0.981	0.976	0.990
Net Heat of Combustion, BTU/lb$_m$	18,478.2	----	17,630.	17,599.	17,638.
Viscosity, cps (333 K)	----	2665.[5)]	7,897.	7,616.	9,997.
Conradson Carbon Residue, wt.%	11.8	8.1	8.8	9.5	9.9
Ash Content, wt.%	1.1	1.3	0.24	0.16	0.16
Pour Point, °F	149.	135.	104.	101.	93.
Elemental Analysis					
C, wt.%	86.4	83.3	86.4	86.4	85.2
H, wt.%	11.7	11.0	11.6	11.5	11.6
N, wt.%	1.1	1.3	1.4	1.1	1.1
S, wt.%	0.5	0.3	0.6	0.4	0.4
O, wt.%	0.3	4.1	----	0.5	1.7
Atomic H/C Ratio	1.63	1.58	1.61	1.60	1.63
Molecular Weight, g mol^{-1}	402.	-----	561.	500.	678.
Ni, ppm	67.	-----	78.	81.	77.
V, ppm	<5.	-----	3.6	2.0	1.3
As, ppm		-----	2.3	2.2	2.3

1) Original Whiterocks tar sand sample provided by Mr. John Fausett.
2) Original 48 drums of run of mine samples were hand picked from the Fausett mine pit.
3) Deep mined drum samples obtained from the Fausett mine in 1989.

14

Table 4
Average Bitumen Properties for the Mined Ore Samples
from the Whiterocks Tar Sand Deposit

	Fausett[1] Outcrop Sample (West Pit)	Fausett[2] Mine Sample (West Pit)	Fausett[3] Mine Sample (West North)	Fausett[3] Mine Sample (West Central)	Fausett[3] Mine Sample (West South)
Simulated Distillation: Volatility (<1000°F), wt.%					
wt.%	30.1	40.5	47.7	49.3	42.1
IBP - 400°F, wt.%	0.	0.0	0.0	0.1	0.3
400 - 650°F, wt.%	2.5	4.9	6.3	7.4	6.6
650 - 1000°F, wt.%	27.6	35.6	41.4	41.8	35.2
1000°F+ Residue, wt.%	69.9	59.9	52.5	50.7	57.9
Simulated Distillation: IBP, °F					
IBP, °F	536.	489.	486.	435.	414.
5, wt.%	718.	651.	635.	592.	594.
10, wt.%	824.	743.	725.	694.	709.
15, wt.%	867.	813.	795.	759.	792.
20, wt.%	921.	849.	842.	815.	844.
25, wt.%	959.	883.	871.	852.	880.
30, wt.%	999.	925.	898.	885.	918.
40, wt.%	----	999.	957.	937.	977.
50, wt.%	----	----	----	----	----
60, wt.%	----	----	----	----	----
70, wt.%	----	----	----	----	----
80, wt.%	----	----	----	----	----
90, wt.%	----	----	----	----	----
95, wt.%	----	----	----	----	----
End Point, wt.%	30.1	<40.5	<47.7	<49.3	<42.1

1) Original Whiterocks tar sand sample provided by Mr. John Fausett.
2) Original 48 drums of run of mine samples were hand picked from the Fausett mine pit
3) Deep mined drum samples obtained from the Fausett mine in 1989.

15

Table 5

Average Bitumen Properties for the Mined Ore Samples
from the Whiterocks Tar Sand Depsoit

	Fausett[1] Outcrop Sample (West Pit)	Fausett[2] Mine Sample (West Pit)	Fausett[3] Mine Sample (West North)	Fausett[3] Mine' Sample (West Central)	Fausett[3] Mine Sample (West South)
Gradient Elution Chromatography					
Saturates, wt%	23.6	18.3			
Mono- and Dinuclear Aromatic Oils, wt%	5.9	5.5			
Polynuclear Aromatic Oils, wt%	14.3	11.5			
Polynuclear Soft Resins, wt%	8.5	13.8			
Hard Resins, wt%	11.7	3.0			
Polar Resing, wt%	13.4	1.6			
Asphaltenes, wt%	18.3	29.6			
Non-Eluted Asphaltenes wt%	4.3	16.9			
Asphaltenes[4], wt%	----	----	3.3	3.6	4.0
Maltenes, wt%	----	----	96.7	96.4	96.0
Compound Type Analysis over Fuller's Earth					
Saturates, wt%	----	----	29.5	30.2	29.2
Aromatics, wt%	----	----	14.5	14.6	12.6
Polynuclear Aromatics, wt%	----	----	5.2	6.8	2.8
Polar Aromatics, wt%	----	----	2.5	3.4	1.4
Resins, wt%	----	----	40.8	38.8	42.0
Asphaltenes, wt%	----	----	1.6	1.3	4.1
Non-Eluted Asphaltenes wt%	----	----	3.3	3.6	6.8

1) Original Whiterocks tar sand samples provided by Mr. John Fausett.
2) Original 48 drums of run of mine samples were hand picked form the Fausett mine pit.
3) Deep mined drum samples obtained from the Fausett mine in 1989.
4) Pentane insolubles.

Core number 2 was drilled in the S 1/2 of the NW 1/4 of Section 17, Township 2 North, Range 1 East and was drilled as a twin to core hole John. The cores were boxed and transported to the University of Utah for analysis. The lithological examination of the cores was conducted and recorded by a consulting geologist. Each box contained a 10-foot section of the core. Average samples from each box were prepared by removing every other 6-inch segment of the core. These segments were crushed to minus-1/2 inch and mixed to produce a representative, composite sample of each box. Six-inch pieces of 1"x1" board were cut and used to replace the removed segments of the core. In this way, the positions of the remaining pieces of core were preserved and subsequent samples could be correlated to the depth of the core. The composite samples were prepared after the geologic inspection had been completed.

The chemical and physical properties of the crushed and composite samples from the individual sections of the boxed core were determined and are reported in Tables 6 through 9. The average properties for core numbers 1 and 2 are reported in Tables 10 and 11.

Lithology of Core Number 1

The Whiterocks core number 1 was geologically logged on 7 and 8 November 1989 by Keith M. Clem, Consulting Petroleum Geologist. The core was located in a laboratory in the HEDCO Building on the University of Utah campus, Salt Lake City, Utah. The inspection was conducted with a binocular microscope (10-70 magnification), an ultra-violet lamp, and a hand lens (10 magnification). The

17

condition of the core was very good with 95 percent of the total core being whole pieces. The lithologic inspection was hampered by the high degree of saturation which masked the rock particles.

The core was cut completely within the Jurassic age Navajo sandstone formation. The Navajo formation is composed primarily of sandstone and has been described as being composed of sub-angular to sub-rounded, well sorted, mostly fine grained sand grains. Occasionally, the sand will be medium to fine grained. The grains are frosted and slightly pitted; the cement, while not visible, is presumed to be a non-calcareous clay. Siltstone lamina between bonds were identified within the Navajo sandstone. The silt grains were sub-angular to angular, occasionally sub-rounded, well sorted and very fine to fine grained. The grains were slightly frosted, and open porosity averaging 15 percent was visible. Clay cement was visible, being bronze colored and slightly effervescent when scratched. Natural fractures were evident in the core, and were classified as follows: sealed with silt, sealed with tar, and open with tar. The fractures sealed with silt and with tar are not readily evident as the core was not broken along the fractured planes. The open fractures with tar were very visible, as evidenced by a broken core and "globs" of tar glistening on the fracture planes. The fractures do not appear to be a controlling factor in the saturation or migration of the tar. Bitumen saturation was consistent across the fractured zones.

The Navajo Sandstone was deposited in a sand-dominated, desert environment. Large dunes are evident by the thick sequences of sand beds. Also evident are "white bands" within the sandstone.

These bands are lenses or lamina of low permeability silt. Most of
the banding is very thin, less than 1/4 inch th ck, however, in
some instances the bands thicken to a couple inches. They appear
to be cross-bedding contacts, wherein a film of silt settled upon
the dune and was subsequently covered by another layer of sand.
The banding grades from very even to braided to contorted to highly
fragmented lenses. This variation suggests extensive slumping or
reworking of the sand. The reworking was a result of both wind-
action and water-action. "White spots" were also noted in the sand
beds. The "spots" appear to be low permeability tubular silt
inclusions. These inclusions may be holes dug by worms which
filled with silt. While the Navajo sandstone was deposited in a
desert environment which was essentially barren of life, episodes
of water saturation are evident throughout the Navajo which may
have created conditions suitable to sustain life.

An attempt was made to decipher the paleo-environment from the
core. Starting from the bottom (first laid sediments) (from 250
ft. to 247 ft.) a silt bed was most probably lain during a wet
period. From 247 ft. to 146 ft., there was an oscillation from dry
sand dunes to moist, silt-accumulating, low areas and back again.
There is evidence that as many as five oscillations occurred in
this interval. The interval from 146 ft. to 127 ft., indicated a
thick, water-lain or moist shallow area dominated, with low
permeability siltstone being predominant. A drying-out period is
indicated in the intervals from 127 ft. to 108 ft., as evidenced by
a progressively cleaner sand being predominant. Small dunes pre-
vailed, from 108 ft. to 90 ft., and massive dunes became dominant

19

in the interval from 90 ft. to 11 ft.

The hydrocarbon resource present in the Navajo Sandstone is a black, odoriferous, tarry-like asphaltum. Under an ultra-violet lamp, the tar does not fluoresce, which is not uncommon for "aged" samples (samples exposed to atmosphere for a period of time) or for a highly naphthenic petroleum resource. The tar appears to fill the pores of the sandstone, with bleeding and oozing indicative of super-saturation. The siltstones are either weakly or not saturated, due to pore filing or permeability choking by clay cement. It does not appear that the "banding" and "spots" (i.e., worm holes) exert significant control over saturation. The hydrocarbon saturation in the core was evident within an upper interval from 11 to 127 feet and a lower interval from 146 to 247 feet. The upper interval is characterized by a rather consistent "rich" grade of saturation, varying a grade higher or lower due to increased silting within the sand. The saturation in the lower interval varied rapidly through all grades. The variation in grades is caused by siltstone permeability barriers. The lower interval has a greater thickness of super saturated (highly and very rich) beds than the upper interval. The details of the inspection of core number 1 are reported in Appendix A.

Lithology of Core Number 2

The Whiterocks core number 2 was geologically logged on, December 20, 21 and 22, 1989, by Keith M. Clem, Consulting Petroleum Geologist. The core was located in the HEDCO Building, on the University of Utah campus, Salt Lake City, Utah. The inspection was conducted with a binocular microscope (10-70 magnification), an

ultra-violet lamp, and a hand-held lens (10 magnification). The condition of the core was very good with 95 percent of total being whole pieces. The lithologic inspection and description was hampered by the high degree of saturation which the masked the rock or sandstone particles.

The core was completely cut in the Jurassic age Navajo Sandstone formation. The Navajo sandstone is primarily composed of sandstone and has been being described as sub-angular to sub-rounded, well sorted, fine grained sand/grains. The grains are mostly clear but occasionally frosted; the cement was primarily a non-calcareous clay although there are sections were the rock effervesced indicative of calcareous cementing. Very little natural fracturing was evident in the core, and all were sealed with either silt or tar. The fractures do not appear to be a controlling factor in saturation or migration of the tar.

The Navajo Sandstone was deposited principally during a sand-dominated, desert environment. Large dunes are evident by the thick sequences of sand beds. Also evident are "white bands" within the sandstone. These bands appear to be lenses or lamina of low permeability silt. Most banding is very thin, less than 1/4 inch thick, however, the bands thicken to several inches in some areas. They appear to be cross-bedding contacts, wherein a film of silt settled on the dune and was subsequently covered by another bed of sand. The banding is mostly braided to slightly contorted lenses.

The hydrocarbon resource in the Navajo Sandstone is a black, odoriferous, tar-like asphaltum. Under an ultra-violet lamp, the

tar does not fluoresce, which is not uncommon for "aged" (samples exposed to atmosphere for a period of time) or for a highly naphthenic petroleum resource sample. The tar occurs as filling in the pores of the sandstone. The hydrocarbon saturation in the core was evident within an upper interval from 152 to 230 feet and a lower interval from 342 to 391 feet. The upper interval is characterized by a rather consistent "rich" grade of saturation. The saturation in the lower interval varies through all grades and quite rapidly. The variation in grades is caused by siltstone permeability barriers. The details of the inspection of core number 2 are reported in Appendix B.

CHARACTERIZATION OF THE NATIVE BITUMEN FROM THE WHITEROCKS TAR SAND DEPOSIT

Bitumen saturations were determined on the three composite mined ore samples and on the composite samples from the 10-foot core intervals. The physical and chemical data were obtained from the extracted toluene-free bitumen samples. Bitumen characterization tests included simulated distillation, specific and API gravity, density, viscosity, heat of combustion, Conradson carbon, ash content, pour point, elemental analysis, molecular weight, and asphaltenes and maltenes analysis. The saturations for the mined ore samples ranged from 6.0 (WC) to 7.6 (WN) wt.%. The bitumen saturations, obtained by Soxhlet extraction using toluene, ranged from 0.7 to 8.4 wt% for core number 1 and 2.2 to 7.2 wt% for core number 2.

Experimental Methods

Bitumen Extraction and Recovery

The bitumen extraction for each sample was carried out in a Dean-Stark Soxhlet apparatus with Whatman, single thickness, cellulose thimbles and toluene as the solvent. Shark skin filter paper was wrapped around the outside of the thimble to trap the fine mineral particles which panned through thimble wall. The extractions were carried out for approximately 24 hours, with the toluene/bitumen solution maintained between 112 and 116°C.

A Büchi, model EL-131S rotary evaporator was used in conjunction with a Precision, model S-35 vacuum pump, to remove the toluene from the solution. The temperature of the cooling water in the condenser was 15°C while that in the water bath was maintained at 85°C. Dry ice and acetone were used to keep the cold trap, between the rotary evaporator and the vacuum pump, at -79°C to prevent backstreaming of the pump oil. The bulk of the toluene was allowed to evaporate at mild conditions (85°C and 300 mm Hg) in order to prevent bumping, after which the pressure was reduced further to 21 mm Hg until dripping of the solvent from the cooling coil ceased. At this point the bitumen sample had been evaporated for five hours.

The residual toluene content of the bitumen samples were determined by simulated distillation. A residual toluene content below 0.2 wt% was achieved with each sample before further analyses were performed.

23

Simulated Distillation

Bitumen samples (3 μl) were injected into an HP model 5730A gas chromatograph, with a dual flame ionization detector, using a temperature program from -30 to 350°C and a ramp of 11°C/min. The 1/4" x 18" stainless steel column was packed with 3% Dexsil 300 on Anakrom Q.

The procedure used was a modification of the ASTM D2887 method. Samples to be injected were diluted to 50% by weight with methylene chloride in order to dissolve all of the bitumen. A second sample was diluted with an internal standard (C_5 to C_9-benzene) and injected. The theoretical total area of the sample was determined from a comparison of the two analyses, allowing the calculation of the percent recovery at 1000°F and the boiling point distribution up to 1000°F.

The volatility is defined as the wt% of the total sample which has been distilled at 1000°F. The naphtha or gasoline fraction is defined to be the material boiling up to 400°F; the middle distillate fraction is defined to be the material boiling between 400 and 650°F; the gas oil fraction is defined to be the material boiling from 650 to 1000°F. The material boiling above 1000°F is defined as the residuum fraction.

Specific Gravity and Density

The specific gravities and densities of the bitumen samples were determined in accordance with the ASTM D70-52 method using a capillary-stoppered pyknometer.

Viscosity

The bitumen viscosities were measured in a Brookfield microviscometer with cone and plate geometry. The viscometer was calibrated using several viscosity-standard silicon oils.

Heat of Combustion

The heats of combustion were measured using a Parr model 1241 adiabatic calorimeter with a model 1108 oxygen combustion bomb. The standardization test was performed using benzoic acid and the net heat of combustion was calculated using sulfur and hydrogen data obtained from elemental analysis of the bitumen.

Conradson Carbon Residue and Ash Content

The Conradson Carbon Residue of the bitumens were determined in accordance with the ASTM D189-65 method; the ash contents were determined in accordance with the ASTM D442-63 method.

Pour Point

The pour point was determined in accordance with the ASTM D97-66 method. The reported values are an average of five determinations.

Elemental Analysis and Molecular Weight

The elemental analysis; carbon, hydrogen, nitrogen, sulfur and oxygen, and molecular weight determinations were performed by Galbraith Laboratories. The oxygen content was a direct determination. The molecular weight was determined using 4-point VPO with toluene as the solvent and benzyl as the standard. Selected samples were also analyzed for carbon, hydrogen, nitrogen and sulfur at the Fossil Fuels Characterization Laboratory,

University of Utah. In general, the analyses were in good agreement between the two laboratories.

Asphaltenes/Maltenes Analysis

Five gram samples of bitumen were mixed with toluene in a ratio of one milliliter of toluene per gram of bitumen in order to dissolve the bitumen. Pentane (40 times the volume of toluene) was then added and the mixture was allowed to settle overnight to achieve precipitation of the asphaltenes. The toluene-pentane-maltenes solution was decanted. The precipitated asphaltenes were washed with pentane and were dried and weighed. The maltenes were calculated by difference.

PHYSICAL AND CHEMICAL PROPERTIES
OF THE WHITEROCKS BITUMEN SAMPLES

The physical and chemical properties of the bitumen from the composite mined ore samples from the Whiterocks tar sand deposit are reported in Tables 3 through 5. The data for the West North, West Central and West South bitumens indicates that there is little lateral variation in the bitumen across the deposit in the Fausett pit (south to north).

The data for the bitumen samples from the cores (Tables 6-9) indicate that there is little vertical variation in bitumen in the two core holes drilled to date. The averaged physical and chemical properties of the bitumen samples from cores number 1 and 2 are presented in Tables 10 and 11. The averaged data from the cores imply there is little lateral variation in the bitumen (west to east) across the deposits; however, it must be recognized that this conclusion is based on limited data.

26

Table 6

Physical and Chemical Properties for the
Whiterocks Bitumen From the Composite Core Samples

Whiterocks Tar Sand Deposit Core Number 1

Interval Number	1	2	3	4	5	6
Depth Range, ft.						
Top	11.0	21.0	31.0	41.2	50.4	59.4
Bottom	21.0	31.0	41.0	50.4	59.4	69.4
Bitumen Saturation, wt%	8.2	7.5	5.7	6.0	6.5	7.7
Specific Gravity (60°F/60°)	0.976	0.979	0.974	0.977	0.981	0.978
API Gravity	13.5	13.1	13.8	13.3	12.7	13.2
Net Heat of Combustion, BTU/lb$_m$	17,600	17,600	17,600	17,700	17,600	17,600
Viscosity, cps (333 K)	10,700	7,240	11,200	7,520	11,100	9,460
Conradson Carbon Residue, wt%	9.6	9.9	9.6	9.8	9.8	11.3
Ash Content, wt%	0.4	0.4	0.4	0.3	0.2	0.3
Pour Point, °F	68	72	68	72	73	69
Elemental Analysis						
C, wt%	86.06	------	------	------	86.22	------
H, wt%	11.90	------	------	------	11.74	------
N, wt%	1.08	------	------	------	1.32	------
S, wt%	0.36	------	------	------	0.53	------
O, wt%	1.07	------	------	------	1.17	------
Atomic H/C Ratio	1.66	------	------	------	1.64	------
Molecular Weight, g/mol	600	------	------	------	573	------
Ni, ppm	6.5	------	------	------	39	------
V, ppm	<1	------	------	------	<1	------
As, ppm	<1	------	------	------	<1	------

27

Table 6 (cont.)
Physical and Chemical Properties for the
Whiterocks Bitumen from the Composite Core Samples

Whiterocks Tar Sand Deposit Core Number 1

Interval Number	7	8	9	10	11	12
Depth Range, ft.						
Top	69.4	79.0	88.6	98.2	107.7	117.7
Bottom	79.0	88.6	98.2	107.7	117.1	126.9
Bitumen Saturation, wt%	8.4	7.4	6.1	5.7	5.8	4.5
Specific Gravity (60°F/60°F)	0.980	0.975	0.976	0.977	0.979	0.978
API Gravity	12.8	13.6	13.4	13.4	13.1	13.2
Net Heat of Combustion, BTU/lb$_m$	17,500	17,700	17,600	17,700	17,700	17,700
Viscosity cps (333 K)	12,200	10,700	8,900	12,200	11,600	12,500
Conradson Carbon Residue, wt%	9.8	12.4	8.8	9.4	9.2	8.5
Ash Content, wt%	0.3	0.2	0.2	0.2	0.2	0.2
Pour Point, °F	75	75	70	70	81	75
Elemental Analysis						
C, wt%	85.85	-----	-----	86.27	-----	-----
H, wt%	11.04	-----	-----	10.64	-----	-----
N, wt%	1.63	-----	-----	1.23	-----	-----
S, wt%	0.33	-----	-----	0.51	-----	-----
O, WT%	0.97	-----	-----	1.59	-----	-----
Atomic H/C Ratio	1.52	-----	-----	1.48	-----	-----
Molecular Weight, g/mol	622	-----	-----	607	-----	-----
Ni, ppm	83	-----	-----	89	-----	-----
V, ppm	2	-----	-----	<1	-----	-----
As, ppm	3	-----	-----	<1	-----	-----

Table 6 (cont.)
Physical and Chemical Properties for the
Whiterocks Bitumen from the Composite Core Samples

Whiterocks Tar Sand Deposit Core Number 1

Interval Number	13	14	15	16	17	18
Depth Range, ft.						
Top	126.9	136.7	146.2	155.8	165.7	175.2
Bottom	136.7	146.2	155.8	165.7	175.2	184.0
Bitumen Saturation, wt%	1.5	0.7	6.6	8.2	6.5	6.5
Specific Gravity, (60°F/60°F)	0.973	0.966	0.979	0.977	0.979	0.983
API Gravity	14.0	15.0	13.0	13.3	13.0	12.5
Net Heat of Combustion, BTU/lb$_m$	17,800	17,800	17,600	17,600	17,600	17,600
Viscosity, cps (333 K)	13,800	8,900	9,680	13,400	17,000	13,600
Conradson Carbon Residue, wt%	8.4	-----	10.2	9.5	9.2	9.5
Ash Content, wt%	0.3	-----	0.2	0.2	0.2	0.2
Pour Point, °F	-----	-----	-----	75	70	75
Elemental Analysis						
C, wt%	-----	-----	-----	85.77	-----	-----
H, wt%	-----	-----	-----	11.69	-----	-----
N, wt%	-----	-----	-----	1.35	-----	-----
S, wt%	-----	-----	-----	0.58	-----	-----
O, wt%	-----	-----	-----	0.87	-----	-----
Atomic H/C Ratio	-----	-----	-----	1.64	-----	-----
Molecular Weight, g/mol	-----	-----	-----	592	-----	-----
Ni, ppm	-----	-----	-----	30	-----	-----
V, ppm	-----	-----	-----	<1	-----	-----
As, ppm	-----	-----	-----	<1	-----	-----

Table 6 (cont.)
Physical and Chemical Properties for the
Whiterocks Bitumen from the Composite Core Samples

Whiterocks Tar Sand Deposit Number 1

Interval Number	19	20	21	22	23	24
Depth Range, ft.						
Top	184.9	195.0	204.1	213.8	223.5	233.1
Bottom	195.0	204.1	213.8	223.5	233.1	242.7
Bitumen Saturation, wt%	5.1	5.0	6.4	7.2	4.8	5.4
Specific Gravity, (60°F/60°F)	0.979	0.984	0.975	0.982	0.980	0.986
API Gravity	13.0	12.3	13.7	12.6	12.9	12.1
Net Heat of Combustion, BTU/lb$_m$	17,600	17,700	17,600	17,600	17,600	17,600
Viscosity cps (333 K)	15,000	16,000	19,400	17,000	11,700	18,200
Conradson Carbon Residue, wt%	11.2	10.0	11.2	9.2	9.9	9.2
Ash Content, wt%	0.3	0.4	0.2	0.2	0.4	0.9
Pour Point, °F	75	-----	81	75	81	75
Elemental Analysis						
C, wt%	-----	86.04	-----	86.27	-----	-----
H, wt%	-----	11.57	-----	11.56	-----	-----
N, wt%	-----	1.52	-----	1.27	-----	-----
S, wt%	-----	0.58	-----	0.37	-----	-----
O, wt%	-----	1.08	-----	0.88	-----	-----
Atomic H/C Ratio	-----	1.62	-----	1.61	-----	-----
Molecular Weight, g/mol	-----	589	-----	617	-----	-----
Ni, ppm	-----	15	-----	86	-----	-----
V, ppm	-----	<1	-----	2	-----	-----
As, ppm	-----	<1	-----	2	-----	-----

Table 6 (cont.)
Physical and Chemical Properties for the
Whiterocks Bitumen from the Composite Core Samples

Whiterocks Tar Sand Deposit Core Number 1

Interval Number	24	-----	-----	-----	-----	-----	-----	-----
Depth Range, ft.								
Top	242.7	---	---	---	---	---	---	---
Bottom	250.7	---	---	---	---	---	---	---
Bitumen Saturation, wt%	3.7	-----	---	---	---	---	---	---
Specific Gravity, (60°F/60°F)	0.972	---	---	---	---	---	---	---
API Gravity	14.1	-----	---	---	---	---	---	---
Net Heat of Combustion, BTU/lb$_m$	17,600	-----	---	---	---	---	---	---
Viscosity cps (333 K)	12,800	-----	---	---	---	---	---	---
Conradson Carbon Residue, wt%	9.8	---	---	---	---	---	---	---
Ash Content, wt%	0.3	---	---	---	---	---	---	---
Pour Point, °F	-----	---	---	---	---	---	---	---
Elemental Analysis								
C, wt%	86.39	---	---	---	---	---	---	---
H, wt%	11.81	---	---	---	---	---	---	---
N, wt%	1.37	---	---	---	---	---	---	---
S, wt%	0.54	---	---	---	---	---	---	---
O, wt%	0.75	---	---	---	---	---	---	---
Atomic H/C Ratio	1.64	---	---	---	---	---	---	---
Molecular Weight, g/mol	571	---	---	---	---	---	---	---
Ni, ppm	72	---	---	---	---	---	---	---
V, ppm	<1	---	---	---	---	---	---	---
As, ppm	<1	---	---	---	---	---	---	---

Table 7
Distillation Analyses for the Whiterocks Bitumen
from the Composite Core Samples

Whiterocks Tar Sand Deposit Core Number 1

Interval Number	1	2	3	4	5	6
Depth Range, ft.						
Top	11.0	21.0	31.0	31.2	50.4	59.4
Bottom	21.0	31.0	41.0	50.4	59.4	69.4
Boiling Point Distribution:						
Volatility (<1000°F), wt%	45.1	47.2	46.6	45.7	50.5	56.7
IBP - 400°F, wt%	0.0	0.0	0.6	0.3	0.7	0.6
400 - 650°F, wt%	7.9	8.5	8.2	8.7	9.4	10.3
650 - 1000°F, wt%	37.2	38.7	37.8	36.7	40.4	45.8
>1000°F Residue, wt%	54.9	52.8	53.4	54.3	49.5	43.3
Simulated Distillation:						
IBP, °F	435	426	394	415	397	432
5 wt%, °F	586	567	556	558	532	529
10 wt%, °F	689	678	675	671	642	637
15 wt%, °F	752	759	754	752	721	712
20 wt%, °F	829	828	826	822	795	777
25 wt%, °F	867	867	867	867	849	829
30 wt%, °F	894	885	894	900	883	862
40 wt%, °F	963	950	961	957	943	912
50 wt%, °F	---	---	---	---	---	963
60 wt%, °F	---	---	---	---	---	---
Asphaltenes, wt%	2.05	1.82	1.49	1.93	1.90	2.83
Maltenes, wt%	97.95	98.18	98.51	98.07	98.10	97.17

Table 7 (cont.)
Distillation Analyses for the Whiterocks Bitumen from the Composite Core Samples

Whiterocks Tar Sand Deposit Core Number 1

Interval Number	7	8	9	10	11	12
Depth Range, ft.						
Top	69.4	79.0	88.6	98.2	107.7	117.1
Bottom	79.0	88.6	98.2	107.7	117.1	126.9
Boiling Point Distribution:						
Volatility (<1000°F), wt%	52.6	45.8	47.6	46.4	48.8	54.8
IBP - 400°F, wt%	0.0	0.4	0.7	0.0	0.0	0.0
400 - 650°F, wt%	8.2	9.2	9.4	8.7	8.0	9.0
650 - 1000°F, wt%	44.4	36.2	37.5	37.7	40.8	45.8
>1000°F Residue, wt%	47.4	54.2	52.4	53.6	51.2	45.2
Simulated Distillation:						
IBP, °F	446	405	405	428	446	453
5 wt%, °F	581	541	536	570	590	577
10 wt%, °F	680	657	631	671	685	667
15 wt%, °F	748	736	716	748	745	730
20 wt%, °F	808	808	784	815	824	790
25 wt%, °F	847	860	842	858	860	840
30 wt%, °F	878	878	874	887	889	871
40 wt%, °F	939	941	943	950	950	921
50 wt%, °F	990	---	---	---	---	979
60 wt%, °F	---	---	---	---	---	---
Asphaltenes, wt%	2.92	2.87	2.60	2.15	1.86	1.44
Maltenes, wt%	97.08	97.13	97.40	97.85	98.14	98.56

Table 7 (cont.)
Distillation Analyses for the Whiterocks Bitumen from the Composite Core Samples

Whiterocks Tar Sand Deposit Core Number 1

Interval Number	13	14	15	16	17	18
Depth Range, ft.						
Top	126.9	136.7	146.2	155.8	165.7	175.2
Bottom	136.7	146.2	155.8	165.7	175.2	184.0
Boiling Point Distribution:						
Volatility (<1000°F), wt%	56.0	63.5	42.7	53.1	51.9	44.8
IBP - 400°F, wt%	0.0	0.0	0.3	0.4	0.0	0.0
400 - 650°F, wt%	8.6	10.1	7.9	10.2	8.6	5.5
650 - 1000°F, wt%	47.4	53.4	34.5	42.5	43.3	39.3
>1000°F Residue, wt%	44.0	36.5	57.3	46.9	48.1	55.2
Simulated Distillation:						
IBP, °F	459	464	410	403	450	457
5 wt%, °F	588	561	570	536	588	613
10 wt%, °F	673	648	682	644	673	691
15 wt%, °F	741	711	792	716	745	801
20 wt%, °F	806	766	835	784	806	853
25 wt%, °F	847	817	878	838	853	887
30 wt%, °F	876	855	910	874	883	914
40 wt%, °F	919	982	981	921	930	970
50 wt%, °F	973	943	---	---	---	---
60 wt%, °F	---	---	---	---	---	---
Asphaltenes, wt%	0.71	-----	2.11	2.36	2.48	2.13
Maltenes, wt%	99.29	-----	97.89	97.64	97.52	97.87

Table 7 (cont.)

Distillation Analyses for the Whiterocks Bitumen
from the Composite Core Samples

Whiterocks Tar Sand Deposit Core Number 1

Interval Number	19	20	21	22	23	24
Depth Range, ft.						
Top	184.9	195.0	204.1	213.8	223.5	233.1
Bottom	195.0	204.1	213.1	223.5	233.1	242.7
Boiling Point Distribution:						
Volatility (<1000°F), wt%	47.7	45.7	52.5	49.7	48.8	50.1
IBP – 400°F, wt%	0.0	0.0	0.0	0.1	0.0	0.0
400 – 650°F, wt%	7.5	7.2	8.4	8.4	7.7	7.9
650 – 1000°F, wt%	40.2	38.5	44.1	41.2	41.2	42.2
>1000°F Residue, wt%	52.3	54.3	47.5	50.3	51.2	49.9
Simulated Distillation:						
IBP, °F	477	448	459	432	459	455
5 wt%, °F	599	621	590	577	594	595
10 wt%, °F	693	696	676	675	689	685
15 wt%, °F	768	770	743	747	763	756
20 wt%, °F	835	831	802	811	828	819
25 wt%, °F	867	867	849	858	864	860
30 wt%, °F	894	889	880	883	894	887
40 wt%, °F	954	957	930	946	952	943
50 wt%, °F	---	---	979	---	---	997
60 wt%, °F	---	---	---	---	---	---
Asphaltenes, wt%	2.15	2.31	2.83	2.37	3.35	2.58
Maltenes, wt%	97.85	97.69	97.17	97.63	96.65	97.42

35

Table 7 (cont.)
Distillation Analyses for the Whiterocks Bitumen
from the Composite Core Samples

Whiterocks Tar Sand Deposit Core Number 1

Interval Number	25	-----	-----	-----	-----	-----	-----
Depth Range, ft.							
Top	242.7	-----	-----	-----	-----	-----	-----
Bottom	250.7	-----	-----	-----	-----	-----	-----
Boiling Point Distribution:							
Volatility (<1000°F), wt%	4.10	-----	-----	-----	-----	-----	-----
IBP - 400°F, wt%	0.4	-----	-----	-----	-----	-----	-----
400 - 650°F, wt%	7.5	-----	-----	-----	-----	-----	-----
650 - 1000°F, wt%	33.1	-----	-----	-----	-----	-----	-----
>1000°F Residue, wt%	59.0	-----	-----	-----	-----	-----	-----
Simulated Distillation:							
IBP, °F	408	-----	-----	-----	-----	-----	-----
5 wt%, °F	579	-----	-----	-----	-----	-----	-----
10 wt%, °F	691	-----	-----	-----	-----	-----	-----
15 wt%, °F	781	-----	-----	-----	-----	-----	-----
20 wt%, °F	849	-----	-----	-----	-----	-----	-----
25 wt%, °F	882	-----	-----	-----	-----	-----	-----
30 wt%, °F	914	-----	-----	-----	-----	-----	-----
40 wt%, °F	982	-----	-----	-----	-----	-----	-----
50 wt%, °F	---	-----	-----	-----	-----	-----	-----
60 wt%, °F	---	-----	-----	-----	-----	-----	-----
Asphaltenes, wt%	-----	-----	-----	-----	-----	-----	-----
Maltenes, wt%	-----	-----	-----	-----	-----	-----	-----

Table 8

Physical and Chemical Properties for the Whiterocks
Bitumen form the Composite Core Samples

Whiterocks Tar Sand Deposit Core Number 2

Interval Number	1	2	3	4	5	6
Depth Range, ft.						
Top	80.0	90.0	100.0	110.0	119.8	129.6
Bottom	90.0	100.0	110.0	119.8	129.6	139.0
Bitumen Saturation, wt%	-----	-----	-----	-----	-----	3.2
Specific Gravity (60°F/60°F)	-----	-----	-----	-----	-----	0.977
API Gravity	-----	-----	-----	-----	-----	13.3
Net Heat of Combustion, BTU/lb$_m$	-----	-----	-----	-----	-----	17,600
Viscosity, cps (333 K)	-----	-----	-----	-----	-----	12,800
Conradson Carbon Residue, wt%	-----	-----	-----	-----	-----	9.8
Ash Content, wt%	-----	-----	-----	-----	-----	0.3
Pour Point, °F	-----	-----	-----	-----	-----	67
Elemental Analysis						
C, wt%	-----	-----	-----	-----	-----	-----
H, wt%	-----	-----	-----	-----	-----	-----
N, wt%	-----	-----	-----	-----	-----	-----
S, wt%	-----	-----	-----	-----	-----	-----
O, wt%	-----	-----	-----	-----	-----	-----
Atomic H/C Ratio	-----	-----	-----	-----	-----	-----
Molecular Weight, g/mol	-----	-----	-----	-----	-----	-----
Ni, ppm	-----	-----	-----	-----	-----	-----
V, ppm	-----	-----	-----	-----	-----	-----
As, ppm	-----	-----	-----	-----	-----	-----

Table 8 (cont.)
Physical and Chemical Properties for the Whiterocks
Bitumen form the Composite Core Samples

Whiterocks Tar Sand Deposit Core Number 2

Interval Number	7	8	9	10	11	12
Depth Range, ft.						
Top	139.0	148.7	158.3	167.9	177.1	186.7
Bottom	148.7	158.3	167.9	177.1	186.7	196.1
Bitumen Saturation, wt%	4.7	4.1	6.4	7.2	5.8	7.0
Specific Gravity (60°F/60°F)	0.972	0.983	0.981	0.977	0.983	0.985
API Gravity	12.5	12.4	12.8	13.4	12.4	12.1
Net Heat of Combustion, BTU/lb/$_m$	17,500	17,500	17,500	17,500	17,700	17,600
Viscosity, cps (333 K)	15,800	11,400	12,800	-----	11,700	12,700
Conradson Carbon Residue, wt%	9.1	8.8	8.8	9.5	9.4	9.6
Ash Content, wt%	0.6	0.3	0.2	0.2	0.3	0.4
Pour Point, °F	70	75	75	75	75	81
Elemental Analysis						
C, wt%	84.97	-----	-----	-----	-----	86.07
H, wt%	11.23	-----	-----	-----	-----	11.44
N, wt%	3.44	-----	-----	-----	-----	1.62
S, wt%	0.35	-----	-----	-----	-----	0.41
O, wt%	0.89	-----	-----	-----	-----	0.88
Atomic H/C Ratio	1.59	-----	-----	-----	-----	1.60
Molecular Weight, g/mol	626	-----	-----	-----	-----	603
Ni, ppm	89	-----	-----	-----	-----	88
V, ppm	2	-----	-----	-----	-----	4
As, ppm	2	-----	-----	-----	-----	2

Table 8 (cont.)
Physical and Chemical Properties for the Whiterocks
Bitumen form the Composite Core Samples

Whiterocks Tar Sand Deposit Core Number 2

Interval Number	13	14	15	16	17	18
Depth Range, ft.						
Top	196.1	206.0	216.2	225.7	235.6	245.5
Bottom	206.0	216.2	225.7	235.7	245.5	255.5
Bitumen Saturation, wt%	7.2	6.4	5.2	8.2	3.4	2.8
Specific Gravity (60°F/60°F)	0.986	0.981	0.980	0.985	0.984	0.986
API Gravity	12.0	12.7	12.9	12.1	12.4	12.0
Net Heat of Combustion, BTU/lb$_m$	17,400	17,700	17,600	17,700	17,600	17,700
Viscosity, cps (333 K)	14,700	15,300	10,100	11,400	13,200	10,000
Conradson Carbon Residue, wt%	9.3	9.7	10.5	9.1	9.8	7.1
Ash Content, wt%	0.4	0.3	0.2	0.3	0.2	0.3
Pour Point, °F	81	81	81	75	-----	-----
Elemental Analysis						
C, wt%	-----	-----	-----	-----	85.25	-----
H, wt%	-----	-----	-----	-----	11.5	-----
N, wt%	-----	-----	-----	-----	1.22	-----
S, wt%	-----	-----	-----	-----	0.36	-----
O, wt%	-----	-----	-----	-----	1.04	-----
Atomic H/C Ratio	-----	-----	-----	-----	1.63	-----
Molecular Weight, g/mol	-----	-----	-----	-----	626	-----
Ni, ppm	-----	-----	-----	-----	87	-----
V, ppm	-----	-----	-----	-----	3	-----
As, ppm	-----	-----	-----	-----	2	-----

39

Table 8 (cont.)
Physical and Chemical Properties for the Whiterocks Bitumen form the Composite Core Samples

Whiterocks Tar Sand Deposit Core Number 2

Interval Number	19	20	21	22	23	24
Depth Range, ft.						
Top	255.5	265.4	275.1	284.6	294.4	304.1
Bottom	265.4	275.1	284.6	294.4	304.1	313.7
Bitumen Saturation, wt%	3.9	2.6	3.5	3.2	6.6	4.7
Specific Gravity (60°F/60°F)	0.985	-----	0.980	0.990	0.984	0.985
API Gravity	12.1	-----	12.9	11.5	12.3	12.2
Net Heat of Combustion, BTU/lb/■	17,300	17,500	17,500	17,600	17,600	17,600
Viscosity, cps (333 K)	13,000	8,550	12,100	10,400	12,500	17,400
Conradson Carbon Residue, wt%	10.0	9.4	10.6	10.1	9.1	9.5
Ash Content, wt%	0.3	0.4	0.2	0.3	0.3	0.2
Pour Point, °F	81	-----	75	75	75	75
Elemental Analysis						
C, wt%	-----	-----	-----	-----	86.37	-----
H, wt%	-----	-----	-----	-----	11.06	-----
N, wt%	-----	-----	-----	-----	1.41	-----
S, wt%	-----	-----	-----	-----	0.37	-----
O, wt%	-----	-----	-----	-----	0.87	-----
Atomic H/C Ratio	-----	-----	-----	-----	1.54	-----
Molecular Weight, g/mol	-----	-----	-----	-----	612	-----
Ni, ppm	-----	-----	-----	-----	89	-----
V, ppm	-----	-----	-----	-----	2	-----
As, ppm	-----	-----	-----	-----	2	-----

40

Table 8 (cont.)
Physical and Chemical Properties for the Whiterocks Bitumen form the Composite Core Samples

Whiterocks Tar Sand Deposit Core Number 2

Interval Number	25	26	27	28	29	30
Depth Range, ft.						
Top	313.7	323.5	333.7	343.2	352.7	363.2
Bottom	323.5	333.4	343.2	352.7	362.2	371.8
Bitumen Saturation, wt%	2.9	3.7	3.0	5.7	3.6	4.5
Specific Gravity (60°F/60°F)	0.978	0.979	0.979	0.983	0.981	0.976
API Gravity	13.2	13.0	13.0	12.5	12.7	13.4
Net Heat of Combustion, BTU/lb	17,700	17,600	17,600	17,500	17,500	17,600
Viscosity, cps (333 K)	8,360	9,440	8,680	11,500	9,580	9,560
Conradson Carbon Residue, wt%	9.1	8.1	9.6	9.4	9.5	9.0
Ash Content, wt%	0.2	0.3	0.1	0.3	0.2	0.3
Pour Point, °F	75	75	-----	-----	-----	67
Elemental Analysis						
C, wt%	-----	-----	-----	-----	-----	85.86
H, wt%	-----	-----	-----	-----	-----	10.29
N, wt%	-----	-----	-----	-----	-----	1.30
S, wt%	-----	-----	-----	-----	-----	0.40
O, wt%	-----	-----	-----	-----	-----	0.84
Atomic H/C Ratio	-----	-----	-----	-----	-----	1.44
Molecular Weight, g/mol	-----	-----	-----	-----	-----	570
Ni, ppm	-----	-----	-----	-----	-----	91
V, ppm	-----	-----	-----	-----	-----	3
As, ppm	-----	-----	-----	-----	-----	2

Table 8 (cont.)
Physical and Chemical Properties for the Whiterocks
Bitumen form the Composite Core Samples

Whiterocks Tar Sand Deposit Core Number 2

Interval Number	31	32	33	34	35	36
Depth Range, ft.						
Top	371.8	381.6	391.2	400.8	410.2	420.0
Bottom	381.6	391.2	400.8	410.2	420.0	425.0
Bitumen Saturation, wt%	3.2	5.4	3.4	2.8	4.1	3.6
Specific Gravity (60°F/60°F)	0.986	0.988	0.982	0.9979	0.982	0.983
API Gravity	12.1	11.7	12.6	13.0	12.6	12.5
Net Heat of Combustion, BTU/lb	17,600	17,600	17,700	17,600	17,500	17,600
Viscosity, cps (333 K)	12,200	14,500	7,030	9,090	10,400	10,600
Conradson Carbon Residue, wt%	9.1	11.1	9.4	8.8	9.8	8.1
Ash Content, wt%	0.2	0.2	0.3	0.2	0.2	0.2
Pour Point, °F	-----	-----	-----	-----	-----	-----
Elemental Analysis						
C, wt%	-----	-----	-----	-----	85.65	-----
H, wt%	-----	-----	-----	-----	11.40	-----
N, wt%	-----	-----	-----	-----	1.30	-----
S, wt%	-----	-----	-----	-----	0.43	-----
O, wt%	-----	-----	-----	-----	0.78	-----
Atomic H/C Ratio	-----	-----	-----	-----	1.60	-----
Molecular Weight, g/mol	-----	-----	-----	-----	575	-----
Ni, ppm	-----	-----	-----	-----	88	-----
V, ppm	-----	-----	-----	-----	2	-----
As, ppm	-----	-----	-----	-----	2	-----

Table 9
Distillation Analyses for the Whiterocks Bitumen from the Composite Core Samples

Whiterocks Tar Sand Deposit Core Number 2

Interval Number	1	2	3	4	5	6
Depth Range, ft.						
Top	80.0	90.0	100.0	110.0	119.8	129.6
Bottom	90.0	100.0	110.0	119.8	129.6	139.0
Boiling Point Distribution:						
Volatility (<1000°F), wt%	-----	-----	-----	-----	-----	49.6
IBP - 400°F, wt%	-----	-----	-----	-----	-----	0.3
400 - 650°F, wt%	-----	-----	-----	-----	-----	8.2
650 - 1000°F, wt%	-----	-----	-----	-----	-----	41.1
>1000°F Residue, wt%	-----	-----	-----	-----	-----	50.4
Simulated Distillation:						
IBP, °F	-----	-----	-----	-----	-----	367
5 wt%, °F	-----	-----	-----	-----	-----	583
10 wt%, °F	-----	-----	-----	-----	-----	673
15 wt%, °F	-----	-----	-----	-----	-----	745
20 wt%, °F	-----	-----	-----	-----	-----	806
25 wt%, °F	-----	-----	-----	-----	-----	855
30 wt%, °F	-----	-----	-----	-----	-----	885
40 wt%, °F	-----	-----	-----	-----	-----	943
50 wt%, °F	-----	-----	-----	-----	-----	---
60 wt%, °F	-----	-----	-----	-----	-----	---
Asphaltenes, wt%	-----	-----	-----	-----	-----	3.28
Maltenes, wt%	-----	-----	-----	-----	-----	96.72

43

Table 9 (cont.)
Distillation Analyses for the Whiterocks Bitumen
from the Composite Core Samples

Whiterocks Tar Sand Deposit Core Number 2

Interval Number	7	8	9	10	11	12
Depth Range, ft.						
Top	139.0	148.7	158.3	167.9	177.1	186.7
Bottom	148.7	158.3	167.9	177.1	186.7	196.1
Boiling Point Distribution:						
Volatility (<1000°F), wt%	49.8	48.4	53.7	51.8	49.4	58.2
IBP - 400°F, wt%	0.0	0.0	0.0	0.4	0.0	0.2
400 - 650°F, wt%	8.4	8.2	9.5	9.8	8.6	10.7
650 - 1000°F, wt%	41.4	40.2	44.2	41.6	40.8	47.3
>1000°F Residue, wt%	50.2	51.6	46.3	48.2	50.6	41.8
Simulated Distillation:						
IBP, °F	459	453	453	408	446	421
5 wt%, °F	590	590	574	549	581	545
10 wt%, °F	676	680	658	648	675	639
15 wt%, °F	745	759	727	721	756	703
20 wt%, °F	806	820	788	815	810	761
25 wt%, °F	849	858	838	842	853	815
30 wt%, °F	880	887	874	876	882	853
40 wt%, °F	930	952	921	930	939	903
50 wt%, °F	---	---	975	982	---	955
60 wt%, °F	---	---	---	---	---	---
Asphaltenes, wt%	3.28	2.25	3.47	2.90	2.62	3.74
Maltenes, wt%	96.62	97.75	96.53	97.10	97.38	96.26

Table 9 (cont.)
Distillation Analyses for the Whiterocks Bitumen
from the Composite Core Samples

Whiterocks Tar Sand Deposit Core Number 2

Interval Number	13	14	15	16	17	18
Depth Range, ft.						
Top	196.1	206.0	216.2	225.7	235.6	245.5
Bottom	206.0	216.2	225.7	235.6	245.5	255.5
Boiling Point Distribution:						
Volatility (<1000°F), wt%	49.8	49.7	51.2	55.6	49.3	45.7
IBP - 400°F, wt%	0.0	0.0	0.0	0.0	0.0	0.0
400 - 650°F, wt%	8.5	7.5	7.7	8.9	6.9	7.2
650 - 1000°F, wt%	41.3	42.2	43.5	46.7	42.4	38.5
>1000°F Residue, wt%	50.2	50.3	48.8	44.4	50.7	54.3
Simulated Distillation:						
IBP, °F	459	459	446	451	462	477
5 wt%, °F	585	603	597	579	601	610
10 wt%, °F	675	691	687	664	687	698
15 wt%, °F	745	763	777	729	757	775
20 wt%, °F	808	826	822	784	815	838
25 wt%, °F	856	864	858	835	858	871
30 wt%, °F	883	891	882	867	883	900
40 wt%, °F	939	945	935	912	936	963
50 wt%, °F	---	---	993	964	---	---
60 wt%, °F	---	---	---	---	---	---
Asphaltenes, wt%	1.89	3.14	3.01	3.02	3.57	2.21
Maltenes, wt%	98.11	96.86	96.99	96.98	96.43	97.79

Table 9 (cont.)
Distillation Analyses for the Whiterocks Bitumen
from the Composite Core Samples

Whiterocks Tar Sand Deposit Core Number 2

Interval Number	19	20	21	22	23	24
Depth Range, ft.						
Top	255.5	265.4	275.1	284.6	294.4	304.1
Bottom	265.4	275.1	284.6	294.4	304.1	313.7
Boiling Point Distribution:						
Volatility (<1000°F), wt%	52.4	62.0	47.6	48.5	46.0	44.8
IBP - 400°F, wt%	0.0	0.0	0.0	0.0	0.0	0.0
400 - 650°F, wt%	9.6	11.1	8.4	8.5	8.0	9.0
650 - 1000°F, wt%	42.8	50.9	39.2	40.0	38.0	35.8
>1000°F Residue, wt%	47.6	38.0	52.4	51.5	54.0	55.2
Simulated Distillation:						
IBP, °F	468	442	457	441	451	469
5 wt%, °F	567	554	585	572	590	585
10 wt%, °F	648	637	678	669	687	669
15 wt%, °F	705	698	752	745	765	745
20 wt%, °F	761	728	820	810	829	815
25 wt%, °F	810	808	862	853	865	860
30 wt%, °F	846	847	891	880	896	892
40 wt%, °F	889	918	954	941	957	959
50 wt%, °F	930	939	---	---	---	---
60 wt%, °F	---	---	---	---	---	---
Asphaltenes, wt%	2.55	2.01	3.18	2.61	3.26	3.28
Maltenes, wt%	97.45	97.99	96.82	97.39	96.74	96.72

46

Table 9 (cont.)
Distillation Analyses for the Whiterocks Bitumen
from the Composite Core Samples

Whiterocks Tar Sand Deposit Core Number 2

Interval Number	25	26	27	28	29	30
Depth Range, ft.						
Top	313.7	323.5	333.7	343.2	352.7	362.2
Bottom	323.5	333.4	343.2	352.7	362.2	371.8
Boiling Point Distribution:						
Volatility (<1000°F), wt%	44.8	46.2	45.9	42.1	41.6	54.1
IBP - 400°F, wt%	0.0	0.0	0.0	0.0	0.0	0.0
400 - 650°F, wt%	7.6	8.3	8.0	7.5	6.8	10.3
65^ - 1000°F, wt%	37.2	37.9	37.9	34.6	34.8	42.9
>1000°F Residue, wt%	55.2	53.8	54.1	57.9	58.4	45.9
Simulated Distillation:						
IBP, °F	451	444	459	448	468	381
5 wt%, °F	588	581	590	595	613	518
10 wt%, °F	694	684	684	694	709	633
15 wt%, °F	777	761	763	779	790	712
20 wt%, °F	837	831	829	846	849	781
25 wt%, °F	871	871	869	882	882	831
30 wt%, °F	880	900	896	912	912	864
40 wt%, °F	961	964	960	986	986	921
50 wt%, °F	---	---	---	---	---	975
60 wt%, °F	---	---	---	---	---	---
Asphaltenes, wt%	----	2.18	2.35	3.22	2.64	3.68
Maltenes, wt%	----	97.82	97.65	96.78	97.36	96.32

Table 9 (cont.)
Distillation Analyses for the Whiterocks Bitumen
from the Composite Core Samples

Whiterocks Tar Sand Deposit Core Number 2

Interval Number	31	32	33	34	35	36
Depth Range, ft.						
Top	371.8	381.6	391.2	400.8	410.2	420.0
Bottom	381.6	391.2	400.8	410.2	420.2	425.0
Boiling Point Distribution:						
Volatility (<1000°F), wt%	45.2	51.9	42.0	44.6	54.6	44.1
IBP - 400°F, wt%	0.0	0.0	0.0	0.0	0.2	0.0
400 - 650°F, wt%	9.3	7.0	7.2	8.7	10.6	8.3
650 - 1000°F, wt%	35.9	44.9	34.8	35.9	43.8	35.8
>1000°F Residue, wt%	54.8	48.1	58.0	55.4	45.4	55.9
Simulated Distillation:						
IBP, °F	468	498	453	435	424	444
5 wt%, °F	581	621	601	567	541	570
10 wt%, °F	662	705	705	673	639	684
15 wt%, °F	741	779	790	763	709	763
20 wt%, °F	820	835	849	829	774	837
25 wt%, °F	867	864	885	864	856	878
30 wt%, °F	896	892	914	898	867	907
40 wt%, °F	968	946	981	904	918	972
50 wt%, °F	---	997	---	---	972	---
60 wt%, °F	---	---	---	---	---	---
Asphaltenes, wt%	2.29	3.82	2.79	2.02	2.88	2.31
Maltenes, wt%	97.71	96.18	97.21	97.98	97.12	97.69

Table 10

Average Chemical and Physical Properties for the Whiterocks Bitumen from the Core Samples

Property	Core 1	Core 2
Bitumen Saturation, wt%	5.9	4.4
Specific Gravity (60°F/60°F)	0.978	0.982
API Gravity	13.2	12.5
Net Heat of Combustion, BTU/lb$_m$	17,600	17,600
Viscosity, cps (333 K)	12,500	11,600
Conradson Carbon Residue, wt%	9.8	9.4
Ash Content, wt%	0.3	0.3
Pour Point, °F	74	76
Elemental Analysis		
C, wt%	86.1	85.7
H, wt%	11.5	11.2
N, wt%	1.3	1.7
S, wt%	0.5	0.4
O, wt%	1.0	0.9
Atomic H/C Ratio	1.60	1.57
Molecular Weight, g/mol	596	602
Ni, ppm	52	89
V, pm	1.2	2.7
As, ppm	1.4	2.0

Table 11

Average Distillation Analyses for the Whiterocks
Bitumen Samples from the Core Samples

Property	Core 1	Core 2
Boiling Point Distribution		
Volatility (<1000°F), wt%	49.4	49.0
IBP - 400°F, wt%	0.2	0.1
400 - 650°F, wt%	8.4	8.5
650 - 1000°F, wt%	40.8	40.5
>1000°F Residue, wt%	50.6	50.9
Simulated Distillation:		
IBP, °F	434	447
5 wt%, °F	573	581
10 wt%, °F	672	674
15 wt%, °F	748	750
20 wt%, °F	813	812
25 wt%, °F	857	856
30 wt%, °F	986	885
40 wt%, °F	944	943
50 wt%, °F	---	---

Summary and Conclusions

The acquisition of deep mined ore and core samples from the Whiterocks tar sand deposit have resulted in a better understanding of the nature of the deposit. Although the data base is somewhat limited at this stage it was concluded that the deposit was laterally and vertically homogenous with regard to the properties of the native bitumen. Confirmation of this conclusion will require opening of a working pit on the eastern flank out-crop of the deposit and the drilling of at least eight more core holes.

The physical and chemical properties of the native bitumen samples were consistent with those previously reported for the Whiterocks bitumen. In particular, the low asphaltene content was confirmed. This observation led to the conclusion that it may be possible to hydrotreat the native Whiterocks bitumen without prior rejection of the asphaltic material thus giving a higher yield of desirable products.

Future Activities

The native Whiterocks bitumen will be separated into several boiling-range fractions for detailed analysis and characterization. The low boiling fraction (400-650°F) will be evaluated for use as a transportation fuel and the residual fraction (>650°F) will be evaluated for use as a road asphalt. In addition to the asphalt specification tests, several spectroscopic techniques will be used to provide detailed characterization data. The analyses to be performed will include combined gas chromatography - mass

spectrometry (GC-MS); Fourier transform infra-red spectroscopy (FTIR); Curie Point pyrolysis mass spectrometry (PY-MS); and Carbon-13 and proton nuclear magnetic resonance. These tests will provide a necessary data base upon which to evaluate a variety of bitumen recovery-upgrading schemes specific to the Whiterocks tar sand deposit.

Acquisition of well defined and precisely located deep mined ore samples from the north, south and central regions of the Asphalt Ridge tar sand deposit for use in recovery, upgrading and characterization studies will be conducted.

Water Based Tar Sand Separation Technology

Principal Investigator: J.D. Miller
Co-Principal Investigator: J. Hupka
Post Doctoral Fellow: K. Bukka
Graduate Students: J. Derlic
                                      Y. Yang

INTRODUCTION

During the year ending June 1990 the research and development program on water-based separation technology included several areas: surface chemistry, process engineering studies, bitumen concentrate clean-up, and characterization of selected tar sands. This section of the report is organized into distinct subsections in which each of the major research activities of the past year are presented and discussed. Four sections are devoted to the characterization of the native bitumens, the mineral matter associated with tar sands and the tar sands themself, whereas two sections are devoted to recovery process technology.

The Whiterocks tar sand bitumen and mineral matter have been characterized. Tar sand samples from three locations in the deposit were collected and analyzed. The bitumen was separated from the sand by toluene extraction and was fractionated into seven different fractions. It was found that the bitumen had a very low asphaltene content regardless of sample location. In order to examine whether a selective distribution of the solids takes place during the flotation step of the modified hot water separation process, a comprehensive analysis was made of the solids which reported to the bitumen froth. A combination of Fourier transform infrared spectroscopy (FTIR), x-ray diffraction (XRD), x-ray

53

fluorescence (XRF), inductively coupled plasma (ICP) and wet chemical analytical techniques were employed.

Data on the electrophoretic mobility of bitumen and fine mineral particles from the Asphalt Ridge and Sunnyside tar sands have been obtained. Negative surface charges were observed for all particles and droplets of bitumen studied for both tar sands. The zeta potentials evaluated from electrophoretic mobilities varied from -65 to -10 mV for bitumen droplets and from -55 to -25 mV for mineral particles depending on the pH of the suspension. These findings suggested that gravity separation might be used to recover a significant portion of the bitumen, since charge minimization is required for an efficient flotation separation process.

An estimate of bitumen viscosity is required before an appropriate processing strategy can be developed for a particular tar sand deposit. A solvent extraction procedure is usually used to separate the bitumen from the tar sand for viscosity measurements or to predict viscosity based on bitumen chemical composition and other properties. Typically toluene is used as the solvent and the effect of residual toluene on bitumen viscosity is frequently questioned. In this regard the intrinsic viscosity of the bitumen is difficult to estimate due to the presence of residual toluene and the loss of light ends during the removal of the solvent in a rotary vacuum evaporator. A correlation between bitumen viscosity and the residual toluene content has been developed. The viscosity decreased by a factor of 2.5 at 30°C and 1.7 at 90°C for a bitumen which contained two weight percent residual toluene with

respect to a bitumen sample from which practically all the toluene (<0.07 wt.% remaining) had been removed.

The investigation of the impact of tar sand slurry viscosity in the digestion step of the modified hot water process has been initiated. Several empirical formulae, reported in the literature, were used to predict the slurry viscosity. Hot water separation experiments were carried out to recover bitumen from Utah tar sands. The slurry viscosity was varied by changing the composition of the pulp from 50 to 80 wt.% solids. The separation efficiency increased with an increase in percent solids and attained a maximum above 70 wt.% solids. The bitumen recovery and concentrate grade from the gravity cell were significantly influenced by the slurry viscosity, while the flotation kinetics remained almost unchanged. The slurry viscosity strongly influences the shear force field available in the conditioning vessel (which may be a stirred tank, rotating drum, or a pipeline reactor). Calculated slurry viscosities have been shown to influence the efficiency of bitumen gravity separation and flotation.

A significant effort has been devoted to the continued development of the moderate temperature separation process for the recovery of bitumen in an economically viable and environmentally acceptable manner. The development of an energy-efficient, water-based process for bitumen recovery from domestic tar sands has been under active study at the University of Utah for over a decade. The great diversity of the various United States tar sand deposits has been a significant variable in the evolution of process technology.

The Canadian hot water separation technique was found to yield unsatisfactory results when used for the U.S. tar sands. A new approach has been developed, taking into consideration diluent addition, a better understanding of digestion chemistry, improved bitumen separation techniques, and a tolerance for fine solids in the recycled water stream (which provides the possibility of a significant reduction in the size of the tailings ponds).

Finally, the results of a study on the separation of a water-in-solvent emulsion in a continuous flow electrostatic coalesce are reported. The study was carried out to develop a better understanding of the potential for bitumen concentrate clean-up in an electric field. Emulsions containing from 9.08% to 0.2% dispersed water with droplet diameters below 20 μm have been separated at an efficiency exceeding 80% for a residence time of 25 seconds. A rapid improvement in the process efficiency was obtained when the field strength was increased to 140 kV/m. When the field strength was increased further from 140 kV/m to 1100 kV/m only a 15% increase in efficiency was realized. The DC electric field pulsation frequency exerted a minor effect on the demulsification yield in the range studied (4 Hz to 25 Hz); nevertheless, a separation optimum was observed for pulsation frequencies between 8 and 11 Hz.

CHARACTERIZATION OF WHITEROCKS TAR SAND BITUMEN AND MINERAL MATTER

Characterization of Whiterocks Tar Sand Bitumen

Bitumen Extraction by the Dean-Stark Method

The composite Whiterocks tar sand sample from each location; West North, West Central and West South was subjected to Dean-Stark toluene extraction for the separation of the bitumen. Multiple extractions were carried out in a 3-liter flask using approximately one kilogram of crushed tar sand ore each time. The toluene was removed from the combined extracts by distillation using a Büchi rotoevaporator. The residual toluene in the bitumen was determined by gas chromatography and toluene removal was monitored such that the bitumen contained no more than 0.1 weight percent toluene. The residual solids from the extraction were saved for size and mineralogical analysis.

Fractionation of the Whiterocks Bitumens

The bitumens extracted from the composite samples from each of the three locations on the Whiterocks tar sand deposit were fractionated and the individual fractions were characterized. The fractionation scheme adopted for these bitumens is outlined in Figure 2. The procedure consisted of the following steps. The bitumen sample was weighed in a tared Erlenmeyer flask (250 ml.) and toluene was added (one milliliter of toluene per gram of bitumen) to the flask. The solution was heated on a water bath to obtain a homogeneous suspension. The suspension was cooled and
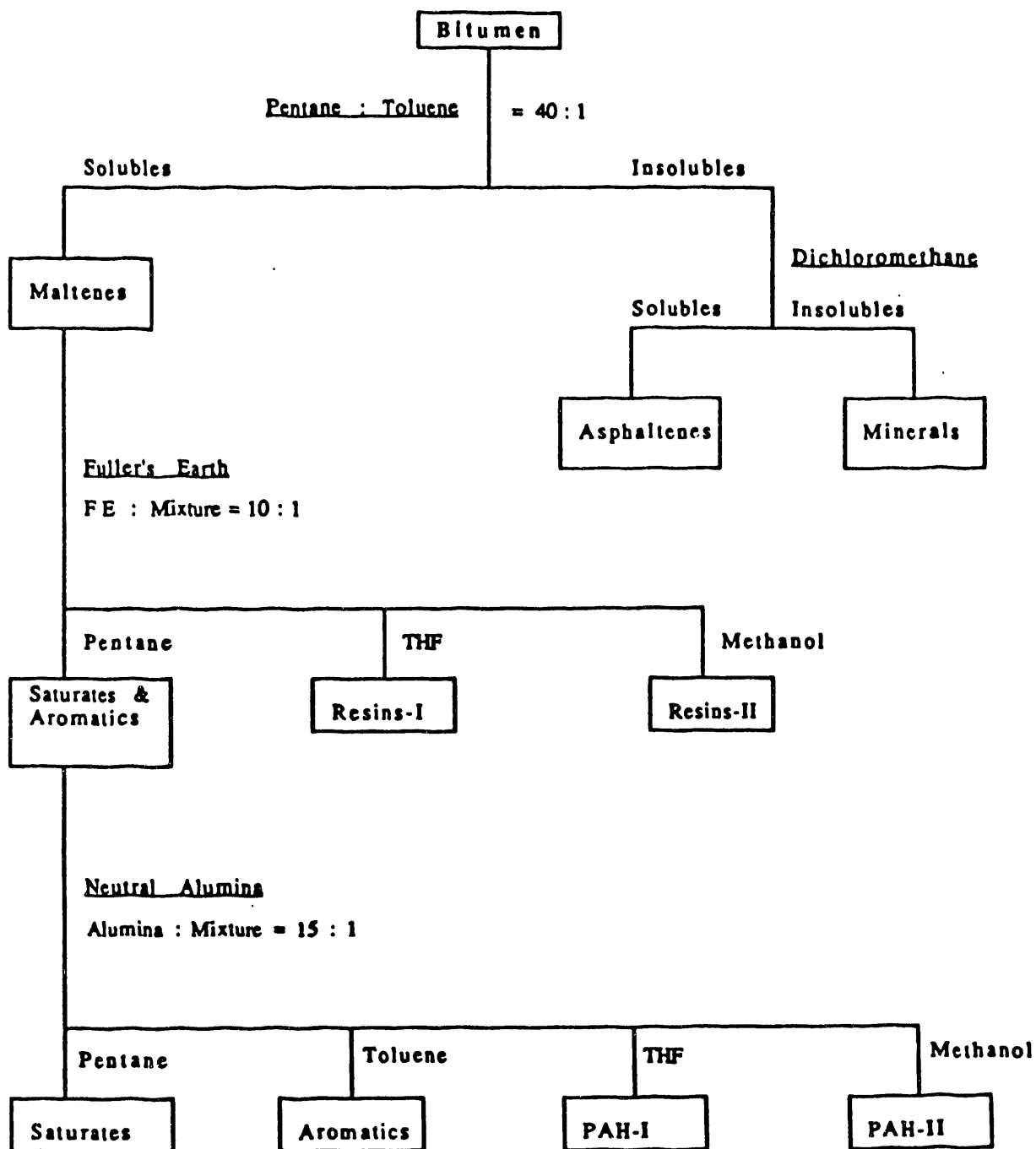
Figure 2.   Bitumen Fractionation Scheme

pentane was added gradually (40 times the volume of toluene) with constant stirring. The resulting mixture was thoroughly shaken and stored in the dark for 16-20 hours. The insoluble solids (asphaltenes) were separated from the solution containing the soluble maltenes by filtration using a fine sintered glass funnel. The solids were washed repeatedly with pentane until the filtrate was colorless. The solids were then dried in an oven at 110°C for two hours and weighed. Since the asphaltene fraction was separated by virtue of its insolubility in pentane, and considering the possibility that mineral fines may have been accumulated in the bitumen, a separation of the fines and asphaltenes was effected by dissolution of the asphaltenes in dichloromethane followed by filtration to remove the fines. The asphaltene fraction was finally isolated from the dichloromethane solution by distillation in a rotoevaporator. The maltene fraction was also recovered by the evaporation of the pentane from the solution.

The maltenes fraction was subsequently separated into saturates and aromatics, and resins. This separation was carried out in a Soxhlet extraction unit. Fuller's Earth was placed in a glass fritted thimble (the ratio of maltenes to Fuller's Earth was 1:10) and washed with pentane prior to use. The maltenes were then loaded onto the Fuller's Earth and the thimble was transferred to the Soxhlet unit. The fractionation of the maltenes was carried out with a sequence of solvents of increasing polarity. The solvents used were (in order of increasing polarity) pentane, tetrahydrofuran and methanol. Extraction with each solvent was

59

carried out for a minimum of 24 hours. The extracts thus collected were labeled as a mixture of saturates and aromatics, resin-I and resin-II respectively. In each case the solvent was removed by rotoevaporation.

In the final step, the mixture of saturates and aromatics was further separated into saturates and aromatics by column chromatography. Neutral alumina, dried at 110°C for 24 hours, was used as the support material. A 15:1 ratio of alumina to saturates/aromatics mixture was used. The saturates and aromatics mixture was dissolved in pentane and the solution was loaded onto the column. The column was eluted in sequence with pentane, toluene, tetra-hydrofuran, and methanol. The extracted solutions were labeled as saturates, aromatics, PAH-I and PAH-II after evaporation of the solvent. The fractions PAH-I and PAH-II were presumed to represent polynuclear aromatic hydrocarbons although they also contain functional groups involving oxygen, nitrogen, and sulfur. After the removal of the solvent on the rotoevaporator, all fractions were placed in a vacuum (1-10 mm Hg) oven at 60°C for 16 hours to remove residual traces of solvent.

Comparison of the Whiterocks Bitumen with the Bitumens from the Asphalt Ridge and Sunnyside Deposits

The compound type analyses of the three Whiterocks bitumens are presented in Table 12. The Whiterocks bitumen from all three locations exhibited similar compositions. The salient feature of the Whiterocks bitumen is the remarkably low asphaltene content.

Table 12. Compound-Type Analyses of the Whiterocks Bitumen Extracted from Mined Ore.

Compound-Type Analysis

Weight, Percent[1]

Bitumen Fraction	West North	West Central	West South	Average[2]
Saturates	29.5	30.2	29.2	29.6
Aromatics	14.5	14.6	12.6	13.9
PAH-I[3]	5.2	6.8	2.8	4.9
PAH-II[3]	2.5	3.4	1.4	2.4
Resins-I[4]	40.8	38.8	42.0	40.5
Resins-II[4]	1.6	1.3	1.1	1.3
Asphaltenes	3.3	3.6	4.1	3.7

1. Mass balances obtained in the fractionation scheme for West North, West Central and West South Whiterocks tar sand bitumens were 97.4%, 98.8% and 93.2%, respectively.

2. Average of the compound-type analyses for West Central, West South and West North bitumens.

3. PAH-I and PAH-II are polyaromatic hydrocarbons with no or very low heteroatom contents. These two fractions differ in their polarities, PAH-II being more polar.

4. Resins-I and Resin-II are also distinguised by their polarities. Resin-II is relatively more polar than Resins-I.

61

Bitumens with low asphaltene content are considered to be of superior quality, as they are relatively easy to integrate into existing hydrogen refinery process schemes. The compound type analyses of the Whiterocks, Asphalt Ridge and Sunnyside bitumen are compared in Table 13. The composition of the Whiterocks bitumen appears to be more like that of the Asphalt Ridge bitumen than that of the Sunnyside bitumen. Comparatively, the Whiterocks bitumen contains less saturates and asphaltenes, but slightly more of resins than the Asphalt Ridge bitumen.

CHARACTERIZATION OF THE MINERAL MATTER FROM THE WHITEROCKS TAR SAND

Size Fractionation of the Feed Solids

The solids obtained from the tar sand after bitumen extraction with toluene were size fractionated and analyzed for mineralogical composition. The size fractionation into seven different size fractions was carried out using a wet sieve analysis. Size analyses of the solids from the three locations are listed in the Table 14. The results indicate that among the coarse particles no discernible trend can be observed. Among the medium to fine size particles viz., 106-38μ, there is a gradual increase in the fines content of the tar sand moving from North to South across the pit. This is perhaps indicative of the topology of the locations. It is observed that the West Central sample contained a higher proportion of the finest fraction (<38μ) of the solids.

Table 13. Compound Type Analyses for the Whiterocks, Asphalt Ridge and Sunnyside Bitumen

Compound Type Fraction	WEIGHT PERCENT[1]			
	WHITEROCKS[2]		ASPHALT RIDGE	SUNNYSIDE
Saturates	29.6	29.6	32.4	24.9
Aromatics	13.9	21.2	22.4	18.1
PAH-I[3]	4.9			
PAH-II[3]	2.4			0.5
Resins-I[4]	40.5	40.5	37.6	30.0
Resins-I[4]	1.3	1.3		0.6
Asphaltenes	3.7	3.7	7.3	23.7

1. Mass balances obtained in the fractionation of Asphalt Ridge and Sunnyside bitumens were 99.7%, and 97.8%, respectively.

2. Average of the compound type analyses for the West Central, West South and West North bitumens.

3. PAH-I and PAH-II are polyaromatic hydrocarbons with no or very low heteroatom contents. These two fractions differ in their polarities, PAH-II being more polar.

4. Resins-I and Resins-II are also distinguished by their polarities. Resin-II is relatively more polar then Resin-I.

63

Table 14. Particle Size Distribution of Solids Obtained
          from Whiterocks Tar Sands.

| | | Weight Percent[1] | | |
Mesh Number	Particle Size, μ	West North	West Central	West South
+ 65	>149	25.9	53.1	11.4
- 65 + 150	149-106	56.9	24.6	60.2
- 150 + 200	106-75	5.4	7.2	11.9
- 200 + 270	75-53	2.7	4.0	5.6
- 270 + 325	53-45	1.3	1.7	2.7
- 325 + 400	45-38	1.4	1.4	2.3
- 400	<38	6.4	8.0	5.9

[1] Solids were separated from the bitumen by Dean Stark extraction with toluene.

Mineralogical Analysis of Feed Solids

Mineralogical analysis was conducted on the feed solids for the West Central ore. The composite feed solids were ground in a micro pulverizer (Fritsch, Puverisette) for 10-15 minutes and the resulting ground material was wet sieved using a VECO (Eerbeek, Holland) precision sieve #254 (circular opening of 45μ). The oversize solids were dried in the oven at 110°C and ground further. These steps were repeated until >95% of the feed solids passed through the sieve. The accumulated slurry containing the undersize particles (<45μm) was centrifuged at 5,000 rpm and the residue was dried in the oven at 110°C.

Finely ground feed solids (<45μ) from the West Central location were analyzed by X-ray diffraction for mineralogical composition. The various minerals present were identified from their characteristic inter-atomic distances. The XRD profile of the sample was compared to that of a pure quartz, and a quantitative estimate of the concentrations of mineral present relative to the quartz in the feed solids was made. The mineralogical composition obtained in this manner is outlined in the Table 15. The mineral matter consisted mainly of quartz (86 wt%) with small amounts of carbonate minerals and clays such as calcite and dolomite and kaolinite and illite/smectites, respectively. As the amount of the 2:1 clays present in the solids was small, it could not be confirmed from the XRD analysis alone whether they were illites, smectites or a mixed layer consisting of these two clays. However, the absence of the swelling clays (smectites) in the feed solids was confirmed by an ethylene glycol expansion test.

Table 15. Mineralogical Analysis of the Solids[1] Derived from Whiterocks Tar Sand as Determined by X-ray diffraction method.

Mineral	Weight Percent
Quartz	86
K-Feldspar	4
Calcite	4
Kaolinite	3
Dolomite	1
Plagioclase	1
Illite & Illite with interlayered smectite	1

[1]Solids from Composite West Central Sample

Determination of the Nature of Clays

The swelling clays such as montmorillonites tend to expand in the presence of certain polar organic molecules, which include amines, alcohols and diols. These organic molecules, upon adsorption, take positions on the interlayer surfaces and prop up the layers. Since layer surfaces of the clays are charged, these adsorbed molecules are firmly anchored to the surface by the electrostatic interactions. These expanded clays show large interlamellar distances, which are recognized from their XRD profiles. The polarorganic used in this study was ethylene glycol.

The solids (<38μ) from the West Central sample (16 g) were suspended in water to which five milliliter of a 5% Calgonite solution was added and thoroughly mixed in a blender. The resulting slurry was centrifuged (Sorvall GLC-1) in two stages to isolate the particles in the size range 0.4-2.0 μm. A thick paste containing solids of 0.4-2.0 μm in size was applied to a glass slide and allowed to dry in the air. Once the paste on the glass

slide had dried, it was analyzed by XRD. After the XRD analysis the slide was placed in an aluminum desiccator containing a small amount of ethylene glycol and transferred to an over at 50°C. After 24 hours the slide was removed from the desiccator and wiped clean of the ethylene glycol and XRD analysis of the ethylene glycol expanded sample was made. This test indicated that there was no detectable montmorillonite in the fines from the West Central sample. Most of the fine fraction consisted of kaolinite and illite interlayered with smectite. The latter mixture was not considered to be a swelling clay, which would indicate that after hot water processing of the tar sands, water recycling from the tailings streams would be expected to be relatively easy.

Effect of Hot Water Processing on the Mineral Matter Distribution

In the hot water separation of bitumen from tar sands, the product from both gravity separation and flotation invariably contains a significant proportion of solids. The solids content of the bitumen from the gravity separation cell is considerably lower than that of the flotation product. A typical size distribution of the solids from the flotation concentrate is presented in the Table 16. As expected the proportion of the fines content, particularly solids of size <38μ, is greatly increased.

Table 16. Particle Size Distribution of the Solids Reporting to the Bitumen Concentrate during Flotation of the Composite West Central Sample.

Mesh Number	Particle Size (microns)	Weight Percent
+ 65	>149	35.5
- 65 + 150	106-149	14.0
- 150 + 200	75-106	11.2
- 200 + 270	53-75	7.9
- 270 + 325	45-53	1.1
- 325 + 400	38-45	2.9
- 400	<38	27.5

Studies were conducted to examine whether minerals present in the tar sand feed undergo selective distribution during the separation of the bitumen in the hot water process. Composite solids from the feed, bitumen concentrates (froth), and tailings of the West Central sample were examined. All these solids were extracted with toluene to remove the bitumen and ground to $<45\mu$ so that more than 95% of the sample material passed through VECO sieve number 254.

Characterization of the Solids
from Different Processing Streams

The finely ground samples were analyzed by FTIR and X-ray fluorescence. The FTIR analysis was conducted by in the diffuse reflectance mode, which involved no sample preparation. Spectra obtained for the solids from the feed, concentrate and tailings are presented in Figures 3 to 5. In spite of the complexity of the
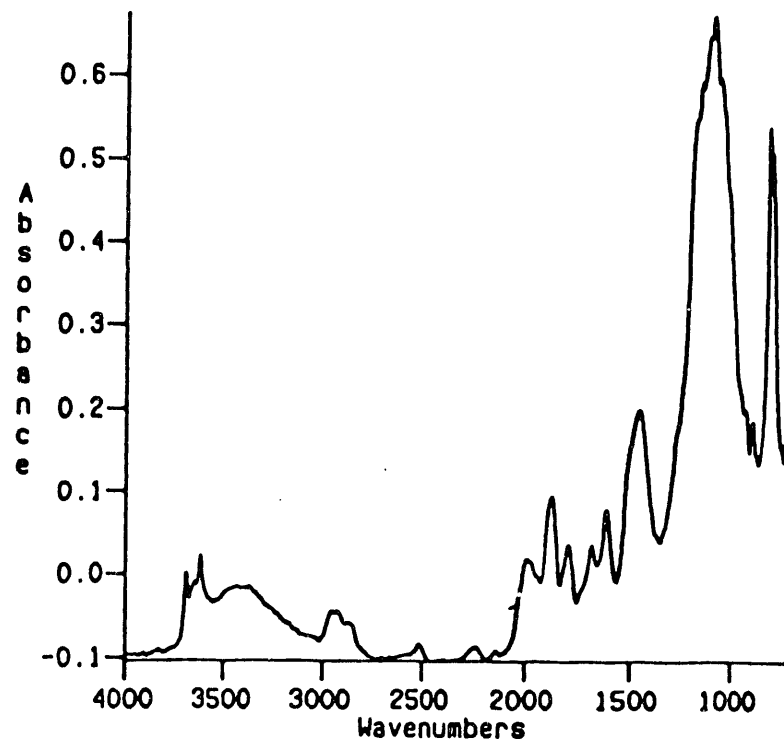
Figure 3. Fourier Transform Infrared Spectrum of Whiterocks Tar Sand Feed Solids ($\leq$ 45μ)
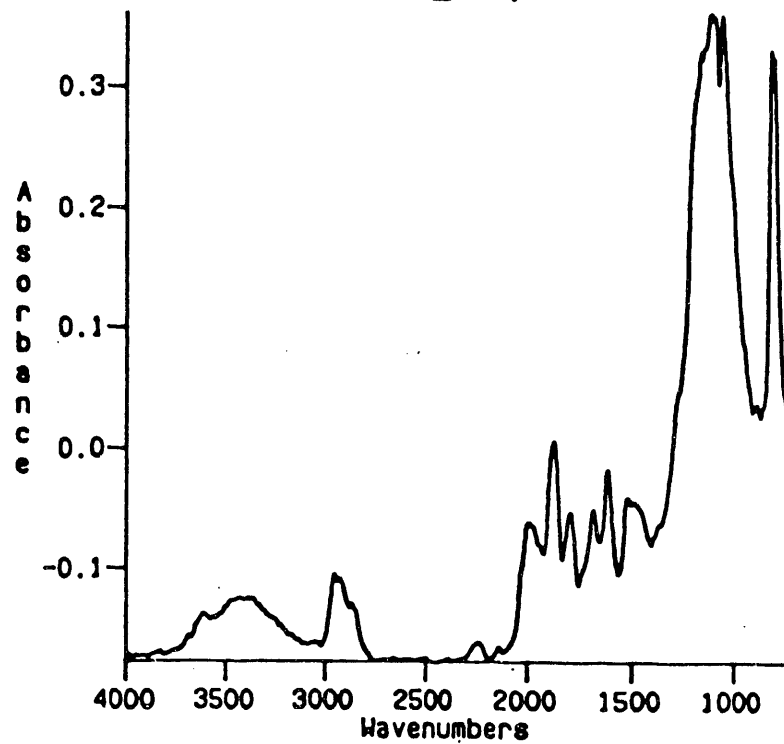
Figure 4. Fourier Transform Infrared Spectrum of the West Central Tailings solids ($\leq$ 45μ)
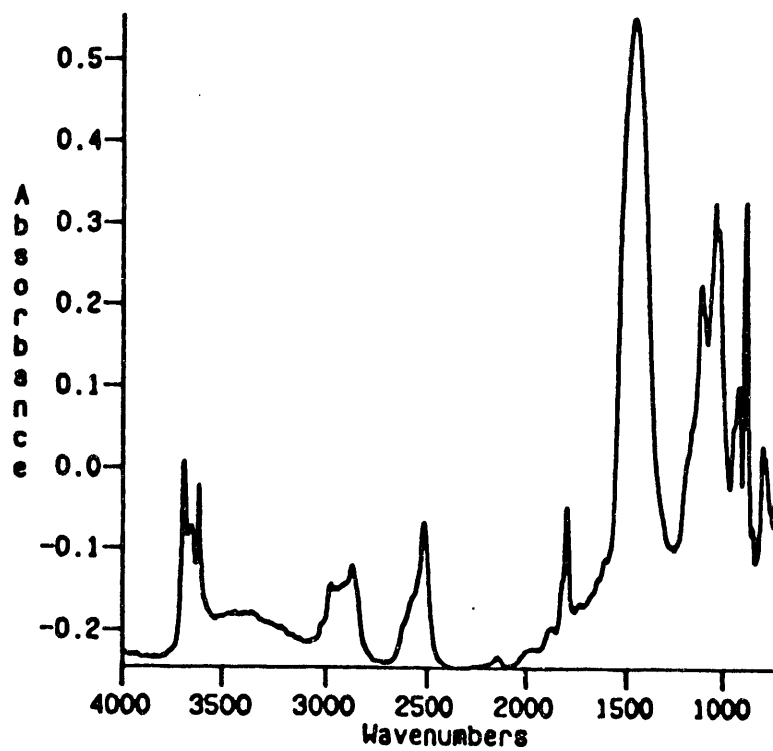
Figure 5. Fourier Transform Infrared Spectrum of the West
Central Solids which Reported to the Bitumen
concentrate ($\leq 45\mu$)

70

spectral features of the constituent minerals, a comparison of the three spectra reveals several important differences. Among the minerals that can be identified are kaolinite, carbonates and quartz. In a qualitative sense the spectra of feed and tailing solids look very similar. Only the spectrum of the concentrates appears distinctly different from the other two, in terms of the nature and intensities of the absorption bands. Further, all samples have noticeable amounts of adsorbed organic material, as characterized by the C-H stretching bands in the region 3020-2825 cm^{-1}. It is known that some organic compounds, particularly those that are highly polar in nature, are bound strongly to the minerals and are difficult to dislodge. These compounds have been referred to as humic acids or humus in general. It is clear that these adsorbed organic species are found predominantly on the solids in the concentrates and least on the solids in the tailings. This may indicate that the adsorption is confined to the fine particles, as their proportion is high in concentrates and lowest in the tailings. Some absorption features also indicate the differences in the nature of the organic material adsorbed on these solids. Details of these differences will be discussed later.

One group of bands observed (which are very distinct in concentrate and feed solids) in the region 3700-3618 cm^{-1} are due to structural hydroxyl present in kaolinite. A comparison of the spectra shows that kaolinite were selectively accumulated in the solids which reported to the bitumen concentrate. This observation may be seen as a corroboration to the finding that in the size analysis of the concentrate solids the fines were shown to increase

71

nearly four-fold (compared to feed solids). Perhaps the most striking difference among the spectra is the presence of an intense band at 2517 cm^{-1} in the spectrum for the concentrate solids. This band is assumed to arise from the carbonate minerals, particularly calcite, dolomite, and siderite. The most intense band for these minerals is observed in the region 1400-1600 cm^{-1}. Although the spectra of the feed solids shows a broad band in the 1456 cm^{-1} region, the tailings and concentrate solids show little evidence of a band in the 1400-1600 cm^{-1} region. This observation seems to be in conflict with the inferences based on the band recorded at 2530 cm^{-1}. This apparent anomaly was resolved by the analysis of the concentrate solids after acid treatment, which would selectively react with the carbonate minerals. In addition there were several other differences in the spectral features of the concentrates, some of which arise from quartz. The others at present remain unresolved.

These solids were also analyzed by X-ray fluorescence to reveal differences in elemental composition. These measurements were made on a mixture containing the sample and cellulose powder (20%, Whatman CF11), which was pressed into a disk under 40,000 psi. Estimation of the concentrations of the measured elements was made using known standard samples. The results are outlined in Table 17. The results presented indicate that there is a considerable enrichment of the minerals containing the elements Ti, Zr, Fe and Mn in the bitumen concentrates.

Table 17. X-ray Fluorescence Analyses of the Solids from
Feed, Concentrates and Tailings

	Iron (as Fe_2O_3) (wt%)	Titanium (as TiO_2) (wt %)	Zirconium (ppm)	Manganese (ppm)
Feed	0.38	0.08	73	124
Concentrate	0.72	0.54	747	1335
Tailing	0.25	0.04	29	37

Acid Treatment of the Solids from Feed
Concentrates and Tailings

In order to verify the carbonate mineral accumulation in the
concentrate solids, the feed, concentrate and tailings solids were
treated with excess hydrochloric acid. The neutralization
reactions were allowed to proceed for 16-24 hours at room
temperature, and the residue was separated by filtration using a
fine pore Whatman #42 filter paper. The filtrate was saved and
analyzed for dissolved ions by ICP.

The ICP method of analysis does not distinguish between
dissolved metal atoms and their ions. However, the detected metals
were presumed to be dissolved ions. The contribution from
dissolved metal atoms, if any, is expected to be very small. The
analyzed solutions were transparent and were filtered through a
0.45 micron filter. The residue was repeatedly washed with
deionized water till the washing were free from chloride ions, and
dried in the oven at 110°C for four hours. Weight loss observed in

each case was recorded and the samples were analyzed by FTIR and X-ray diffraction.

The weight loss of the three samples from acid treatment is presented in the Table 18. Since the precise nature of the minerals was not known, it was assumed that only the carbonate minerals would react with the acid and other minerals would remain unaffected. It is seen from the Table 18 that the weight loss from the concentrate is extremely high in comparison with that of feed and tailing solids. This provides strong evidence that the carbonate minerals are selectively accumulated in the concentrates.

Table 18. Weight Loss of Feed, Concentrate, and Tailings Solids as a Result of Acid Treatment

	Feed	Concentrate	Tailing
% Weight Loss	7.2	73.7	3.7

FTIR spectrum of the residue from the concentrates is presented in Figure 6. The band at 2517 cm^{-1} which was observed in the case of the solids from concentrates (Figure 5), is entirely absent in the residue after acid treatment. This would clearly indicate that 2517 cm^{-1} band is due to the presence of carbonate minerals. Elemental analysis of the filtrates from the acid treatment of the three samples are presented in the Table 19.

Element	Feed	Concentrate	Tailings
Sodium	1.1	0.7	<0.4
Potassium	1.4	1.3	0.6
Calcium	33.0	751	0.7
Iron	1.0	6.7	0.3
Aluminum	1.7	2.7	0.7
Titanium	<0.1	0.2	<0.1
Strontium	0.02	0.38	<0.01
Manganese	0.3	5.7	<0.2

Table 19.   Elemental Analysis of the Feed, Concentrate and Tailings Filtrates Following Acid Treatment.
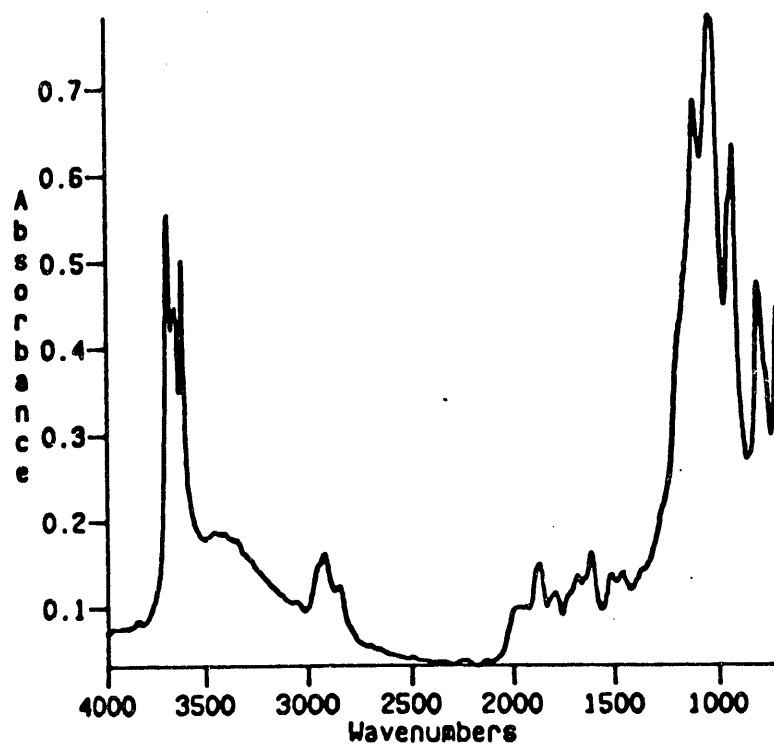
Figure 6. Fourier Transform Infrared Spectrum of the Acid
Treated West Central Solids from the Bitumen
Concentrate (≤45μ)

The results indicate that the concentration of calcium, magnesium, iron, manganese, and strontium in the filtrate from the concentrate solids relative to the feed sand increased by almost an order of magnitude. X-ray diffraction analysis of the solids from the concentrate indicated that the main carbonate minerals were calcite, dolomite and magnetite. The XRD profiles of the same solids after the acid treatment show a total absence of the peaks attributed to the carbonate minerals (Figure 7). The ICP analysis of the acid treated filtrates indicated the presence of siderite, strontianite and rhodochrosite.

The results from all these experiments unequivocally demonstrate that, in general, very fine particles such as kaolinite and quartz, and in particular carbonate minerals are intimately associated with bitumen and follow the bitumen into the concentrate product during the flotation process. The reporting of kaolinite to the bitumen froth can be explained by mechanical entrapment and are distributed according to the water split between concentrate and tailings. The mineral particles acquire a hydrophobic nature as a result of adsorbed organic molecules from the bitumen at their surfaces. The intimate association between carbonate minerals and bitumen may indicate some specific interactions between them. Bitumen is known to contain significant amounts of carboxylic acids, and it is conceivable that through these acid groups complex carboxylate are fixed at the surface of the carbonate minerals. It is rather difficult to define the exact nature of the adsorption phenomenon but chemisorption and surface precipitation reactions are known to occur in other flotation systems.
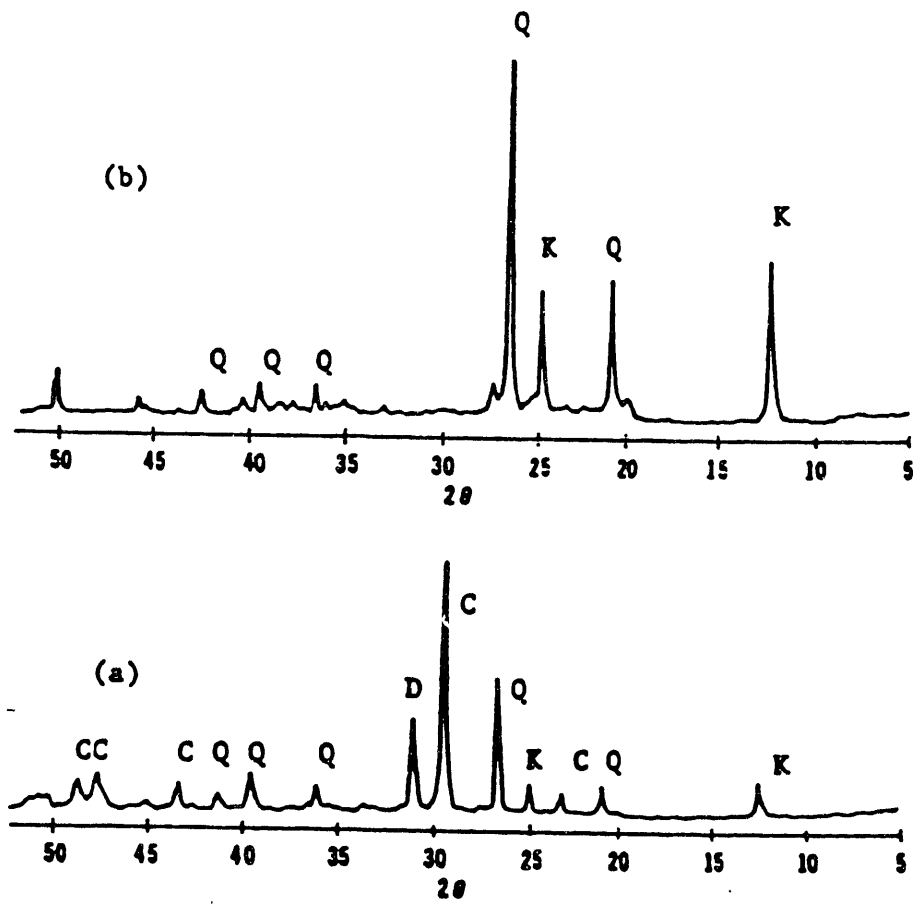
Figure 7. XRD Profiles of Solids (a) from Bitumen
Concentrates,and After Acid Treatment (b)
(K = kaolinite, Q = quartz, C = calcite,
D = Dolomite).

78

Summary and Conclusions

Samples from the Whiterocks tar sand deposit were collected from three different locations for bitumen and solids characterization. The bitumen was separated from the tar sand by toluene extraction and compound-type analyses were performed. The analyses indicated that the composition of the bitumens obtained from the three different locations were similar. The most significant feature of the Whiterocks bitumen was the low concentration of asphaltenes. The Whiterocks bitumens were somewhat similar to the Asphalt Ridge bitumen with respect to other compositional properties.

The mineralogical analysis of the tar sand solids, after bitumen extraction, indicated that it consisted mainly of quartz, calcite, dolomite and kaolinite. It was observed that in the hot water processing of tar sands, some solids always reported to the bitumen concentrate in both the gravity separation and flotation steps. In order to determine whether a selective distribution of the solids takes place in the flotation process, a comprehensive analysis of the solids reporting to the bitumen concentrate was made. A combination of FTIR, XRD, XRF, ICP and wet chemical techniques was employed in the analyses. The results indicated that kaolinite and carbonates concentrated in the bitumen concentrate. The accumulation of kaolinite and carbonates in the bitumen concentrate solids was explained based on their size and the presence of organic compounds on the particle surfaces. Although the precise nature of these adsorbed organic compounds is unknown, it was presumed that they contain carboxylic acid groups which would cause these species to adsorb on the mineral surfaces.

79

ELECTROPHORETIC CHARACTERIZATION OF BITUMEN AND FINE MINERAL PARTICLES FROM ASPHALT RIDGE AND SUNNYSIDE TAR SANDS

Introduction

A considerable portion of Utah's tar sand resource can be mined and processed above ground to recover bitumen by means of a modified hot water separation process. A similar strategy has been successful in Canada for processing of the Athabasca tar sands.[1] The hot water process remains economically sound when compared to other bitumen recovery methods which have been proposed.[2] The efficiency of the hot water separation process is strongly influenced by the surface properties of the bitumen and sand phases of which the tar sand material is composed.[3] Surface charges on bitumen droplets and mineral particles conceivably could influence the final bitumen recovery and sludge settling characteristics in the tailings pond as shown by Hall and Tollefson[5]. Physical and chemical properties of the Athabasca tar sands have been determined to a much greater extent than the properties of Utah tar sands.

In this phase of the research program, tar sand samples from the Asphalt Ridge and Sunnyside deposits have been studied. Bitumen from the Asphalt Ridge tar sand has been recognized to be easy to separate, and the process efficiency, measured by the coefficient of separation is comparable to the separation efficiency reported for Athabasca tar sands as reported by Hupka et. al.[6] The coefficient of separation (CS) is defined as the fraction of feed which undergoes perfect separation and is calculated as the difference between bitumen and sand recovery in the concentrate. Processing of Sunnyside tar sands results in a significantly inferior separation. The main reason for lower

separation efficiency is undoubtedly the consolidated nature of the material from the Sunnyside deposit and the substantially greater bitumen viscosity in comparison to the viscosity of the Asphalt Ridge bitumen. Feed size reduction below two millimeters and subsequent prolonged contact with a suitable amount of diluent (kerosene) did not increase the coefficient of separation for the Sunnyside tar sand above 0.81. This coefficient of separation should be compared to the coefficients of separation for the tar sand, 0.94, and for the Asphalt Ridge tar sand, 0.91 as reported by Hupka et al.[6]. Electrophoretic characterization was undertaken to determine if differences in electrical surface properties of the tar sand components could be detected.

The results may also contribute to a better understanding of the mechanisms underlying the separation of the bitumen from the tar sand matrix and its subsequent flotation for bitumen recovery.

Processing Strategy for Utah Tar Sands

Bitumen recovery from tar sands by means of hot water processing involves two steps: digestion and phase separation.[4] In the digestion step the organic bitumen phase is disengaged from mineral particles by preferential wetting of the particles by the aqueous phase and by the introduction of mechanical energy into the system. In the hot water process developed for Utah tar sands, digestion requires a more intense shear force field than that used for Athabasca tar sands because of the inherent differences in physical and chemical properties as reported by Miller and Misra.[4] Moreover, effective separation is controlled by bitumen viscosity

81

which should not exceed 1.5 Pa s at the processing temperature.[7] After displacement from the sand, the bitumen remains suspended in the aqueous phase. Phase separation of the bitumen by dilution of the pulp and subsequent flotation is the second step of the processing strategy.

Experimental

Hot Water Separation Experiments

Bitumen recovery from batch experiments was carried out by digestion of 400 gram feed samples in a specially designed stirred-tank reactor and flotation in a Denver-type four dm^3 flotation cell according to procedures described elsewhere[4,6] (see also Table 20). Kerosene was used as a diluent to control bitumen viscosity in the range 0.5 to 1.5 Pa.s at the processing temperature. The aqueous phase alkalinity was adjusted by Na_2CO_3 addition. Processing temperatures of 30°C, 60°C, and 90-95°C were used. Due to contamination with sand and kerosene, the bitumen concentrate as such was not used for electrophoretic experiments, with one exception. Instead the bitumen was obtained by toluene extraction from tar sand feed samples.[7]

Analytical Methods

Electrophoretic mobility was measured at 25 ± 0.5°C in a quartz cell (1.5 mm thick). The zeta meter was equipped with a video-viewing system as described by Stachurski and Michalek[8] and a system for statistical evaluation of the data. Particle mobility measurements at positions of zero electrolyte flow were found to be

Table 20. Processing Conditions and Tailings Water Properties for Asphalt Ridge and Sunnyside Tar

Tar Sand	Processing Conditions[a]			Coefficient of Separation	Tailings Water Properties at 20°C			
	Temperature °C	Na_2CO_3 Added (g/kg)	Flotation pH		Surface Tension, mN/m		MBAS [b] mg/dm³	Specific Conductivity μScm⁻¹
					air-tailings water	kerosene-tailings water		
Asphalt Ridge	95[c]	2.5	8.5	0.93	47.9	23.7	4.5	610
11.5 wt%	60	1.25	8.1	0.88	54.5	27.7	1.0	310
bitumen	30	2.5	8.9	0.82	52.3	25.9	2.4	400
Sunnyside	90	7.5	9.9	0.80	46.2	18.9	4.4	1650
9.5% wt%	60	5.0	8.5	0.79	51.0	23.7	2.0	1150
bitumen	30	2.5	8.7	0.72	48.8	24.2	1.5	800

a) Constant processing parameters:
   - bitumen viscosity at processing temperature: 0.5 to 1.5 Pa·s (controlled by diluent addition)
   - digestion time: 15 min.
   - flotation time: 10 min.
   - percent solids in reactor: 63%
   - percent solids in flotation cell: 12%

b) Methylene blue active substances (mainly surfactant with sulfate, sulfonate carboxyl and groups)

c) Experiment in which diluent was not applied

83

sufficiently reproducible (error limits are indicated in Figure 9).
Mineral particles under observation were in the range of one to two
μm while kerosene and bitumen droplets had diameters of five to 10
μm. Zeta potentials (ζ) were calculated from the average velocity
of five to seven particles at both positions of zero electrolyte
flow based on the Smoluchowski equation[9]. Bitumen and kerosene
emulsions in distilled water and in tailings water (after
filtration) were prepared in a homogenizer. Sunnyside bitumen
required the combined action of mechanical and ultrasonic force
fields in order to achieve satisfactory emulsification.
Suspensions of fine minerals in tailings water were used as
withdrawn from the flotation cell after allowing the sand to settle
for approximately 10 to 20 minutes. Suspensions of fine minerals
in distilled water and suspensions prepared from roasted minerals
(five hours at 550°C) in distilled and tailings water (after
filtration) were equilibrated for one hour prior to measurements.
Emulsions and suspensions were also equilibrated following pH
adjustment with HCl or NaOH. Interfacial tensions at kerosene-
tailings water and air-tailings water interfaces were measured with
a semiautomatic DuNouy ring type tensiometer (Mallinckrodt Dyno-
meter, FRG). The kerosene-tailings water interface was allowed to
equilibrate for 30 minutes. The average error in the determination
was ± 0.5 mN/m. Tailings water was also analyzed for anionic
surface active agents by the methylene blue method and results were
reported as methylene blue active substances ("Standard Methods,"
APHA, 14th ed., 1976, .600). Specific conductivity measurements

84

for tailings water were made with a Radelkis conductivity meter (Hungary). The experimental error was less than 0.5%.

Results and Discussion

Bitumen separation efficiencies reported as the coefficient of separation are presented in Table 20. The coefficient of separation for Asphalt Ridge tar sands was found to be significantly greater than that for Sunnyside tar sands as previously reported.[6,7]. Data in Table 20 also confirm earlier results reported on the increase of surface active agents released to the aqueous phase ("free" surfactant) with increasing processing temperature and alkalinity[4,10]. It has been widely accepted that naphthionic acids present in the crude oil or bitumen interact with the alkali to form a surface active soap. All detailed findings on this matter, however, can be related to research on the Athabasca tar sands, in which case carboxylic acids have been found to be primarily responsible for the observed surface activity[3,4,10-13]. The significance of other anionic surfactant, namely sulfate and sulfonate compounds, in oil recovery efficiency has also been reported[10].

General observations concerning the zeta potential plots presented in Figures 8-16 are that the surface of all particles and droplets had negative charges in the pH range from pH 3 to pH 10. Emulsions and suspensions, whether of Asphalt Ridge or Sunnyside origin, exhibited similar electrokinetic behavior despite changing the ionic strength of the solution in each experiment.
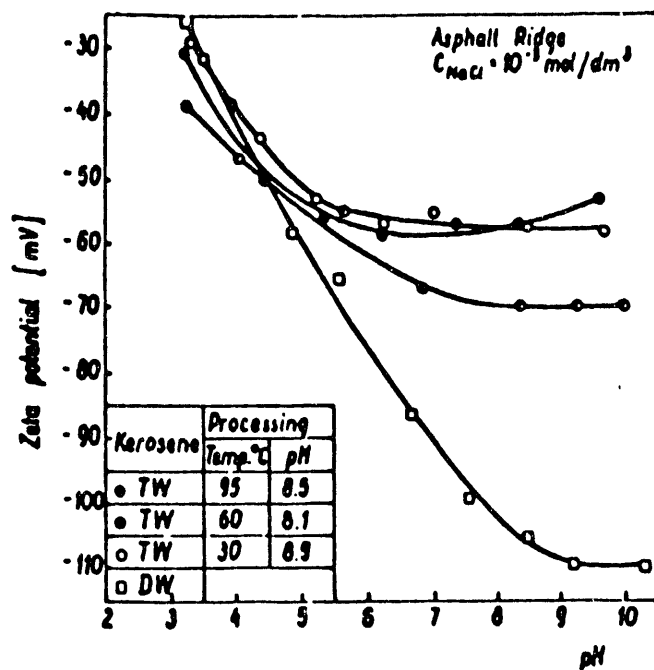
Figure 8.   Zeta Potential of Kerosene Droplets in Asphalt Ridge Tailings Water (TW) and in Distilled Water (DW).
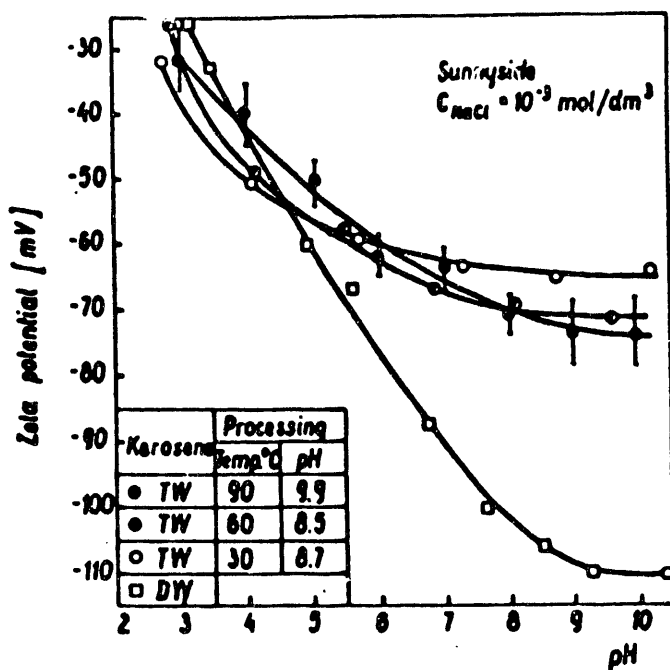
Figure 9.   Zeta Potential of Kerosene Droplets in Sunnyside Tailing Water (TW) and in Distilled Water (DW).
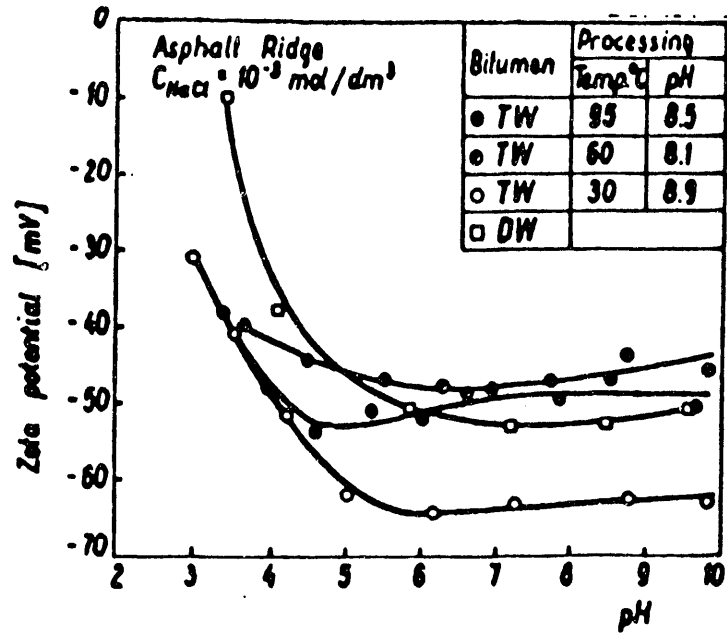
Figure 10. Zeta Potential of Toluene Extracted Bitumen Droplets in Asphalt Ridge Tailing Water (TW) and in Distilled Water DW).
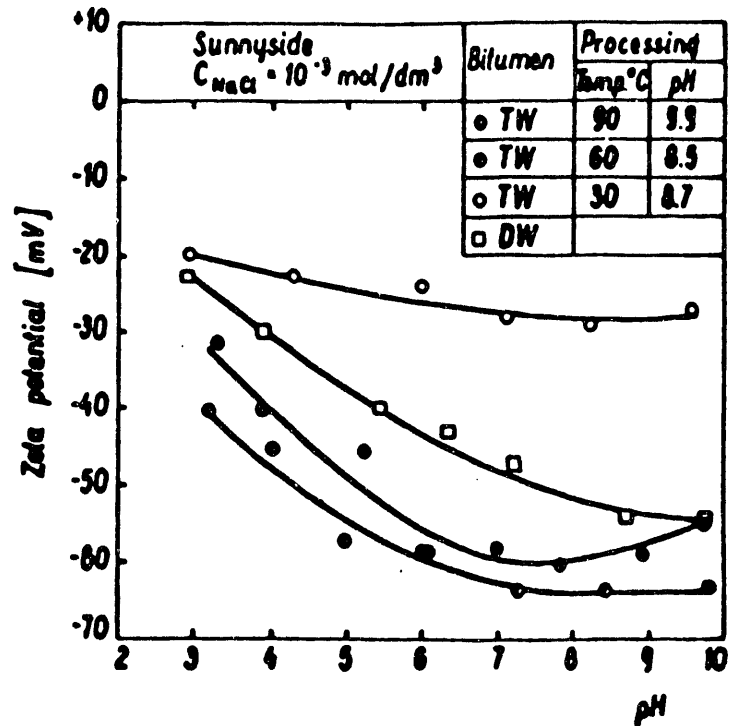
Figure 11. Zeta Potential of Toluene Extracted Bitumen Droplets in Sunnyside Tailing Water (TW) and in Distilled Water (DW).
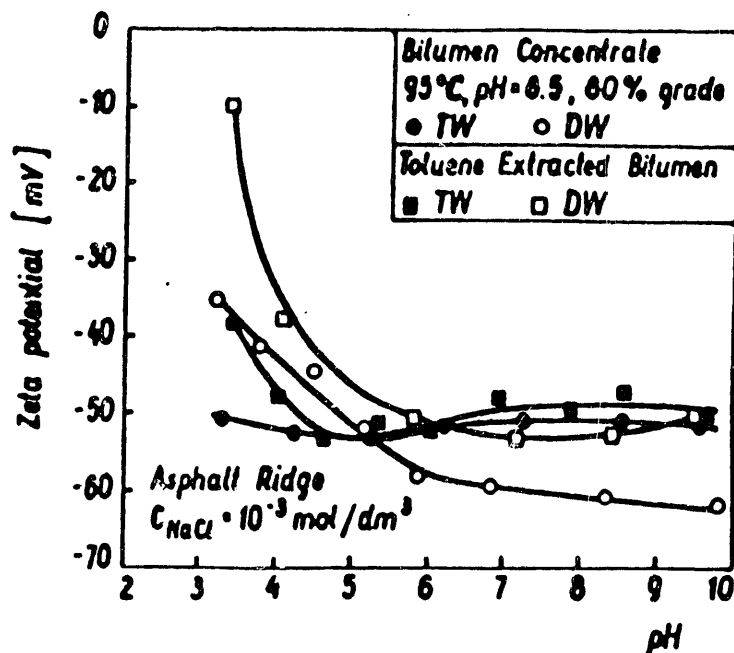
Figure 12. Zeta Potential of Toluene Extracted Bitumen Droplets and Bitumen Concentrate Droplets in Asphalt Ridge Tailing Water (TW) and in Distilled Water (DW).
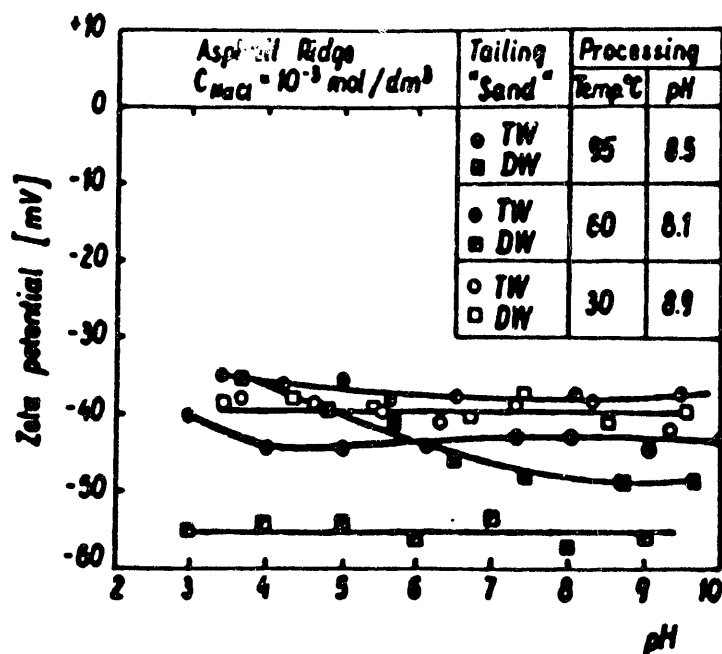
Figure 13. Zeta Potential of Fine Mineral Particles in Asphalt Ridge Tailing Water (TW) and in Distilled Water (DW)
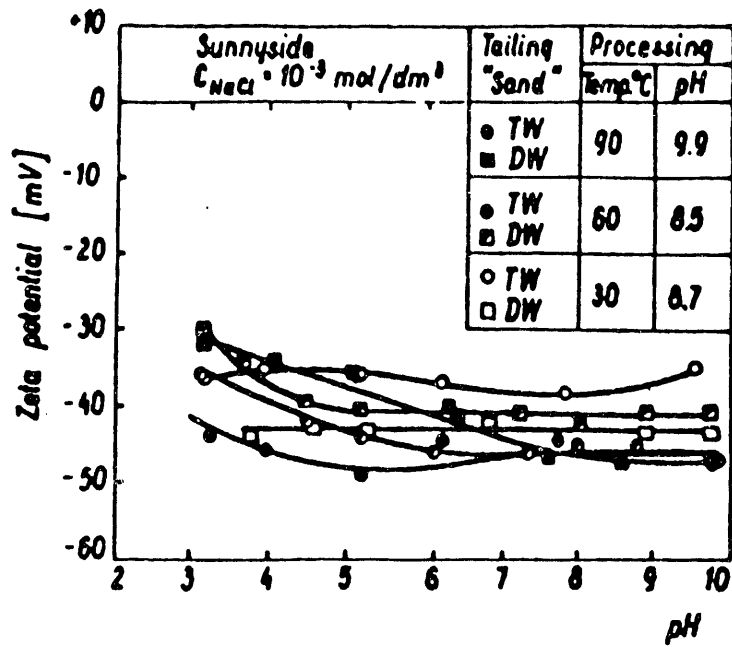
Figure 14.   Zeta Potential of Fine Mineral Particles in Sunnyside Tailing Water (TW) and in Distilled Water (DW).
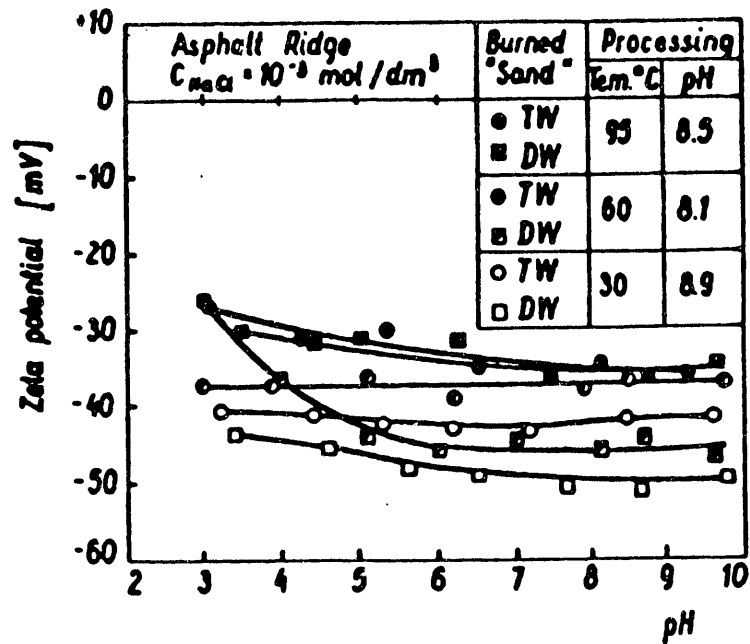
Figure 15.   Zeta Potential of Roasted Fine Mineral Particles in Asphalt Ridge Tailing Water (TW) and in Distilled Water (DW).
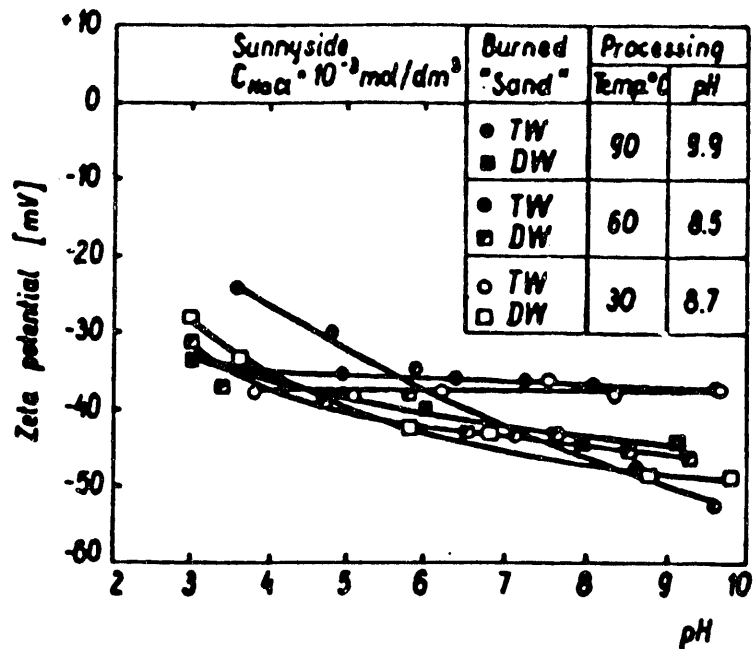
Figure 16. Zeta Potential of Roasted Fine Mineral Particles in Sunnyside Tailing Water (TW) and in Distilled Water (DW).

Mobility of Bitumen Droplets

Investigations performed with the Athabasca tar sands showed a maximum in bitumen droplet mobility at certain concentrations of surface active compounds[10]. It appears that a similar effect was observed with the Utah tar sands. The bitumen zeta potential curves in Figures 10 and 11 indicate that a critical surfactant concentration might be reached for both bitumens under certain conditions (particularly at elevated temperatures). The lowest charged droplets were from Asphalt Ridge bitumen at 60°C and from Sunnyside bitumen at 30°C. These results, presented in Figure 10 and 11, correlate with the "free" surfactant contents given in Table 20. The presence of "free" carboxylate surfactant in the tailings water can be deduced from the behavior of the kerosene droplets' zeta potential (Figures 8 and 9). Above pH five the zeta potential remains unchanged within experimental uncertainty (± five mV) — particularly for the Asphalt Ridge sample. Below pH five the zeta potential becomes increasingly less negative because of protonation of the carboxylate. A similar trend can be observed in Figures 10 and 11 for bitumen droplets. The stabilizing effect of the negative electrical charge is more pronounced here due to the additional influence of surfactant remaining in the bitumen phase and those adsorbed from the aqueous phase. The shape of the Sunnyside bitumen and kerosene in tailings water zeta potential curves provided evidence of the presence of other surface active agents more polar than the carboxylate surfactant. Most recently a comparison of the electrophoretic mobilities and the dynamic

mobilities obtained by electroacoustical methods for an Athabasca bitumen in water emulsion was presented by Babchin et al[14].

The agreement for both methods is relatively good in an acidic environment. In an alkaline solution the electroacoustical method yielded much lower mobilities. The exact cause of this is not known and eventually may be attributed to the particle size distribution. In the present work a TV monitor was used, and only the particles of a desired size were selected for velocity measurements. In this regard errors attributed to polydispersed systems should be minimized.

The bitumen from the hot water concentrate appears to be more stabilized by negatively charged hydrophilic groups than bitumen extracted from the tar sand by means of toluene (Figure 12). This observation is in agreement with previous observations that bitumen hydrophobicity can be destroyed during digestion[15].
The solubility of fatty acids was found to increase as the system pH was increased[4]. This phenomenon appears to account for the polar bitumen surface and the loss in the hydrophobic character of the digested bitumen.

Mobility of Fine Mineral Particles

The zeta potentials for fine mineral particles from the tailings product (most probably clay and precipitated carbonates) are presented in Figures 13 through 16. The results for the fine particles suspended in tailings water and in distilled water are presented in Figures 13 and 14 respectively. Zeta potentials of roasted fine mineral particles (from which organic matter has been

removed) suspended in tailings water and distilled water are presented in Figures 15 and 16. Comparison of the plots in these figures suggests that adsorbed surfactant are not significant in determining the electrophoretic properties of the mineral particles. According to Srinivasan et al.[16], the surface electrical properties of mineral fines from the tailings produced from the Athabasca tar sands are due to fixed surface charges of mixed clay systems and organic species. On the other hand, electrophoretic mobility of the solids from Athabasca tar sands as measured by Schramm and Smith[10] increased with an increase in free surfactant concentration of process extracts. There was little change in the zeta potential pH for the fines (Figures 13 and 16). Nevertheless, at higher temperatures and alkalinities, there was an increased organic removal from the fines' surface as clearly seen for the Sunnyside tar sand and in distilled water suspensions of the fines recovered at a processing temperature of in the range 90-95°C for both tar sands.

Zeta potential plots for roasted fine solids, Figures 8 and 9, suggest adsorption of certain substances from the tailings water. Experimental plots obtained for Sunnyside fines in distilled water representing three different hot water separations carried out at 90, 60 and 30°C, indicate very good experimental reproducibility. On the other hand, lack of superposition of the zeta potential curves for Asphalt Ridge roasted fines suspended in distilled water may indicate a variation in the fines mineralogical composition due to different sedimentation kinetics after flotation. There are

93

still many uncertainties regarding the condition of the surfaces during tar sands processing, as indicated by Kotlyar et al.[17], particularly with respect to the interaction of polyvalent cations and unidentified surfactant at the bitumen-water and solid-water interface.

Hot Water Processing Technology

The negative zeta potential at the bitumen surface is in the range of -65 mV to -45 mV during flotation and is significantly reduced during digestion due to high ionic strength of the aqueous phase. The negative electrical charge at the surface of both phases (bitumen and sand) should facilitate disengagement during digestion if the viscosity criterion of <1.5 Pa.s is satisfied. Hupka et al[7] have verified this conclusion for a number of U.S. tar sand samples. Clay particles, also negatively charged, do not separate as easily from the bitumen and thus report to the concentrate. As suggested for Utah tar sands by Misra et al.[15] and Hupka and Miller[18] and as shown in detail in the study of Athabasca tar sands by Schramm et al.[12], an excessive addition of NaOH or Na_2CO_3 during digestion should be avoided in the hot water process due to the increased release of surfactant to the aqueous phase. Surfactant exceeding a critical concentration reduce the bitumen zeta potential[12] (Figures 10 and 11), and diminish the disjoining pressure at the bitumen - mineral interface[13]. Thus, forces leading to phase displacement and disengagement are weakened. Excessive addition of alkalies significantly reduced the quality of separation for the Asphalt Ridge sample[4] as indicated in Figure 17.

A.

lb/ton of Tar Sand

Coefficient of Separation vs NaOH Concentration, M

Asphalt Ridge samples
Temperature : 95 °C
Percent Solids : 70-80%

B.

lb/ton of Tar Sand

Coefficient of Separation vs Na₂CO₃ Concentration, M

Asphalt Ridge Tar Sand
Temperature : 95 °C
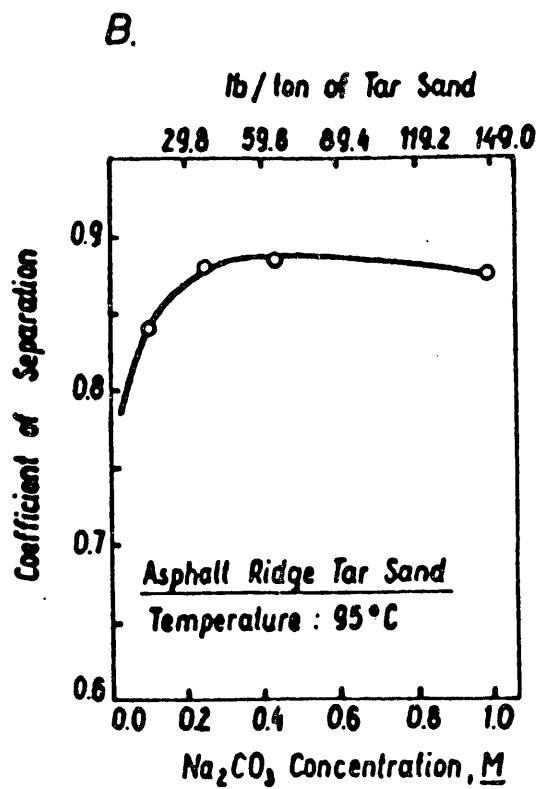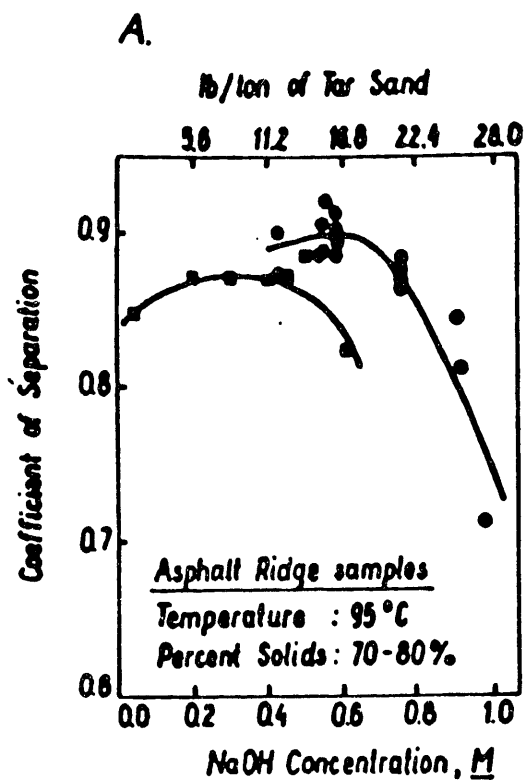
Figure 17.   Quality of Separation as a Function of: (a) Sodium
Hydroxide Concentrations and (b) Sodium Carbonate
Concentration for the Asphalt Ridge Sample[4].

95

The influence of sodium carbonate was not as severe due to limited hydrolysis and buffering. From the electrophoretic mobility point of view, it would be expected that a decrease in processing temperature would not diminish the separation efficiency for bitumen recovery. An earlier investigation confirmed that the coefficient of separation remained essentially constant when the processing temperature was lowered from 90°C to 60°C provided the viscosity of the bitumen was controlled by diluent addition[6]. Mechanical entrapment of high viscosity Sunnyside bitumen in consolidated sandstone and bitumen resistance to dilution by kerosene are still the only reasonable explanations for the difference in separation efficiency between the Sunnyside and Asphalt Ridge tar sands.

Also, during the flotation step of the modified hot water process, it is evident that all interfaces in the aerated tar sand slurry are negatively charged. Efficient flotation of minute bitumen droplets may therefore be in question. The fast flotation of large bitumen droplets is expected at the outset, followed by relatively slow flotation of tiny residual droplets. The rate of rise to the surface of large droplets is controlled by an air bubble entrapment mechanism, as shown by Miller and Misra[4] and Misra et al.[15] Bubble entrapment can take place only in bitumen droplets considerably larger than the air bubbles. The encapsulation of air bubbles in bitumen droplets having a diameter below 0.5 mm (i.e., smaller than that of the air bubbles generated in the flotation cell) can occur in the process of bubble and

96

droplet attachment and filming. Nevertheless, the preliminary condition has to be fulfilled as given by Leja and Bowman[19]:

$$\gamma_{a/w} > \gamma_{o/w} + \gamma_{a/o} \tag{1}$$

where: γ is the interfacial tension, mN/m, at the air-water (a/w), the oil-water (o/w), and the air-oil (a/o) interfaces.

According to Bowman[3], Potoczny et al.[20] , and Burchfield and Hepler[21], the following γ values can be anticipated for conditions in the flotation cell (depending on temperature). (see Table 20).

$$\gamma_{a/w} = 45 \text{ to } 55$$
$$\gamma_{o/w} = 5 \text{ to } 25$$
$$\gamma_{a/o} = 20 \text{ to } 35 \tag{2}$$

Note that the largest possible value of $\gamma_{o/w}$ is required for bitumen retraction from sand grains during digestion, contrary to the in-situ process[13]. This high $\gamma_{o/w}$ is also maintained in the flotation step in the absence of additives. Therefore filming, understood as advantageous for effective flotation, will not necessarily follow attachment.

The degree of bitumen dispersion in the slurry depends on the shear force field applied during digestion. Excessive agitation might, therefore, contribute to a slower flotation rate and a lower grade of the bitumen concentrate.

Data presented in Table 21 leave no doubt that after flotation of the large bitumen droplets, flotation of negatively charged mineral particles competes with the flotation of negatively charged fine bitumen droplets. The lowest possible zeta potential at the bitumen surface will facilitate its flotation. The same conditions

Table 21. Bitumen Recovery by Flotation as a Function of Time at 90-95°C

Time of Flotation (min)	Bitumen Grade of Concentrate, wt.%			Bitumen Distribution in Concentrate, wt.%		
	Athabasca	Asphalt Ridge	Sunnyside	Athabasca	Asphalt Ridge	Sunnyside
0-1	84	81	55	82	75	48
1-3	62	52	34	13	15	28
3-6	37	34	26	3	5	14
6-10	25	28	18	<1	1	5
Average/Total**	78	71	40	98	96	95

* dry mass
** average grade and total recovery after 10 minutes flotation

were used to process each of these tar sand samples. The variation in overall bitumen concentrate grade can be attributed to the presence of undigested agglomerates which report to the concentrate and account for the inferior separation efficiency.

Summary and Conclusions

A study of the electrophoretic mobility of the Asphalt Ridge and Sunnyside tar sand components at pH 3 to 10 revealed that the surfaces of the mineral particles, and of the bitumen and kerosene droplets have a negative electrical charge. The zeta potential of bitumen droplets in tailings water at pH 8 to 9 (processing temperatures $\geq$ 60°C) was found to be -45 to -65 mV, while the zeta potential of the fine mineral particles was found to be -35 to -45 mV. These fine mineral particles will float with the bitumen droplets, but at a slower rate. Therefore, a higher grade bitumen concentrate is obtained at shorter flotation times. Of course, the smallest possible zeta potential for bitumen droplets is desired for most efficient flotation. Despite variations in the processing temperature and carbonate addition (which influenced the pH and ionic strength of the aqueous phase) and the use of tar sands from two different locations, no significant differences in the zeta potential curves were observed. Apparently in each run a sufficient amount of organic surfactant was present at the bitumen and mineral fines surfaces, to stabilize the negative surface charge. Additionally, the comparable negative electrical charge on both bitumen droplets and mineral particles suggests that bitumen gravity separation should precede flotation. Flotation could then be used to scavenge the remaining bitumen droplets.

99

RESIDUAL SOLVENT EFFECT ON THE VISCOSITY
OF BITUMEN FROM WHITEROCKS TAR SAND

Introduction

The viscosities of U.S. tar sand bitumens vary over several orders of magnitude, e.g., from 0.1 Pa·s (10 cP) at 90°C for the bitumen from the McKittrick deposit in California to 1000 Pa·s (10^5cP) at 90°C for specific locations on the P.R. Spring deposit in Utah. A solvent extraction procedure is usually used to isolate the bitumen for analytical purposes, particularly for the highly viscous bitumens present in the Utah deposits.

The solvent is recovered from the bitumen-solvent solution by evaporation under vacuum. Dissolved gases and volatile species are carried overhead with the solvent at higher temperatures and lower vacuum. Thus the viscosity determined for the extracted bitumen is not that which would be determined for the native bitumen. The sensitivity of the viscosity to the residual solvent content was found to be significant for the Athabasca bitumen,[22,23]. The bitumen viscosity was lowered by a factor of two to three by two weight percent residual toluene.

An estimate of bitumen viscosity is required before any processing strategy can be developed for a particular tar sand deposit. This requirement is also relevant to surface processing of mined tar sand by means of hot water extraction. As reported earlier[7], the suitability of the modified hot water separation process for a specific tar sand is related to the bitumen viscosity and the selection of process operating conditions is related to the classification system developed by Hupka et al[7]. A proper bitumen

viscosity determination is therefore of importance. Studies on tar sand bitumen properties are also preceded with solvent extraction[20], even in the case when the viscosity is predicted from bitumen chemical and physicochemical properties[24].

Wallace and Henry[25] proposed an alternative procedure to complete solvent removal which involves solvent extraction, removal of most of the solvent under mild conditions of rotary evaporation, and mathematical correction of the measured viscosity for residual solvent using the Cragoe equation. The ratio of the corrected viscosity to the measured viscosity should not exceed a factor of six to hold the uncertainty in the corrected viscosity to 20% relative.

The objective of this phase of our research was to evaluate the effect of the residual toluene content and simultaneous loss of light ends on the bitumen viscosity. In addition, the rheological behavior of the Whiterocks bitumen which contained a diluent was examined.

Experimental

Tar Sand Sampling

Tar sand properties vary due to site removal, storage and handling, all of which influence the extent of bitumen deterioration. No standard procedures have been established for tar sand sampling and for the acquisition of representative samples. In order to overcome this problem a simplified equation derived by Gy[26], based on a detailed analysis of the statistics of

sampling in mineral processing technology, has been applied:

$$\frac{1}{M_s} - \frac{1}{M_L} = \frac{s^2}{Cd} \qquad (3)$$

where:

M_s is the minimum sample weight, g,

M_L is the lot weight, g,

d   is the linear dimension of the largest particle, in the lot to be sampled, cm, (in this case 0.67 cm),

s   is the relative standard deviation, and

C   is the sampling constant for specific particle mixture, g.

The sampling constant is given by a product of four parameters,

$$C = f \cdot g \cdot l \cdot m \qquad (4)$$

where f is the shape factor, g is the particle size distribution factor, l is the liberation factor and m is the mineralogical composition factor. In the case of tar sands, the following values can be assigned to three of the factors: $f = 0.5$, $g = 0.25$, and $l = 0.122$. The m factor is calculated from the following formula:

$$m = (1-a)/a \cdot [(1 - a) \, \rho_c + a \, \rho_g] \qquad (5)$$

where:

a   is the weight fraction of the critical component (in this case the average bitumen content of the Whiterocks tar sand which is equal to 7.5 wt%)

ρ_c is the density of critical component (bitumen), g/cm^3, (in this case the bitumen has a density of 0.98 g/cm^3)

ρ_g is the density of gangue (mineral components of tar sand, g/cm^3), (in this case the gangue has a density 2.55 g/cm^3).

Following Gy's equation[26] the sample of tar sand to be cut from a larger mass of material (a 55 gal drum of crushed ore) was found to be not less than 1.4 kg, assuming a confidence level of 95±0.1%.

The tar sand sample used in the investigation was obtained from the Whiterocks deposit in Utah. The elemental analysis of the bitumen was 86.4 % carbon, 11.5 % hydrogen, 1.1 % nitrogen, 0.5 % oxygen, and 0.4 % sulphur.

Extraction Procedure

The bitumen used in this study was obtained by extraction of five 1.4 kg samples with spectro-grade toluene, obtained from a crushed, screened and averaged sample from the West Central region of the Fausett pit on the Whiterocks deposit.   The mined ore contained approximately 6.0 wt.% bitumen.   Each extraction was carried out using a Dean-Stark apparatus with Whatman, single thickness, cellulose thimbles. Shark skin filter paper was wrapped around the outside of the thimble to trap the fine mineral particles which penetrated the thimble wall. The extractions were carried out for 24 hours. The toluene/bitumen solution was held at 112-116°C. A total of two liters of the toluene/bitumen solution, containing 23 wt.% bitumen, was obtained from each extraction.

Toluene Evaporation Procedure

A Büchi, model EL-131S rotary evaporator was used in

conjunction with a precision, model S-35 vacuum pump, to remove the toluene from the solution. The temperature of the cooling water in the condenser was 15°C while that in the water bath was maintained at 85°C. Dry ice and acetone were used to keep the cold trap, between the rotary evaporator and the pump, at -79°C.

The two liter toluene/bitumen solution was added to the round-bottom boiling flask which rotated at 100 rpm. The bulk of the toluene was allowed to evaporate at mild conditions (85°C and 3.10^3 Pa, in order to prevent excessive foaming) until dripping of the solvent from the cooling coil ceased. Approximately two hours were required to reach this stage of solvent removal. At this point (time zero) a 15 cm³ sample of the bitumen was taken for analysis, along with a six cm³ of the toluene from the cold trap, after which the vacuum was increased to 2.1 kPa. The next 15 cm³ bitumen samples were withdrawn after one, two, four, eight and 16 hours of evaporation, whereas six cm³ cold trap samples were withdrawn after four, eight and 16 hours.

The residual toluene content of the bitumen samples was determined by simulated distillation. The three μl bitumen samples were injected into an HP model 5730A GC using a temperature program from -30°C to 350°C with ramp of 11°C/min. The internal standard consisted of C_5 to C_{10}-benzene. The procedure was a modification of the standard ASTM method D-287.

Viscosity Measurements

Bitumen viscosity was measured in a Brookfield microviscometer with cone-plate geometry. Several silicon oils were used as

viscosity standards to calibrate the viscometer. Experimental error, resulting primarily from uncertainty of temperature determination (±0.2°C accuracy), did not exceed one percent.

Results and Discussion

Bitumen Viscosity

Viscosity data for the Whiterocks bitumen (with changing residual toluene content) as a function of temperature are presented in Figure 18. The Arhenius plot is non-linear in the temperature range investigated, however, some of the data in Figure 18 can be fitted with the following empirical equation, proposed by Vogel as reported by Christensen et al.[27]:

$$\mu^* = \exp\left(A(T^*-1)/(T^*-B)\right) \tag{6}$$

where: μ^* and T^* are the dimensionless viscosity and temperature, respectively.

The dimensionless viscosity may be computed from

$$\mu^* = \mu(T,X_T)/\mu(T = 310.8 \text{ K}, X_T) \quad \mu(T = 310.8 \text{ K}, x_T) \tag{7}$$

where: $\mu(T,X_T)$ is the viscosity at the given absolute temperature (T) and for the given diluent weight fraction (X_T);

293 K ≤ T ≤ 422 K; 0.5% ≤ X_T ≤ 10%

$$\mu(T=310.8\text{K},X_T) = [299.0 \cdot (X_T)^{-0.84}] - 40, \text{ Pa·s} \tag{8}$$

$$A = (X_T-20.4)/1.206$$

$$B = (X_T+99.2)/152$$

The predicted and experimental viscosities are presented in Table 22. The viscosity calculated from the Vogel equation is in good

105
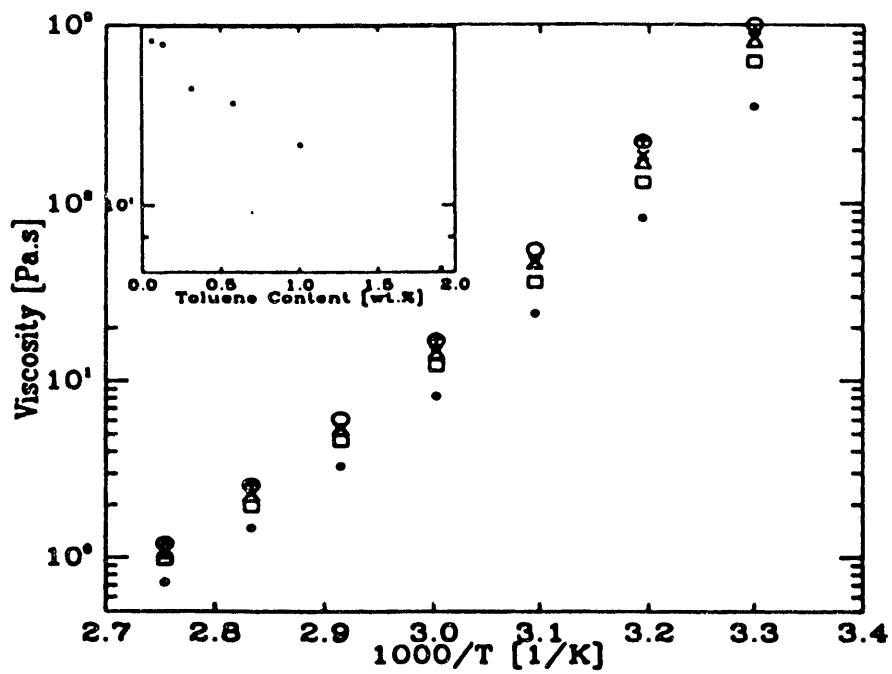
Figure 18. **Viscosity of the Whiterocks Bitumen**

Table 22. Bitumen Viscosity at Various Temperatures and Toluene Dilutions

Residual Toluene Weight Percent		Viscosity Pa$						
		30°C	40°C	50°C	60°C	70°C	80°C	90°C
1.91	1*	346.6	82.74	24.08	8.13	3.30	1.48	0.73
	2**	410.3	93.70	26.08	8.80	3.50	1.60	0.78
1.03	1	619.3	131.7	36.07	12.23	4.62	1.97	0.98
	2	876.0	176.8	46.70	15.30	5.80	2.50	1.23
0.58	1	786.4	165.8	45.59	14.01	5.14	2.17	1.04
	2	1530.0	30.30	78.60	25.00	9.47	4.06	1.94
0.32	1	850.3	186.5	47.06	14.67	5.43	2.32	1.08
	2	2646.0	515.0	132.0	41.00	15.60	6.60	3.13
0.14	1	983.1	221.20	56.93	16.96	6.14	2.60	1.23
	2	5486.0	1059.0	268.0	84.62	31.00	13.20	6.20
0.07	1	1100.0	226.1	--	17.20	--	2.61	1.23
	2	9771.0	1880.0	496.0	149.0	55.0	23.20	10.90

* experimental
** calculated

agreement with the measured values for the elevated temperatures (assuming that the toluene content in bitumen remains within the recommended values: $0.5\% \leq X_T \leq 10\%$), but there is a discrepancy below 50°C where the calculated bitumen viscosity was greater than the measured one in all cases.

The effect of diluent on bitumen viscosity is diminished with increasing temperature that is the dependence of the viscosity of the diluted bitumen on temperature was diminished. This trend can be observed in Figure 18 and is presented explicitly in Figure 19.

A brief investigation of the shear rate — shear stress relationship was carried out and the bitumen exhibited Newtonian behavior in the temperature (above 40°C) and shear rate ranges, (Table 23). Non-Newtonian behavior of bitumens is usually attributed to high asphaltene content[23,25]. The Whiterocks bitumen, used in this study contained less than five percent asphaltenes which explains its Newtonian behavior.

Toluene and Light Ends Removal

The extent of toluene removal and the corresponding bitumen viscosity as a function of evaporation time are presented in Figure 20. After 16 hours of rotoevaporation the toluene content in the bitumen dropped from 1.91% to 0.07%. The bitumen viscosity increased by a factor of 2.2 as a result of toluene removal (and light ends loss) at 60°C. Almost no bitumen viscosity change was observed after eight hours evaporation. The toluene removal data fit (correlation coefficient R=0.997) second order kinetics as indicated by the curve in Figure 21. These results indicate that
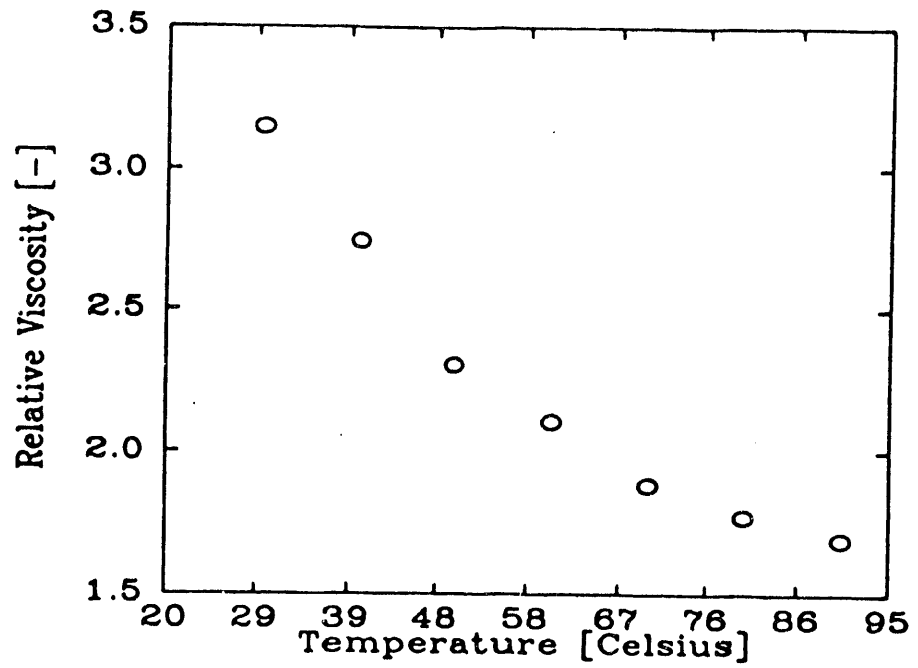
Figure 19. Influence of Toluene on Whiterocks Bitumen Viscosity at Various Temperatures
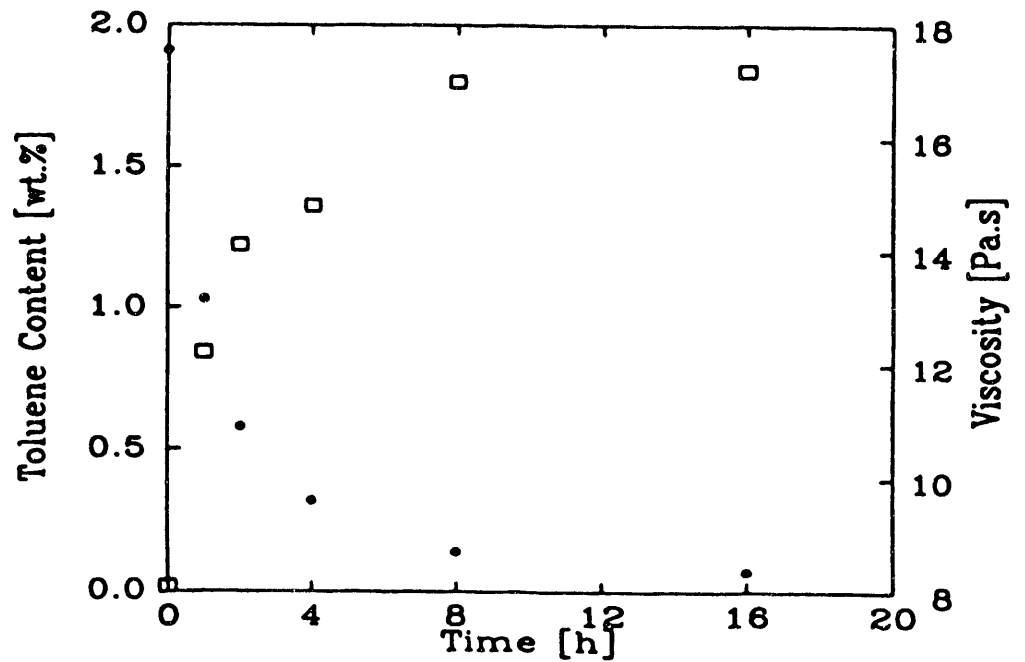
Figure 20. Toluene Content and Bitumen Viscosity versus Time

Table 23 Rheological Behavior of the Whiterocks Bitumen for Different Residual Toluene Contents

Temperature [°C]	Shear Rate [s⁻¹]	Shear Stress [dyn/cm²]	Viscosity Coefficient [Pa·s]

1.9 wt% Toluene

Temperature [°C]	Shear Rate [s⁻¹]	Shear Stress [dyn/cm²]	Viscosity Coefficient [Pa·s]
60	10	816	
	20	1622	
	40	3264	8.13
	100	8081	
50	5	1204	
	10	2408	24.08
	20	4817	
40	1	836	
	2	1642	82.74
	5	4129	

1.03 wt% Toluene

Temperature [°C]	Shear Rate [s⁻¹]	Shear Stress [dyn/cm²]	Viscosity Coefficient [Pa·s]
70	20	934	
	40	1838	4.62
	100	4591	
60	10	1229	
	20	2433	12.23
	40	4866	
50	5	1794	
	10	3588	36.07
	20	7225	
40	1	1327	
	2	2625	131.68
	5	6502	

110

Table 23   Rheological   Behavior   of   the   Whiterocks   Bitumen   for
            Different Residual Toluene Contents (continued)

0.58 wt% Toluene

70	20	1032	
	40	2045	5.14
	100	5141	
50	1	467	
	2	904	45.59
	5	2261	
40	1	1671	
	2	3736	165.77
	5	8208	

0.32 wt% Toluene

70	20	1101	
	40	2163	5.43
	100	5407	
50	2	934	
	5	2359	47.06
	10	4719	
40	1	1868	
	2	3736	186.53
	5	9290	

0.14 wt% Toluene

70	20	1229	
	40	2458	6.14
	100	6124	
50	2	1101	
	5	2753	54.93
	10	5456	

111
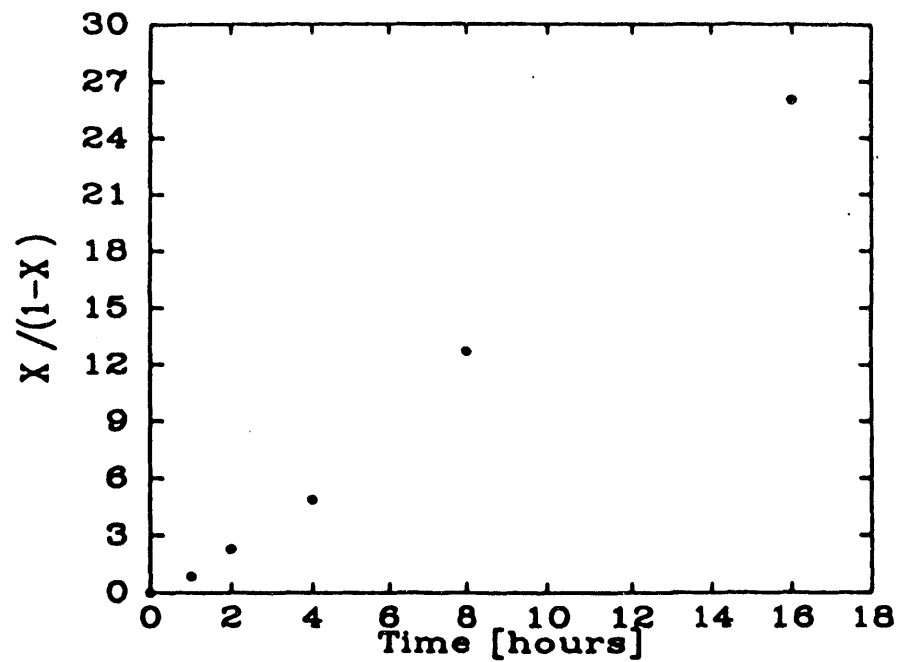
Figure 21.   **Kinetics of Toluene Removal from Bitumen**

112

diffusion is not the controlling mechanism, and toluene is brought to the bitumen surface due to mixing within the evaporation flask. The rate constant is k=0.88 min^{-1}. Thus it is estimated that lowering the toluene content from 0.07% to 0.01% might take an additional 100 hours of evaporation.

Attenuated total reflection FTIR spectroscopy was used to characterize the light ends which were released from the bitumen and collected in the cold trap. A ZnSe rod was used as the internal reflection element. The subtracted spectra with the time zero sample as background are reproduced in Figures 22 and 23. The absorbencies are very weak indicating a low concentration of light ends. The spectrum in Figure 22 indicates the presence of aliphatic groups. The presence of heteroatoms cannot be excluded. The amount of light ends collected in the cold trap increased with evaporation time (Figure 23).

The amount of light ends removed from 340 cm^3 Whiterocks bitumen after 16 hours evaporation was about 0.5 cm^3 (as analyzed by GC, Figure 24), which is equivalent to a weight loss of 0.1 %. The light ends start to distill at approximately 180°C. Assuming the light ends possess the same dissolution power as toluene, the bitumen viscosity change due to their loss should not exceed 15%. The residual toluene in the amount of 0.1% can eventually make-up for the viscosity increase due to the light ends loss.

Residual Organic Material on Extracted Sand

Toluene is not sufficiently polar to extract all the bitumen from the sand. A sample of the sand from which the bitumen
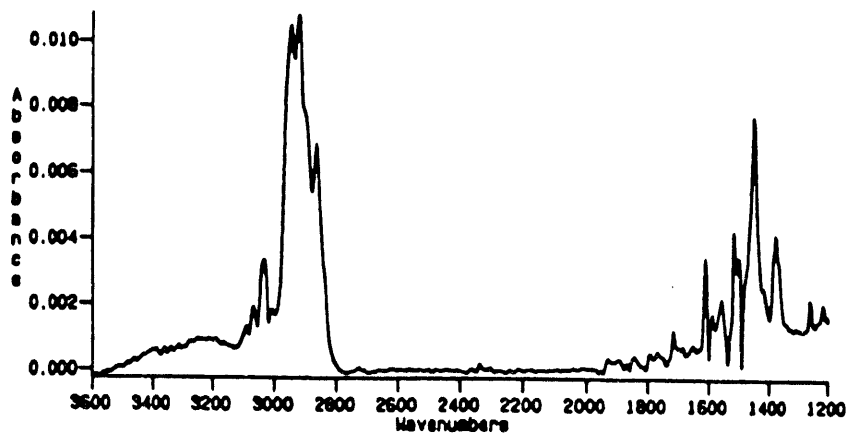
Figure 22. Subtracted Spectrum of Light Ends Removed from bitumen
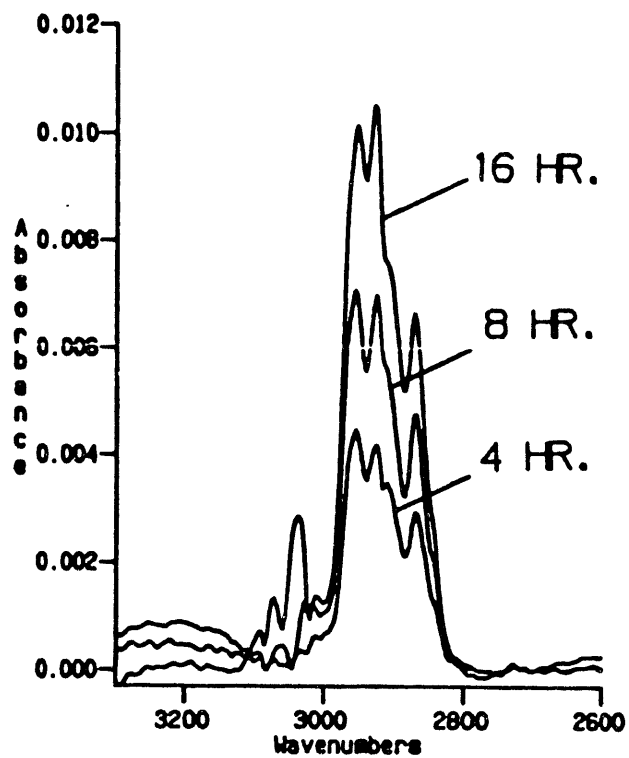
Figure 23. Infra Red Spectrum of Cold Trap Samples as a Function of Evaporation Time 4 hr, 8 hr, 16 hr

114
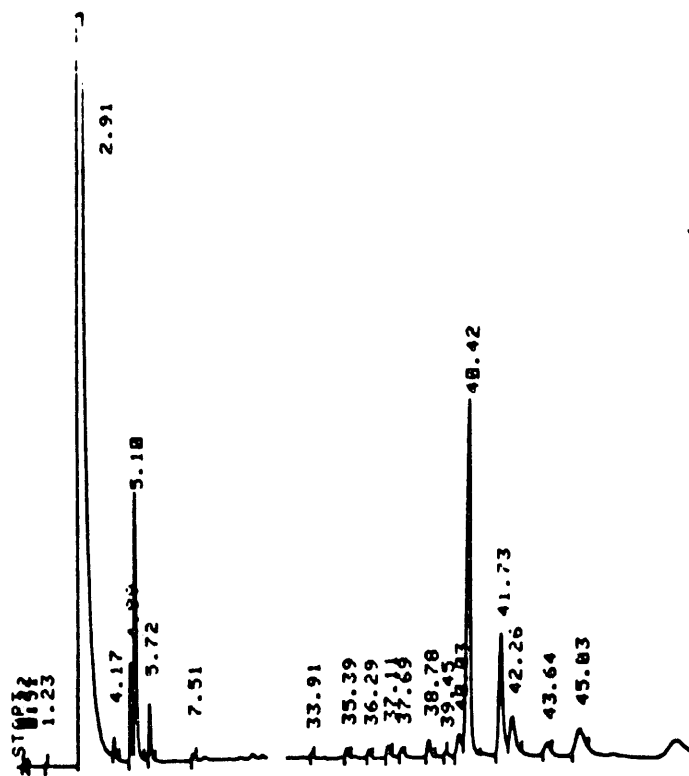
Figure 24. Chromatogram of Sample from Cold Trap

Table 24. Roasting of Toluene Extracted Whiterocks Sand at 550°C
(Dried at 110°C)

Size Fraction [mesh]	Mass Loss [wt.%]
+150 -65	0.31
+400 -150	0.51
-400	6.0

had been removed exhibited a loss of weight upon rousing in air (Table 24). The weight loss can be attributed to the combustion of residual organic material, to the removal of chemically bonded water from clays and silica, and to the decomposition of ferric carbonate. The weight loss contribution due to burning residual organics has been estimated 30% for the -400 mesh fraction of the Whiterocks tar sand sample. A more detailed study on residual organic material on the extracted and tailing sand, including contact angle and electrophoretic mobility measurements, and FTIR spectra analysis, is contained in the 1990/91 research program.

Effect of Kerosene on Bitumen Viscosity

The evaluation of selected organic solvents as diluents in the modified hot water process has been discussed previously[28]. Naphtha or kerosene were the recommended solvents for industrial application with the Athabasca tar sands, despite slightly greater dissolution power of some other solvents. The bitumen viscosity as a function of kerosene content in the bitumen-kerosene blend is presented in Figure 25. The amount of kerosene added depends on the original bitumen viscosity, tar sand grade, and temperature of
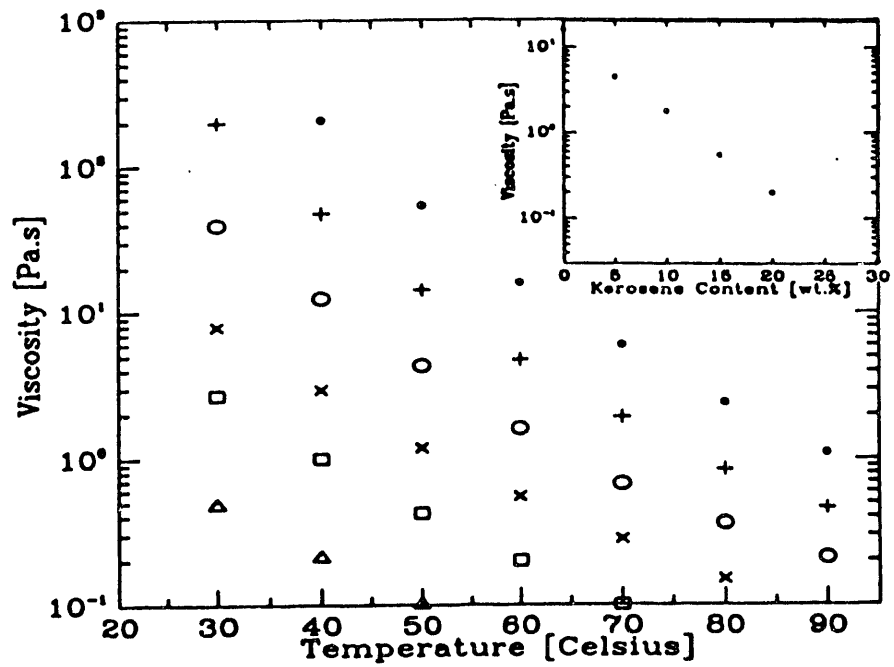
Figure 25. The Influence of Kerosene Content on the Viscosity of Whiterocks Bitumen

processing. The required amount of kerosene to obtain the optimum viscosity, 0.5 to 1.5 Pa·s, can be determined from the shaded region on the plot. The reduction of bitumen viscosity due to kerosene dilution can be also predicted using Vogel's equation[27], (Table 25). The calculated values correspond to the experimental data only at elevated temperatures. If the solvent content is more than 10 weight percent Vogel's equation cannot be applied (yields negative viscosity).

The dependence of bitumen viscosity reduction on kerosene or toluene content is presented in Figure 26. Linear regression analysis for both sets of data resulted in regression coefficients of 0.997 for kerosene and 0.988 for toluene. Comparing the slope of both lines it is evident that toluene exhibits a greater plasticizing effect than kerosene.

Summary and Conclusions

Whiterocks bitumen was found to exhibit Newtonian behavior (in the temperature range 40 to 90°C) which can be attributed, in part, to its low asphaltene content. The Whiterocks bitumen released 0.1% of its mass as lightends during rotoevaporation (vacuum 2.1 kPa, water bath temperature 85°C, cold trap temperature -79°C, time 16 hours). After 12 hours at these rotoevaporation conditions the residual toluene in bitumen compensated for the loss of lightends, and thus the impact on bitumen viscosity was negligible. The native bitumen may have a lower viscosity due to the presence of dissolved gases which are lost during bitumen preparation. The influence of residual toluene on bitumen viscosity diminishes with

118

Table 25. Bitumen Viscosity at Various Temperatures and Kerosene Contents

Temperature [°C]	Bitumen Viscosity [Pa·s]	
	5 wt. % kerosene	10 wt. % kerosene
30	110.00*	7.40
	198.00**	39.30
40	28.00	3.60
	47.30	12.40
50	9.00	1.20
	14.10	4.32
60	3.80	0.74
	4.70	1.60
70	1.60	0.40
	1.90	0.07
80	0.79	0.22
	0.84	0.36
90	0.44	0.14
	0.46	0.21

* Calculated value based on Vogel equation
** Experimental value.
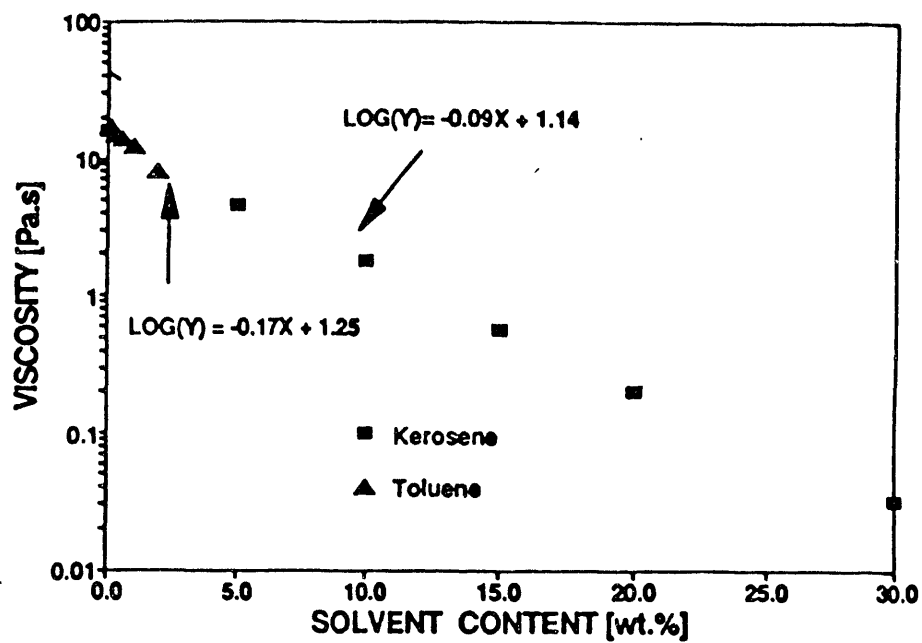
Figure 26. Plasticizing Effect of Kerosene and Toluene on the Viscosity of the Whiterocks Bitumen at 60°C

increasing temperature.

1. The Whiterocks bitumen was found to behave like a Newtonian fluid in shear (in the temperature range from 40 to 90°C). This behavior, in part, can be attributed to the low asphaltene   content of this bitumen.

2. The influence of residual toluene on the bitumen viscosity appeared to be balanced by the loss of light ends after 12 hours evaporation, therefore its influence was negligible. The measured viscosity also reflects the absence of high molecular, insoluble components of the native bitumens which were not removed from the sand granules in the extraction procedure. Thus, the viscosity determined for a sample of bitumen from

   which nearly all the solvent has been removed is a practical and reasonable estimate of viscosity of the native bitumen.

3. Approximately, 0.1 wt% volatiles from the Whiterocks bitumen were driven overhead at the rotoevaporation conditions (vacuum 2.1 kPa, water bath temperature 85°C, cold trap temperature - 79°C, time 16 hours).

4. The influence of residual toluene on bitumen viscosity diminishes with increasing temperature. In the system studied the difference at 30°C and 90°C was 100%.

THE INFLUENCE OF TAR SAND SLURRY VISCOSITY ON THE HOT WATER DIGESTION-FLOTATION PROCESS

Introduction

Mechanical energy is necessary for bitumen liberation from sand grains during the digestion step in hot water processing of tar sand. This energy is used for the development of a sufficient shear stress field in the tar sand slurry; the magnitude of the stress depending on the processing conditions and reactor design. The viscosity of the slurry plays a major role in the establishment of the stress field, as given below:

$$\tau = \mu_a (du/dx) \tag{9}$$

where: τ is the shear stress, Pa;

du/dx is the shear rate, s^{-1};

μ_a is the viscosity of a Newtonian fluid or the apparent viscosity for a non-Newtonian fluid, Pa s.

The highly concentrated slurry encountered in the digestion step of the modified hot water process is expected to behave like a non-Newtonian liquid and the apparent viscosity can be described by a power law correlation:

$$\mu_a = k(du/dx)^{m-1} \tag{10}$$

where: k   is the laminar consistency index; and;

m   is the flow behavior index.

The flow behavior index is a measure of the deviation of the

behavior of a given liquid from that of a Newtonian liquid. (m =1 for a Newtonian fluid; m <1 for a pseudoplastic fluid; m >1 for a dilatant fluid).

Simultaneously, in the turbulent flow field, bitumen droplets released from the tar sand may undergo disintegration, depending on the energy dissipation in the system, the physical properties of the liquid phases, and how far the system is from equilibrium. At equilibrium, the bitumen droplet size can be found from the relation[29]:

$$D_{32} = K(\sigma/\rho_c)^{0.6}E^{-0.4} \tag{11}$$

where: D_{32} is the Sauter diameter, m;

σ is the interfacial tension, mN/m;

ρ_c is the density of the continuous phase, kg/m^3 ;

E   is the dissipation energy, J; and;

K   is a constant.

In order to prevent unnecessary bitumen dispersion the residence time of the tar sand slurry in the digester after bitumen disengagement from the sand should be minimized.

Due to the very complex nature of the tar sand slurry during digestion the slurry rheological behavior is difficult to model or to measure in situ. The viscosity of tar sand slurry changes with time due to the bitumen liberation process during digestion. Initially a bitumen film exists around almost every sand particle, additionally serving as the binding medium for the tar sand aggregates. When in contact with the alkaline aqueous phase,

123

bitumen (of the proper viscosity, controlled by temperature or diluent application) forms droplets which are separated from sand under the influence of shear forces. Gradually all unconsolidated tar sand aggregates disappear leaving a suspension of dispersed bitumen droplets and mineral particles.

The method used to investigate the impact of tar sand slurry viscosity on the hot water separation efficiency includes calculation of slurry viscosity from several equations reported in literature, and experimental measurements to determine how the tar sand slurry viscosity varies with percent solids during digestion.

Viscosity of the Tar Sand Slurry

Evaluation of the relative viscosity of the tar sand slurry during digestion has been carried out using several equations selected from the literature which describe the relationship between relative viscosity and concentration for dispersed systems[30-33]. These equations had been originally formulated for a specific type of dispersion (usually uniform rigid spheres), a restricted range of concentration, and a particular shear rate. A limited number of equations include solids concentrations above 50 volume percent the concentration most often encountered in tar sand processing.

The following equations were used to estimate the tar sand slurry viscosity:

1) Bednarski[30]

$$\mu_s = \mu_1 [1+k/\psi_s \cdot \phi_e/(1-\phi_e)]$$ (12)

where: μ_s is the viscosity of the slurry, cps;

μ_1 is the viscosity of bitumen-in-water dispersion

(calculated to be 0.7 cp at 80°C), cps;

k   is a proportionality constant (for particles of size from 0.1mm to 0.001mm k = 30);

ψ_s is the shape factor (assumed to be 0.8); and;

ϕ_e is the volume fraction of solids in the slurry.

2) used by Goddard and reported by Cheng[31]:

$$\mu_s = \mu_1 \cdot 9/8 \cdot (\phi_e/\phi_m)^{1/3}/[1-(\phi_e/\phi_m)^{1/3}]$$ (13)

where: ϕ_m is the maximum volume fraction of solids in the

slurry (approximately 0.62).

3) derived by Eiler and reported by Rutgers[32]

$$\mu_s = \mu_1 [1+1.25\phi_e+3.0\phi_e^2)/(1-1.5\phi_e)]^2$$ (14)

4) derived by Mooney and reported by Rutgers[32]:

$$\mu_s = \mu_1 \cdot \exp[2.5\phi_e/(1-1.4\phi_e)]$$ (15)

The dependence of slurry viscosity versus percentage tar sand, assuming that the temperature is 80°C and tar sand composition is 13 wt.% bitumen and 0.8 wt.% water, is presented in Figures 27 through 29.   The bitumen has been treated as a solid (which corresponds to the beginning of digestion) and as a liquid, present in the slurry in the form of oil-in-water emulsion (which corresponds to the final state of the slurry after bitumen liberation from the sand).   The initial moments of digestion are

very poorly represented here because it was necessary to assume that the suspension consisted of individual sand particles covered by a film of bitumen.

A significant change in consistency can be expected for solids contents in the slurry of greater than 40 volume % (Figure 27-29). Above 50 volume %, a region of great uncertainty exists because the viscosity can vary by an order of magnitude for a small change in solids content. Viscosity values estimated from the above mentioned equations differ within 20 to 100% depending on the assumptions and the mechanism of particle-particle interaction assumed in the derivation of each equation. The mineral particle size distribution is not taken into account by the equations which seriously limits their applicability to a complex systems such as a tar sand slurry.

An experimental verification of the above equation will be considered during 1990/91 after evaluation of various viscometers, suitable for slurry consistency measurements. The rheology of Newtonian and non-Newtonian suspensions have been presented in many papers, dealing mostly with model systems, but also with some actual slurries. The methods and viscometers used in these studies are reported in Table 26.

Water-Based Bitumen Recovery Experiments

Procedure

Tar sand surface samples from the western outcrop of the Whiterocks deposit were used for bitumen recovery experiments in the laboratory. The ore contained 7.8 wt.% bitumen. The bitumen

126
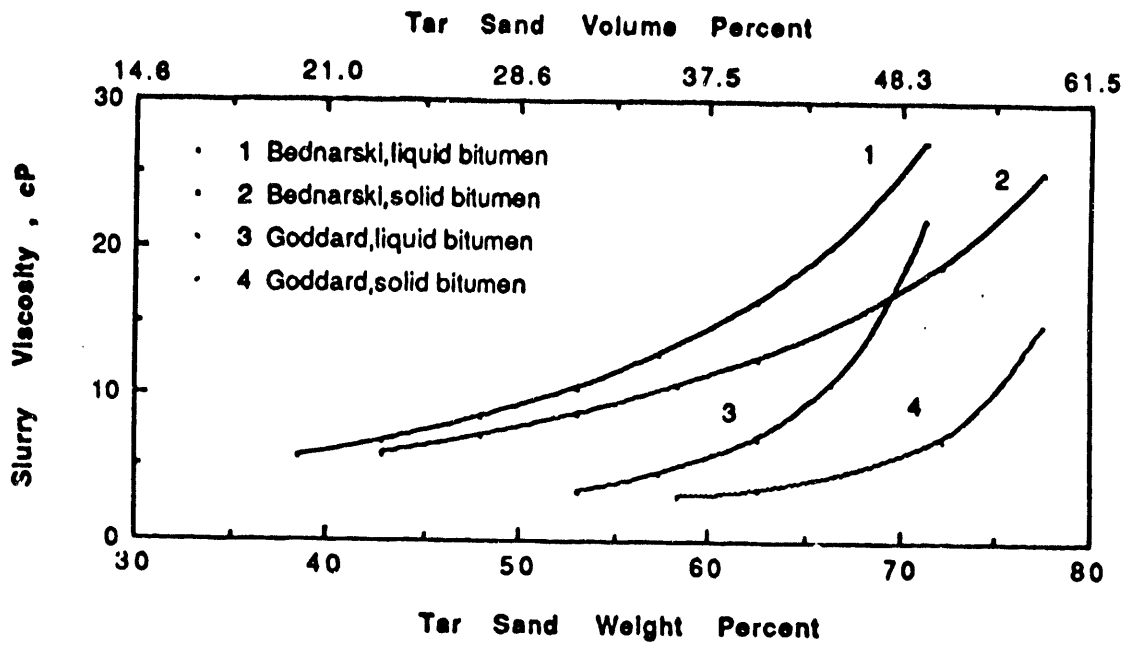
Figure 27. Calculated Viscosity of Tar Sand Slurry
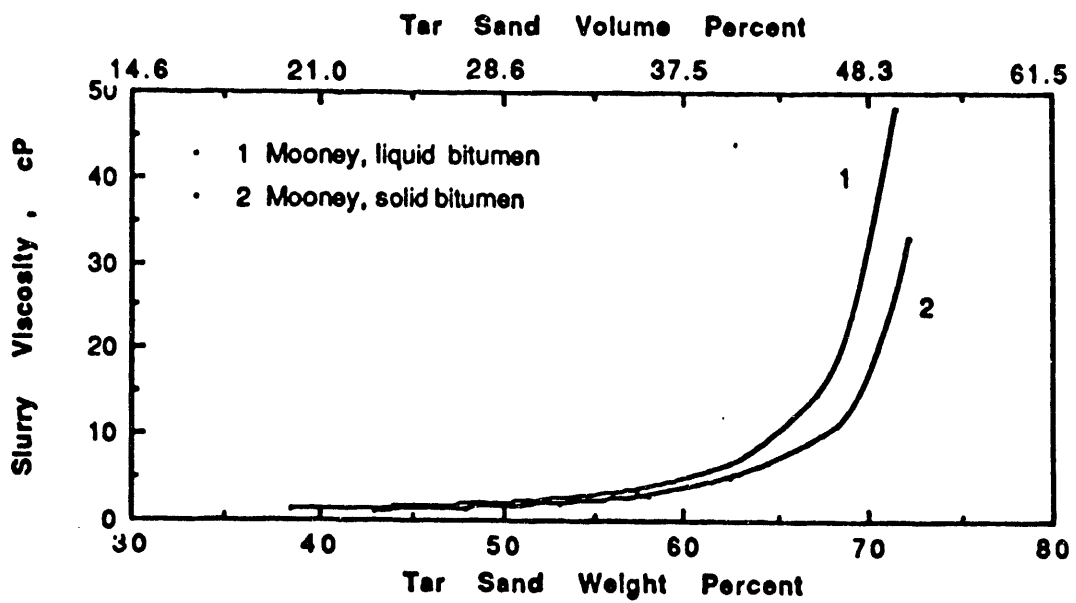
Figure 28. Calculated Viscosity of Tar Sand Slurry

127
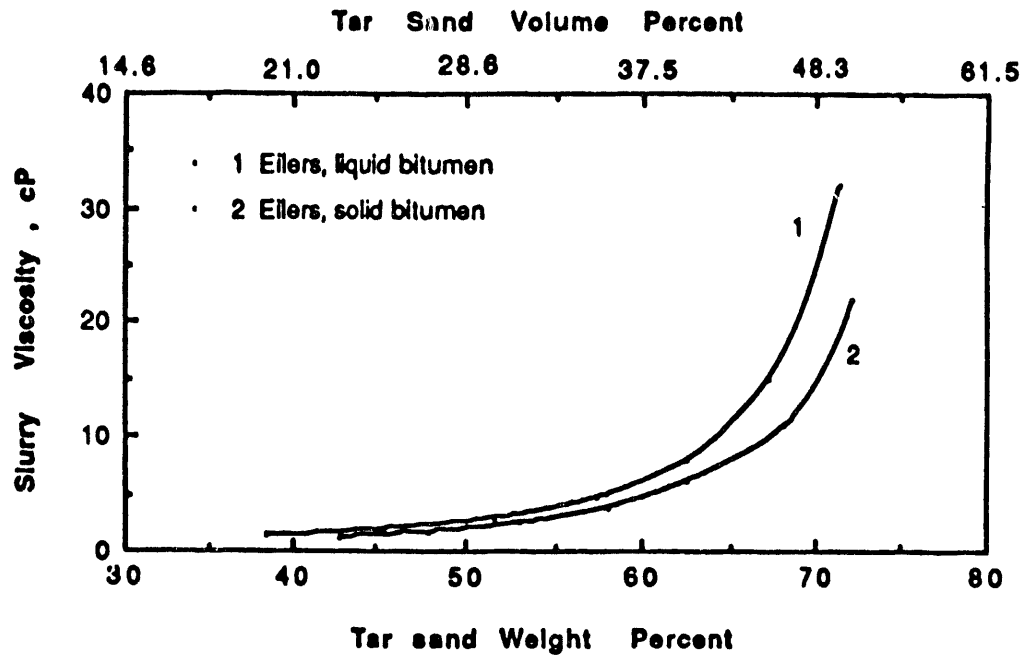
Figure 29. Calculated Viscosity of Tar Sand Slurry

128

Table 26. Comparison of Viscometers and Experimental Conditions Used for Slurry Rheology Research

Types of Viscometer	Kind of Slurry	Solid Percent Volume Fraction %	Slurry Stability	Particle Size (Microns)	Rheological Behavior	Temperature °C	Viscosity Limit (Pa.s)	References
Capillary tube	Polystyrene+ ethylene glycol	< 20	---	84 - 398	nN*	25-37	< 0.05	5 - 33
Haake Rotovisco	quartz and coal + water	< 60	stable	20 - 200	N**	< 25	< 1.0	6 - 34
Orifice	glass beads + polyisobutylene	< 65	stable	25 - 250	N	20-40	---	7 - 35
Couette Rheometer	coal + coal derived solvents	< 50	stable	< 75	N	25-500	---	8 - 36
Rotary Viscometer	coal + creosole oil, tetralin	< 35	stable	10 - 230	--	25-400	< 12.0	9 - 37
Rheometrics	methyl-methacrylate + decalin	< 55	stable	10 - 100	nN	20-50	---	10 - 38
Rotary with revolving mixer modified (Searll type)	quart and hematite + silicone oils	< 55	stable	10 - 100	nN	20-50	---	11 - 39
Submersible (pendulum type)	quartz + water	< 55	---	---	nN	---	< 0.11	12 - 40

*nN = non-Newtonian
**N = Newtonian

129

had a viscosity of 2.5 Pa·s (2.5×10^3 cp) at 90°C. Feed material was prepared by mechanical crushing and mixing, according to the procedure described earlier. The crushed ore was subsequently sprayed with kerosene. A pretreatment time of two hours was allowed for the kerosene to penetrate into the tar sand and dilute the bitumen phase.

Batch hot water (55 to 60°C) separation tests were performed in an agitated, baffled stirred-tank reactor (3.8 L) equipped with two turbine impellers (75 wt.% solids). The bitumen was separated from the sand by batch gravity separation (40 wt.% solids) and by batch flotation in a Denver-type 38 liter flotation cell (20 wt.% solids). The air flow rate was fixed at five liters/minute and a flotation time of 10 minutes was used for each test. The bitumen concentrate was collected as a function of time, for the study of the flotation kinetics. Sodium carbonate and sodium tripoly-phosphate (one gram Na_2CO_3 and 0.5 gram of $Na_5P_3O_{10}$ per kilogram of tar sand, respectively) were added to the digester to control the pH and wetting ability of the aqueous phase. No flotation agents were used.

Results and Discussion

Results from hot water experiments with varying tar sand percent in the slurry are presented in Figures 30 to 34. The processing efficiency was evaluated by determining the bitumen contents in the concentrate and tailings, by determining the bitumen recovery in the concentrate, and by calculating the coefficient of separation (CS). The coefficient of separation is
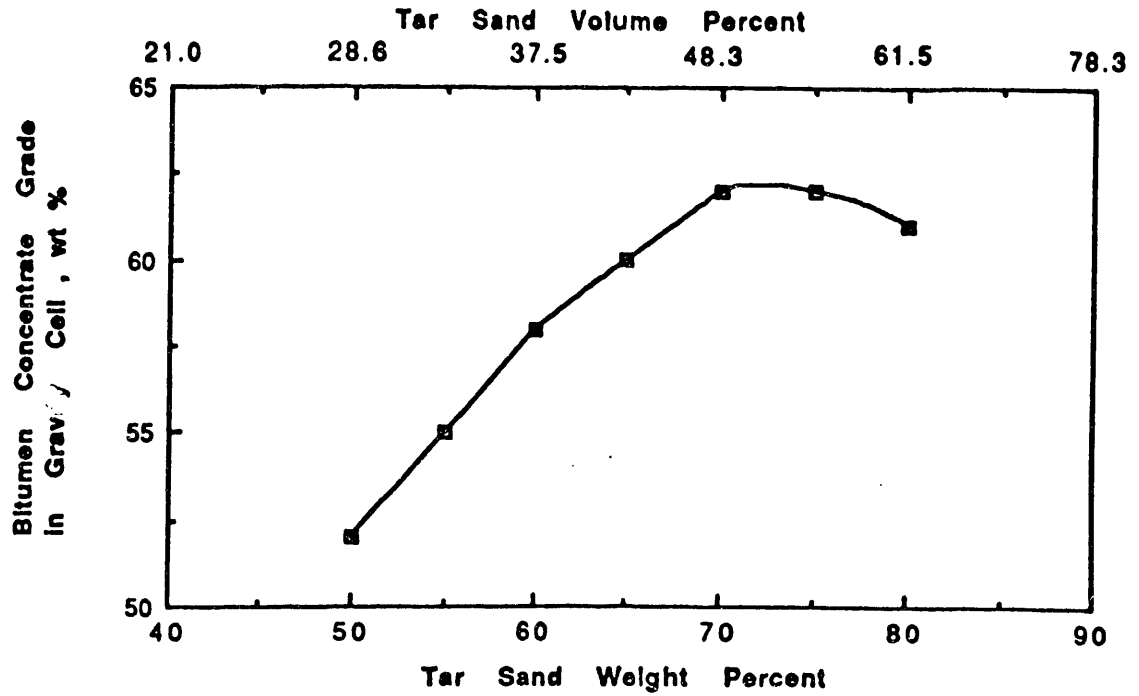
Figure 30.   Bitumen Concentrate Grade in Gravity Cell
versus Tar Sand Percent During Digestion
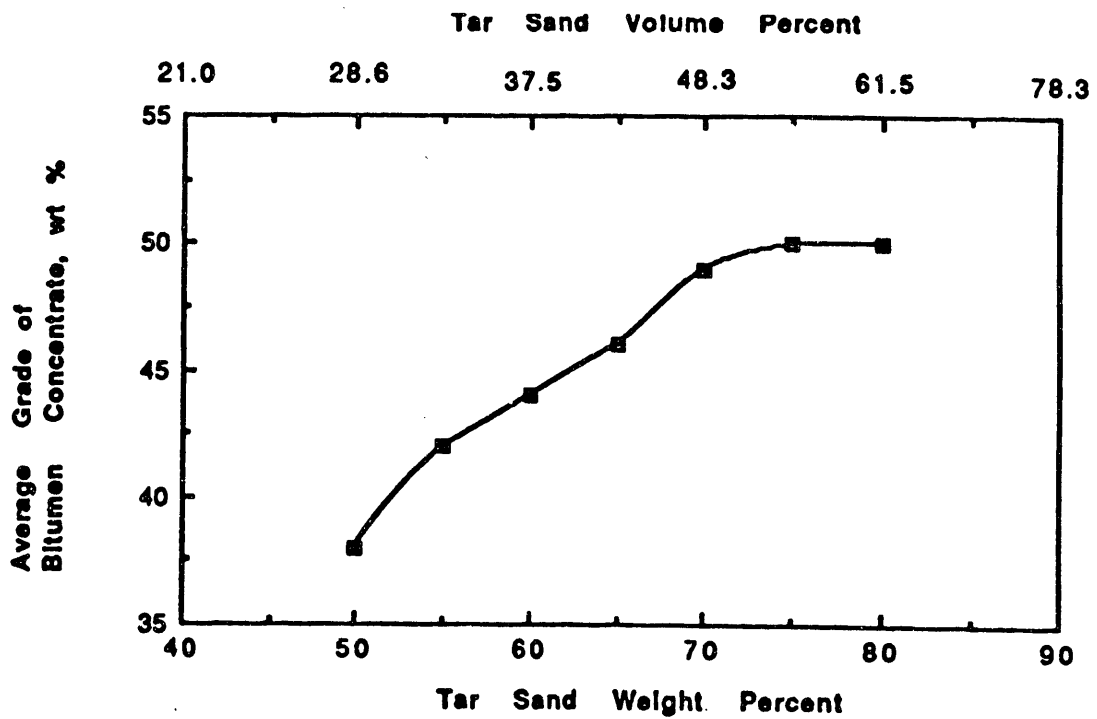
Figure 31.   Average Grade of Bitumen Concentrate
versus Tar Sands Percent During Digestion
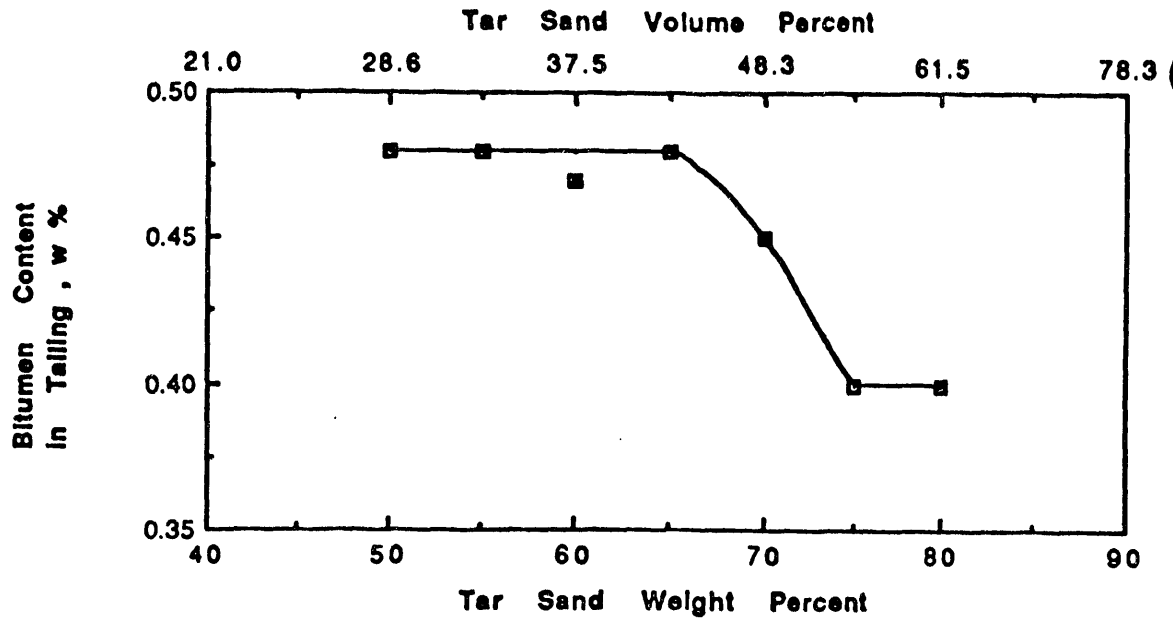
Figure 32. Bitumen Content in Tailings versus Tar Sand Percent During Digestion.
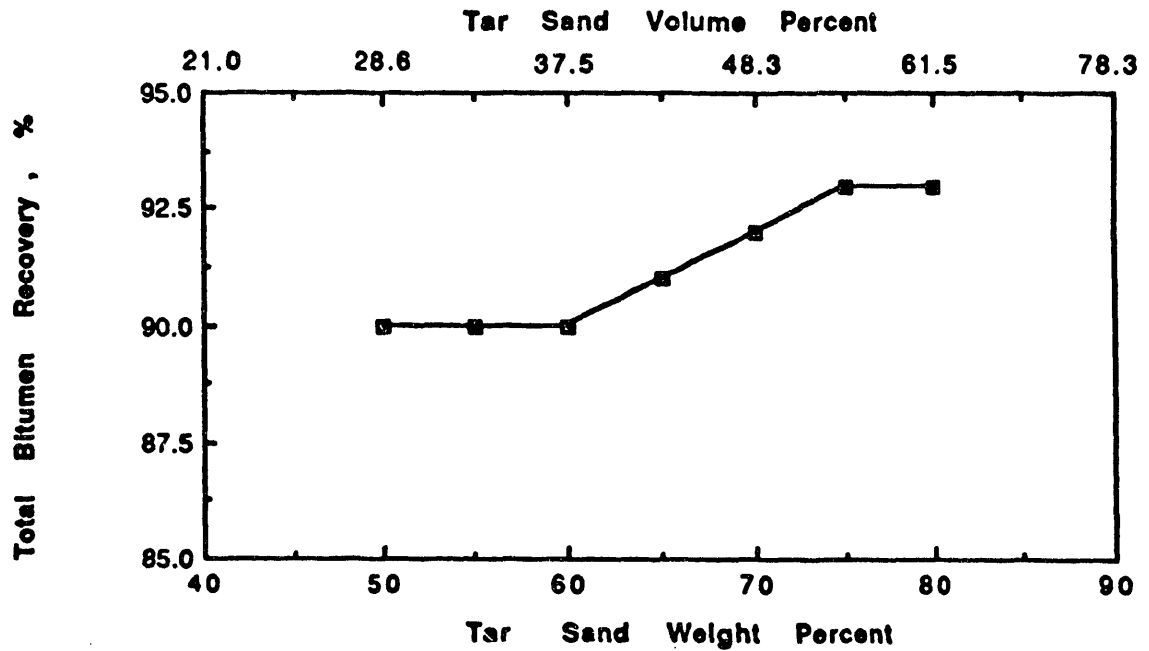
Figure 33. Total Bitumen Recovery in the Concentrate as a Function of Tar Sand Concentration during Digestion.
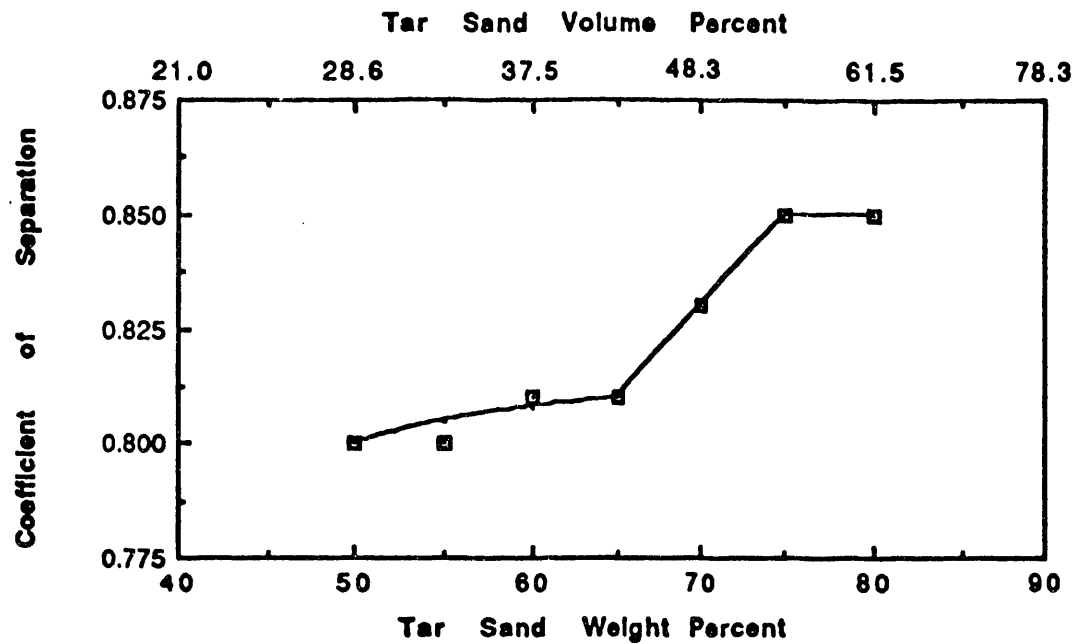
Figure 34. Coefficient of Separation as a Function of Tar Sand Concentration during Digestion.

an appropriate measure of the separation efficiency which is equal to the difference between weight percent recovery of bitumen and weight percent recovery of sand in the concentrate. The trends in all the plots indicate the impact of tar sand concentration in the slurry on the digestion during process efficiency. A significant portion of the impact may be related to the diminished shear force field at lower solids contents in the slurry during digestion. The development of the shear force in the digester is a function of the slurry viscosity. The grade of the bitumen concentrate in the gravity cell increases steadily with an increase in percent tar sand reaching a maximum at 75 wt% (Figure 30). Similar results were obtained for the combined concentrates from gravity separation and flotation (Figure 31). Simultaneously, residual bitumen content in tailings dropped significantly in tests in which the weight percent solids exceeded 68%. These results may also be attributed to the increased shear developed in more concentrated slurries (Figure 32). The overall bitumen recovery did not change due to the extended flotation time, amounting to 10 minutes, which was intended to provide sufficient residence time to recover the bitumen attached to sand grains (Figure 33). The coefficient of separation, on the other hand, remained practically constant at low weight percent tar sand, and then increased significantly to 0.85 for slurries containing more than 65 wt% tar sand. (Figure 34).

Summary and Conclusions

The Whiterocks tar sand slurry viscosity was varied by changing the composition of the pulp during digestion. The separation efficiency increased with an increase in percent solids

reaching a maximum at 70 weight percent tar sand and above. The bitumen recovery and concentrate grade from the gravity cell were significantly influenced by changes in the slurry viscosity while the flotation kinetics remained almost unchanged. The slurry viscosity is expected to strongly influence the shear force field available in the conditioning vessel used for tar sand digestion. Slurry viscosities calculated from several semiempirical formulae vary by an order of magnitude for a small change in solids content when the solids content in the slurry exceeds 50 volume percent.

DEVELOPMENT OF A MODERATE TEMPERATURE SEPARATION PROCESS FOR TAR SANDS

Limitations to Bitumen Recovery

The efficiency of bitumen recovery from tar sands by the hot water digestion-flotation technique depends not only on the process operating variables but also on the origin of the tar sand. The importance of bitumen viscosity on the separation efficiencies has been shown to be significant for all tar sands tested and has led to the development of the modified hot water separation technology[7,41]. It was found that the bitumen viscosity must be reduced below 1.5 Pa.s (15 Poise) to achieve a satisfactory coefficient of separation at the temperature of digestion and that a predetermined conditioning time, termed penetration time, may be necessary for the diluent to effectively interact with the bitumen thus reducing its viscosity. Generally this was the case regardless of the tar sand origin and characteristics. More detailed studies on Athabasca tar sands have indicated that bitumen recovery can also be correlated with tar sand grade[42], fraction of fine solids[43], solids mineralogical composition, chemical composition of the bitumen and the surfactant released to the aqueous phase[43].

Large streams of tar sand slurry have to be handled in the water based separation technologies, therefore, gravity separation after digestion is desirable from a materials handling point of view. Unfortunately, gravity separation of the bitumen from the sand accounts for only a small fraction of the total bitumen recovered for most tar sands even after diluent pretreatment.

The exception is the Athabasca tar sands which contain a bitumen of favorable density and viscosity for gravity separation.

A detailed process model of the hot water separation mechanism has not yet been developed. Nevertheless, near optimum values of the controlling variables (temperature, mechanical energy, wetting agents dosage, solids/water amount) are known and used in practice, resulting in satisfactory separation efficiencies for most tar sand samples tested. An example of a tar sand for which poor separation results were obtained despite running the hot water separation tests at optimal experimental conditions, is the Whiterocks tar sand (Figure 35). The Whiterocks tar sand contains a bitumen of moderate viscosity which can easily be diluted with an appropriate amount of an organic solvent, such as kerosene, with a penetration time of less than two hours at 20°C. This bitumen-impregnated sandstone is an unconsolidated tar sand which means that the sand grains are, generally, not cemented with calcareous or siliceous material. However the Whiterocks tar sand does contain a significant amount of fine mineral particles, of which 10% by weight pass through 400 mesh (38 μm) and 75% by weight pass through 65 mesh (210μm). Unlike the Whiterocks tar sand, other tar sands of similar fines content yield higher grade bitumen concentrates during the modified hot water separation process[7]. It appears that these differences can be attributed to the mineralogical composition of the sand and to the different chemical composition of the bitumen from the Whiterocks tar sand deposit.
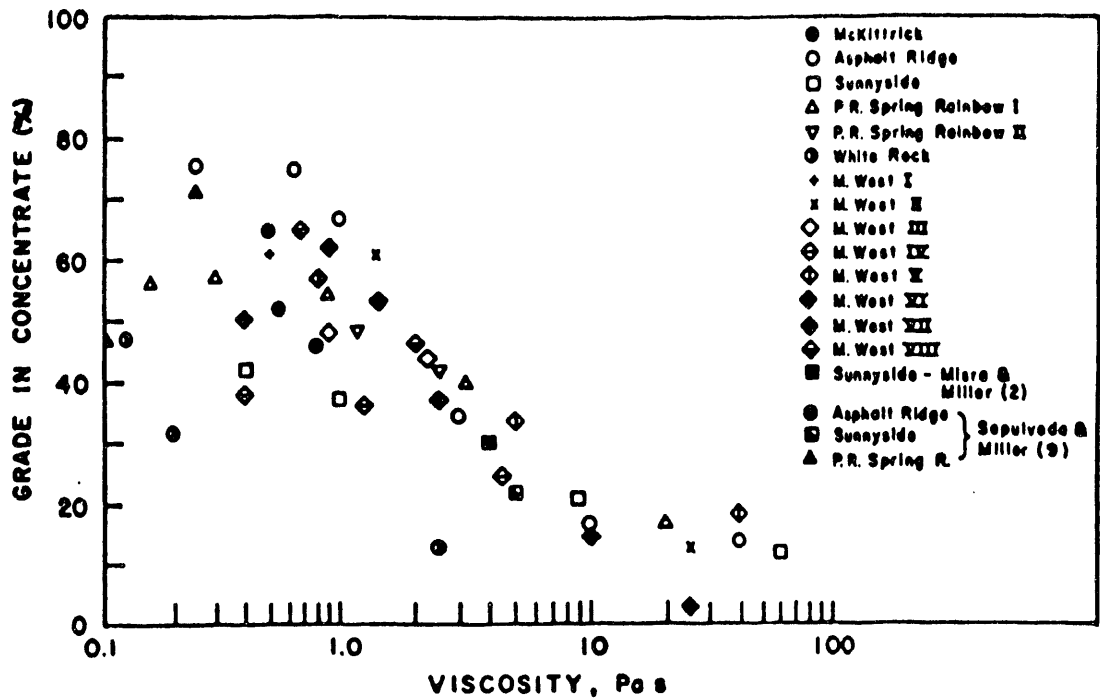
Figure 35. Concentrate Bitumen Content versus Bitumen Viscosity at the Temperature of Digestion

Most of the tar sands tested have been shown to be amenable to bitumen recovery by the modified hot water process, nevertheless bitumen recovery by gravity separation does not yield a high percentage of the recovered bitumen and hence the need for flotation. These limitations to bitumen recovery have led to the development of a new processing strategy.

The New Method

One reason for the relatively poor separation of bitumen after digestion (influencing the overall bitumen recovery and separation efficiency) can be the insufficient wetting power of conventionally used sodium hydroxide or sodium carbonate solutions as dispersents. Also, interference from polyvalent cations present in the aqueous

138

phase may limit the efficiency of the separation. In order to improve the digestion step a controlled amount of sodium tripolyphosphate was added to the aqueous phase, in addition to sodium carbonate, before mixing with the diluent-pretreated tar sand. After several minutes of digestion at 50 to 60°C the slurry was discharged into a container and diluted with an equal amount of warm water, gently agitated and left one minute for gravitational separation of the bitumen from the sand. The bitumen was skimmed from the surface of the cell. Unexpectedly, a very high quality product was obtained. In the case of the Whiterocks tar sand (with the exception of the north-west location of the deposit) more than 50% bitumen was recovered, containing, on a dry basis, over 55 wt.% bitumen. These results should be compared to the poor gravitational release of bitumen in the absence of sodium tripolyphosphate $(Na_5P_3O_{10})$. In warm aqueous solutions tripolyphosphate is known to gradually lose its dispersing ability which is accentuated above 60°C, due to hydrolysis and degradation to the orthophosphate. Therefore a moderate temperature for digestion and bitumen separation (gravity separation and flotation) should be maintained. The gravity separation data on Whiterocks and Asphalt Ridge tar sands are presented in Table 27. In addition to experiments in which fresh water was used, Table 27 also contains data for experiments in which 80% water (containing up to five percent fine solids) was recycled, simulating the continuous process. The beneficial effect of sodium tripolyphosphate addition was also observed in the recycle water experiments. As indicated

Table 27. Influence of Surfactant Addition on Tar Sand Processing

Tar Sand Sample	Gravity Conc. Bitumen Grade wt.%	Recov. %	Flotation Conc. Bitumen Grade wt.%	Recov. %	Tailings Bitumen Grade wt.%	Recov. %	Sedimentation Solids in Water for Recycle ppm
Fresh Water Processing							
Asphalt Ridge							
– with phosphate	78	80	49	20	<0.1	<0.1	200
– without phosphate	75	40	56	58	0.4	2	700
Whiterocks (W-C)							
– with phosphate	57	36	31	57	0.6	7	170
– without phosphate	55	14	32	77	0.7	9	
Whiterocks (N-W)							
– with phosphate	60	22	35	70	0.8	8	440
– without phosphate	62	11	40	81	0.9	8	950
Recycled Water Processing (6 recycles; 80% water recycled)							
Whiterocks (W-C)							
– with phosphate	58	41	36	52	0.5	7	1140
– without phosphate	51	14	34	78	0.6	8	1880
Whiterocks (N-W)							
– with phosphate	62	29	39	64	0.7	7	640
– without phosphate	51	1–	37	82	0.9	8	2130

Tripolyphosphate concentration: 0.5g kg^{-1}

140

in the block diagram (Figure 36) both gravity separation and air flotation are used for bitumen recovery from the digested tar sand slurry due to the broad size distribution of the bitumen droplets. Large bitumen droplets are separated in the gravity cell, while fine bitumen droplets require flotation for fast and complete recovery.

Finally, with respect to tailings disposal, it should be noted that sodium tripolyphosphate undergoes hydrolysis to orthophosphate (acting as a mild flocculating agent), the hydrolysis being accelerated above 60°C. Therefore after fines sedimentation the tailings water should be heated (to such a temperature that the amount of heat introduced equals the total amount of heat loss in the processes of digestion, gravity separation, flotation and tailings disposal/water recycle) in order to stimulate tripolyphosphate decomposition.

In this manner the recycled water serves also as a heating medium during gravity separation and flotation. Consequently additional, unnecessary heating of the coarse and fine sand (more than 95% of the total mineral matter) is diminished. Steam heating systems for the gravity separation and flotation are also avoided. Under these conditions most of the process water can be directly recycled, as indicated on the flowsheet presented in Figure 36, while the aqueous phase present in the combined tailings sand (coarse sand and fine sand slurry) is sufficient for hydraulic transport of the tailings sand to the disposal site.

Figure 36. Block Diagram of Hot Water Separation Process for Bitumen Recovery From Tar Sands

142

The new process strategy embodies the following advantages:

- Low process temperature thus there exists the potential for significant thermal energy savings with respect to conventional hot water processing strategies.

- Moderate mechanical energy is required for phase disengagement, thus there is a possibility for digestion under low shear conditions such as encountered in a rotating drum.

- Higher grade combined concentrate, from the gravity and the flotation cells.

- Very clean tailings sand which may be used for valuable minerals recovery and other purposes.

- Complete water recycle, thus reducing potential pollution hazard.

- Suspended mineral fines are tolerated in the recycled water allowing a short sedimentation time and flocculent savings.

- Improved sedimentation of fine mineral particles due to tripolyphosphate conversion to orthophosphate.

The tar sand (solvent conditioned if necessary) is digested in a solution of sodium carbonate and sodium tripolyphosphate having a weight ratio of 2:1 based on the anhydrous compounds. The total concentration of each additive should range from 0.5 to 1.5 g per kg of tar sand depending upon the bitumen content and chemical composition. The pH of the aqueous phase, at any stage in the process, should remain below 11. The slurry from the digester was transferred to a settler after screening, diluted with warm, fresh water, stirred gently with steam, to which 0.1 to 0.5 volume

143

percent air is added — and the bitumen was skimmed from the surface. The solids concentration in the gravity separation step is 40 wt%. After bitumen skimming the slurry undergoes flotation with a controlled amount of air corresponding to 0.1 to 0.15 liter per minute per liter of slurry in the first two minutes of flotation and 0.2 to 0.3 liter per minute per liter of slurry in the next two minutes. The solids concentration during flotation is 20 wt.%. The ionic strength of the aqueous phase, expressed as specific conductivity, should remain below 10 $mScm^{-1}$. The temperatures during digestion, gravity separation, flotation and fines sedimentation should not exceed 60°C. After the thickening step the process water is heated to above 65°C. Other processing conditions are indicated on the block diagram (Figure 36).

Summary and Conclusions

A moderate temperature (50-60°C), water-based tar sand recovery process, specific to deposits containing high viscosity bitumens has been developed. Adequate diluent pretreatment combined with a dispersing agent, sodium tripolyphosphate, made it possible to recover a significant portion of the bitumen in a gravity cell as a high grade concentrate. It was observed that recycling process water containing four to five weight percent suspended matter had no deleterious effect on the separation efficiency when sodium tripolyphosphate was used, which indicates that the sedimentation time of the tailings in the thickener can be significantly reduced.

THE EFFECT OF ELECTRIC FIELD PULSATION FREQUENCY ON BREAKING WATER-IN-OIL EMULSIONS

Introduction

It has been known for over half a century that water-in-oil emulsions can be efficiently broken in an electrostatic coalescer. The reliability and effectiveness of electric field dehydrators contributed to their wide application, particularly in the petrochemical industry since the early work by Cotrell in 1911[44]. Alternating, direct, and direct-pulsating electric fields and combinations have been used in dehydration equipment[44,45]. Renewed research interest in emulsion separation in the presence of electric fields has resulted, in part, from its usefulness in liquid membrane processes, implemented for industrial scale-up by Li in the late sixties[46]. The data obtained by many authors indicate that a high voltage electric field exerts a beneficial effect on the separation kinetics for liquid membrane emulsions [47-52] as well as for emulsions originating from conventional solvent extraction processes[53,54].

The facts that water droplets can oscillate at the electrical field frequency[55], and that electrically generated vibrations at the water-oil interface can promote coalescence[56] have been known for some time. Nevertheless, the electric field pulsation frequency was considered a rather unimportant variable in dehydration processes[57,58]. Little attention was directed to this phenomenon until the last decade, when separation in electric fields received new attention as a promising method for the separation of stable,

145

high water content (30-50%) emulsions, such as encountered in liquid membrane processes. The existence of an optimum in water separation efficiency versus DC electric field pulsation frequency was first reported by Bailes & Larkai in a series of papers published in the early eighties[59-61]. The separation efficiency reached an optimum in the frequency range 2.5 to 13.5 Hz depending on the thickness of the insulation (polymethylmethacrylate) layer on the electrode. The effect was very clear for voltages up to 800 volts and for very concentrated emulsions (up to 50% water). The effect of a high frequency electric field has been reported for liquid membrane emulsions[62-65]. Satisfactory separations were obtained for such systems at 500 Hz (the highest frequency generated in the cell) in combination with a DC electric field[62]. High-speed photography showed that water droplets vibrated with a frequency several times greater than that of the electric field. There are also reports of industrial application of a high voltage electric cell of a special design for the treatment of phenolic waste water by means of liquid membranes[63,64]. An AC field[63] and a modulating pulse wave field[64] were used in these applications. The best results were obtained in the range of 200 to 8000 Hz. A linear correlation between the separation efficiency for a stabilized acid solution in kerosene emulsions and frequencies in the range of 200 to 2000 Hz has been reported[65].

Additional effects which should be investigated include: drop vibrational frequency[62,66], electrical properties at the interface[61], dipole moments of the drops[66], and the average magnitude of the

electric field imposed on the emulsion[64,67].

The present study was intended to determine the impact of the pulsation frequency on the separation efficiency for a water-in-oil emulsion with a water content below 0.2% over the frequency range used by Bailes & Larkai[59-61]. Thin insulating layers were used on the anode to prevent short-circuiting. No surfactant were used for emulsion stabilization thus resulting in shorter coalescence time between colliding water droplets.

Experimental

Emulsion Preparation

Distilled water of specific conductivity: 9×10^{-6} scm^{-1}, was emulsified in an aromatic solvent having a density: 702 kg/m^3, viscosity: 1.12×10^{-3} Pa.s and dielectric permittivity: 2.1. Emulsification was accomplished in a homogenizer (type MPW-302, Precise Mechanics Works, Warsaw) for one minute at 10,000 rpm and a volumetric phase ratio (aqueous to organic) of 1:100. The emulsion was subjected to sedimentation for 40 minutes to eliminate larger water droplets.

Experimental Apparatus

An electrostatic coalescence cell (ECC) constructed of polymethylmethacrylate, with dimensions 150 mm x 100 mm x 70 mm was used in the study. The system was comprised of two electrodes: a cathode (copper plate) fixed to the bottom of the cell and an anode installed in the cell cover guides which made setting and replacement of this electrode possible. The anode was made of

copper sheet insulated with epoxy resin having a dielectric permittivity 3.6. The thickness of insulation was either 0.2 mm or 2 mm. The protective coating was used to prevent short-circuits. A high voltage pulse generator was used having the following characteristics; current: one mA, voltage: up to 20 kV, electric current pulsation frequency: from four to 30 Hz.

Procedure

A schematic of experimental apparatus is presented in Figure 37. The water/oil emulsion (having the water droplet size distribution presented in Figure 38) was fed from a storage tank to the ECC with a metering pump . The distance between the electrodes was adjusted to 20 ± 2 mm. The emulsion leaving the cell was diverted to a settling tank in which large droplet were separated by gravity in two minutes. The Karl Fisher method was used for water determination in both the original and processed emulsion. The water droplet size distribution was determined with a MP-3 projection microscope (Polish Optical Works, Warsaw) at 1000x magnification. The dielectric permittivitoes of the water/oil emulsion and the extraction solvent were determined experimentally in a cylindrical capacitor using a Wheatstone bridge. The permittivity of the emulsion was found to be between 2.10 and 2.16. The strength of the electric field generated in the cell was calculated from the following equation[68]:

$$E = \frac{U}{(i/\varepsilon_1 + d/\varepsilon_2)\varepsilon_1} \tag{16}$$

148
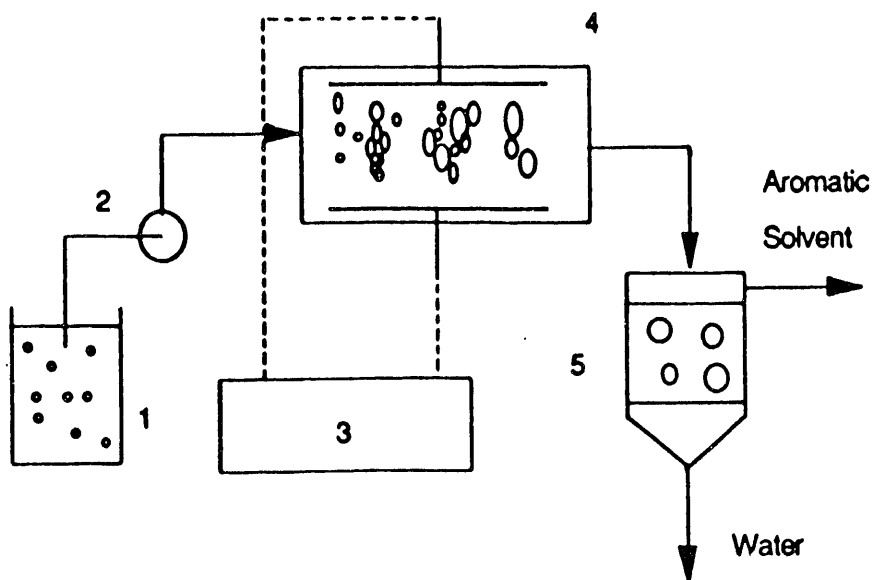
Figure 37.   Schematic of Experimental Apparatus; 1. o/w
                  Emulsion Container, 2. Metering Pump, 3. High
                  Voltage Generator, 4. Electrical Cell, 5.
                  Settler.
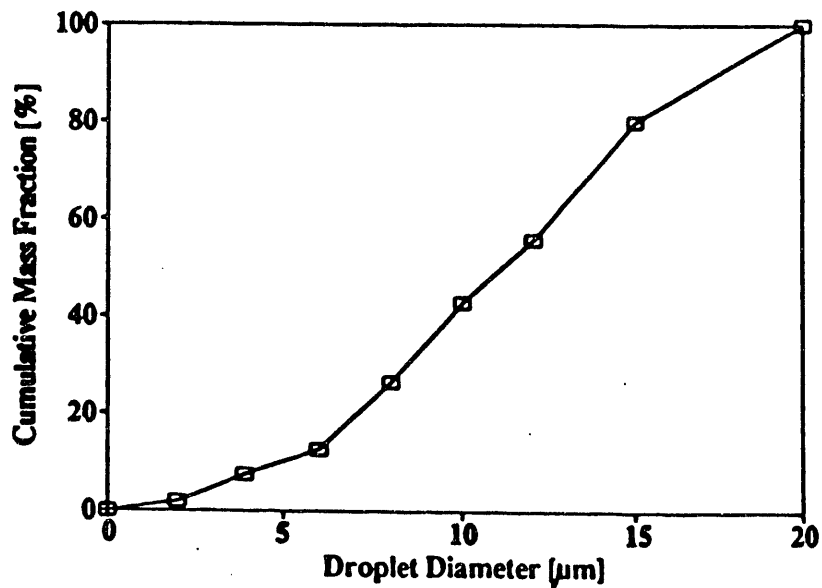
Figure 38.   Water Droplet Size Distribution.

where:

U is the applied voltage, V;

L is the distance between electrodes, m;

d is the thickness of insulation, m;

ε_1 is the permittivity of the emulsion; and,

ε_2 is the permittivity of the anode insulation.

The efficiency of the separation process was calculated from the difference in water content before and after processing divided by the value of the initial water content.

Results and Discussion

The effect of the electric field strength on the efficiency of phase separation is presented in Figure 39. The separation efficiency increases sharply until an efficiency of 63% is reached at approximately 140kV/m, while imposition of a higher voltage gradient up to 1100 kV/m improves demulsification only slightly. A simplified interpretation of the results will be presented here. Linear changes in the separation efficiency versus field strength are considered in the two ranges: 0 to 140 kV/m and 140 to 1100 kV/m. Thus the increase in water removal efficiency can be expressed by the linear function, $\Delta W/\Delta E = 3.8 \times 10^{-4}$ %m/V, for the first range and $\Delta W/\Delta E = 0.2 \times 10^{-4}$ %m/V for the second one. The data presented in Figure 39 corresponds to data obtained by Bailes and Larkai[69]. Bailes and Larkai[69] reported a transition point at approximately 30 Kv/m for concentrated emulsions containing more than 16% water and at approximately 100 kV/m for emulsions containing less than nine percent water. A stronger electric field

150
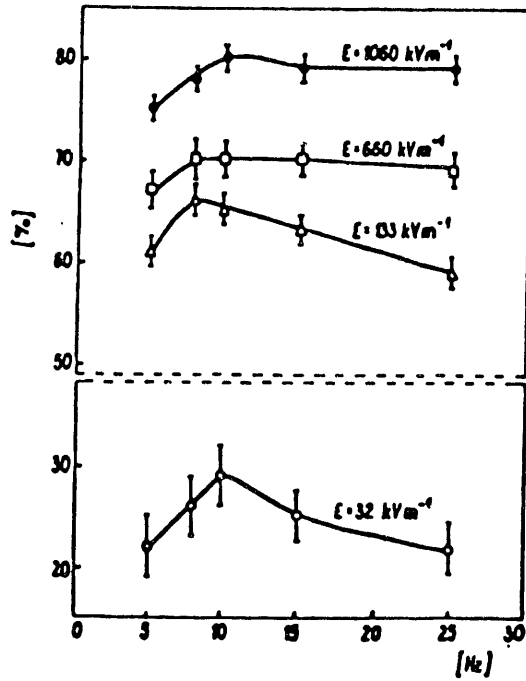
Figure 39. Water Separation Efficiency versus Electrical Field Strength

is required for dilute emulsions in which inter-droplet distances are greater, and a significantly greater electrostatic attraction is required to initiate the coalescence. Further, the extent of phase separation is reduced considerably as is evident from the data. The dependence of the phase separation efficiency on the electric field pulsation frequency is shown in Figure 40. At a frequency of eight to 11 Hz a slight increase in the efficiency takes place independent of the electric field intensity and a more distinct optimum is found at low intensity values. The increase in the phase separation effectiveness, however, does not exceed seven percent. Demulsification rates are similar for both anode insulation thicknesses (0.2 and 2 mm), providing essentially the same field strength (E_1 = 133 kV/m and E_2 = 140 kV/m) after a uniform electric field has been achieved. In the case of a thicker coating the phase separation is lower at an electric field pulsation frequency of less than 11 Hz. The results obtained confirm findings from the literature on the importance of electrode design for organic phase dewatering[59,67]. Of particular interest here is the insulation thickness[59] and eventually the kind of material used for insulation[47]. The impact of electrode insulation on the change in separation efficiency might be even more pronounced than the influence of field frequency itself (in the four to 25 Hz region) on time coalescence time between droplets.
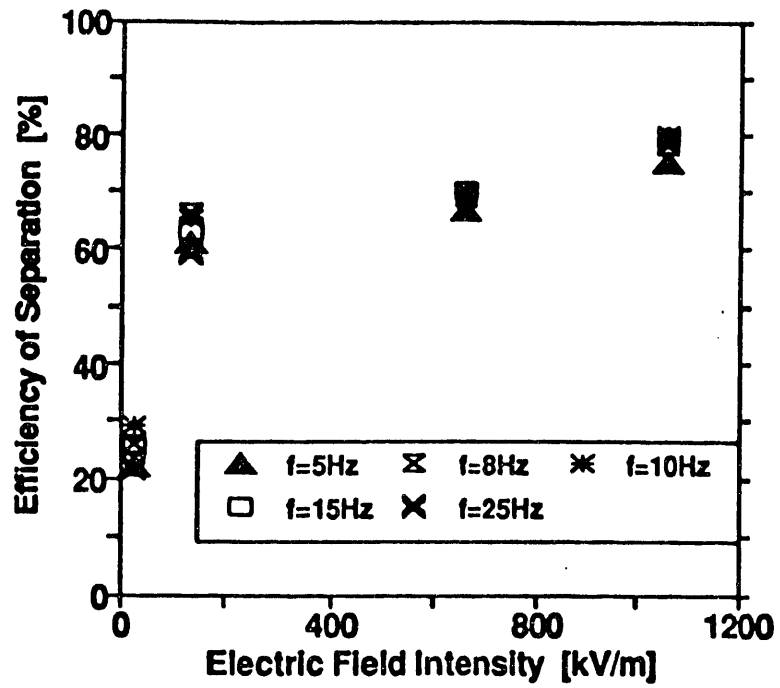
Figure 40. Water Separation Efficiency versus Field Pulsation Frequency (anode insulation thickness d = 2 mm)

Summary and Conclusions

A water-in-oil emulsion containing from 0.08 to 0.2% water has been separated with an efficiency exceeding 80% for a 25 second nominal residence time in a continuous flow electric field coalescence cell. The electric field strength was found to be the controlling parameter for demulsification. A rapid improvement in the separation efficiency was obtained when the field strength was increased up to 140 kV/m. However, the increase in separation efficiency was only 15% when the field strength was increased from 140 to 1100 kV/m.

The electric field pulsation frequency in the range studied (four to 25 Hz) exerted no significant influence on the demulsification yield for dilute and unstable water-in-oil emulsions (below 0.2% dispersed phase). Nevertheless, a separation optimum exists for pulsation frequencies between eight Hz and 11 Hz, particularly at lower field strengths. The increase in the separation efficiency optimum is larger by only five to seven percent.

154

Overall Summary and Conclusions

In the past year our attention has been focused on tar sands from the Uinta Basin of Utah which would be amenable for mining and processing in a demonstration plant, namely: Asphalt Ridge, Whiterocks, and Sunnyside. Four sections of the water-based processing technology report are devoted to the characterization of the native bitumens, the mineral matter associated with the tar sands and the tar sands themselves, whereas two sections are devoted to recovery process technology.

1. The analyses of the Whiterocks tar sand indicated that the composition of bitumens obtained from three different locations were similar. The most significant feature of the Whiterocks bitumen was the low concentration of asphaltenes. Kaolinites and carbonates were concentrated in the bitumen froth from the hot water process. The accumulation of kaolinites and carbonates in the bitumen froth solids can be explained based on their size and the presence of organic compounds on the particle surfaces. Although the precise nature of these adsorbed organic compounds is unknown, it was presumed that they contain carboxylic acid groups which would cause these species to adsorb on the mineral surfaces.

2. Whiterocks bitumen was found to exhibit Newtonian behavior (in the temperature range 40 to 90°C) which can be attributed, in part, to its low asphaltene content. The Whiterocks bitumen released 0.1% of its mass as light ends during rotoevaporation (vacuum 2.1 kPa, water bath temperature 85°C, cold trap

temperature -79°C, time 16 hours). After 12 hours at these conditions the residual foluene in the bitumen was found to compensate for the loss of light ends, and thus the impact on bitumen viscosity was negligible. The native bitumen may have a lower viscosity due to the presence of dissolved gases which are lost during bitumen preparation. The influence of residual toluene on bitumen viscosity diminishes with increasing temperature.

3. A study of the electrophoretic mobility of the Asphalt Ridge and Sunnyside tar sand components at pH 3 to 10 revealed that the surfaces of mineral particles, and of bitumen and kerosene droplets have a negative electrical charge. The zeta potential of bitumen droplets in tailings water at pH 8 to 9 (processing temperatures $\geq$ 60°C) was found to be -45 to -65 mV, while the zeta potential of the fine mineral particles was found to be -35 to -45 mV. These fine mineral particles will float with the bitumen droplets, but at a slower rate. Therefore the shorter the flotation time, the higher the grade of the bitumen concentrate. Of course, the smallest possible zeta potential for bitumen droplets is desired for most efficient flotation. Despite variations in the processing temperature and carbonate addition (which influenced the pH and ionic strength of the aqueous phase) and the use of tar sands from two different locations, no significant differences in the zeta potential curves were observed. Apparently in each run a sufficient amount of organic surfactant was present

156

at the bitumen and mineral fines surfaces to stabilize the negative surface charge. Additionally, the comparable negative electrical charge on both bitumen droplets and mineral particles suggests that bitumen gravity separation should precede flotation. Flotation could then be used to scavenge the remaining bitumen droplets.

4. The Whiterocks tar sand slurry viscosity was varied by changing the composition of the pulp during digestion. The separation efficiency increased with an increase in percent solids reaching a maximum at 70 weight percent tar sand and above. Both the bitumen recovery and concentrate grade from the gravity cell were significantly affected by slurry viscosity changes, while the flotation kinetics remained almost unchanged. The slurry viscosity is expected to strongly influence the shear force field available in the conditioning vessel used for tar sand digestion. Slurry viscosities calculated from several semiempirical formulae vary by an order of magnitude for a small change in solids content when the solids content in the slurry exceeds 50 volume percent.

5. A water-based tar sand bitumen recovery process (particularly, containing bitumen of high viscosity, which is typical for most U.S. deposits) characterized by 50-60°C moderate temperature has been finalized. Adequate diluent pretreatment combined with a dispersing agent, sodium tripolyphosphate, made it possible to recover a significant portion of the

bitumen in a gravity cell as a high grade concentrate. It was observed that the recycle of process water containing four to five weight percent suspended matter had no deleterious effect on the separation efficiency when sodium tripolyphosphate was used, which indicates that the sedimentation time of the tailings in the thickener can be significantly reduced.

6.   A water-in-oil emulsion containing from 0.08 to 0.2 weight percent water has been separated with an efficiency exceeding 80% for a 25 second nominal residence time in a continuous flow electric field coalescence cell. The electric field strength was found to be the controlling parameter for demulsification. The electric field pulsation frequency in the range studied (4 to 25 Hz) exerted no significant influence on the demulsification yield for dilute and unstable water-in-oil emulsions below 0.2 weight percent dispersed phase.

Future Activities

Unlike the Canadian tar sands of Alberta, the surface properties of Utah tar sands and their influence on the hot water process separation efficiency have not been studied extensively Characterization of all phases present during the digestion and flotation of the tar sand slurry should be conducted using FTIR spectroscopy, contact angle measurements, interfacial tension measurements, x-ray composition, analysis of fine minerals and hot water separation experiments. Particular attention should be given

158

to the microstructure of Utah tar sands and its impact on the water-based separation technology. In this regard, computer-aided x-ray tomography may be included as a research tool.

Investigation of the chemistry of the tar sand digestion process and its correlation with the mechanical energy required for satisfactory bitumen disengagement should be continued. Beside conventional dispersed air flotation other bitumen flotation techniques, including air sparged hydrocyclone and column flotation, need to be considered and tested. An optimization study would be required with respect to the amount of air and the properties of the aqueous phase for each flotation device. The bitumen concentrate clean-up research should be continued using modified electrostatic cells, including the study of the principal variables which control water and fine solids separation in a pulsating electrical field as well as the coalescence mechanism of both oil and water droplets. Finally, the impact of recycled water on the hot water process needs continuous evaluation including fines sedimentation and tailings thickening characteristics.

Extraction of Bitumen from Western Tar Sands

by An Energy-Efficient Thermal Method

Principal Investigator: J.D. Seader
Graduate Student: C.J. Coronella

Introduction

In order to accurately scale up and optimize a coupled fluidized-bed process for the thermal pyrolysis of Utah tar sands, an in-depth mathematical model has been under development for computer simulation of the process. Using the combustion bed as a starting point, a literature review, previously reported, was conducted to gather information on the hydrodynamics, transport, and kinetics of fluidized beds. The results of a simulation capable of predicting hydrodynamic characteristics, concentration profiles, and the mean conversion of O_2 and coke are presented here. In addition, a preliminary proposal is made for modification of the existing two-stage fluidized-bed process to reduce the residence time in the combustion bed by withdrawing incompletely oxidized coked sand from the bed. Subsequently, the partially combusted coked sand is fed into a third "after burner" bed that would operate adiabatically at a higher temperature to significantly increase the rate of coke oxidation and complete the removal of coke from the sand.

Simulation Algorithm Flowchart

A simplified flowchart of the simulation algorithm is presented in Figure 41. The first step is to read the operating parameters from an external data file. These parameters include the

160
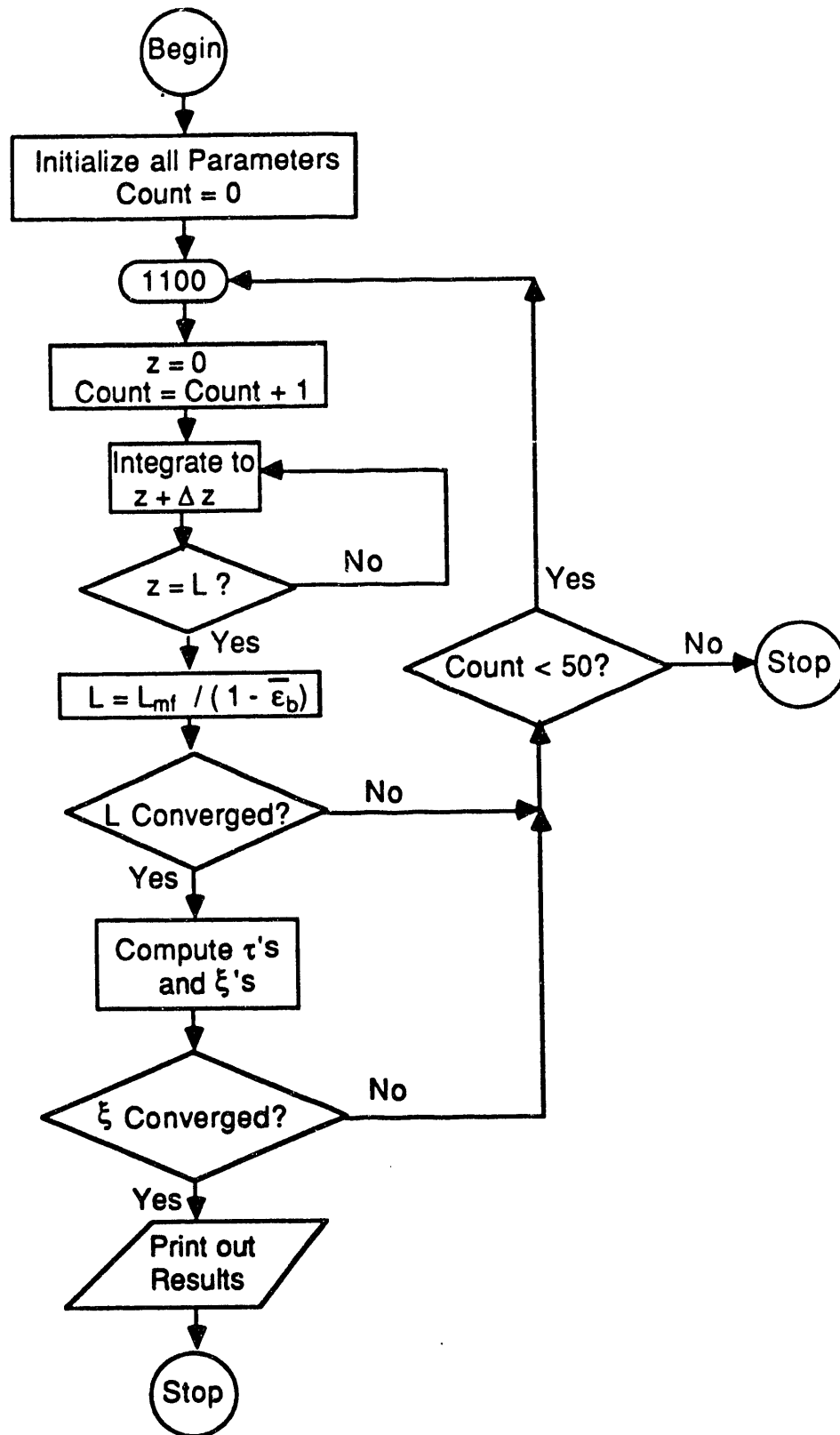
Figure 41
Flowchart of Simulation Algorithm

161

particle size distribution as well as the following:

ρ_s, the grain density of sand particles;

ϵ_{mf}, the void fraction at minimum fluidization;

ϕ_s, the particle shap factor;

P_{out}, the pressure at bed outlet;

$Y_{H_2O}(0)$, the inlet mole fraction of water vapor;

$x_{gas} = u(0)/u_{mf}$, the net conversion of oxygen in the combustion bed;

d_{hp}, the particle diameter;

ΔX, the physical dimensions of the heat pipe geometry;

A_o, the catchment area of the distributor;

T, the combustion bed operating temperature;

$X_{\phi_b} = \phi_b/\epsilon_b$, the solids volume fraction of the bubble phase;

f_{cc}, the mass fraction of the entering coked sand;

ρ_c, the density of the coke;

$M_{flux} = M_{CB}/A_b$, the mass flux of coked sand entering the bed; and;

$\bar{t}$, the mean particle residence time.

The s0*0*d step is to initialize several variables, including the gas viscosity $\mu_g = 2.4169 \times 10^{-7} T^{0.76}$ (Robinson,[70]), ρ_g the gas density from the ideal gas law, Re_{mf}, $u(0) = x_{gas} \cdot U_{mf}$, L_{mf}, ΔP_{total}, and $d_{b,max}$. An estimated representative bubble diameter d_b, is used to specify a first approximation for L, the total bed height. Based on experience, this was taken to be 0.044 meters. The total bed height L, is then calculated from two-phase fluidized-bed theory, as presented previously.

The initial value for τ_t, the time required for the complete combustion of the coke on a single particle of size d_p, is calculated by dividing the mass of coke on the particle by the mass rate of combustion C_o. The amount of coke on a particle, C_o, of

size d_p is computed first from

$$C_o = \frac{\pi}{3} \delta \phi_s^3 (3 d_i^2 + 6 d_i \delta + 4 \delta^2) \rho_c \qquad (17)$$

In this equation, δ is the thickness of the layer of residual coke on the particles entering the combustion bed from the pyrolysis bed. The reaction rate is calculated from

$$r_c = A_p k_p P_{o_2} \qquad (18)$$

where P_{o_2} is 0.2 atm and A_p is the particle surface area equal to $\pi (\phi_s d_p)^2$. The initial value for τ_i is then calcualted by dividing C_0 by the reaction rate. Thus τ_i is computed from

$$\tau_i = \frac{\delta \phi_s \rho_c}{3 M_c k_p P_{o_2}} \left[3 + 6 \left(\frac{\delta}{d_p} \right) + 4 \left(\frac{\delta}{d_p} \right)^2 \right] \qquad (19)$$

Using Equation 19 with $d_p = \bar{d}_p$, we find $\tau_i = 120$ S. Although this is not always a good initial guess, it was for used for all cases. The only effect of this being a poor initial guess was that some cases required a greater number of iterations to converge to τ_i than others, as discussed below.

At this point, control of the execution of the program is at line number 1100 of the main program, after which the next step is to perform the integrations by use of subroutine LSODA, in the ODEPACK numerical integration package, in increments of $\Delta z = L/500$. The use of 500 elements in the vertical direction was selected based on an optimal error control criterion. Using fewer elements resulted in somewhat different solutions, and using more elements

163

yielded no additional accuracy. The values of the error control parameters required for LSODA were selected in a similar fashion. Initially, the error control parameters were set at a large value, proportional to the value of the expected integrated values. Subsequently, the magnitudes of these parameters were reduced monotonically until no additional improvement in accuracy was noticeable. The absolute errors were finally taken as

1. $(uC_{co,b})$ ATOL $= 10^{-16}$

2. $(u \ C_{o_2,b})$ ATOL $= 10^{-15}$

3. $\int (dp/dz)dz$ ATOL $= 10^{-2}$

4. $\int \epsilon_b \ dz$ ATOL $= 10^{-8}$

The actual integration is performed by subroutine LSODA, which is able to integrate both stiff and non-stiff systems, depending on the characterization of the system. Subroutine LSODA calls subroutine DERIV, which requires evaluation of many parameters, to evaluate the four differential equations. An outline of the procedure followed in subroutine DERIV is presented in Figure 42. The dense-phase concentrations $C_{co,d}$ and $C_{o_2,d}$ are determined in subroutine DENSE by first substituting for $C_{co,d}$ from the dense-phase mass balance equation for CO into the dense-phase mass balance equation for O_2 and subsequently solving the latter equation for $C_{o_2,d}$ by application of the secant method.

The four derivatives (or integrands) may be evaluated as follows:

1. $d (u C_{co,b})/dz$ from the bubble-phase mass balance equation

2. $d (u C_{o_2,b})/dz$ also from the bubble-phase mass balance equation

164

$T, u, \varepsilon_b C_{CO,b} C_{O_2,b} d_b$

From LSODA

$z,$ $(u \cdot C_{CO,b})$

$(u \quad C_{O_2,b})$

ΔP

$\int_0^z \varepsilon_b \, dz$

Subroutine DENSE

1. Call Subroutine MTCOEF.
2. Evaluate $A_{p,d}$, Γ, γ, ψ, and η.
3. Make Initial Guess for $C_{O_2,d}$
4. Apply Secant Method to dense-phase mass balance equation for O_2.

Subroutine DERIV

1. Evaluate $P, u, C_{CO,b}, C_{O_2,b}, d_b, \varepsilon,$ and ε_b.
2. Call Subroutine DENSE
3. Call Subroutine MTCOEF
4. Call Subroutine RATES
5. Evaluate the two differential equations and two integrands.

$C_{CO,d}, C_{O_2,d}$

$d_b, \varepsilon_{mf}, T, P, u, u_{mf}$

Subroutine MTCOEF

1. Evaluate $k_{q,i}$.

$k_{q,CO}, k_{q,O_2}$

$\dfrac{d}{dz}(u \cdot C_{CO,b})$

$\dfrac{d}{dz}(u \cdot C_{O_2,b})$

$\dfrac{dP}{dz}$

ε_b

$C_{i,p}, T, P, u$

Subroutine RATES

Evaluate reaction rate equations...

$n_b^o, n_b^e, n_d^o, n_d^e$

Back to LSODA

Figure 42

Schematic Drawing of the Evaluation
of the Three Differential Equations
and Two Integrands

165

3. $dp/dz = (\rho_s - \rho_g)g (1-\epsilon)$

4. $d/dz [\int \epsilon_b dz] = \epsilon_b$

Upon successful completion of the integration up to $z = L$, L is recomputed and checked for convergence. Convergence is deemed satisfactory if $|L - L_{old}| < 10^{-4} L$, where L_{old} represents the previous value of L. If L does not converge satisfactorily, control returns to line 1100 of the main program, after which the integrations are performed again. Execution of the simulation is halted if the convergence of L is not attained in fifty iterations to prevent excessive iterations. However, it should be noted here that the simulation converged to a solution for L in less than 15 iterations in all cases, validating the previously presented conclusions regarding the successive substitution scheme.

After a value for L has been determined, the next step is to determine the values of τ_i of each particle size with subroutine FINDTA according to the following relationship:

$$\tau_i = \frac{C_o A_c^T}{A_p r_c^T} \qquad (20)$$

where:

C_0 is the amount of coke present on a particle in the pyrolysis bed,

A_p is the external surface area of the particle,

A_c^T is the total surface area of coked particles in the bed, and

r_c^T is the cumulative rate of coke combustion in the bed.

166

The convergence of τ_t is checked in a manner similar to that used for the convergence to L. If the values of τ_t are unsatisfactorily converged, control is once again returned to line 1100 to find another value for r_c^T as described below. Excessive iteration is prevented using the same loop-counter that was described in the previous paragraph.

Following successful solution for τ_t, subroutine CCONV finds the mean exit coke conversion. We can compute x_i, the time averaged coke conversion for particles of size d_i and subsequently, x, the overall mean exit coke conversion can be computed. Finally, output is printed according to the needs of the specific case.

Previously, the dense-phase concentrations, $C_{0_2,d}$ and $C_{co,d}$, were computed by solving the two dense-phase mole-balance equations simultaneously by a two-dimensional application of the Newton-Raphson method, making use of the calculated bubble-phase concentrations. However, by reducing the dense-phase mole-balance equations to one equation (by eliminating $C_{co,d}$), $C_{0_2,d}$ can be found by application of the secant method to the following equation:

$$0 = C_{0_2,b} - C_{0_2,d} + d_1 \left\{ -\gamma C_{0_2,d} \eta - \frac{\Gamma}{2} C_{0_2,d}^{0.3} \left(\frac{C_{co,b} + d_2 \gamma \Psi C_{0_2,d}}{1 + d_2 \Gamma C_{0_2,d}^{0.3}} \right) \right\} \qquad (21)$$

Subsequently, $C_{co,d}$ is found from

$$C_{co,d} = \frac{C_{co,b} + d_2 \gamma \Psi C_{0_2,d}}{1 + d_2 \Gamma C_{0_2,d}^{0.3}}$$

(22)

where d_1 and d_2 are constants resulting from the mass transfer correlations, and γ, Γ, η, and Ψ are constants in the kinetic rate expressions. Using the secant method to solve a single equation reduces computing time substantially when compared to using the Newton-Raphson method to solve two equations.

Equation 20 is used to find values for r_i. Previously, the value of r_c^T was found by integrating

$$r_c^T = A_b \int_0^L (e_b n_b^\theta + (1-e_b) n_d^\theta) \, dz$$

(23)

However, the total coke combustion rate in the bed can be found instead from the exit gaseous concentrations. Each mole of CO and CO_2 leaving the bed corresponds to a mass of coke being burned, and the concentration of CO_2 can be found using the fact that the number of oxygen atoms leaving the bed is equal to the number entering the bed.

$$\frac{r_c^T}{A_b} = u(C_{co,b}(L) + C_{co_2,b}(L)) \frac{M_c}{m_c}$$

(24)

$$C_{CO_2,b}(L) = \frac{4(1-f_H)\left(\frac{P(L)}{P(O)}C_{O_2,b}(O) - C_{O_2,b}(L)\right) - (2-f_H)C_{CO,b}(L)}{4-3f_H} \qquad (25)$$

Using these expressions, the number of ordinary differential equations being integrated reduced from five to four, resulting in further reduction in CPU time required for execution of the program.

Results

Unless otherwise noted, the operating conditions in each of the computer simulations of the combustion bed were those given in Table 28. The mean coke conversion for this base case was found to be x= 99.2%, and the exit oxygen conversion was 40.2%.

The oxygen and carbon monoxide conversion profiles for this case are presented in Figures 43 and 44, respectively. In Figure 43, the "kink" in the dense phase curve at z = 0.275 meter corresponds to the point in the bed where the bubble size has reached the maximum allowable size, $d_{b,max}$, determined by the heat-pipe geometry according to:

$$d_{b,max} = \frac{\sqrt{3}}{2}\Delta x - d_{hp} \qquad (26)$$

The oxygen conversion is noticeably higher in the dense phase than in the bubble phase. This is expected since oxygen, which reacts with coke and with carbon monoxide, a product of the oxidation of

Particle Density	ρ_s	2600 kg / m^3
Void Fraction at Minimum Fluidization	ε_{mf}	0.46
Particle Shape Factor	ϕ_s	0.80
Exit Pressure	$P(L)$	89.16 kPa
Heat Pipe Spacing	Δx	0.055 m
Heat Pipe Diameter	d_{hp}	0.019 m
Area Per Orifice of Grid	A_0	1×10^{-4} m^2
Combustion Bed Operating Temperature	T	848 K
Volume fraction of bubble phase that is particles	ϕ_b/ε_b	0.005
Entrance Water Vapor Mole Fraction	$y_{H_2O}(0)$	0.008
Entrance Gas Velocity Coefficient	u_0/u_{mf}	19
Coke Mass Fraction of Solids Entering Bed	f_{cc}	0.01961
Mass Flux of Solids Entering Bed	M_{CB}/A_B	0.137 kg / (m^2 s)
Mean Particle Residence Time	$\bar{t}$	7400 s
Atomic Hydrogen Mass Fraction of Coke	m_H	0.03
Atomic Carbon Mass Fraction of Coke	m_C	0.88

Table 28.   Base Case Operating Parameters

170
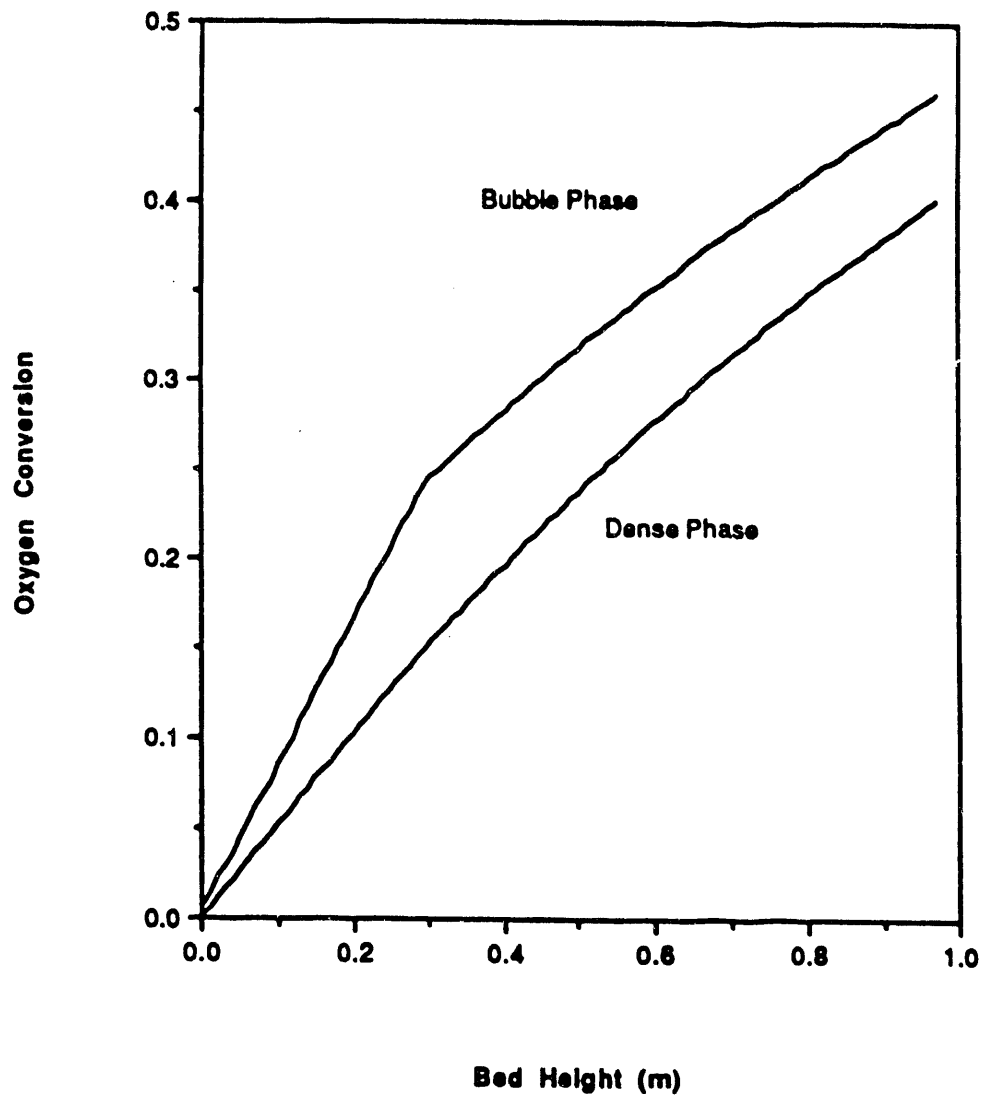
Figure 43
Oxygen Conversion Profile

171
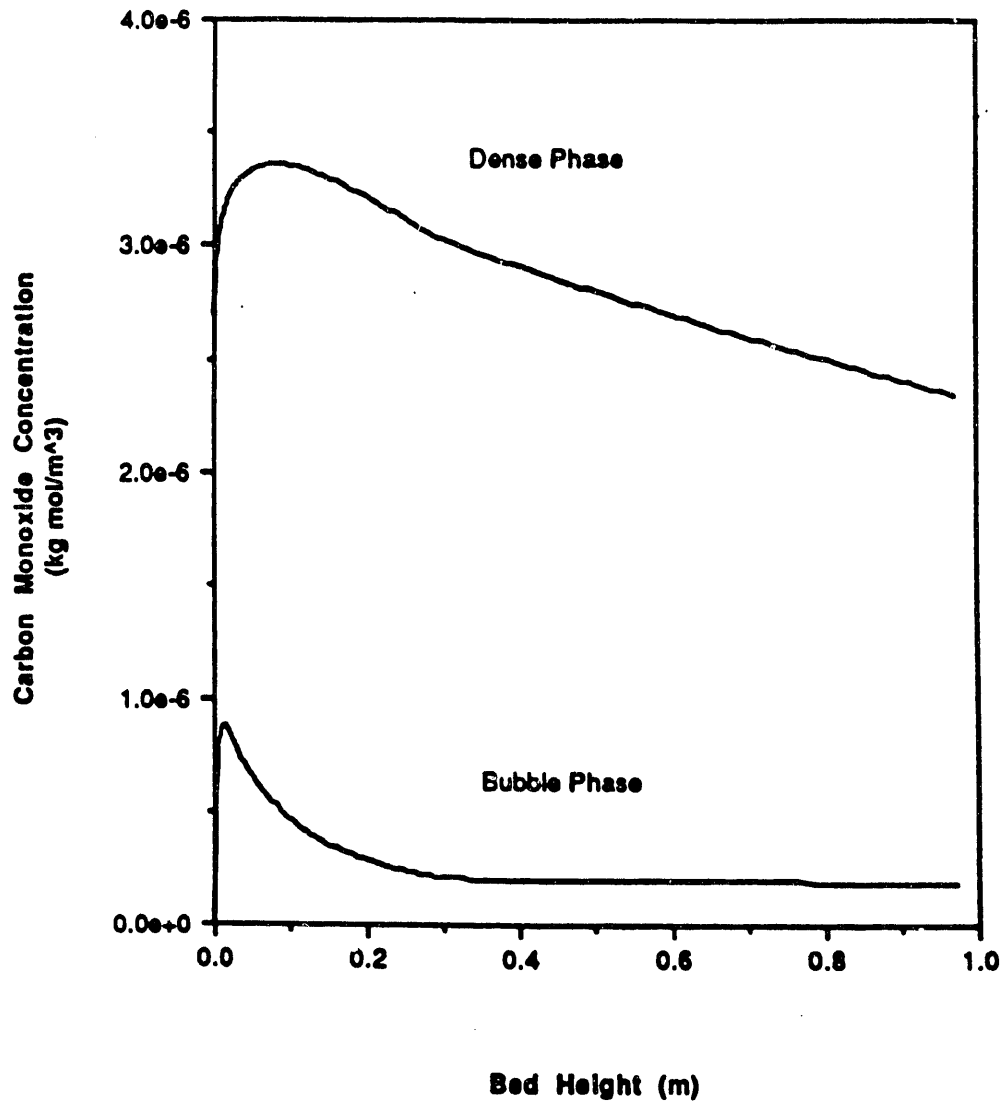
Figure 44
Carbon Monoxide Concentration Profile

coke, is consumed almost exclusively in the dense phase. The carbon monoxide concentration is substantially higher in the dense phase than in the bubble phase (Figure 44). Again, this is due to the fact that carbon monoxide is produced in the coke oxidation reaction, which occurs primarily in the dense phase. The outlet CO concentration is low with respect to the amount O_2 consumed. In all cases considered thus far, the exit CO represents a fraction of less than 10^{-4} of O_2 consumed in the reactor.

The values of τ_t, the residence time required for complete conversion of the coke on a single particle, are plotted against particle diameter in Figure 45 for the base case. Insight into the relationship between τ and d_p can be obtained by examining the following form of Equation 19:

$$\tau = \alpha \left[3 + 6 \left(\frac{\delta}{d_p}\right) + 4 \left(\frac{\delta}{d_p}\right)^2\right] \tag{27}$$

Instead of evaluating the coefficients in the front of Equation 18, we evaluate a single constant α by fitting a curve to the predictions of the simulation. Using regression analysis we find $\alpha = 41.1$. In Figure 45, Equation 26 is plotted along with the predictions of the simulation, where the fit is seen to be quite good. Hence, Equation 26 adequately describes the relationship between τ and dp significance of Figure 45. To find the value for δ, the assumed uniform thickness of coke residue remaining on each sand particle after pyrolysis, the relationship equating the coke exiting the pyrolysis bed to the coke entering the combustion bed
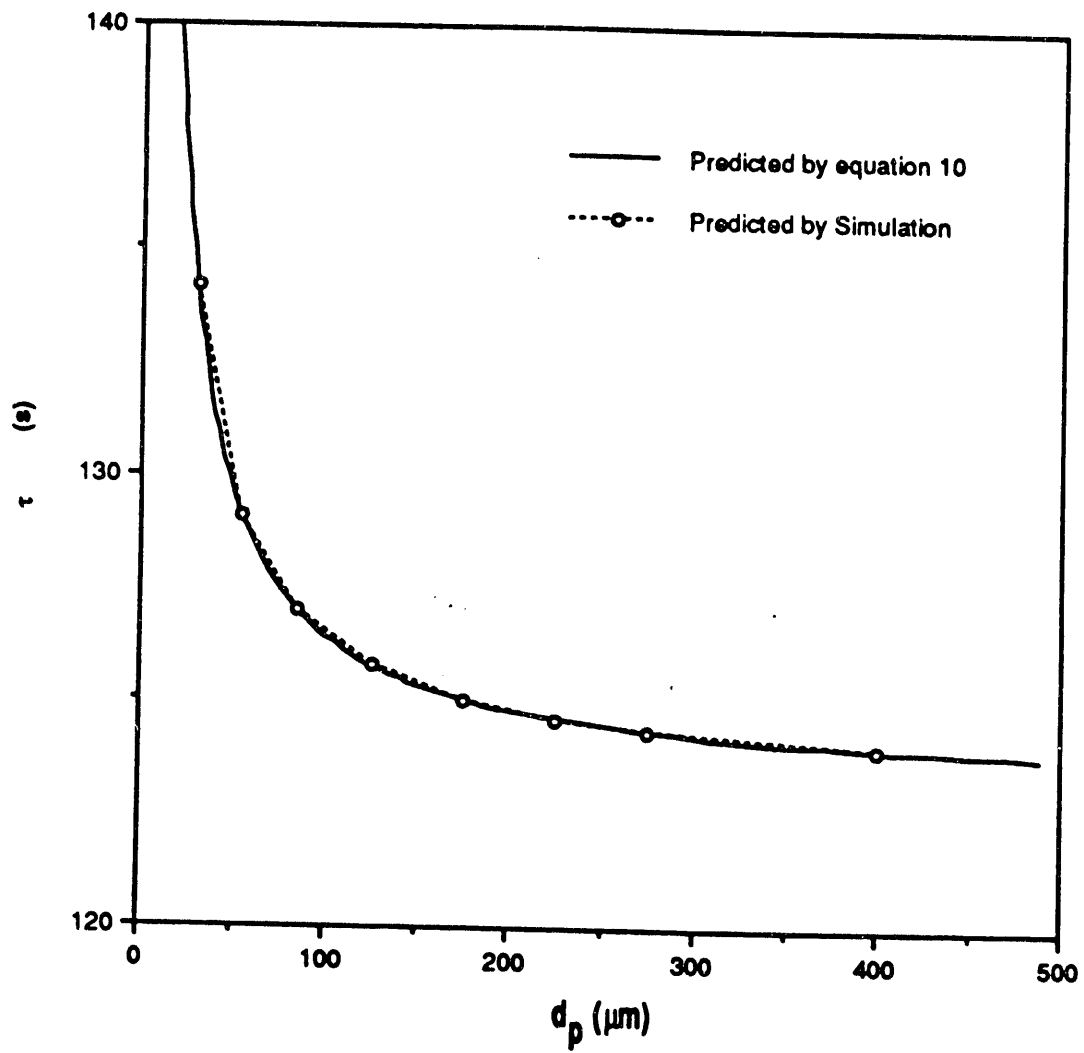
Figure 45
Time for Complete Combustion of Coke
as a Function of Particle Size

174

was solved by a secant method. With all the parameters taking the base case values, we find $\delta = 1.30$ μm.

The results of a parameter-sensitivity study are presented in Table 29. In each case, the value of only one parameter was changed from the base-case value. Values of some of the parameters for the base case, presented in Table 28, were assigned somewhat arbitrarily. The particle shape factor, ϕ_s, was taken to be 0.80based on typical values reported in the literature[71] and work done on an isolated sample of clean tar sand[72]. It is expected that the shape factor might vary somewhat from sample to sample. However, as shown in Table 29, the effect on mean coke conversion of varying ϕ_s from 0.70 to 0.92 is negligible, although the effect on oxygen conversion is somewhat more significant. Similarly, ϵ_{mf}, the void fraction at minimum fluidization, is taken to be 0.46 in the base case based on fluidization experiments with the same generic sand at ambient conditions and on typical literature values. In terms of coke and oxygen conversions, the effect of changing ϵ_{mf} is similar to that observed when the particle shape factor is changed, and is shown in Table 29.

Values of the bed exit pressure, $P(L)$, and of the entering mole fraction of water vapor, $y_{H_2O}(0)$ were assumed to be typical Utah desert values. The effects of changing these parameters on the coke and oxygen conversions are shown to be small in Table 29.

Smart[72,] reported on the operation of the coupled fluidized-bed reactor (four-inch-diameter) at various temperatures. The effect of operating the combustion bed at different temperatures was investigated. Increasing the temperature by 20°C increased the

175

Table 29. Results of Parametric Study

Variable	Base Case Value*	Parametric Value *	Overall Coke Conversion	Overall Oxygen Conversion	Total Bed Height	Iterations Required for Convergence
			x	XO_2	L(m)	
Base Case (See Table 28)			0.992	0.402	0.975	11
ϕs	0.08	0.70	0.991	0.525	0.918	16
ϕs	0.80	0.92	0.992	0.304	1.053	11
ε_{mf}	0.46	0.48	0.992	0.341	1.057	12
ε_{mf}	0.46	0.44	0.991	0.476	0.905	15
P(L)	89.2k	8.6x104	0.991	0.415	0.976	13
P(L)	89.2k	1.01 x10^4	0.993	0.359	0.974	13
$YH_2O^{(0)}$	0.008	0.001	0.992	0.399	0.975	12
$YH_2O^{(0)}$	0.008	0.032	0.991	0.412	0.975	11
T	848	823	0.984	0.379	0.981	13
T	848	873	0.995	0.425	0.970	15
M_{CR}/A_R	0.137	0.160	0.991	0.462	1.138	14
M_{CR}/A_R	0.137	0.100	0.992	0.302	0.716	12
f_{cc}	0.0196	0.0220	0.990	0.451	0.973	12
f_{cc}	0.0196	0.0175	0.993	0.359	0.977	12
mH	0.03	0.02	0.992	0.390	0.975	11
mH	0.03	0.04	0.991	0.414	0.975	12
mC	0.88	0.90	0.991	0.410	0.975	11
mC	0.88	0.86	0.992	0.394	0.975	11
$\phi b/\omega b$	0.005	0.001	0.992	0.402	0.975	11
$\phi b/\varepsilon b$	0.005	0.010	0.992	0.402	0.975	11
u_0/u_{mf}	19	25	0.992	0.306	1.056	12
u_0/u_{mf}	19	15	0.990	0.509	0.921	15
u_0/u_{mf}	19	10	0.985	0.759	0.853	28
u_0/u_{mf}	19	7.5	0.953	0.979	0.818	118
u_0/u_{mf}	19	4	0.519	1.000	0.767	24

average coke conversion to 0.995 and decreasing the temperature by 25°C caused a decrease to 0.984. Obviously, the effect of temperature is significant.

Smart[72] reported a typical tar-sand feed rate of 12 pounds per hour, from which the value for the mass flux of coked sand entering the combustion bed given in Table 28 (0.137 kg/(m^2 s)) was derived. Since several other values were reported, the effect of changing the feed rate, represented here as the mass flux, M_{CB}/A_B, was explored. Note that since only this parameter is changing, i.e., the residence time is held constant, hold up in the bed increases directly with feed rate. As show in Table 29, this parameter primarily affects the total bed height, and the conversions do not change appreciably.

Similarly, f_{cc}, the weight fraction of the coked sand that is coke, was derived from the bitumen fraction of the tar sand and from the residue fraction of the bitumen left behind as coke for a single run of Smart[72]. Increasing f_{cc} by as much as 12% reduced the coke conversion insignificantly.

Additionally, the composition of the coke itself can vary as reported by Bunger[73]. The amount of O_2 consumed changes slightly as the values of m_H and m_C, the weight fractions of atomic hydrogen and carbon change, however, the overall conversion of coke is barely affected.

The overall reaction rate in a fluidized bed may be bounded by bubble-to-dense-phase mass-transfer considerations or by heterogeneous reaction kinetics or by a combination of the two[74]. If the

presence of particles in the bubble phase greatly affects overall conversions, then the reaction is most likely limited by interphase mass transfer. According to Grace[74], the volume fraction of the bubble phase occupied by solids, ϕ_b/ϵ_b, is bounded by $0.001 < \phi_b/\epsilon_b < 0.01$. An examination of the data in Table 29 reveals an insignificant dependence of coke and oxygen conversions upon the presence of particles in the bubble phase. Hence, the system considered here is controlled by reaction kinetics. In Table 29, the dependence of coke conversion is seen to be relatively independent of air flow rate as long as the entering gas velocity, u_0, is above a minimum threshold value. Decreasing u_0 from 25 u_{mf} (0.241 m/s) to 7.5 u_{mf} (0.72 m/s) results in a decrease of $\bar{\bar{x}}$ from 99.2% to 95.3%. However, as the gas flow is decreased further to $u_0 = 4\ u_{mf}$ (0.0386 m/s), the coke conversion decreases to 51.9%. For the base case operating conditions, then, the threshold of dependence upon fluidizing air velocity lies between 7.5 u_{mf} and 4 u_{mf}.

Further insight may be gained by examining the dependence of oxygen conversion upon excess gas velocity, which was expected to be more significant than that for coke. Oxygen conversion profiles at several different gas flow rates are presented in Figure 46. As u_0 decreased from 25 u_{mf} to 7.5 u_{mf}, the oxygen conversion increases from 30.6% to 97.9%, and at $u_0 = 4U_{mf}$, the oxygen is fully converted (to four significant figures). Apparently, the coke will combust at a sufficient rate to allow for high conversion as long as the oxygen is not completely consumed in the reactor. In other words,

178
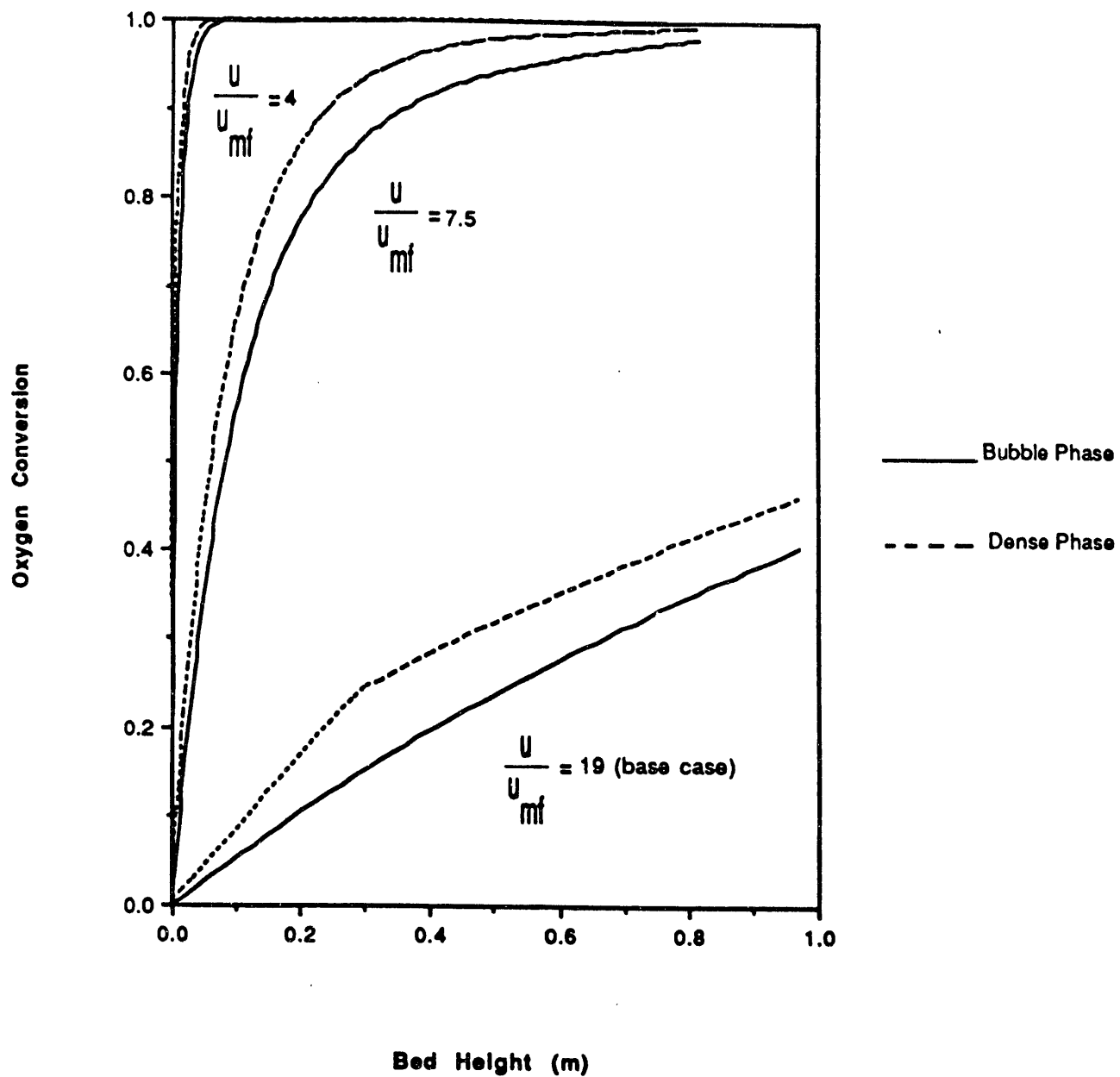
Figure 46
Effect of Gas Flow Rate
on Oxygen Conversion

high coke conversion can be expected whenever the oxygen flow rate into the bed is in excess of the stoichiometric requirement.

The effect of varying only the mean particle residence time, $\bar{t}$, upon the overall coke conversion, $\bar{\bar{x}}$, is shown in Figure 47. Note that an incremental improvement in $\bar{\bar{x}}$ requires greater increases in $\bar{t}$ (i.e., hold up) at higher conversions. The conversion increases from 94.2% to 97.0% with an increase in $\bar{t}$ from 20minutes to 40 minutes, but only increases further to 98.1% with an increase in $\bar{t}$ to 60 minutes. Above a conversion level of about 99%, an incremental increase in $\bar{\bar{x}}$ requires much greater increases in the particle residence time.

If a single-sized particle distribution is assumed, an estimate of the accuracy of the computations can be assumed. We take $\bar{d}_p$ = 139 μm, δ = 1.30 μm, and compute C_0 = 1.49 x 10^{-10} kg by Equation 17. An approximate coke combustion rate can be found by evaluating the kinetic rate expression of the coke combustion reaction with p_0 = 0.2 atm. This predicts a coke combustion rate of r_c = 1.17 x 10^{-12} kg/s, and an estimate of $\tau \approx 127.3$ s. The net coke conversion for the single-sized particles, $\bar{x}$, can be found as a function of $\bar{t}$, the mean particle residence time according to:

$$\bar{x} = \frac{\bar{t}}{\tau} (1 - e^{-\tau/\bar{t}})$$ (28)

The coke conversion predicted by these approximate calculations at T = 575 °C is shown in Figure 47 with the solution found by the simulation. For residence times greater than about 1000 s, we find very good agreement.

The simulation of the combustion bed is robust from a numerical perspective. Convergence was obtained for all the cases that were tried. As seen in Table 29, convergence to L and τ_i was achieved in less than twenty iterations over the integrations for all cases expect those where the fluidizing-gas velocity was unusually low. Apparently, the initial guesses for τ_i and d_b were appropriate for high fluidization gas flow rates/velocities. In light of the strong dependence of bubble growth upon $(u - u_{mf})$ given by the correlation of Stubington et al.[76], this might be expected. The bed height, L, is largely dependent upon the volume fraction of bubbles, and so a good initial guess of d_b is crucial for rapid convergence to L.

Based on the above results, it is possible to identify the parameters that influence the overall conversions of the fluidized-bed reactor under consideration here. The most important parameters are those related to the operation of the bed itself. The mean particle residence time, the gas flow rate, the mass feed rate, and the bed operating temperature are significant. Of the physical parameters considered, only ϵ_{mf}, the void fraction at minimum fluidization, and f_{cc}, the fraction of feed that is coke, seem to have a minimal influence on the predictions for coke conversion.

In the previous annual reports, mention has been made that a grid region model may be necessary to account for the enhanced mass transfer between the bubble and dense phases near the distributor. Such models may be important for modelling beds in which
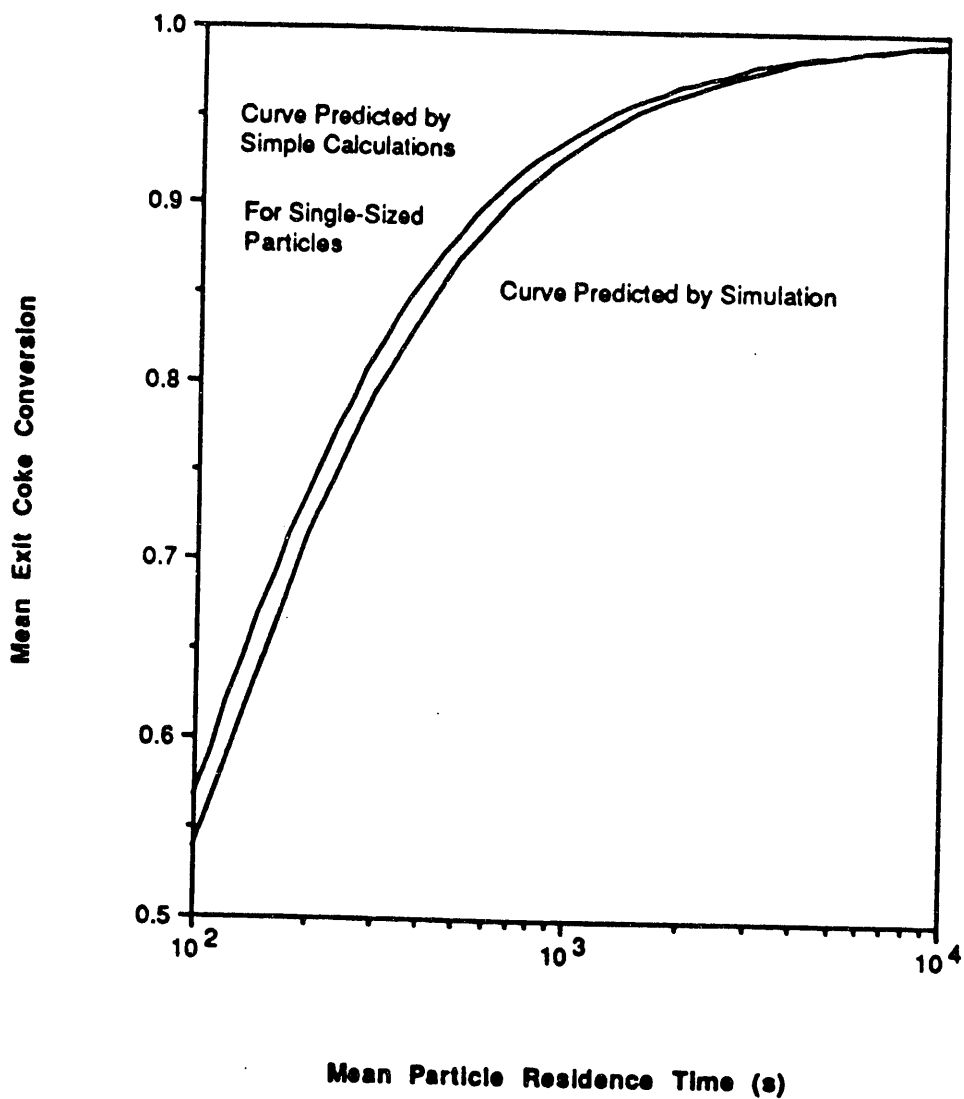
Figure 47
Coke Conversion vs Residence Time

heterogeneous reactions take place.[75] To get a qualitative feel for the applicability of a grid-region model we can simply increase the mass transfer coefficients $k_{q,0}2$ and $k_{q,co}$. Multiplying each of these numbers by a factor of five results in very little difference. This procedure increases the mass transfer between phases through the whole bed, and so should produce more drastic changes then simply a grid model.

Apparently, the combustion reaction is not limited by the supply of oxygen. From Figure 46, we can see that the oxygen concentration in the dense phase, where most of the reaction is occurring, is rather close to that in the bubble phase. As modelled here, the mass transfer between phases is fast enough to keep up with the oxygen consumption. On the basis of these findings, an analysis of the grid region will be pursued no further.

Process Modification Proposal

A comparison of Figures 45 and 47 reveals quite different residence times. Figure 45 shows that a particle must reside in the bed for approximately 125 s before all of the coke is burned and Figure 47 indicates that an average residence time of 7000 s is required for a mean exit coke conversion of 99.1%. This can be explained by realizing that the particles are assumed to be well mixed throughout the reactor, resulting in a wide distribution of particle residence times. Although the exit stream of particles contains mostly clean sand, there will always be some particles containing coke. To ensure a high coke conversion, the mean

183

particle residence time $\bar{t}$ must be many times τ, the residence time required for the conversion of 100% of the coke on a single particle.

Concern has been raised over the large particle residence time necessary to achieve high coke conversion. This large residence time represents a significant hold up in the reactor, along with concomitant high compressor costs. In the case with $\bar{t}$ = 7000 s, the pressure drop across the bed is 9.2 kPa, or 1.3 psi. A high rate of mixing, generally considered to be an advantage of fluidized-bed reactors, is the ultimate source of this difficulty. In such a well-mixed reactor, the particle residence times have a wide distribution. A key to limiting the mean particle residence time is controlling this distribution. A common way to gain some degree of control over the residence time distribution in well-mixed reactors is to link more than one reactor in series. As discussed above, the coke conversion very quickly achieves a state of diminishing returns with respect to $\bar{t}$, i.e., coke coversion increases at a slower rate as the value of $\bar{t}$ increases. It is feasible to limit the particle residence time to a low value, say 2000 seconds, while still achieving a high degree of energy extraction for transfer to the upper pyrolysis bed. The predicted coke conversion $\bar{x}$ as a function of $\bar{t}$ is presented in Figure 47. At a residence time of 2000 seconds the coke conversion was 96.4%. Decreasing the mean residence time (and the reactor hold up) by a factor of more than three resulted in a decreasing coke conversion from 99.2% to 96.4%.

Thus, it is proposed to add a third reactor to the bitumen extraction process. A schematic diagram of the proposed process is shown in Figure 48. Residence time in the combustion bed would be reduced from the time required for high coke conversion. Hence, sand withdrawn from this bed and fed into the third "after-burner" bed would contain a fraction of the original coke. This fraction might be about five percent, although the exact amount would be found by an optimization procedure. The "after-burner" bed would operate adiabatically, and therefore at a higher temperature than that in the combustion bed, and the reaction rate would be higher than that in the combustion bed, so that the mean residence time in this bed need not be great.

The reduced coke conversion in the combustion bed means that slightly less energy is available for transfer to the pyrolysis bed. However, some of the lost energy can be recovered in a heat recovery unit, perhaps by preheating the fluidizing gas for each of the beds.

As an illustrative example, let us suppose that the residence time in the combustion bed is reduced to 2000 s, although the exact residence time will be found by optimization. Preliminary calculations show that under this condition, 96.4% of the coke is oxidized in the combustion bed, and the third "after-burner" bed would operate at 876 K, assuming the combustion bed operates at 848 K. At this higher temperature, the coke combustion rate increases to just about twice the rate at 848 K. As noted above, the operating temperature inside the combustion bed has a large
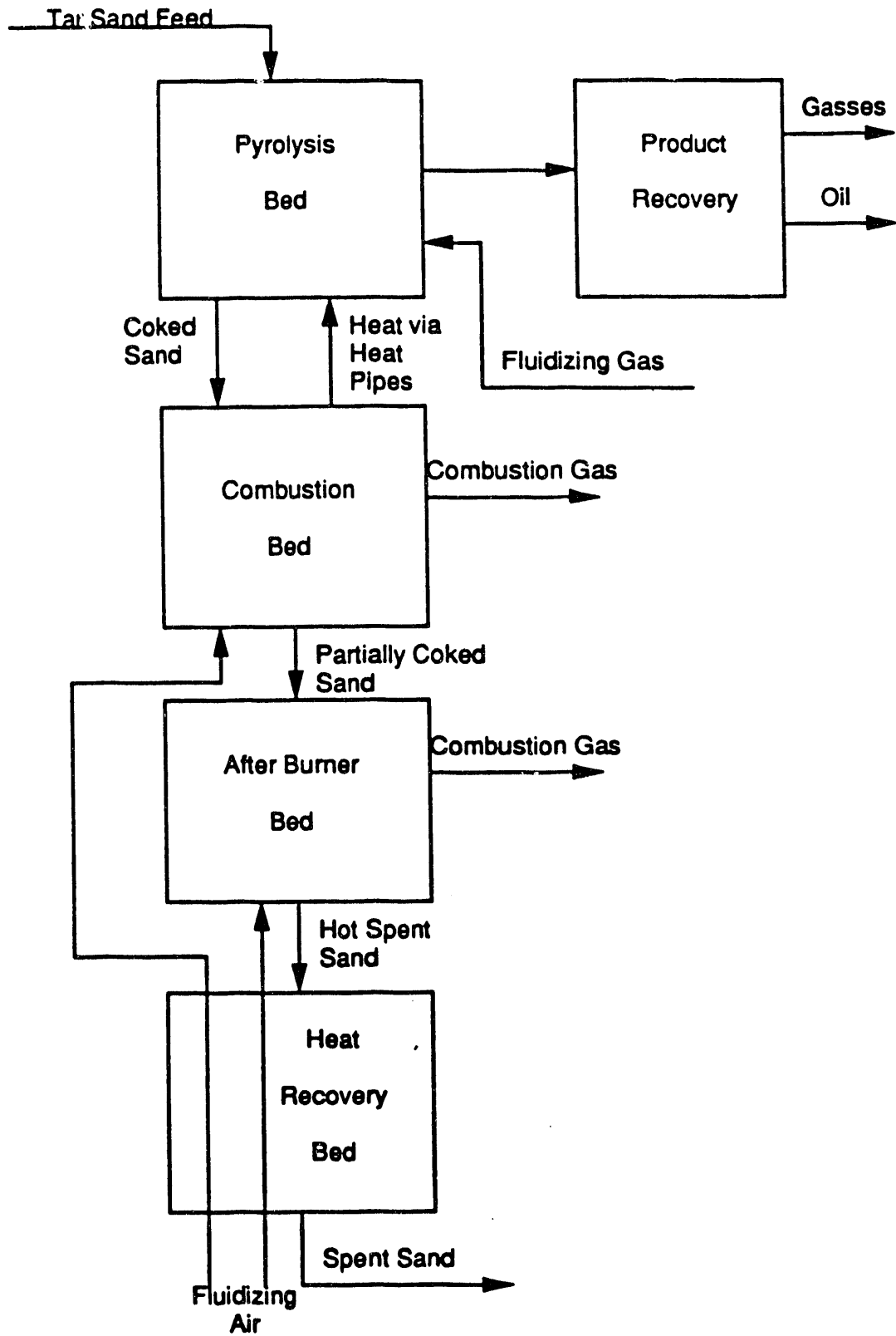
Figure 48

Schematic of Modified Process

186

effect on the coke conversion. Hence, a substantial benefit can be realized by incorporating this modification into the process.

The cost of adding a third fluidized-bed reactor is likely to be substantial, and must be assessed. Although free from the cost of the heat pipes (which contribute greatly to the cost of the pyrolysis and combustion beds), this reactor would have to be built of temperature resistant materials. Additionally, operation of this bed may require an additional compressor with its accompanying utility cost. Note, however, that the increased compressor cost would be offset by the reduced compressor cost of the combustion bed.

The usefulness for this third bed needs to be assessed. The model predicts that an average residence time of about two hours is necessary to burn 99% of the coke in the combustion bed. This corresponds to a bed height of a little less than one meter. By operating the combustion bed with a particle residence time of about one half hour, 96% of the coke is burned, and the bed height is reduced by a factor of nearly four. The questions to be resolved is whether or not the cost of an additional bed is worth reducing the height of the combustion bed by about 0.7 meter.

Summary and Conclusions

The fluidized-bed model of the existing process is as yet incomplete. The hydrodynamics and the related kinetics of reaction which transpire in the lower combustion bed have been modelled. The model is numerically robust for a wide range of input parameters and is capable of predicting exit gaseous concentrations and

mean exit coke conversion. However, this represents only a first step, albeit an important one, in a sophisticated model of the complete system.

Future Activities

It still remains to model the upper pyrolysis reactor. Hopefully, a literature review will reveal the hydrodynamics of the two beds are alike, and a similar hydrodynamic model can be utilized. However, the effect, if any, of particle agglomeration must be investigated. It is widely recognized that the fluidization of particles that experience inter-particle forces is subject to phenomena not important otherwise. (See, for example, Geldart[77]).

The two fluidized-bed reactors are thermally linked by heat transfer via a network of heat pipes. This link must be modelled by application of the energy balances previously presented. This will cause the operating temperatures of the two beds to become unknown variables in the simulation, rather than explicitly set, as was done here.

Upon successful compilation of the steady-state model described above, a dynamic simulation could be developed by rewriting the mass and energy balance equations with time-dependent quantities. The resulting partial differential equations could be solved and used to predict start up effects or the effect of perturbing the system through the input parameters. Eventually, the two simulations will be used for optimization of the physical configuration to be used for commercial-scale plant design.

Nomenclature

A_b	Cross-sectional area of bed, m^2
A_c^T	Cumulative Surface area of all reacting particles in bed, m^2
A_p	External Surface area of a single particle, m^2
A_0	Catchment area, defined by Darton et al.[78] as the number of orifices per total area, m^2
$c_{i,p}$	Molar concentration of species i in the p phase (bubble or dense), kg mol/m^3
$_{0,i}$	The volume of coke on a particle of diameter d_i upon entering the combustion bed, kg
d_b	Characteristic-bubble diameter, m
$d_{b,max}$	Maximum bubble diameter achieved in a bed, m
d_{hp}	Diameter of heat pipes, m
$d_i, d_{p,i}$	Diameter of particle belonging to size cut i in a distribution, m
$\bar{d}_p$	Harmonic mean particle diameter, m
d_p	Particle diameter, m
d_1, d_2	Constants from dense-phase mass balance equations.
f_{cc}	Mass fraction of coke in combustion bed solids feed
f_H	Molar fraction of coke consisting of H atoms,
i	As a subscript, used as an index to specify a discrete size cut in a particle-size distribution
k_p	Rate coefficient for coke-combustion reaction, kg/m^2Pa s
L	Total bed height, m

L_{mf}	Total bed height at minimum fluidization , m
M_c	Molecular weight of carbon, kg mol/kg
m_c	Carbon mass fraction of coke,
M_{CB}	Mass feed rate of solids into combustion bed, kg/s
m_H	Hydrogen mass fraction of coke
n_p^e	Molar rate of heterogeneous reaction corresponding to rate of disappearance of coke in phase P (bubble or dense), kg/mol/m^3 s
P	Bed Pressure, Pa
$P_{O_2,P}$	Partial pressure of oxygen in the p phase (bubble or dense), Pa
r_c^T	Total reaction rate of coke in combustion bed, kg/s
Re	Particle Reynolds number = $\bar{d}_p u\, \rho_g/\mu_g$
Re_{mf}	Particle Reynolds number at minimum fluidization
$\bar{t}$	Mean particle residence time, s
T	Bed Temperature, K
u, u_0	Superficial gas velocity, m/s
u_{mf}	Superficial gas velocity at minimum fluidization, m/s
$\bar{\bar{x}}$	Mean exit conversion of coke in the fluidized bed
$\bar{x}_i$	Time averaged exit conversion of the coke on particles of size d_i
x_{O_2}	Net conversion of oxygen in the combustion bed
Y_{H_2O}	Mole fraction of water vapor in fluidizing gas
z	Axial bed height, m
α	Constant used in Equation 27
δ	The thickness of coke on a particle entering the

	combustion bed, m
ΔP	Pressure drop through a section of bed, Pa
Δx	Center-to-center spacing of heat pipes in fluidized bed, m
ϵ_{mf}	Void fraction in bed at minimum fluidization conditions
ϵ_b	Volume fraction of bubble phase in bed
$\gamma, \Gamma, \psi, \eta$	Constants from dense-phase mass balance equations
ϕ_p	Volume fraction of a fluidized bed that is particles in the p phase (bubble or dense)
ϕ_s	Shape factor of particle defined to be the ratio of the surface areas of a round particle to an irregularly shaped particle
μ_g	Viscosity of fluidizing gas, Pa s
ρ_c	Density of coke on coked particles, kg/m^3
ρ_g	Density of fluidizing gas, kg/m^3
ρ_s	Density of solid sand particles, kg/m^3
$\tau(d_i), \tau_i$	Residence time in combustion bed required for the complete combustion of the coke on a single particle size of d_i, s

**Process Concepts for the Recovery and Upgrading
of Bitumen and Bitumen-Derived Liquids**

Co-Principal Investigator: F. V. Hanson
Co-Principal Investigator: M. D. Deo

SMALL-DIAMETER FLUIDIZED BED REACTOR STUDIES

EXPLORATORY PROCESS VARIABLE STUDIES

Minimum Fluidization Velocity - Temperature Relationship

Graduate Student: J. V. Fletcher

The small-diameter fluidized-bed reactor system has been used to study the pyrolysis of the bitumen-impregnated sandstones from a number of the tar sand deposits of Utah.   The deposits investigated included Tar Sand Triangle[79,80]; Whiterocks[80,81]; PR Spring[79]; Sunnyside[79]; and Circle Cliffs.[82]   The process variables investigated included reaction temperature, solids retention time, fluidization gas flow rate and the feed sand particle size distribution.   Throughout the course of these studies the quality of fluidization has been a constant source of concern when interpreting the experimental results and the influence of process variables on the product distribution and yields and on the product quality.

The small-diameter fluidized-bed reactor system was scheduled for significant modification during the 1989-1990 contract period. The proposed modifications included the acquisition of an Acrison, Inc., dry material feeder; the design and fabrication of a new, 2.5-inch diameter reactor; and the design and fabrication of an improved product recovery system.   It was intended that completion

192

of the modifications would be followed a resumption of the process variable studies with the Asphalt Ridge tar sand ore.

The design of the reactor led us into a detailed evaluation of the nature of the fluidization in the small diameter fluidized bed, pyrolysis process studies. This evaluation focused on an examination of the design parameters and of the quality of fluidization in laboratory scale fluidized bed reactors. The examination of the data for Group B sands reported in the fluidization literature and of the coked tar sand fluidization data obtained in our laboratory led to the development of an improved correlation for the prediction of minimum fluidization velocities at elevated temperatures. Fourteen previously published variations of the Ergun equation were studied and found to be unreliable predictors of minimum fluidization velocity for some Group B sands, including coked sands, at ambient conditions. Three simplified versions of the Ergun equation were found to adequately correlate published fluidization data for over 25 Group B sands at ambient temperatures. A relationship between U_{mf} and T was developed and incorporated into a proposed method for predicting U_{mf} at elevated temperatures.

The key parameters for the design of laboratory scale fluidized bed reactors have been identified and the design equations are currently being used to design the new reactor system to insure that the system operates in the particulate fluidization mode.

Introduction

One of the challenges a researcher in fluidized bed process development must surmount is the simulation of commercial operating conditions in laboratory scale fluidized beds. This goal can be accomplished through the appropriate application of experimental and laboratory equipment design. The impact of process variables such as temperature, pressure, and fluidizing gas flow rate are commonly evaluated in the laboratory for their importance in scale up design and process modelling. Central to the description of a fluidized bed process is the minimum fluidization velocity, U_{mf}.

As evidenced by many recent publications [83-86], the relationship between temperature, pressure, and fluidizing gas velocity is not yet fully understood for the range of powder types known to be fluidizable. As a practical matter, while many researchers choose to work and publish results at ambient conditions, it is often necessary for others to adjust reported parameters to the conditions of their interest in order to use the reported findings. This need to adjust and predict beyond ambient conditions has most assuredly contributed to the continuing interest in the hydrodynamics of gas fluidized beds and to the development of predictive correlations for U_{mf}.

For example, silica sand, often reported simply as sand, density 2.5-2.7 g/cm^3, has been widely studied in fluidized beds, yet such fundamental parameters as U_{mf}, particle diameter, d_p, and heat transfer coefficient, h_w, are still being studied and discussed in the literature [81,84,85] thirty years after Leva's landmark text was

published.[88]   It is now generally accepted that sand is the prototype material for powders that fit the Group B classification of Geldart [89], a convenient grouping for particles with similar fluidization behavior. Couderc succinctly summarized this classification scheme in the recent book edited by Davidson et al.[86] Published data on the fluidization of Group B sands is available at ambient and elevated temperatures and pressures, and when the particle diameter, temperature and pressure are explicitly reported, it is possible to apply the data to predictive correlations for U_{mf}.

The predictive correlations of interest here are those for U_{mf} based on a modified Ergun equation. The derivation of this equation has been described by others.[86] In order to predict U_{mf} from a modified Ergun equation, temperature and pressure must be determined so that the gas density and viscosity can be specified. The Ergun equation infers that it is possible to predict U_{mf} at any temperature and pressure provided gas viscosity and density values are available. Reviews have noted that some correlations are applicable to more than one powder type within a group.[86,89]

Accordingly, published data on the fluidization of Group B sands at ambient and elevated temperatures was examined to develop a predictive correlation that could be extended to fluidization data for sands containing up to two weight percent carbonaceous residue. The fluidization of coked sands is of interest in a process for pyrolysing tar sands in a fluidized bed reactor. Details of the process concept have been described elsewhere.[90]

195

Two problems became immediately apparent as this review progressed. First, fluidization data are often reported at "ambient" or "room temperature" with no numerical value given. Second, very few researchers report ambient pressure unless they have studied pressure as a variable. One atmosphere pressure must be assumed for the purpose of determining gas density, but any ambient temperature assumption would make the ambiguity in the Ergun equation unacceptable.

A simplified procedure for predicting U_{mf} for Group B sands at both ambient and elevated temperatures was developed and verified, building on the findings of several comprehensive reviews of predictive correlations.[91-96] This procedure reduces the search for a predictive U_{mf} or Reynolds number at minimum fluidization, Re_{mf} correlation from 14 or more variations of the Ergun equation to three choices and was found to yield a good fit to data over a wide range of Archimedes numbers. The procedure was applicable to both Group B sands and coked sands and was found to predict Re_{mf} as well or better than any of the individual Ergun equations. The procedure is also more reliable at ambient temperatures than any of the 14 modified Ergun equations reviewed.[91-96]

Finally, given a valid experimental value of U_{mf}, two methods were found to reliably predict U_{mf} at elevated temperatures. The first relies on a choice of one of the three modified Ergun equations mentioned above. The second method, based on comparisons with published sand fluidization data, is superior to any method published to date, and requires only a valid U_{mf} and its correspond-

ing temperature.

The correlations developed in this study were compared to the coked sand fluidization data of three researchers from the University of Utah tar sands research group.[79,97,98] Agreement between experiment and the proposed predictive methods is excellent in the ambient to 870 K temperature range.

Correlations for Predicting Minimum Fluidization Velocity

Fluidization Parameters

Most U_{mf} or Re_{mf} correlations include values for gas density, gas viscosity, particle density, and particle diameter.[86] The variations of the modified Ergun equation studied here, incorporated these parameters as part of the Archimedes number, Ar.

$$Ar = \frac{d_p^3 g \, \rho_g \, (\rho_s - \rho_g)}{\mu_g^2} \qquad (29)$$

The other parameters in the Ergun equation are bed voidage and particle shape factor, but adopting the method of Wen and Yu[99], these parameters may be lumped into a pair of constants, C_1 and C_2, to give a relationship for Re_{mf}

$$Re_{mf} = [C_1^2 + C_2 \, Ar]^{\frac{1}{2}} - C_1 \qquad (30)$$

from which U_{mf} may be calculated:

$$U_{mf} = \frac{\mu_g \, Re_{mf}}{d_p \, \rho_g} \qquad (31)$$

Although gas viscosity is usually considered independent of pressure[100], density is not. The variation in gas density and

197

viscosity in the "ambient" region when not corrected for temperature results in a potential error in U_{mf} calculated using Equation 30. For example, if "ambient" is 291 K (18°C), then μ/ρ for air is 0.1484 cm²/s; but if "ambient" is 298 K (25°C), then μ/ρ is 0.1550 cm²/s. This is a difference of 4.4% assuming "ambient" pressure to be constant at one atmosphere. Thus, an experimentally measured and reported U_{mf} cannot be properly compared with a predictive correlation unless the experimental temperature and pressure are also reported. Some potentially useful sand fluidization studies could not be included in the present review[87] for this reason.

Mathur et al.[93] recently reviewed eight permutations of Equation 30, including the one originally proposed by Wen and Yu.[98] Mathur et al.[93] concluded that none of the cited correlations adequately fit their new data for four different sized sands. Fortunately, they gave sufficient experimental detail to permit testing their data with several more correlations based on Equation 29. In Table 30, the constants for Equation 30 are expanded from the eight reported by Mathur et al.[93] to fourteen, with the original eight listed first in the order in which they appeared in the original publication.[93]

Table 31 is based on Table 2 from Mathur et al.[93] for 559 μm sand, a sand clearly in the Group B category. The top section of the table gives Ar, U_{mf} and Re_{mf} as reported at six temperatures. The Archimedes number was calculated using Equation 29, U_{mf} was experimentally measured, and Re_{mf} was recalculated using Equation 30. Reported Ar and Re_{mf} are followed by calculated values using

198

Table 30. Values of Parameters C_1 and C_2 Reported for Equation (30) for the Reynolds Number at Minimum Fluidization

Investigators	C1	C2	Notes
1. Wen and Yu[99]	33.7	0.0408	a
2. Bourgeois and Grenier[102]	26.46	0.0384	a
3. Richardson and Jeronimo[103]	25.7	0.0365	a
4. Saxena and Vogel[104]	25.28	0.0571	a
5. Babu et al.[105]	25.25	0.0651	a
6. Thonglimp et al.[106]	19.9	0.0320	a,b
7. Grace[107]	27.2	0.0408	a
8. Zheng et al.[108]	18.75	0.0313	a
9. Thonglimp et al.[95]	31.6	0.0425	c
10. Lucas et al.[92]	32.1	0.0571	
11. Lucas et al.[92]	29.5	0.0357	
12. Lucas et al.[92]	25.2	0.0672	
13. Chitester et al.[109]	28.7	0.0494	
14. Nakamura et al.[94]	33.95	0.0465	

Notes:
  (a)   In the same order as reported in Mathur et al.[93]
  (b)   These constants are for binary mixtures. See number 9.
  (c)   These constants are for multi-sized powders.

Table 31. Experimental and Predicted Values of the Reynolds Number at Minimum Fluidization

Powder: 559 μm sand

Reported by Mathur et al[93]

T, (K)	1200	1050	725	525	375	300
Ar,	612	812	1910	3990	9130	15700
U_{mf}, (cm/s)	13	14	15	17	20	22
Re_{mf},	0.46	0.59	1.22	2.35	4.81	6.39

Recalculated for this Investigation

Ar, (-) [a)	622	831	1904	4006	9063	15790
Re_{mf} (-) [b)	0.46	0.61	1.19	2.31	4.84	7.84

Re_{mf} Predicted Using Equation 30

Investigators						
1. Wen and Yu[99]	0.37	0.50	1.13	2.34	5.10	8.49
2. Bourgeois and Grenier[102]	0.46	0.62	1.40	2.86	6.10	9.96
3. Richardson and Jeronimo[103]	0.44	0.58	1.32	2.70	5.78	9.47
4. Saxena and Vogel[104]	0.69	0.92	2.07	4.18	8.73	13.97
5. Babu et al.[105]	0.79	1.05	2.35	4.72	9.79	15.56
6. Thonglimp et al.[106]	0.49	0.66	1.48	3.00	6.29	10.12
7. Grace[107]	0.46	0.62	1.39	2.85	6.11	10.00
8. Zheng et al.[108]	0.51	0.68	1.53	3.09	6.45	10.33
9. Thonglimp et al.[95]	0.42	0.55	1.25	2.59	5.60	9.26
10. Lucas et al.[92]	0.55	0.73	1.65	3.38	7.24	11.85
11. Lucas et al.[92]	0.37	0.50	1.13	2.33	5.05	8.37
12. Lucas et al.[92]	0.82	1.08	2.42	4.87	10.07	15.98
13. Chitester et al.[109]	0.53	0.71	1.59	3.26	6.96	11.35
14. Nakamura et al.[94]	0.42	0.56	1.28	2.64	5.72	9.49

a) from Equation 29
b) from experimental U_{mf} and Equation 30

densities and viscosities at one atmosphere from an appendix of White.[101] The latter values of Ar and Re_{mf} were used for this study in the interest of consistency.

Listed with the reported and calculated Reynolds numbers in Table 31 are Re_{mf} calculated from Equation 30 using the constants in Table 30. Unfortunately, even after using this expanded list, the conclusion of Mathur et al.[93] that their data cannot be described by a modified Ergun equation is not changed. Perhaps even more important is the finding that the modified Ergun equations are the least accurate at 300 K, the lowest temperature reported. The failure of the modified Ergun equation at ambient temperature suggests the need to reexamine the predictive methodology.

Predictive Methodology for Reynolds Number at U_{mf}

Re_{mf} at Ambient Temperatures

Following the method of Mathur et al.[93], the parameter of interest is the value of Re_{mf}. This can be predicted from modifications of the Ergun equation and then compared to Re_{mf} as calculated from the experimental U_{mf}

$$Re_{mf} = \frac{d_p\,\rho_g\,U_{mf}}{\mu_g} \tag{32}$$

Alternately, Re_{mf} may be predicted from Equation 30, U_{mf} can be predicted using Equation 31, and the predicted U_{mf} can be compared directly with the experimental U_{mf}. These approaches were well

illustrated by Mathur et al.[93], Wen and Yu[100], and Thonglimp et al.[95]

Values for C_1 and C_2 in Equation 30 have been reported by many researchers over the years[92,94,95,99,102-109] and the equation has been applied to powders of many sizes and densities. The motivation in searching for a comprehensive correlation to predict Re_{mf} is in part stimulated by the desire to avoid the necessity of measuring bed voidages and shape factors.[96] Using this approach one wishes to predict Re_{mf} and then U_{mf} at the temperature and pressure of interest given a knowledge of the particle diameter and density. Sands are usually found to have a singular density but a distribution of diameters.

For this study an average particle diameter was calculated by the conventional method[83] using the following equation:

$$\overline{d_p} = \Sigma \frac{1}{(x_i/d_{p_i})} \tag{33}$$

from sieve analysis or other data. If other researchers identified another calculation method, their data was not used. Clearly Equation 29 will magnify any error in calculating $\overline{d_p}$, and using the wrong $\overline{d_p}$ ranks with use of the wrong distributor as the greatest error in fluidized bed research.[110]

With a value for $\overline{d_p}$ and ρ_s, one needs only the gas density and gas viscosity to calculate the Archimedes number at any temperature and pressure. Gas densities and viscosities may be obtained from tables or, in the case of densities, calculated from an appropriate gas law. If the gas is a mixture, then its viscosity may be

calculated using one of the methods recommended by Reid et al.[100]

Re_{mf} at Elevated Temperatures

As noted above and demonstrated in Table 31, the prediction of Re_{mf} using Equation 30 and constants from Table 30 is not a satisfactory procedure at ambient 300 K, yet Table 31 indicates that several pairs of constants gave excellent predictions at the higher temperatures. One of the best correlations, as noted by Davidson et al.[86], is that of Thonglimp et al.[95] provided the correct constants are used (See Table 30 notes).

Hartman and Svoboda[89] cautioned researchers against fitting a room temperature value of U_{mf} to a modified Ergun equation and then assuming it held at elevated temperatures. In addition, the variation in Re_{mf} from Equation 30 using constants from Table 30 or other sources is almost overwhelming. It is thus tempting to simply default to the frequently quoted Wen and Yu equation.[99] Lucas et al.[90] proposed a set of three modified Ergun equations which reportedly give a good fit to experimental data over a broad range of Archimedes numbers range. As indicated in Table 31, these equations also fail near room temperature for the 559 μm sand, but one of the three is actually the best of all 14 surveyed.

Simplified Ergun Equations

From time to time, reference has been made to the simplified solution to the Ergun equation, which itself is a quadratic, proposed by Goroshko et al.[112] Botterill et al.[111, 113] described the Goroshko approach as "fortuitous" and points out how neglecting the

product term when solving the Ergun quadratic tends to compensate for changes in bed voidage which is assumed constant in Equation 30. They further suggest that Re_{mf} might be predicted for elevated temperatures by "fitting" the equation at ambient operating conditions.[111]

Adopting the above suggestion, three simplified Ergun equations were obtained using a broad range of published data for sands.[84,87,93,111,114-119]

For round sands (with $\epsilon_{mf} < 0.48$)

$$Re_{mf} = \frac{Ar}{1400+5\sqrt{Ar}} \qquad Ar \geq 1480 \qquad (34)$$

$$= \frac{Ar}{1400} \qquad Ar < 1480$$

For moderately sharp sands (with $0.45 < \epsilon_{mf} < 0.55$)

$$Re_{mf} = \frac{Ar}{1170+\sqrt{Ar}} \qquad (35)$$

For very angular sands and coked sands

$$Re_{mf} = \frac{Ar}{790+7\sqrt{Ar}} \qquad (36)$$

The form of Equations 34-36 is the same as that proposed by Goroshko et al.[112] and the 1400 in the denominator of Equation 34 is unchanged.[111] All other parameters in these equations were fit to

published data as part of this study. The requisite criteria was to minimize differences between predicted and published Re_{mf} based on standard deviations of the mean differences.

As shown in Table 31, none of the modified Ergun equations formulated from Equation 30 and Table 30 will predict Re_{mf} at 300 K for the 559 μm sand data of Mathur et al.[93] Recalculated experimental Re_{mf} from Table 31 are reproduced in Table 32 along with Re_{mf} as predicted using Equation 34 to demonstrate the improved match of predicted and experimental Reynolds numbers using Equation 34. Agreement is excellent, and more importantly, this calculation method predicts Re_{mf} at 300 K.

Geldart[119] has shown that not all sands are the same, even if their average size is the same. Thus, while Equation 34 success-fully predicts Re_{mf} for the data of Mathur et al.[93] as shown in Table 32 and the data of many others as shown in Table 33, some sands require different constants in the simplified Ergun equation. This is demonstrated for Geldart's data[119] in Table 33 where Equations 34, 35, and 36 are required to match his experimental data. Thresholds for the use of Equations 34-36 are tentative and based on bed voidage at minimum fluidization as reported by Geldart.[119]

Equation 36 is of special interest for our tar sand research because it also gives reasonable predictions of Re_{mf} at ambient temperatures for coked sand. Data from three different fluid bed reactors used in tar sand studies[79,97,98] is compared to Equation 36 in Table 34. It should be noted that the best agreement is for the 10.2 cm diameter reactor of Sung[98] and that the other reactors were

of much smaller diameter. Original pressure drop versus gas velocity data suggests slugging was common to all three reactors and U_{mf} values were reinterpreted as part of this study following the method of Botterill et al.[111]

Table 32. Experimental and Predicted Values of the Reynolds Number
at Minimum Fluidization

	Data Reported by Mathur et al.[93]						
T, (K)	1200	1050	725	525	375	300	
Ar, (−)	622	831	1905	4006	9063	15790	from Eqn 29
Re_{mf}, (−)	0.46	0.61	1.19	2.31	4.84	7.84	from Eqn 30
	Predicted Using Equation 34						
Re_{mf}, (−)	0.44	0.59	1.18	2.33	4.83	7.78	
% Diff.	−4.3	−3.3	−0.8	+0.9	−0.2	−0.8	$|X| = 1.7\%$

Table 33. Experimental and Predicted Values of the Reynolds Number at Minimum Fluidization Velocity for Sands

Investigators	Reported $d_{p(\mu m)}$	Experimental Re_{mf}	Predicted Re_{mf}	(Eqn)
Macek & Amin[115]	720	1.43	1.51	(35)
Grewal & Gupta[84]	237	0.61	0.71	(34)
	545	4.64	6.22	(34)
	896	25.2	22.0	(34)
Yan et al[116]	181	0.59	0.60	(36)
Pattipati & Wen[116,117]	250	0.88	0.93	(34)
	462	5.29	5.03	(34)
	240	0.79	0.95	(34)
Cited in Mori & Wen[118]				
Geldart (1971)	128	0.10	0.14	(34)
Whitehead (1967)	150	0.20	0.23	(34)
Miwa (1971)	160	0.26	0.28	(34)
Tomita (1971)	202	0.54	0.56	(34)
BOTTERILL ET AL[111]	380	3.8	4.1	(35)
	460	5.23	4.96	(34)
	820[a]	23.8	22.5	(35)
	2320	140	172	(34)
Hong et al[87]	194	0.61	0.58	(35)
	359	2.74	2.55	(34)
Geldart[83]	RW-128	0.12	0.17	(34)
	RW-175	0.44	0.44	(34)
	RW-100	0.104	0.097	(35)
	RW-275	1.2	1.46	(34)
	AW-75	0.057	0.057	(36)
	AW-250	1.4	1.4	(35)
	AW-470	9.0	9.0	(35)

[a]   Coal Ash

Table 34. Experimental and Predicted Values of the Reynolds Number at Minimum Fluidization for Coked Sand.

$d_p = 143 \ \mu m$ Data of Jayakar[97]   Reactor Diameter = 5.5cm

Temperature (K)	Experimental Re_{mf}	Predicted Remf	% Difference	Average % Difference
298	0.215	0.238	+10.7	
473	0.0811	0.0793	-2.22	$\|X\| = 12.9\%$
673	0.0415	0.0352	+15.2	$\sigma = 8.6$
873	0.0258	0.0199	-22.9	

$d_p = 202 \ \mu m$ Data of Sung[98]   Reactor Diameter = 10.2cm

582	0.150	0.153	+2.00	
674	0.107	0.111	-3.74	$\|X\| = 2.08\%$
778	0.0820	0.0809	-1.34	$\sigma = 1.15$
870	0.0642	0.0634	-1.25	

$d_p = 202 \ \mu m$ Data of Venkatesan[79]   Reactor Diameter = 3.5cm

293	0.863	0.872	+1.04	
473	0.345	0.298	-13.6	$\|X\| = 15.6\%$
723	0.155	0.118	-23.9	$\sigma = 10.9$
773	0.134	0.102	-23.9	

The modified Ergun equations of Thonglimp et al.[95] and Wen and Yu[99] were developed using many sets of data spanning a wide range of Reynolds numbers. This suggests that the correlations will be valid at elevated temperatures provided appropriate values for gas density and viscosity are used. Testing this hypothesis has produced mixed reviews[91,111] however, as shown in Table 31, the results can be very acceptable in some cases. The problem has been that Equation 30 often does not give adequate predictions ambient temperatures. Equations 34, 35, and 36 appear to fit a broader range of data than any one or more variations of Equation 30 with the added advantage of a good fit at ambient temperatures.

Minimum Fluidization Velocity at Elevated Temperatures

Equation 34 was shown to predict the 559 μm sand data of Mathur et al.[93] at all temperatures in Table 32, and Equations 34 - 36 were shown to yield good ambient predictions in Table 33. The emphasis in developing Equations 34 - 36 was to correct for the failures of Equation 30 at ambient temperatures and to use a simpler method to predict U_{mf} at elevated temperatures. It will be shown however, that Equations 34 - 36 may also be used to predict U_{mf} at elevated temperatures.

Based on data for two sands, Macek and Amin[115] suggested that a relationship exists between U_{mf} and T in the form

$$U_{mf} \ T^{0.38} = k_f \tag{37}$$

This investigation indicated that many published sets of data for U_{mf} and temperature are better correlated by an equation of the form

$$U_{mf} \ T^{0.27} = k_f \tag{38}$$

including the data reported by Macek and Amin.[115] Although the form of Equations 37 and 38 is the same, in each case tested, Equation 38 yields a constant with a much smaller standard deviation than Equation 37.

The validity of Equation 38 is demonstrated in Table 35 where the U_{mf} $T^{0.27}$ product is shown to be constant for the Table 2 experimental data of Mathur et al.[93], and previously published experimental data of Botterill et al.[111] and of Pattipati and Wen.[113] It should be noted that except for Table 31 data, U_{mf} values were obtained in part from plotted points of published graphs. It appears that, given one experimental value of U_{mf} for a Group B sand, Equation 38 can be used to predict U_{mf} at a different temperature. In some cases, calculating k_f from a value for U_{mf} at 400°C or above appears to give even more reliable predictions.

A method for predicting U_{mf} at elevated temperatures is therefore proposed:

1. Determine a value for U_{mf} at a selected temperature either by experiment or by use of Equations 34-36.

2. Calculate the fluidization constant, k_f, using Equation 38.

3. Predict U_{mf} at another temperature by solving Equation 38 at that temperature using the k_f calculated in Equation 30.

The method for predicting U_{mf} is compared with experiment and with two representative Ergun correlations in Table 36. The data

Table 35. Application of Temperture-Minimum Fluidization Velocity Relationship to Published Data

Mathur et al.[93] 559μm Sand		Pattipati & Wen[117] 240μm Sand		Botterill et al.[111] 380μm Sand	
T (K)	k_f	T (K)	k_f	T (K)	k_f
1200	88.2	1020	64.9	1073	62.5
1050	91.6	766	66.1	673	58.0
725	88.8	554	66.1	573	59.4
525	92.2	473	73.8	473	63.3
375	99.1	291	78.7	293	69.5
300	102.6				
$|X|$	93.8	$|X|$	69.6	$|X|$	62.5
σ	5.8	σ	6.1	σ	4.5
$\dfrac{\sigma}{|X|}(100)=6.2\%$		$\dfrac{\sigma}{|X|}(100)=8.7$		$\dfrac{\sigma}{|X|}(100)=7.2\%$	

Botterill et al.[111] 460μm Sand		Botterill et al.[111] 820μm Coal Ash		Botterill et al.[111] 2320μm Sand	
T (K)	k_f	T (K)	k_f	T (K)	k_f
1088	71.3	893	194	988	675
884	65.6	788	188	718	667
548	68.6	473	185	603	619
292	79.3	298	200	293	436
$|X|$	71.2	$|X|$	192	$|X|$	654*
σ	5.9	σ	6.7	σ	30*
$\dfrac{\sigma}{|X|}(100)=8.3\%$		$\dfrac{\sigma}{|X|}(100)=8.7\%$		$\dfrac{\sigma}{|X|}(100)=4.6\%$	

* T = 293 K excluded

Table 36. Comparison of Methods for Prediction of U_{mf} for Sands

---

$d_p = 380$ μm Data of Botterill et al.[111]

Temperature Experimental   Predicted U_{mf} (cm/s)

(K)	U_{mf} (cm/s)	Eqn (38)	Wen & Yu[99]	Thonglimp et al.[95]	Eqn (35)
293	15	13.5	11.8	13.0	16.4
473	12	11.8	8.6	9.5	12.2
573	10.7	11.3	7.6	3.4	10.8
673	10	10.8	6.8	7.5	9.6
1073	9.7	9.5	5.1	5.7	7.2

$d_p = 460$ μm Data of Botterill et al.[111]

Temperature Experimental   Predicted U_{mf} (cm/s)

(K)	U_{mf} (cm/s)	Eqn (38)	Wen & Yu[99]	Thonglimp	Eqn(34)
293	17.1	15.4	17.1	18.8	16.2
548	12.5	13.0	11.5	12.8	11.9
884	10.5	11.4	8.6	9.5	10.2
1088	10.8	10.8	7.6	8.4	9.0

$d_p = 559$ μm Data of Mathur et al.[93]

Temperature Experimental   Predicted U_{mf} (cm/s)

(K)	U_{mf} (cm/s)	Eqn (38)	Wen & Yu[99]	Thonglimp	Eqn (34)
300	22	20.1	23.8	25.9	21.8
375	20	18.9	21.1	23.2	20.0
525	17	17.3	17.3	19.1	17.2
725	15	15.8	14.2	15.8	14.8
1050	14	14.3	11.5	12.7	13.6
1200	13	13.8	10.6	12.0	12.6

---

of Mathur et al.[93] for 559 μm sand, and the data of Botterill et al. [113] for 380 μm and 460 μm sands, have been used in these calculations. The predicted U_{mf} values from Equation 38 are found using the average fluidization constant k_f in Table 35. Comparison of the experimental U_{mf} values in Table 36 with those predicted from the correlation of Thonglimp et al.[95], the Wen and Yu equation[99], and Equations 34-36 as appropriate, shows Equation 38 to be superior predictive tool in a majority of cases.

Predicting U_{mf} for Coked Sand

Several researchers[79,97,98] have published U_{mf} data for sand produced in a bitumen recovery process using a fluid bed. This data is for both nitrogen and air fluidized beds from ambient to over 850 K. Reexamination of this data shows that Equation 36 will successfully predict the Re_{mf} at ambient temperatures, and that Equation 38 is valid at all temperatures investigated. This is illustrated in Tables 34 and 37.

Table 34 compares experimental Re_{mf} values to ones predicted by applying Equation 36 to the data of Jayakar [97], Sung [98], and Venkatesan.[79] As mentioned above, these data suggest slugging occurred, and it is not surprising that the best fit is for the largest diameter bed. Unfortunately, Sung did not report a U_{mf} for coked sand at an ambient temperature. The fluidization constant, k_f, calculated using Equation 38 and the experimental data reported in Table 34 is presented in Table 37. Based on the standard deviations, Equation 38 is valid $\pm$ 10% at the 99% confidence level.

Table 37. Application of Temperature-Minimum Fluidization Velocity Relationship to Coked Sand Data.[79,97,98]

	$d_p = 143\ \mu m$		Data of Jayakar[97]	
Temperature (K)	Experimental U_{mf} (cm/s)	k_f (cm·K/s)	Average	k_f
296	2.71	12.6	$\lvert X \rvert =$	12.4%
473	2.30	12.1	$\sigma =$	0.2
673	2.13	12.4	$\dfrac{\sigma}{k_f}$	
873	2.02	12.6		$(100)=1.6\%$

	$d_p = 202\ \mu m$		Data of Sung[98]	
582	4.09	22.8	$\lvert X \rvert =$	21.8%
674	3.73	21.7	$\sigma =$	0.7
778	3.61	21.8	$\dfrac{\sigma}{k_f}$	
870	3.39	21.1		$(100)=3.2\%$

	$d_p = 225\ \mu m$		Data of Venkatesan[79]	
293	6.8	31.5	$\lvert X \rvert =$	32.5%
473	6.2	32.7	$\sigma =$	0.7
723	5.6	33.1	$\dfrac{\sigma}{k_f}$	
773	5.4	32.5		$(100)=2.2\%$

The data of Venkatesan[79] was studied over the temperature range 293 K to 773 K to test the validity of the proposed method. Assuming no experimental value of U_{mf} was available, the following calculation procedure was followed and compared with the experimental data in Table 38:

Step 1   Using Equation 36 and then Equation 31, calculate Re_{mf} at 293 K (or any other convenient temperature) and U_{mf}. U_{mf} (calculated) = 6.9 cm/s at 293 K

Step 2   Using Equation 38, calculate k_f based on U_{mf} and T, from Step 1 above. k_f = 32.0 cm·K/s

Step 3   Solve Equation 38 for U_{mf} at the other temperatures of interest using k_f from Step 2 above. See Table 38 for predicted U_{mf} at 473 K, 723 K, and 773 K.

It should be noted that given the preferred case of an experimental U_{mf} and temperature, Step one would be skipped and Steps two and three would still be used to predict U_{mf}.

As can be observed from Table 38, the experimental and predicted values of U_{mf} are in close agreement.

Table 38.   Experimental and Predicted Values of the Minimum Fluidization Velocity using Coked Sand Data.[79]

Temperature (K)	Experimental Re_{mf}	Predicted Remf	% Difference	Average % Difference
293	6.8	6.9 (a)	+1.5	$|X|$ = 2.2%
473	6.2	6.1 (b)	-1.6	σ = 1.0
723	5.6	5.4 (b)	-3.6	
773	5.4	5.3 (b)	-1.9	

(a) from Equation 36
(b) from Equation 36 at 293K, then Equation 38 at T

Conclusions

Based on this study, the following conclusions may be drawn:

1. The Ergun equation in one of the forms popularized by Wen and Yu[99] is more likely to predict an accurate Re_{mf} at temperatures well above ambient and must be used with caution at room temperatures.

2. A simplification of the Ergun equation, adjusted for the degree of sand roundness, will predict Re_{mf} at ambient temperatures:

    (a) For round sands

$$Re_{mf} = \frac{Ar}{1400 + 5\sqrt{Ar}} \qquad Ar \geq 1480 \qquad (34)$$

$$= \frac{Ar}{1400} \qquad Ar < 1480$$

    (b) For moderately sharp sands

$$Re_{mf} = \frac{Ar}{1170 + 5\sqrt{Ar}} \qquad (35)$$

    (c) For very angular sands and coked sands

$$Re_{mf} = \frac{Ar}{790 + 7\sqrt{Ar}} \qquad (36)$$

3. The simplified Ergun equation for very angular sands reliably predicts Re_{mf} for coked sands produced through

216

fluid bed pryolysis of tar sands.

4. A simple relationship exists between U_{mf} and the corresponding temperature of some Group B sands and coked sands. The relationship

$$k_f = U_{mf}T^{0.27} \tag{38}$$

was found to be valid up to 1200 K for particles with average diameters from 143 μm to 2320 μm. There was an exception at 293 K for the largest sand, which is more likely a Group D sand.

5. The uncertainty of the 14 possible modifications of the Ergun equations or the three simplified versions of the Ergun equation may be avoided when predicting U_{mf} versus temperature. Given one experimental U_{mf} and corresponding temperature, it is recommended that one calculate the fluidization constant, k_f, using Equation 38 and predict U_{mf} at other temperatures by solving Equation 38 based on the experimental k_f.

Future Activities

The correlations for minimum fluidization velocity and the minimum fluidization velocity-temperature relationship will be used in the design of the large-diameter fluidized bed reactor. The reactor will be fabricated and installed for preliminary fluidization studies. The coked sand withdrawal system will be designed and a prototype will be evaluated prior to fabrication and installation on the reactor. The product recovery system will be designed, fabricated and installed.

The assembled unit will undergo preliminary testing with coked sand produced in the previous fluidized bed production run. The reactor furnace (propane gas burner) will be installed and tested during hot fluidization tests with coked sands. The correlations will also be used to redesign the small diameter fluidized bed reactor system.

Nomenclature

Ar	Archimedes number, Ar, from Equation (28),
C_1 C_2	Constants in Equation (29)
$\bar{d}_p$	Average size of particles, from Equation (32),m
d_{pi}	Size of particles in ith fraction, m
g	Acceleration due to gravity, m/s^2
h_w	Total heat transfer coefficient, W/m^2 · K
k_f	Fluidization constant in Equation (37), m · K/s
Re_{mf}	Reynolds number at minimum fluidization from Equation (29) or (31), --
U_{mf}	Superficial gas velocity at minimum fluidization conditions from Equation (30), m/s
x_i	Mass fraction of particles in ith fraction, --
$|\bar{x}|$	Average of absolute values of x

Greek Symbols

ϵmf	Bed voidage at minimum fluidization, --
ρ_g, ρ_s	Density of gas and solid respectively, k$_g$/m^3
μ_g	Gas viscosity, k$_g$/m · s
σ	Standard deviation, --

Catalytic Activity of the Circle Cliffs Mineral Matter

Graduate Student   D. Shun

The mined and crushed ore from the Circle Cliffs tar sand
deposit produced significantly less bitumen-derived hydrocarbon
liquid than the ore from the Tar Sand Triangle tar sand deposit at
comparable pyrolysis conditions.[82] This decrease in liquid product
was accompanied by a significant increase in the C_1-C_4 hydrocarbon
gas yield.   The production of hydrocarbon products was also
accompanied by a significant yield of water.

Analysis of the host rock from the Circle Cliffs tar sand
deposit indicated that it contained an appreciable amount (up to 14
wt.%) of kaolinite which appeared to be activated at pyrolysis
conditions and acted as a catalytic cracking agent in the presence
of the varporized bitumen-derived hydrocarbon liquid. The cracking
function of the kaolinite caused the shift from the higher
molecular weight liquid products to the lower molecular weight
gaseous products.

The catalytic cracking activity of the kaolinite containing
mineral matter was confirmed by cracking normal hexane over the
bitumen-free Circle Cliffs host rock. The hexane cracking product
distribution obtained with the bitumen free Circle Cliffs host rock
indicated that a carbonium ion mechanism was operative which would
be expected for catalytically active materials. The bitumen-free
host rock from the Whiterocks tar sand deposit, shown to be free of
kaolinite, was also evaluated for hexane cracking.   The product

219

distribution from these experiments indicated a thermal cracking mechanism was operative.

If the kaolinite were determined to persist throughout the saturated zones of the Circle Cliffs tar sand deposit then it would seem reasonable to conclude that thermal recovery methods would not be feasible for the recovery of hydrocarbon values. This conclusion may also extend to in-situ thermal recovery methods. The lean nature of the resource, less then four to five weight percent bitumen saturation, significantly impacts the economics of the other mining-surface recovery process schemes: aqueous separation and solvent extraction processes. These factors coupled with the proximity of Capitol Reef National Park severely limit the potential for the development of the hydrocarbon resource in the Circle Cliffs tar sand deposit. Thus, the focus of the thermal process development program has shifted to the Uinta Basin tar sand deposit.

Large-Diameter Fluidized-Bed Reactor Studies

Graduate Student   J.V. Fletcher

The production run conducted in the large diameter (4-inch) fluidized bed reactor system was successful in that it identified all of the significant operating problems associated with long-term operation of the system. The problem and proposed solutions to each have been discussed in detail by Sung[97] and several have been implemented by Fletcher during the current period.

Design, Specification and Evaluation of the Tar Sand Feeder

Based on successful tests of feeding tar sand/coked sand mixtures with a dry materials, bin discharge feeder used by Harper Electric Furnace on their rotary kiln, and past experience with similar equipment, an Acrison bin discharge feeder was selected to feed tar sand on the redesigned fluid bed reactor. Discussion with factory and local representatives lead to a set of specifications for flow rate, pressure rating, and fittings for purge gas and thermocouples.

The Acrison Model BDF-1.5/E2 was received in late fall of 1989, installed in December, and subjected to calibration tests in the first months of 1990. This feeder has all of the factory heavy duty service options, most notable is the solid shaft feed anger. It has a variable speed D.C. motor and calibration of the controller showed excellent linearity but a 3.3 second delay from start to actual shaft movement. This should not be a problem in operation since the feeder will operate at a fixed, continuous speed.

Using coked sand previously produced from the 4-inch fluidized bed reactor, mass versus time data was collected for the feeder at 15%, 30%, 45%, 60%, and 75% of total speed. The feed rate data exhibited excellent linearity in all cases (Figure 49). At 100% of speed this feeder (E/2) will feed 1.86 kilograms of coked sand per minute. Similar tests were conducted using mixtures of coked sand and tar sand: coked sand to tar sand ore ratios of 1:1 and 1:3. No observable performance changes were noted so the calibration using 100% (Whiterocks West North) tar sand was carried out. A lower mass output was observed: (Figure 50) at a 90% setting with coked sand the feeder delivered 1674 grams per minute but at the same setting with 100% tar sand only 660 grams per minute were delivered. Thus the maximum feed rate decreased from 1.86 kg to 0.72 kg per minute. This reduction in feed rate with time on stream is believed to be caused by an increase in temperature in the tar sand within the feed hopper due to shear. It is also possible that the incorporation of higher temperature ambient air into the agitated tar sand could contribute to the increased temperature.

In the process of redesigning the fluid bed reactor the range of feed rates needed were calculated at 300 to 2000 g per minute. Thus, the reduction in feed rate noted for 100% tar sand required specification of an auger with a different pitch. Since augers are interchangeable on this feeder, we selected the larger Model H/2 auger to complement the E/2 and give a broader experimental range for feed composition and feed rates. The new auger was ordered in June 1990 and a water jacket will be specified for the discharge cylinder to help maintain lower temperature in the feeder conduit.
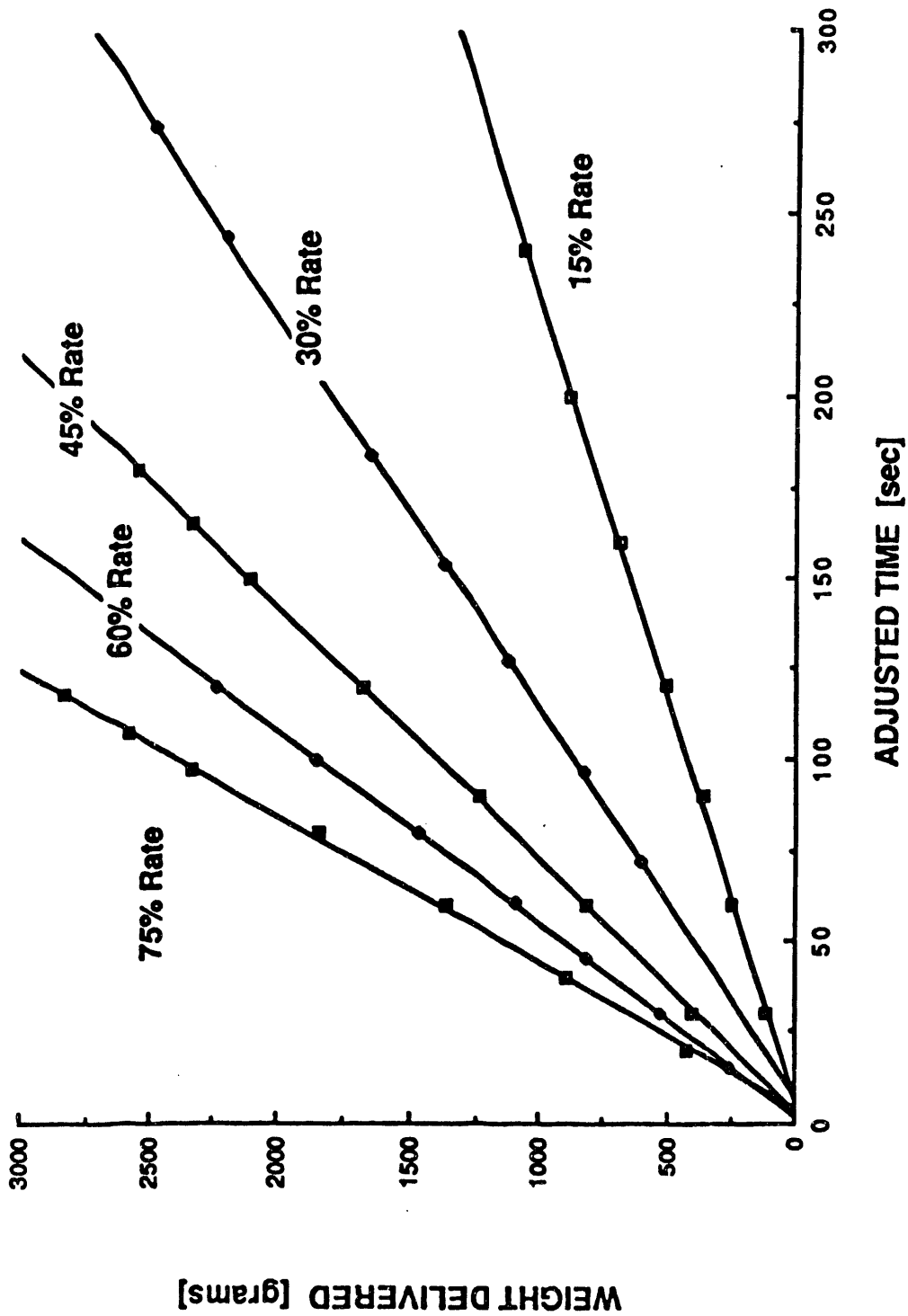
Figure 49. Acrison Dry Materials Feeder Calibration with Coked Sand

223
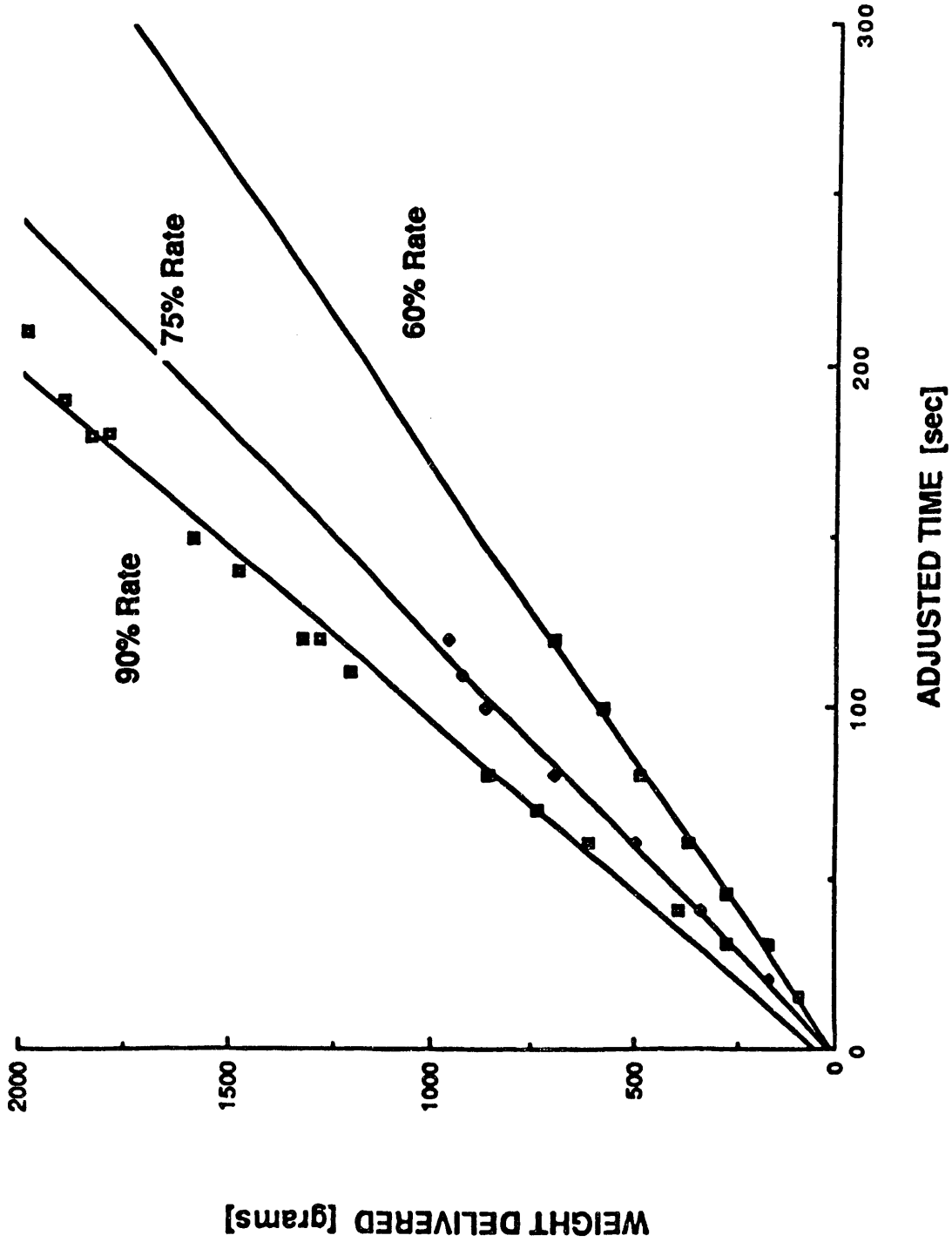
Figure 50. Acrison Dry Materials Feeder Tar Sand Feeding Test with Whiterocks Ore

224

Design of the Overall Fluidized-Bed Unit

Previously, the University of Utah has tested 1 1/4-inch and a 4-inch diameter fluid bed reactors. Reevaluation of performance data for these reactors suggested that they were prone to slugging. With the intent of avoiding this behavior and studying key operating parameters in the fluidized regime, we determined that a 6" diameter reactor was the minimum size that would avoid wall effects and allow operation as a true fluidized bed. At this diameter, a bed holdup of six kilograms was calculated to be the maximum amount that will avoid slugging. Six kilograms is also the bed holdup used in the 4-inch diameter reactor, thus it should be possible to compare fluidization data for the two reactors.

Heat for the 6-inch diameter reactor will be provided using a natural gas burner fired into a heating jacket built around the lower third of the bed. This will allow greater heat flexibility than the previously used resistance heaters but more importantly it will allow us to recycle cracked hydrocarbon product gases and burn them as a first step toward demonstrating an energy sufficient process.

The other serious problem reported with earlier rectors was the erratic performance of the coked sand discharge valve. This problem was addressed in the new reactor specifying a conical base grid design which permits withdrawal of coked sand down the center of the cone using a nonmechanical L valve.[119,120] The design and operation of a prototype nonmechanical valve will be studied during the 1990-1991 contract period.

Summary and Conclusions

The Acrison feeder has solved the tar sand ore feeding problems encountered in the continuous production run with the large diameter fluidized bed reactor apparatus. It is also anticipated than an Acrison feeder would be feasible for the revamped small diameter fluidized bed reactor system.

Future Activities

The fluidized bed reactor will be fabricated and assembled during the 1990-1991 contract period. It should also be possible to conduct hydrodynamic studies with the assembled reactor to test the coked sand withdrawal system, the conical distributor design and the fluidized bed design equations.

Rotary Kiln Pyrolysis Reactor

Principal Investigator: F. V. Hanson

Graduate Student: S. Cha

Introduction

The successful completion of the preliminary rotary kiln pyrolysis reactor test with the Whiterocks tar sand ore at the Harper Electric Furnace Corporation Development Laboratories in Lancaster, New York, led to the purchase of a Model HOU-6D60-RTA-25 rotary kiln. The reactor-furnace assembly and the control module, scheduled for delivery in December 1989, were finally delivered in late February 1990. Electrical and water utility services were connected in March 1990.

The unflighted kiln barrel was installed in the furnace and the Acrison dry material feeder was calibrated with coked sand and mixtures of coked sand and fresh tar sand. A series of preliminary experiments were conducted to refine the operating procedures, to establish material balance capabilities and to determine the reproducibility of the product distribution data.

Reproducibility of Rotary Kiln Pyrolysis Experiments

A series of three experiments was conducted at 798 K and a solids retention time of 21 minutes to specifically evaluate reproducibility of the operating procedures. The normalized product distributions and yields are presented in Figure 51 and Table 39. The C_1-C_4 gas, the C_5^+ hydrocarbon liquid and the
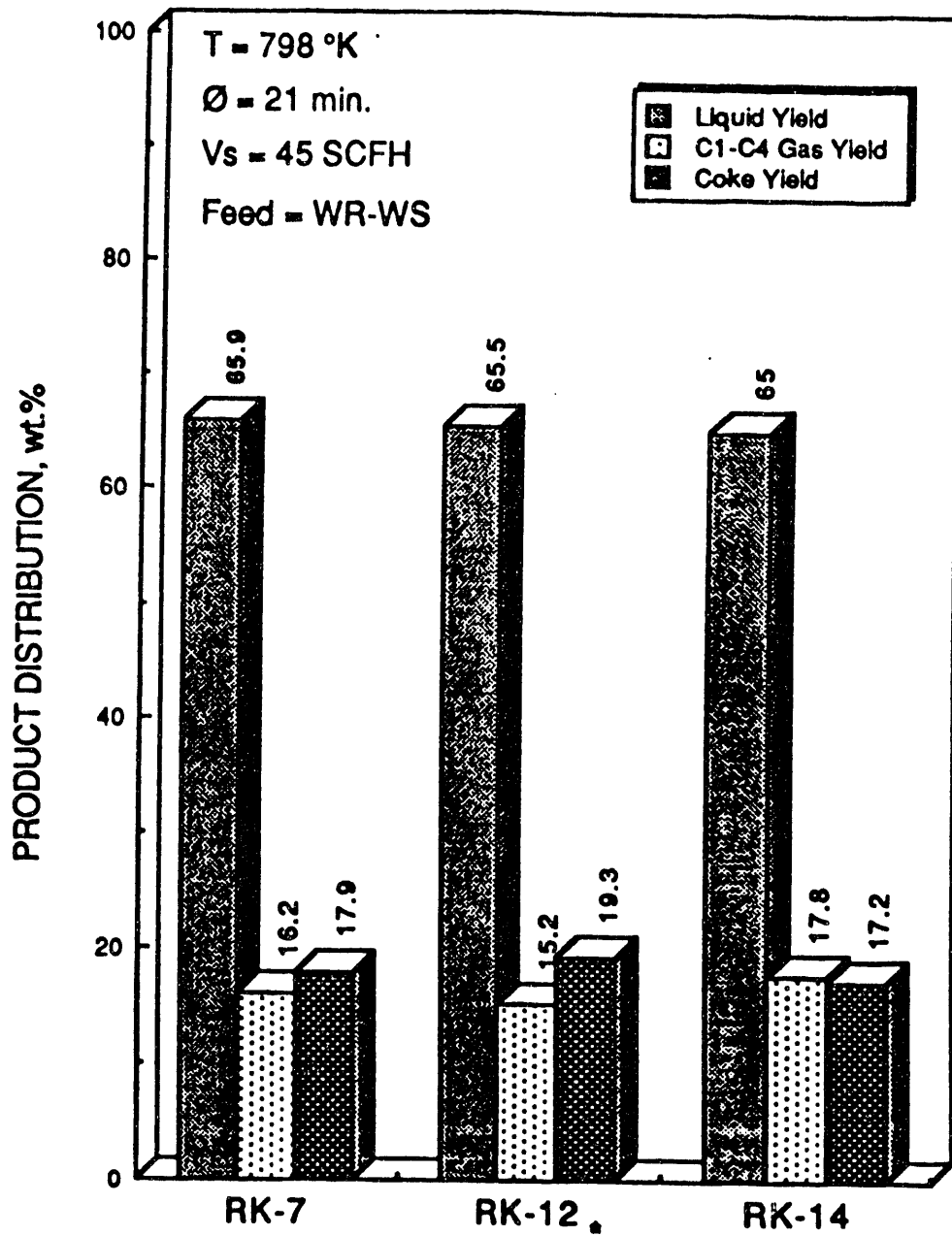
Figure 51. Reproducibility of Normalized Product Distributions and Yields with the Rotary Kiln

Table 39. Reproducibility of Product Distribution and Yields with
          the Rotary Kiln

Run I.D.	RK-7	RK-12	RK-14
Feed Sand	WR-WS	WR-WS	WR-WS
Reactor Temp.	525 C	525 C	525 C
Retention Time	21 min	24 min	21 min
Gas Flow Rate	45 SCFH	45 SCFH	45 SCFH
Obtained Yields			
Liquid, wt%	59.9	57.5	60.0
Gas, wt%	14.2	13.2	16.4
Coke	15.7	16.9	15.9
Total Mass Balance, wt%	87.8	87.6	92.3
Losses, wt%	12.2	12.4	7.7
Normalized Yields*			
Liquid, wt%	65.9	65.5	65.0
Gas, wt%	16.2	15.2	17.8
Coke, wt%	17.9	19.3	17.2
Total Mass Balance, wt%	17.9	19.3	100
Gas Product Distribution			
H2, wt%	0.10	0.10	0.11
CH4, wt%	1.94	1.94	2.09
CO2, wt%	1.01	1.21	1.03
C2H4, wt%	1.04	0.91	1.20
C2H6, wt%	1.23	1.22	1.42
C3H6, wt%	4.48	3.46	5.27
C3H8, wt%	1.39	1.27	1.62
i-C4, wt%	0.11	0.14	0.16
n-C4=, wt%	1.84	1.80	2.17
n-C4, wt%	0.82	0.93	1.10
i-C4=, wt%	0.21	0.21	0.23
C5's, wt%	1.54	1.68	1.88
C6's, wt%	0.36	0.50	0.72

*Normalization of obtained yields: (obtained yield) + (osses x
obtained yield/obtained mass balance)

carbonaceous residue yields for the three experiments were in excellent agreement. Unfortunately, run RK-12 was carried out at a slightly higher solids retention time than was used in runs RK-7 and RK-14; however, this difference did not alter the conclusion regarding the reproducibility. The raw material balance data indicate that the operating procedures and material balance practices still require improvement.

A second series of preliminary experiments were conducted to evaluate the product recovery systems: liquid product recovery and spent sand recovery systems. After several modifications, based on operating experience gained in the preliminary runs both product recovery systems functioned satisfactorily.

Liquid Product Recovery System

The recovery of the hydrocarbon mist formed during the pyrolysis of tar sand is important in obtaining an acceptable material balance and in performing an economic evaluation of the process. This initial study was intended to lead the development of an efficient liquid product recovery system for the rotary kiln pyrolysis reactor.

A hydrocarbon vapor is produced whenever fresh tar sand is added to a reactor at temperature above 673°K. When the hydrocarbon vapor-carrier gas mixture is cooled in the condenser, a hydrocarbon mist or aerosol is formed. Brink, Jr., et al.[121] have reported on the effectiveness of the various demisting devices as a function of the droplet size of the aerosol. Demisting equipment such as packed-bed scrubbers, electrostatic precipitators, and

230

fiber mist collectors are most effective for the coalescence of aerosols over a wide range of droplet size (10 to 0.01 microns and below), while cyclone separators and impingement separators such as demisting wire mesh pads are effective over a narrow size range of mist droplets (5 to 10 microns). Several of these demisting devices were evaluated either alone or in combination for the coalescence of the hydrocarbon mist produced in the rotary kiln.

Fiber mist eliminators which were tested as one of demisting options in these experiments have been widely used for the removal of acid mist.[121] The reported collection efficiencies are high (> 95%) because of the combination of three mechanisms operative during demisting; that is, inertial impaction, direct interception, and adsorption/absorption. When a gas stream containing an aerosol moves across the fibers, the large size droplets are coalesced and condensed on the fibers by inertial impaction and by direct interception and become a part of the liquid film which wets the fibers. When small mist droplets in the gas impinge on the surface of the wet fibers, they are absorbed by the liquid film.

Design of Liquid Product Recovery System

The liquid product recovery system consisted of two condensers in series, a demister with demisting pad and a fiber mist collector for the recovery sand fines and the hydrocarbon mist. All elements in the demisting system were operated at room temperature. A schematic of the liquid product recovery system is presented in Figure 52.

231
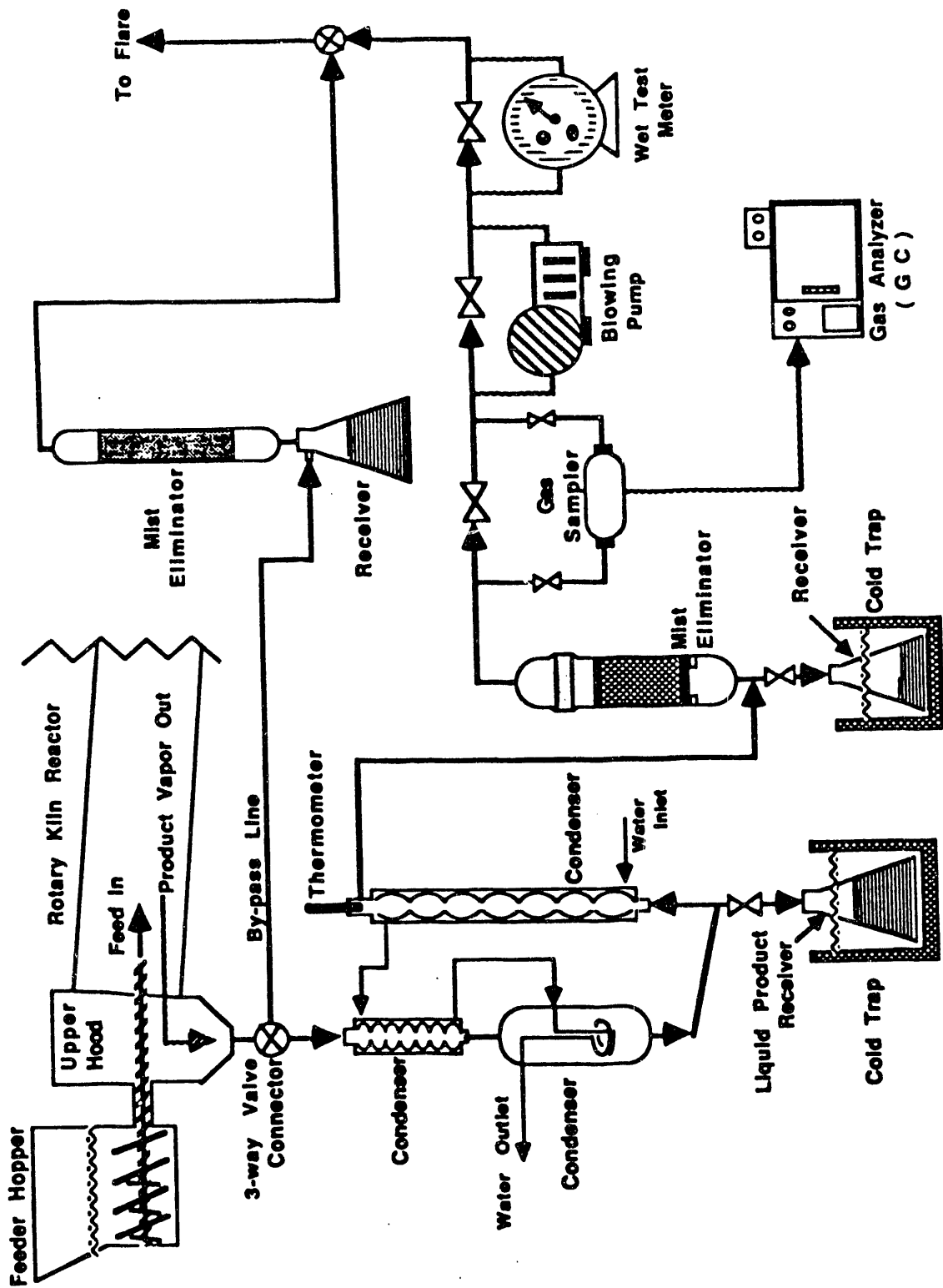
Figure 52. Flow Diagram Of The Liquid Product Recovery System

The hydrocarbon vapor, along with the carrier gas leaving the reactor, enters the product recovery system where it is cooled in two water-cooled Pyrex Brand Allihn condensers and where a significant porition of the hydrocarbon is vapor condensed and collected in the liquid product receiver. A fraction of the vapor which condensed on the wall of the inner tube in both condensers were collected in the liquid product receiver and was drawn off periodically.

The remaining condensible vapors, in the form of a hydrocarbon mist suspended in the sweep gas, were passed through a demisting pad where most of the mist and the sand fines were condensed and collected, respectively. Once the demisting pad was saturated with hydrocarbon liquid, the efficiency of the demister increased.

Conventional chromatographic gas analysis was used to analyze the unit off gas. The condensed hydrocarbon liquids contained small amounts of the fine sand and were filtered or centrifuged before physical and chemical analyses were performed. The demisting train was estimated to operate above 95% efficiency during their experiments.

Calculation of Product Condensers Cooling Water Duty

Calculation of the maximum condenser water duty was carried out assuming that the condenser is a simple shell and tube heat exchanger using cold water as the cooling fluid.

Maximum gas flow rate = 250 CFH (9000 g/hr)

Maximum liquid yield
 (assuming the gas
 yield is 30 wt%) = 70 wt%

233

Maximum bitumen saturation	= 10 wt%
Maximum feed rate	= 30 kg/hr
Average temperature of entering water	= 17°C
Heat of vaporization for liquid products; $\underline{H}_v$ (C_5^+)	= 80 cal/g
Maximum bitumen condensation rate	= 2100 g/h
Maximum gas product flow rate, $\underline{M}_g$	= 900 g/h
Average heat capacity of nitrogen; C_{p,N_2}	= 0.253 cal/g/°C
Average heat capacity of liquid products; $C_{p,l}$	= 0.8 cal/g/°C
Average heat capacity of water, $C_{p,w}$	= 1 cal/g/°C
Heat capacity of gas products (C_1 - C_4), $C_{p,g}$	= 0.83 cal/g/°C

Thus, the total energy balance for the maximum condenser heat duty is,

$$M_w \, C_{p,w} \, (T_{cb} - T_{ca}) = M_{N2} \, C_{pN_2} \, (T_{ha} - T_{hb})$$
$$+ M_g \, C_{p,g}^2 \, (T_{ha} - T_{hb})$$
$$+ M_1 \, [\underline{H}_v + C_{p,1} \, (T_{ha} - T_{hb})] \quad (39)$$

Therefore, the water rate calculated from this equation is:

M_w = 957,600 g/hr = 4.22 gal/min

Assuming that the efficiency of the heat exchanger is 0.8, the water rate required for the condensers is

M_w = 4.22 gal/min / 0.8 = 5.3 gal/min.

Control of Pressure Drop Across the System

In the rotary kiln unit, the pressure drop on the system must be limited to 16 inches of water because a pressure drop in excess

234

of 16 inches of water in the kiln will cause vapor/gas leaks through the rotary seals. This makes it difficult to operate the liquid product recovery train and the off gas monitoring device because it creates a back pressure the rotary kiln. It is proposed to connect the exit line from the liquid product recovery train to the suction or inlet line of a properly sized blower (Figure 52). The pressure inside the rotary kiln and concomitantly the pressure drop across the rotary seals will be controlled by means of a metering by-pass valve around the blower. This pressure control system will be developed early in the 1990-1991 contract period prior to the start of the process variable study.

Summary and Conclusions

The reproducibility of the product distribution and yields provided confidence that the rotary kiln reactor system would provide reproducible process variable data for the pyrolysis of tar sands.

Future Activities

The rotary kiln tar sand pyrolysis process variable study will be conducted during the 1990-1991 contract period. The primary process variables to be investigated include the pyrolysis zone temperature, the feed sand retention time in the pyrolysis zone and the sweep gas flow rate. The crushed and sized tar sand ore from the Whiterocks tar sand deposit will be used in these initial process studies. The analyses of produced gases and liquids will be initiated.

Riser Reactor for the Combustion of Coked Sand

Co-Principal Investigator: F. V. Hanson:
Postdoctoral Fellow   L. C. Lin:

The feasibility of the riser reactor for the combustion of the carbonaceous residue produced during tar sand pyrolysis was evaluated for the Whiterocks tar sand. The analyses indicated that both the dilute phase and the dense-phase transport reactor would be suitable. The mathematical analysis and the design parameters determined are reported in the subsequent discussion.

Introduction

The recovery of hydrocarbon values from bitumen-impregnated sandstone can be accomplished by any one of several mining-surface recovery schemes. These recovery process concepts include aqueous separation,[4,15] diluent-assisted aqueous separation,[6,7,18] solvent extraction,[122-124] and pyrolysis[79-82] as well as combinations of these processes.[124-126] The pyrolysis process include both fluidized-bed[79-82] and rotary kiln[127] reactors.

The product distribution from tar sand pyrolysis included a carbonaceous residue ("coke") on the spent sand in addition to hydrocarbon gases and liquids.[90] The carbonaceous residue is an important thermal energy source, as its combustion can contribute a substantial portion of the energy required for surface retorting. Typically, 15-30 weight percent of the bitumen fed to a pyrolysis reactor is converted to a carbonaceous residue on the spent sand. This corresponds to one to two weight percent based on the spent sand which is not unlike the coke content of a catalytic cracking

236

catalyst in heavy oil cracking service.

The fluidized-bed pyrolysis of Utah tar sand has been extensively investigated in both single-stage[78-82,98] and two-stage[72] applications. The single-stage pyrolysis reactor was continuously fed with fresh, crushed and sized bitumen impregnated sandstone. The fluidized-bed inventory was maintained constant by simultaneously adding fresh feed sand to the reactor and withdrawing the spent sand. Thus the carbonaceous residue was not used to provide thermal energy for the pyrolysis process. The two-stage, thermally efficient fluidized-bed pyrolysis reactor consisted of two distinct zones: an upper pyrolysis zone and a lower combustion zone. The thermal energy generated in the combustion zone was transferred to the pyrolysis zone by means of internal heat pipes. The reactor was in heat balance at all times with this configuration.

The single-stage pyrolysis reactor concept has evolved with an external loop in which the carbonaceous residue on the spent sand would be burned in a riser reactor. A portion of the clean, residue-free sand would be recycled to the pyrolysis zone to provide the thermal energy required for the pyrolysis process.

The objective of this sub-project was to evaluate the feasibility of the riser reactor for the combustion of the carbonaceous residues left on the spent sand produced during the pyrolysis of bitumen-impregnated sandstone. Subsequent to the feasibility analysis a preliminary design of the riser reactor was initiated. The next phase of the project will include completion

237

of a final design for the riser reactor and construction of the apparatus based upon the final design.

Theoretical Considerations

The concept of a vertical transport reactor (riser-combustor) has been investigated for application to the combustion of coked sand particles.

The minimum fluidization and particle terminal velocities are frequently used design parameters in fluid-solid systems.[71] For small particles, the minimum fluidization velocity is calculated from[71]

$$U_m = \frac{d_p^2 (\rho_s - \rho_g) g}{1650 \mu}; \quad Re < 20 \tag{40}$$

and the particle terminal velocity is given by

$$U_t = \left[\frac{4 (\rho_s - \rho_g)^2 g^2}{225 \rho_g \mu} \right]^{1/3} d_p; \quad 0.4 < Re_p < 500 \tag{38}$$

where $Re_p = \rho_g u_o d_p / \mu$ is the particle Reynolds number. Pneumatic conveying of solids has generally been classified into two categories: dilute-phase (lean-phase) transport and dense-phase transport. The two possible classes of behavior are illustrated in Figure 53 as the gas velocity passes from a high to a low value at a fixed solid flow rate.[128,129] Several criteria have been proposed to predict when choking of the bed would occur. Yousfi and
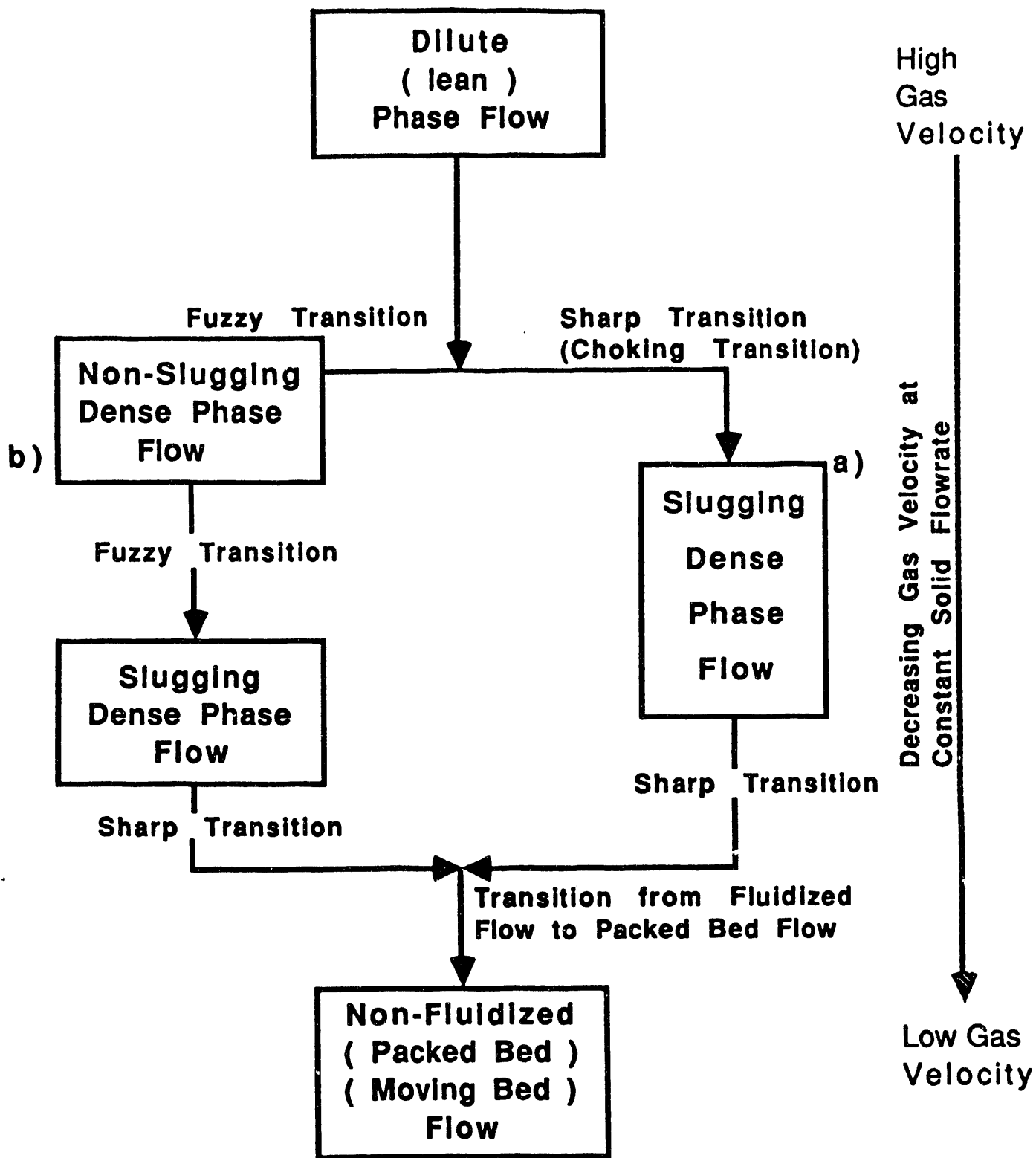
Figure 53.   Possible Flow Patterns in Vertical Pneumatic
              Conveying a) Choking-Type System and b) Non-
              Choking-Type System.

239

Gau[128,129] predicted that choking will occur when the Froude number exceeds 140:

$$\frac{u_t^2}{gd_p} > 140 \tag{42}$$

Yang[128,129] extended this concept further and developed the following criterion to predict choking:

$$Fr = \frac{U_t^2}{gD} < 0.35; \text{ no choking}$$

$$\tag{43}$$

$$Fr = \frac{U_t^2}{gD} > 0.35; \text{ choking occurs}$$

where Fr is the Froude number. In general, light and small particles in large tubes tend towards nonslugging dense-phase mode, while choking is more likely to occur with coarse particles in small tubes.

Zenz and Othmer[130] considered choking as the degeneration of dilute gas-solid flow into dense phase, slugging flow. A flow characteristic in vertical transport based on Zenz and Othmer's schematic representation is presented in Figure 54.[129] The pressure drop in pneumatic transport is due to gas-to-pipe and solid-to-pipe friction. Assume solids at a rate G1 are introduced into a gas stream which is flowing at a velocity corresponding to point B. Line AB represents the pressure drop versus velocity relationship for gas alone (no solid) passing through the transport line. The pressure drop decreases as the gas flow rate is reduced gradually
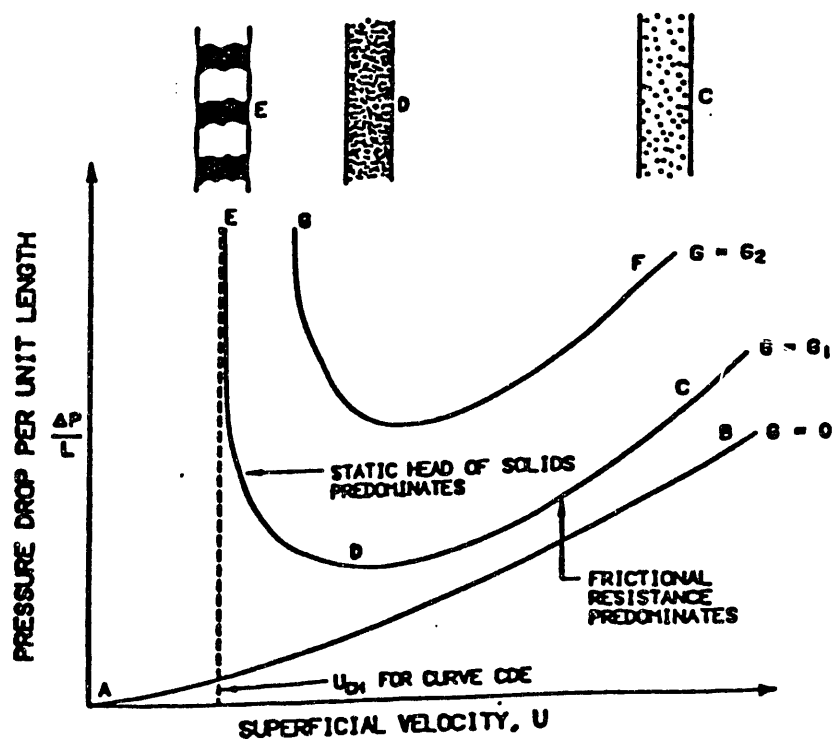
Figure 54. Phase Diagram for Dilute Phase Vertical Pneumatic Conveying

from point C to D. Simultaneously the velocity of the particles and the voidage decrease while the static head of the particles increases. At point D, the solid head begins to exceed the gas friction and a further lowering of the gas flow causes a sharp rise in pressure drop. As point E is approached the gas can no longer support the mass of the solid suspended and the solid collapse into a dense-phase slugging mode. The gas velocity at point E is called the choking velocity and is the lower limit of the gas velocity which is able to maintain a dilute-phase vertical flow.

Several correlations for predicting choking velocity have been proposed.[71,128-131] Among them the Zenz and Othmer[130] correlation is simple and applicable to a system of varying gas density. They are shown below:

$$U_{ch} = U_o \frac{100 G_s}{3_n D^2 \rho_s (3^- \rho_s)}$$ (44)

An alternative method to estimate choking velocity is given by the following relationships[130]:

$$W_{ch} = \rho_s (1 - \varepsilon_{ch}) (U_{ch} - U_t)$$ (45)

and

$$\varepsilon_{ch} = 0.03 \rho_s + 0.91$$ (46)

where ρ_s is in g/cm^3. The critical voidage, ε_{ch} is nearly independent of the mass velocity of solids and of the particle diameter in the range of 0.17-1.7 mm.

The optimum gas velocity for dilute-phase vertical transport has been investigated. Zhang and Yang[131] found the optimum gas velocity was 1.3 times that of choking velocity for a tube with dimension less than 56 cm. Ahland[131] developed a correlation for cases in which the tube diameter is less than 15 centimeter:

$$u_{op} = 3.4 g^{0.2} D^{0.2} u - t^{0.6} \tag{48}$$

The optimal gas velocity for a mixture of different particle sizes should be estimated based on the maximum particle size which is to be transported.

The modified Konno and Saito correlation[129] was found to give better prediction of pressure drop in vertical dilute-phase transport reactor and is presented below:

$$\Delta p = \frac{u_o^2 \rho_g}{2} + \frac{4 G_s u_p}{\pi D^2} + \frac{2 f u_o^2 \rho_g L}{D} + \frac{0.057 G_s L g}{(gD)^{1/2}} + \frac{4 G_s L g}{\pi D^2 u_p} + \rho_g L g \tag{48}$$

where

$$u_p = u_g - u_t \tag{49}$$

$\dfrac{U_o^2}{2} \rho_g$ is the pressure drop due to gas acceleration,

$\dfrac{4 G_s u_p}{\pi D^2}$ is the pressure drop due to particle acceleration,

$\dfrac{2 f u_o^2 \rho_g L}{D}$ is the pressure drop due to gas-to-pipe friction,

243

$$\frac{4G_sLg}{\pi D^2 u_p}$$ is the pressure drop related to solid-to-pipe

friction

$$\frac{0.057G_sLg}{(gD)^{1/2}}$$ is the pressure drop related to the static head of

the solids,

$$\rho_g Lg$$ is the pressure drop due to the static head of the

gas.

If the gas and the solids are already accelerated in the lift line, then the first two terms should be omitted from the calculation of the pressure drop.

The pressure drop due to vertical dense-phase transport with voidage less than 0.8 was given by Wen and Galli[132]

$$\frac{\Delta P}{L} = \left[\frac{150\mu(u_o/\varepsilon - u_p)(1-\varepsilon)^2}{d_p^2\phi^2\varepsilon^2} + \frac{1.75(1-\varepsilon)\rho_g(u_o/\varepsilon - u_p)^2}{d_p\phi\varepsilon} \right]$$

$$+ (1-\varepsilon)(\rho_s - \rho_g)g + \frac{2fu_o^2\rho_g}{D} \tag{50}$$

where

$$[\frac{150\mu(u_o/\varepsilon - u_p)(1-\varepsilon)^2}{d_p^2\phi^2\varepsilon^2}]$$ is the pressure drop due to viscous

friction between gas and,

$$\frac{1.75(1-\varepsilon)\rho_g(u_o/\varepsilon-u_p)^2}{d_p\Phi\varepsilon}$$

is the pressure drop due to inertial friction between gas and particles,

$$(1-\varepsilon)(\rho_s - \rho_g)g$$

is the pressure drop due to static head of the solids,

$$\frac{2fU_o^2\rho_g}{D}$$

is the pressure drop due to gas-to-pipe friction

The first two terms represent the pressure drop due to the friction between fluid and particles in a fixed bed or in a particulate fluidized bed of voidage less than 0.8.[71,132]

The relationship between voidage, ε, and particle velocity,[132] u_p is given by

$$u_p = 4\frac{G_s}{\pi D^2\rho_s(1-\varepsilon)} \tag{51}$$

The relationship between voidage ε and the superficial gas velocity u_o is given by

$$\varepsilon^{4.7}\frac{d_p^3\rho_g(\rho_s-\rho_g)g}{\mu^2} = 18\frac{d_p(u_o-\varepsilon u_p)\rho_g}{\mu}$$
$$+ 2.7\left[\frac{d_p(u_o-\varepsilon u_p)\rho_g}{\mu}\right]^{1.687} \tag{52}$$

The power requirement for the vertical solid-gas transport section may be calculated from the following equation[71]

$$-\omega_a = 3.5 p_2 v_2 [1 - p_2^{-2/7}] / \eta \qquad\qquad (53)$$

This set of equations, Equation 40 through 53, form the basis for the design of a transport reactor.

Design Calculations for the Transport Reactor

In practice, vertical pneumatic conveying is usually carried out in the dilute-phase regime and much of the published literature on vertical pneumatic transport has been restricted to this mode. Dense-phase conveying is used less often because of the erratic nature of the flow, the pressure fluctuations, high pressure drops, and pipe line vibration.[128] However, dense-phase flow is sometimes preferred in a solid-riser reactor, to give a high solid concentration in the tube and/or high solids residence time in the reactor. Moving-bed flow is generally avoided because of high pressure drop and the problem of blockage.[128]

It is important in the design of a solid-riser reactor to be able to predict the flow behavior of a particular gas-solid system, the transition velocity (choking velocity), and the pressure drop for each flow regime.

Coke Combustion Reaction Time

The intrinsic kinetics for the combustion of coked sand has been investigated by thermal gravimetric analysis.[133] The coked sand was formed during the fluidized-bed pyrolysis of the mined and crushed ore from the Whiterocks tar sand deposit. First-order and second-order dependence of the fraction of carbonaceous residue

remaining was reported; however, a second-order rate expression is not appropriate for the calculation of the complete reaction time since $t \rightarrow \infty$ as $X \rightarrow 1$. The first-order rate expression was given by:

$$dx/dt = A \exp(-E/RT) (P_{O_2})^{0.5}(1-X) \qquad (54)$$

and

$$t = \frac{-\ln(1-X)}{A \exp(-E/RT)(P_{O2})^{0.5}} \qquad (55)$$

from which the following kinetic parameters and reaction times were determined:

$A = 2.67 \times 10^6$ 1/s atm$^{0.5}$

$E = 25.27$ kcal/mol

for $X = 0.99$,

$T = 500°C$, $t = 57$ seconds;

$T = 550°C$, $t = 21$ seconds;

$T = 650°C$, $t = 4$ seconds.

Dilute-Phase Vertical Transport Mode

The reaction time calculation revealed that a dilute-phase riser-combustor is practical only when the combustor temperature is high enough to minimize the reaction time (a few seconds) since gas and solid velocities are very high in this flow pattern and the length of the riser must be limited.

The particle size distribution of the Whiterocks coked sand was determined to be as follows:

247

greater than 42 standard Tyler mesh   5.5%

42-60 standard Tyler mesh (0.351-0.246 mm) 59.4%

60-100 standard Tyler mesh (0.246-0.147 mm) 14.6%

less than 100 standard Tyler mesh   20.5%

The coked sands are treated as spherical particles for simplicity. If the transport gas is assumed to be air, at 650°C, and one atmosphere then the density, ρ_g is 3.83×10^{-4} g/cm^3 and the viscosity, μ_g, is 3.9×10^{-4} g/cm s. The grain density of the coked sand, ρ_s, is 2.3 g/cm^3.

The minimum fluidization velocity and particle terminal velocity are calculated from Equations 40 and 41 respectively, the results are shown below:

mesh size	d(cm)	u_{mf}(cm/s)	u_t(cm/s)	$Fr = u_t^2/gD$
42	0.0351	4.32	297	71
48	0.0295	3.15	254	52
100	0.0147	0.76	124	12

The minimum fluidization velocity and particle terminal velocity versus particle size in the range 0.01 to 0.1 cm are presented in Figure 55. A tar sand feed rate of 20 kg/hr was used in the 4-inch fluidized-bed reactor. The coked sand mass flow rate of 10 kg/hr was used in this calculation. A steel pipe of inside diameter of 1.27 cm (0.5 inch) was chosen so that the solid mass flux would be in the range of values reported in the literature.
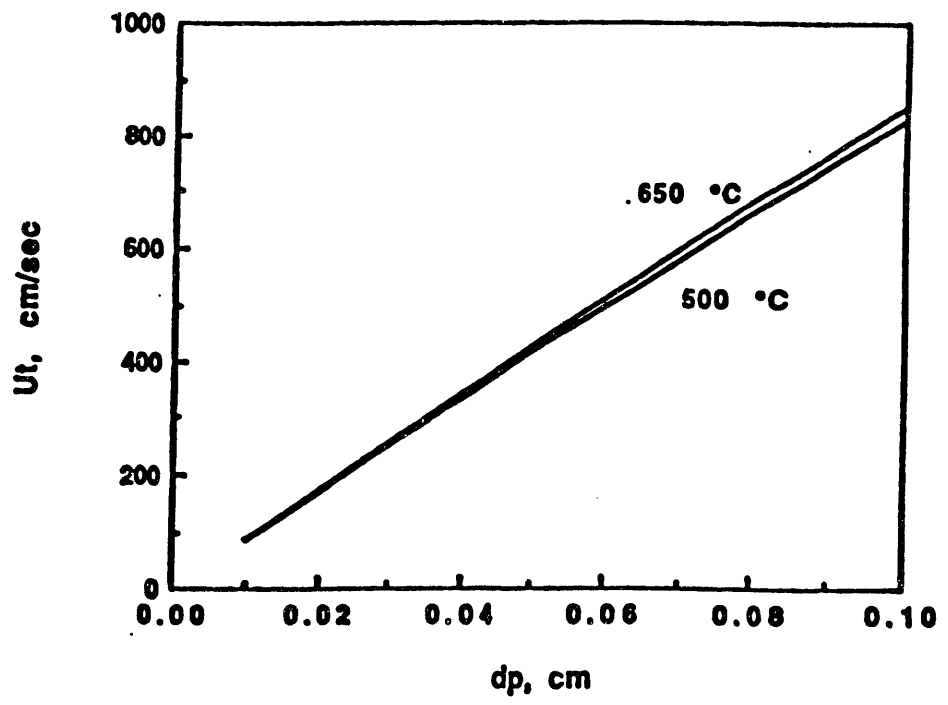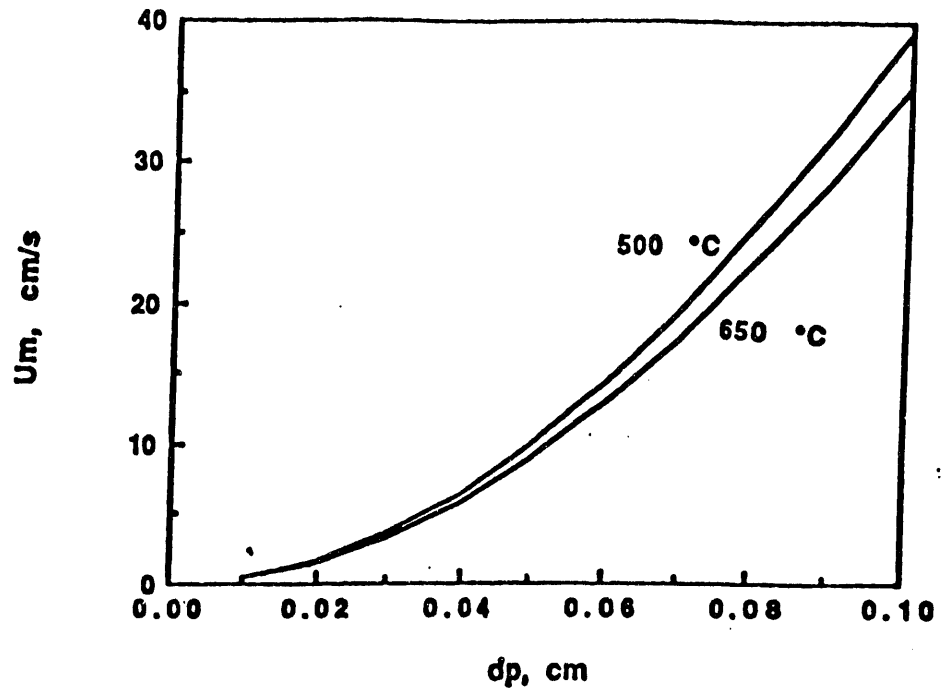
Figure 55. Minimum Fluidization Velocity and Particle Terminal Velocity Versus Particle Size

249

Yang's correlation, Equation 44, can be applied to predict when choking would occur if the gas velocity in a dilute-phase vertical flow is decreased. It was concluded that choking was likely to occur for particles larger than 100 mesh based on the values of the Froude number. The terminal velocity was 297 cm/s for a 42-mesh particle and the choking velocity, estimated from Equation 44, was 342 cm/s. The choking velocity can also be calculated from Equations 45 and 46: if ϵ_{ch} = 0.98, G_s = 10 kg/hr = 2.78 g/s, D = 1.27 cm, and W_{ch} = 2.1946 g/cm^2 s, then u_{ch} = 345 cm/s. Thus in a dilute-phase riser-combustor system, a velocity higher than 345 cm/s is required to vertically convey particles with sizes up to 42 mesh. Particle velocity in vertical dilute-phase conveying can be approximated by Equation 47 with ± 20% accuracy.[128,129]

The optimum gas velocity is calculated as 1.3 times choking velocity, that is 448 cm/s. Optimum gas velocity estimated by Equation 47 based on a 42-mesh particle is 431 cm/s. If a superficial gas velocity, u_o, of 440 cm/s is assumed and if it is assumed that the coked sand to be burned has a particle size larger than 100 mesh the terminal velocity would be 124 cm/s, and the particle velocity, u_p would be 316 cm/s. Since four seconds is needed to burn the coke at 650°C in air, a riser-combustor of length 1264 cm is required. Thus a steel pipe of 1.27 cm diameter, 1300 centimeter long is needed for the dilute-phase riser-combustor.

The pressure drop of the riser-combustor under dilute-phase

transport is calculated by Equation 48 with the first term dropped since the gas is already accelerated in the riser. In the second and fifth terms, a value of u_p based on a 100-mesh particle was used. In the third term, a frictional coefficient f is needed. For laminar flow,[134] $f = 16/R_e = \rho_g u_0 D/\mu$, and since the Reynolds number is 545 the system is in the laminar flow regime, and f is 0.029. The pressure drop, calculated from Equation 48, was 17,908 $g/cm\ s^2$ or 0.018 atm.

Dense-Phase Vertical Transport Mode

In dense-phase vertical conveying, the particle velocity is much less than in dilute-phase transport, and particle residence time increases dramatically. Thus, a feasible riser-combustor temperature would be less than that in dilute-phase flow. Assume a combustor temperature of 500°C. Sandy et al.[135] reported a voidage of 0.6 to 0.7 in a dense-phase vertical conveying experiment with 70- to 80-mesh alumina pellets. Hikita et al.[136] studied the dense-phase vertical transportation of coke particles and the voidage was calculated to be in the range of 0.60-0.72. Therefore, a voidage of 0.7 was used in these calculations.

A sphericity, ϕ_s, of 0.6, and a particle size of 48 mesh (60% of coked sand is in the range of 42 to 60 mesh) were used in the calculation[133]: the transport fluid was air at 500°C, and one atmosphere with a density, ρ_g, of 0.00046 g/cm^3 and a viscosity, μ, of 0.00035 g/cm s. The particle velocity, u_p was calculated from Equation 51 and was 3.2 cm/s.

When the riser-combustor temperature is 500°C, 57 seconds are

needed to completely burn out the coke, thus a riser-combustor of length 3.2 cm/s x 57 s = 182 cm is required. A steel pipe with 1.27 cm inside diameter and 200 cm long is needed for a dense-phase vertical riser-combustor. The superficial gas velocity, u_0, calculated from Equation 52, was 60 cm/s and $\Delta P/L$, calculated from Equation 50, and was 3263 g/cm s^2. Thus for a riser-combustor reactor 200 centimeters long, the pressure drop, ΔP, was 0.64 atmosphere.

The gas-to-pipe friction can be neglected in dense-phase flow since the gas flow rate is low. It should be noted that the calculated gas flow rate and pressure drop are in the range of experimental observation for alumina pellets.[135] The gas flow rate (60 cm/s) for dense-phase vertical transport is less than that of particle terminal velocity (254 cm/s, 48-mesh), and the upward movement of solids is caused by the large pressure difference across the bed. The pressure drop in dense-phase transport was reported to be an order of magnitude higher than that in dilute-phase transport[135] which is consistent with this calculation.

The power requirement for the solid-gas vertical conveying system is calculated by Equation 53[71] and was 7.74 watts with $\eta = 0.8$ and $P_2 = 1.70$ atmosphere. V_2 was computed from the expression $U_o A P_3/P_2$ where P_3 is 1.64 atmosphere and was 73 cm^3/s or 0.073 liter/s. The power requirement could also be estimated from the bed pressure drop and the gas flow rate. The superficial gas rate is 60 cm/s and is equivalent to a mean flow rate of 126 g/h which leads to a power requirement of 6.33 watts. Thus, a minimum 10-watt blower is required.

Discussion

The potential energy recovery due to the combustion of coked sand in tar sand pyrolysis is analyzed below. The thermodynamic properties used in the calculation were as follows[133]:

1. The standard heat of pyrolysis (25°C, 1 atm) for the reaction 1 g bitumen $\longrightarrow$ 0.15 g coke + 0.70 g oil + 0.15 g gases is 5 cal/g bitumen.

2. The enthalpy change H_{oil} vapor at 475°C - H_{oil} liquid at 25°C = 319 cal/g oil as estimated for oil with API gravity 20° and mean average boiling point 371°C (700°F).

3. The enthalpy change H_{HC} gases at 475°C - H_{HC} gases at 25°C = 292 cal/g gas.

4. The enthalpy change H_{coke} at 475°C - H_{coke} at 25°C = 189 cal/g coke.

5. As a first approximation in the temperature range of 25 to 650°C, the following constant specific heats were assumed:

$$C_p, \text{ sand} = 0.24 \text{ cal/g } °C$$

$$C_p, \text{ nitrogen} = 0.25 \text{ cal/g } °C$$

$$C_p, \text{ oxygen} = 0.24 \text{ cal/g } °C$$

$$C_p, \text{ carbon dioxide} = 0.26 \text{ cal/g } °C$$

6. Standard heat of combustion of coke = 8256 cal/g coke.

The heat of pyrolysis for different product distributions is assumed to be the same since this energy is small compared to the total energy requirement for the pyrolysis. The heat of combustion of coke at any combustion temperature is assumed equal to the

standard heat of combustion since they are so close.

If we assume a basis of 100 g tar sand with 10% bitumen saturation, then the amount of coke produced would be 1.5 g. The energy released from the combustion of this coke would be 12,384 cal. Significant burning of coked sand starts around 375°C.[133] The energy requirement to heat the coked sand from 25°C to 375°C would be 7686 cal (91.5 g coked sand x 0.24 cal/g °C x 350 °C). Thus the coked sand should be utilized immediately upon leaving the pyrolysis reactor.

The energy and mass balance calculations for the pyrolysis of tar sand with coked sand combustion/recycle are illustrated below: basis:

feed sand: 100 g (cold tar sand plus recycled hot clean sand)

recycled clean sand: R,g

tar sand bitumen saturation: 10%

pyrolysis temperature: 475°C

The pyrolysis reaction is expressed as:

(100 - R) x 0.9 g sand, 25°C +   (100 - R) x 0.9 g sand, 475°C+

(100 - R) x 0.1 bitumen, 25°C --→ (100 - R) x 0.015 g coke, 475°C+

                                          (100 - R) x 0.015 g oil, 475°C+

                                          (100 - R) x 0.070 g gases, 475°C
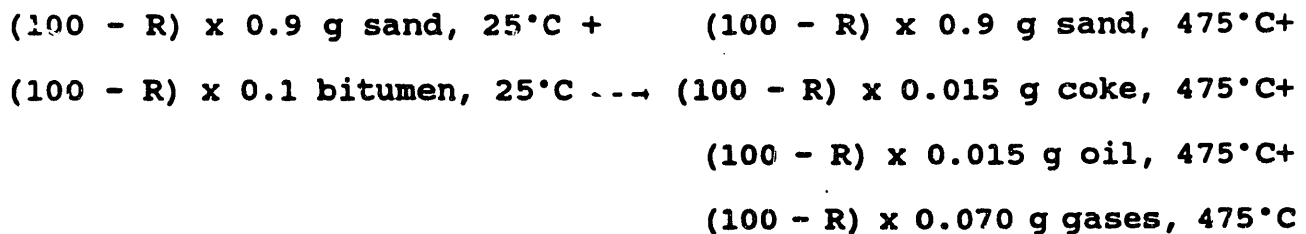
The amount of energy needed for pyrolysis (excluding the energy needed to preheat the fluidization nitrogen gas)

    =   energy to heat (100 - R) x 0.9 g of sand matrix from 25 to 475°C

    +   standard heat of pyrolysis for (100 - R) x 0.1 bitumen

+   enthalpy difference for $(100 - R) \times 0.015$ g coke (25 to 475°C)

+   enthalpy difference for $(100 - R) \times 0.070$ g oil (25 to 475°C)

+   enthalpy difference of $(100 - R) \times 0.015$ g gases (25 to 475°C).

Thus, the energy required for pyrolysis

= $(100 - R)$ g x 0.9 x (475-25)°C x 0.24 cal/g°C

+ 5 x $(100 - R)$ x 0.1 cal

+ $(100 - R)$ x 0.015 x 189 cal

+ $(100 - R)$ x 0.070 x 319 cal

+ $(100 - R)$ x 0.015 x 292 cal

The energy released from the combustion of the coke is

= 8256 cal/g coke x $(100 - R)$ x 0.015 x fr

where fr is the fraction of the coked sand produced in the pyrolysis reactor that is charged to combustor. Assume stoichiometric air is supplied for the combustion process, and that the molecular weight of the coke is 12 g/g mole. Thus the amount of air needed in $[(100 - R) \times 0.015 / 12] \times fr \times 5 \times 29$ g and the amount of carbon dioxide produced is $[(100 - R) \times 0.015/ 12] \times fr \times 44$ g. The amount of nitrogen carried in is $[(100 - R) \times 0.015/ 12] \times fr \times 4 \times 28$ g. The adiabatic equilibrium temperature of clean spent sand and the flue gases is calculated from the following expression assuming the average flue gas specific heat is the same as the specific heat of nitrogen.

$$8256 \text{ cal/g} \times (100 - R) \times 0.015 \times fr = [(100 - R) \times 0.0125] \times fr \times (44 + 4 \times 28)\text{g} \times 0.025 \text{ cal/g } ^\circ\text{C} \times (T_a - 475^\circ\text{C}) + [100 - (100 - R) \times 0.1] \times fr \times 0.24 \text{ cal/g } ^\circ\text{C} \times (T_a - 475^\circ\text{C})$$

Thus it can be seen that the fraction of coked sand charged into the combustor, fr, does not influence the adiabatic equilibrium temperature T_a. However, the more coked sand that is burned, the more hot clean sand and flue gases are produced.

The condition that all coked sand produced was charged into combustor ($fr = 1$) is illustrated in the following calculations.

The energy carried by the recycled hot sand into the pyrolysis reactor is given by $R \text{ g} \times 0.24 \text{ cal/g } ^\circ\text{C} \times (T_a - 475^\circ\text{C})$.

The energy required to heat the stoichiometric amount of air is given by

$$[(100 - R) \times 0.015/12] \times 5 \times 29 \text{ g} \times 0.25 \text{ cal/g } ^\circ\text{C} \times (475 - 25) ^\circ\text{C}.$$

A typical mass ratio of feed sand to fluidization gas is 0.05, thus the energy required to preheat the fluidization gas (nitrogen) is 563 cal. The results of the energy balance calculation as a function of R are presented in Table 40. As the recycle sand ratio increased, the total energy needed for pyrolysis decreased and the percentage of energy released from coke sand combustion to total energy needed decreased. However, the ratio of energy carried by recycled hot sand into the pyrolysis reactor to total energy required increased. When there is no recycle of hot clean sand,

256

Table 40. Energy Balance Calculations for
Combustion of Coked Sand in Riser

R	Ta	Energy from recycled sand to pyrolysis	Energy needed for pyrolysis (preheat of N₂ air excluded)	Energy released from all coke combustion	Total energy needed (include preheat of N₂ air)	Energy released from all coke combustion/ total energy needed	Energy recycled/ total energy needed
g	°C	cal	cal	cal	cal	%	%
0	943	0	12725	12384	15331	80.8	0
10	900	1020	11452	11146	13850	80.5	7.4
20	856	1829	10180	9907	12374	80.1	14.8
30	812	2426	8907	8669	10897	79.6	22.3
40	767	2803	7635	7430	9421	78.9	29.8
50	720	2940	6392	6192	7945	77.9	37.0
60	673	2851	5090	4954	6469	76.6	44.1
70	625	2520	3817	3715	4992	74.4	50.5
80	576	1939	2545	2477	3516	70.4	55.1
90	526	1102	1272	1238	2039	60.7	54.0

a: basis: 100 g feed, i.e., (100 - R) g tar sand at 25°C plus R g recycled clean sand at Tc.

The basis could be taken as 100 kg with the energy units in kcal.
tar sand saturation = 10%
pyrolysis temperature = 475°C, fluidization gas to feed sand mass ratio = 0.05
pyrolysis products = coke 15%, oil 70%, gases 15%.

the tar sand processing rate is maximized, as is the production of coke. Under this condition, 81 percent of total energy needed for pyrolysis can be obtained from the combustion of coked sand. The energy can be utilized to preheat the tar sand feed, the fluidizing gas (nitrogen) and the air for combustion of coked sand. A schematic diagram of the riser-combustor is shown in Figure 56. The size of the cyclone will depend on the flow mode chosen.

Future Activities

Detailed design calculations will be performed during the 1990-1991 contract period. The coked sand produced in the fluidized bed and the rotary kiln reactors will be analyzed for elemental composition, metals and heating value. The coke combustion kinetic data previously obtained will be reviewed and evaluated for use in the design process.

Hot Flue Gas

Cycolne

Sand after Combustion

Coked Sand Feed Hopper

Furnace

Air

Blower
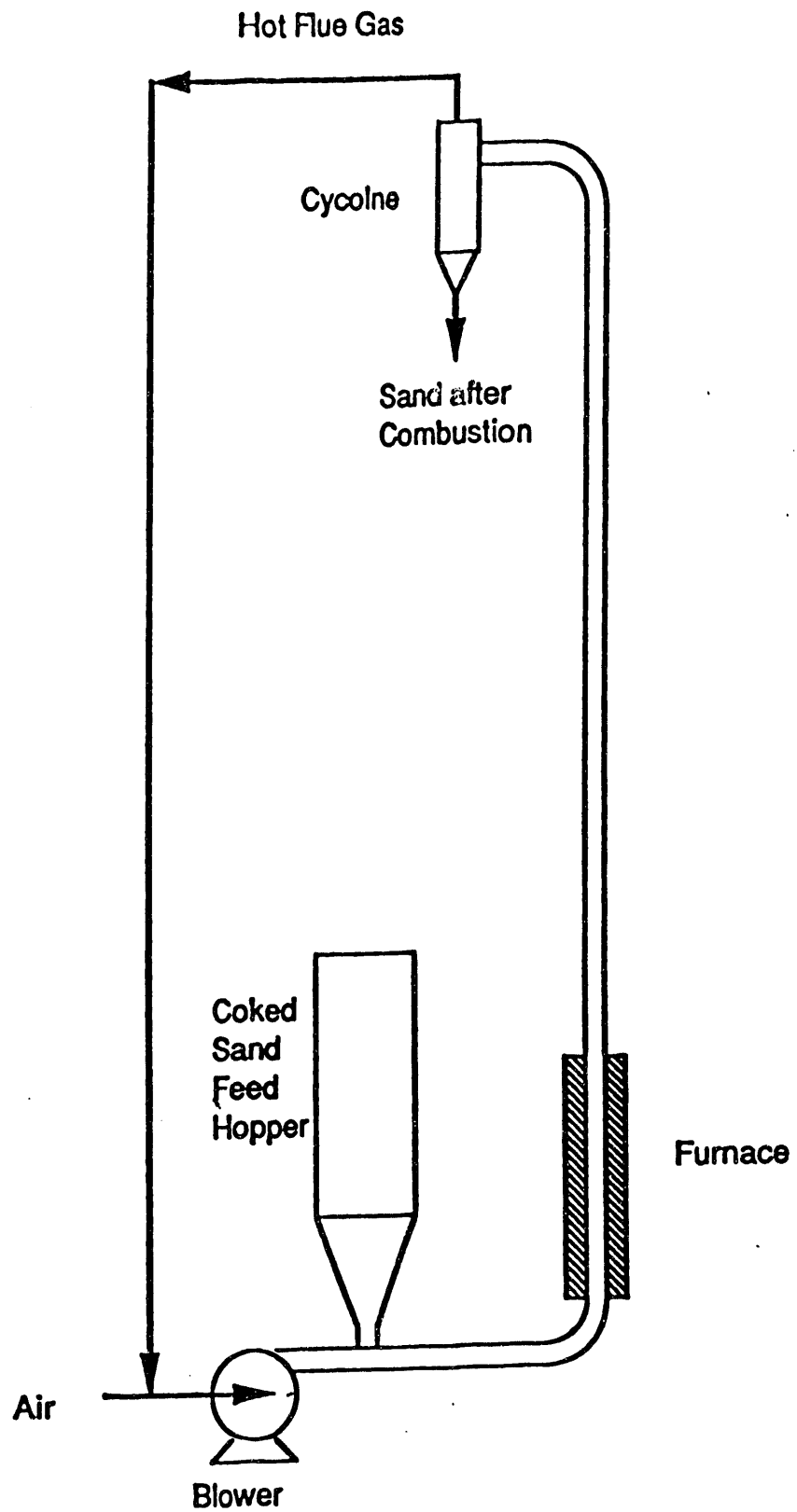
Figure 56. **Schematic of Riser-Combustor Transport Reactor**

259

Nomenclature

A	preexponential factor, $1/s\ atm^{0.5}$
C_p	heat capacity, cal/g $\cdot$C
d_p	particle diameter
D	pipe diameter, cm
E	activation energy, kcal/mol
f	friction factor
fr	fraction of coked sand charged into combustor
Fr	$= u_{t2}/g\ D$ Froude number
g	gravitational acceleration, 980 cm^2/s
G_s	mass flow rate, g/s
Kp	thermal conductivity, cal/cm s $\cdot$C
L	length of pipe, cm
R_e	$= \rho_g U_o D/\mu$, Reynolds number
Re_p	$= \rho_g U_o D/\mu$, particle Reynolds number
p	pressure, $g/cm\ s^2$, atm
Δp	pressure drop, $g/cm\ s^2$, atm
R	radius of particle, cm
t	time, s
T	temperature, $\cdot$C, K
T_a	adiabatic temperature, $\cdot$C
U_o	superficial gas velocity (based on empty tube), cm/s
U_{ch}	choking velocity, cm/s
U_g	gas velocity, cm/s
U_m	minimum fluidization velocity, cm/s
U_{op}	optimum gas velocity for dilute-phase transport, cm/s
U_t	particle terminal velocity, cm/s
ω_a	actual pumping work, watt
W_{ch}	solid mass choking velocity, $g/cm^2 s$
X	conversion
P_g	gas density, g/cm^3
P_s	solid density, g/cm^3
ϵ	voidage
ϵ_{ch}	voidage at choking velocity
η	pumping efficiency
μ	viscosity, g/cm s
ϕ	sphericity of a particle

Solvent Extraction of Tar Sands

Principal Investigator: F.V. Hanson

Co-Principal Investigator: M.D. Deo

Post Doctoral Fellow: L.C. Lin

Graduate Student: J. Hwang

A variety of solvents have been proposed for the recovery of the native bitumen from the mined ore from Utah's tar sand deposits. Unfortunately, those working on solvent extraction tend to publish little or no information regarding their process studies. This is due in large measure to the presumed proprietary nature of the solvent and/or solvent-mixture and of the process operating conditions.

The solvent extraction program initiated during the contract period was intended to develop an adequate background in the literature of solvent extraction as it relates to tar sands and to examine the experimental techniques employed in solvent extraction studies. A second objective was to design a suitable experimental system for process variable studies related to solvent extraction of tar sands.

These preliminary considerations led to an understanding that it would be beneficial to study the extraction of tar sands at both super- and subcritical conditions in a reactor that would insure good contacting between the extract and residual phases and effective separation of the phases. The contacting of a suitable solvent and the bitumen or tar sand at supercritical conditions is

261

not difficult to achieve; however, the separation of the supercritical fluid extract phase from the residual phase at supercritical conditions is a demanding task. Thus, it was decided that a complete system would be purchased from a vendor if possible. The supercritical fluid extraction system selected for purchase was manufactured by Autoclave Engineers, Inc.

Laboratory Scale Solvent Extraction of Tar Sand Bitumen

Introduction

Numerous methods have been developed for the mining-surface recovery of the bitumen from tar sands. Each of these fall into one of four categories: (1) hot water separation processes; (2) solvent-assisted aqueous separation processes; (3) solvent extraction processes; and (4) thermal processes[133]. Currently, bitumen is separated and recovered from the Athabasca tar sands by a variation of the Clark hot water process. The bitumen recovery or yield from this process is high (88-91%); however, it also produces an aqueous sludge which is a significant economic and environmental debit. Both solvent extraction and direct coking have been examined in an attempt to develop alternative bitumen recovery techniques which do not produce aqueous tailings. The purpose of this sub-project is to investigate the influence of process operating conditions on bitumen recovery for the solvent extraction method. Laboratory-scale experiments are essential before the full potential of the solvent extraction process can be understood and realized.

262

General Discussion

In the solvent extraction process, the bitumen is dissolved and separated from the sand by mixing the solvent with tar sand in an appropriate vessel. The bitumen-solvent mixture is then drained from the sand matrix or sand slurry, and the bitumen is recovered from the mixture, usually by evaporation or distillation of the solvent. Solvent extraction studies with tar sand bitumen have been described by several investigators[1,79,81,137-139]. The solvent has a higher economic value than the bitumen, thus, a large fraction (~100%) of the solvent must be recovered if the process is to be economical. Although a supercritical solvent separation process has been developed[140] separation of the solvent from the bitumen is usually accomplished by distillation (evaporation). The residual solvent physically entrained in the interstitial void volume of the wet sand can be driven off and recovered by heating the waste sand using methods such as stripping. Complete recovery of solvent entrained in the waste sand may not be energy-efficient, since a small amount of solvent may be strongly bound to the sand matrix. At the boiling point of n-pentane (36°C), 3.75% of the pentane is entrained in the sand matrix; at 90°C, 0.90% of the pentane is entrained; at 100°C, there is still a measurable amount of bound pentane at one atmosphere, although the vapor pressure of pentane is nearly 10 atm[141]. This results in a substantial energy loss because of the need to heat the waste sand itself, from which it is not possible to recover all of the heat.

The solubility of bitumen in various solvents[142,143] is listed

263

in Table 41. The normal boiling temperatures, and the critical temperatures and pressures of the solvents are also included[144].

Williams and Martin[145] described a process for the extraction of oil shales and tar sands which consisted of heating the shale or tar sand in the presence of an extractant in the supercritical fluid state. The critical temperatures of the solvents were in the range from 0° to 550°C. The extraction pressure should not be less than the critical pressure of the solvent and the extractant temperature should not be more than 200°C above the critical temperature of the solvent. The operating conditions and results are summarized in Table 42, and the ultimate analyses of the raw materials, extracts, and residues are listed in Table 43[145]. As indicated in Table 41, the bitumen is totally extractable by toluene; the solubility of Athabasca bitumen in n-pentane is 83% with the remaining 17% rejected as asphaltene.

The Residuum Oil Supercritical Extraction (ROSE) process uses the solvent in its supercritical state;[140,146] however, the title of the ROSE process is somewhat misleading, since the extraction step is not carried out in a supercritical state. A schematic of a ROSE process unit designed to separate asphaltenes, resins, and oils from residuum is presented in Figure 57. The residuum is charged to a mixer (M-1), where it is contacted with several volumes of a light hydrocarbon solvent (such as pentane) at elevated temperature and pressure. The mixture passes to the first vessel, (V-1). The heavy high softening point asphaltene fraction is withdrawn as a liquid from the bottom of V-1 and passes through the heater (H-1)

Table 41

The Solubility of Bitumen in Various Solvents
Boiling Point, Critical Temperature and Pressure of Solvents

Solvent	Bitumen Solubility (%)	$T_{n.p}$ (°C)	T_c (°C)	P_c (atm)
carbon dioxide	---	-79	31	72.9
propane	52	-42	97	42
n-butane	73	0	152	37.5
n-pentane	80-83	36	197	33.3
n-hexane	84	69	234	29.3
n-heptane	88	98	267	27
n-octane	90	126	296	24.5
n-decane	91	174	344	20.8
cyclopentane	99	49	239	44.6
carbon disulfide	100	46	279	78
benzene	100	80	289	48.6
toluene	100	111	321	41.6
pyridine	100	116	347	----

Table 42

Supercritical Fluid Extraction Data and Product Yields
Pressure = 1500 psig

Charge	Solvent	Temperature (°C)	Extraction Time (min)	Solvent to Dry Charge Ratio	Solvent Flow (g/min)	Extract % total organic	Organic Residue % total organic
Colorado oil Shale	toluene	395	60	20.3	31.6	77	15
Athabasca tar sand	toluene	395	30	11.0	30.8	89	5
Athabasca tar sand	pentane	230	60	----	----	75	13

266

Table 43

Ultimate Analysis of Oil Shale and Tar Sand, Extract and Residue Supercritical Fluid Extraction

Species	% H_2O	% Ash	C	H	O	N	S	Cl	CO_2
						% (dry base)			
Colorado oil shale (toluene)									
Shale	0.5	60.6	17.5	2.4	1.0	0.55	0.90	–	17.1
Extract	–	–	83.0	10.3	2.6	2.20	1.75	0.03	–
Residue	0.3	75.6	1.9	0.30	–	0.15	0.65	0.03	21.5
Athabasca tar sand (toluene)									
Tar sand	2.9	89.1	8.3	0.9	1.2	0.10	0.45	–	0.04
Extract	–	–	84.0	10.3	1.3	0.40	3.85	0.09	–
Residue	0.3	98.4	0.5	0.1	–	0.02	0.10	–	0.28
Athabasca tar sand (pentane)									
Extract	–	–	83.2	10.8	1.2	0.30	4.25	–	–
Residue	0.2	37.8	1.25	0.20	–	0.05	0.15	–	0.07
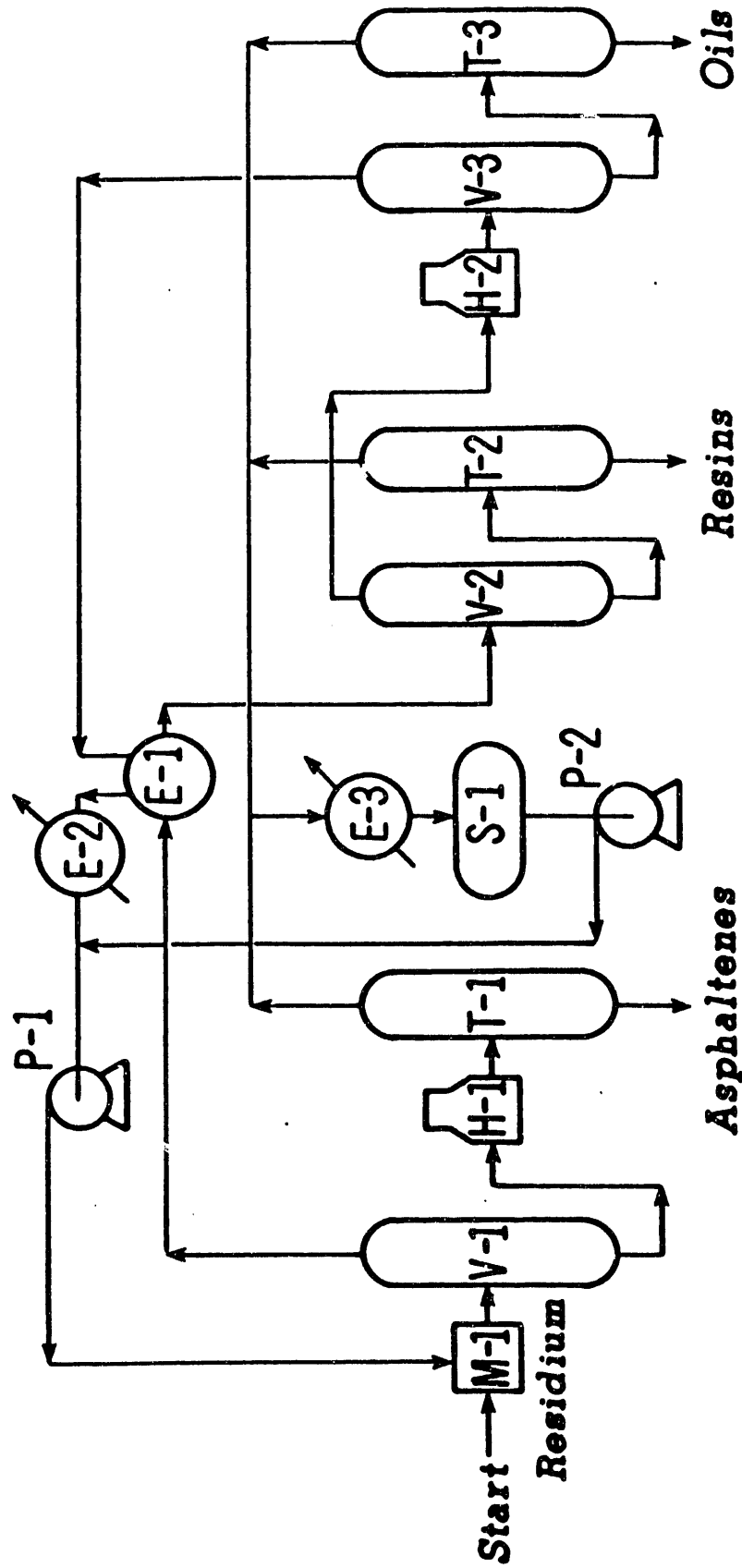
Figure 57 Schematic of the ROSE Process

to the flash tower (T-1), where the solvent is flashed and stripped from the asphaltenes. The solvent-resin-oil phase flows from the top of (V-1) through heat exchanger (E-1) to vessel (V-2). As a result of the increase in temperature, a second separation takes place from the solvent, yielding an intermediate resin fraction which is removed, again as a liquid, from the bottom of (V-2) and stripped of its solvent in a flash tower (T-2). The remaining solvent-oil phase proceeds overhead from (V-2) through a heater (H-2), where its temperature is further raised to a super-critical level with resultant separation of the oils from the solvent. The mixture then passes to the final settling vessel, (V-3) where the separation of the solvent and the oil takes place. The oil-free supercritical solvent exits from the top of the settling vessel (V-3) and passes through a heat exchanger (E-1), and is further cooled in a second heat exchanger (E-2) to a subcritical temperature for recycle back to the process by pump (P-1)[140].

Results from the extraction studies on virgin, visbroken and hydrocatalytically refined Athabasca tar sand bitumens[146] are presented in Tables 44, 45, and 46. One feature of the ROSE process is that approximately 90% (at a 10:1 solvent to residue ratio) of the solvent is recovered from its supercritical state through the heat exchanger as a condensed liquid rather than as a vapor by evaporation, to be further compressed and condensed as in a conventual solvent extraction process[140]. It has been claimed that the ROSE process results in a utility savings of about 50% over the

Table 44

ROSE Unit Product Yield and Quality Results for
n-Butane and n-Pentane Extractions of Athabasca
Tar Sand Bitumen 340°C Plus Resid

Solvent	340°C+ Bitumen	n-Butane		n-Pentane	
		Asphaltene	DAO	Asphaltene	DAO
Yields, wt.%	100	35.0	65.0	20.0	80.0
Lv. %	100	31.5	68.5	17.4	82.6
S.G. @ 15°C/4°C	1.031	1.146	0.978	1.183	0.999
API Gravity	5.7	-8.0	13.2	-11.9	10.1
Nitrogen, Wt.%	0.52	0.97	0.28	1.12	0.37
Sulfur, Wt.5	5.4	8.6	3.7	9.4	4.4
Con Carbon, Wt.%	15.6	36	4.5	48	7.6
Nickel, ppm	115	290	20	400	43
Vanadium, ppm	287	700	67	930	125
R&B Softening, Pt., °C	--	280	--	177	--
Viscosities, mPa's (est)					
@ 99°C	2000	--	144	--	254
@ 135°C	265	--	37	--	55

Table 45

ROSE Unit Product Yield and Quality Results for n-Butane and n-Pentane Extractions of Visbroken Athabasca Tar Sand Bitumen Resid

	Feedstock	Asphaltene	Resin	Resin + DAO	DAO
Solvent: n-Butane					
Yields, Wt.%	100	53.8	13.7	46.2	32.5
Lv. %	100	50.0	14.3	50.0	35.7
S.G. @ 15°C/4°C	1.085	1.168	1.038	(1.001)	0.986
API Gravity	-1.1	-10.4	4.8	(9.90)	12.0
Nitrogen, Wt.%	0.60	0.80	0.48	(0.37)	0.32
Sulfur, Wt.%	5.4	6.3	4.8	(3.9)	3.6
Con Carbon, Wt.%	31.3	52	19.2	(10.5)	6.8
Nickel, ppm	160	330	42	(16.)	5
Vanadium, ppm	400	750	90	(32.)	8
R&B Softening Pt., °C	71	156	38	--	6
Viscosities, mPa's (est)					
@ 99°C	23,000	--	800	(113.)	60
@ 135°C	1400	--	115	(31.)	17
Solvent: n-Pentane					
Yields, Wt.%		37.4	12.5	62.6	50.1
Lv.%		33.8	12.5	66.2	53.7
S.G. @ 15°C/4°C		1.202	1.084	(1.025)	1.011
API Gravity		-13.8	-1.0	(6.6)	8.5
Nitrogen, Wt.%		0.92	0.68	(0.50)	0.46
Sulfur, Wt.%		6.9	5.5	(4.5)	4.2
Con Carbon, Wt.%		57	30.8	(15.3)	11.5
Nickel, ppm		350	110	(42.)	25
Vanadium, ppm		960	260	(89.)	46
R&B Softening Pt., °C		186	72	--	--
Viscosities, mPa's (est)					
@ 99°C		--	23,500	(277.)	135
@ 135°C		--	120	(60.)	28

( ) indicates calculated data.

Table 46

ROSE Unit Product Yield and Quality Results
for n-Pentane Extraction of the Resid
from Hydrocatalytically Refined
Athabasca Tar Sand Bitumen

	Feedstock	Asphaltene	Resin	Resin + DAO	DAO
Yields, Wt.%	100	47.8	27.4	52.2	24.8
Nitrogen, Wt.%	0.95	1.42	0.59	(0.48)	0.36
Sulfur, Wt.%	5.8	6.7	3.2	(3.3)	3.5
Con Carbon, Wt.%	39.1	62	22.4	(16.3)	9.6
Nickel, ppm	133	214	51	(36.)	20
Vanadium, ppm	378	652	106	(62.)	13
R&B Softening Pt., °C	86	220	37	--	--
Viscosities, mPa's (est)					
@ 99°C	14,000	--	360	(205.)	115
@ 135°C	925	--	135	(55.)	35
Ash, Wt.%	0.80	1.64	0.13	(0.07)	<0.01

( ) Indicates calculated data.

usual evaporative method[140]; however, this is questionable since a solvent such as pentane with a normal boiling temperature of 36°C could be easily separated from the oil-solvent mixture by evaporation and condensation.

A Soxhlet extractor is usually used in the laboratory for tar sand bitumen extraction. The extraction study using solvents with normal boiling temperatures below room temperature, such as n-butane and propane, could be carried out by the high-pressure Soxhlet extractor which is shown in Figure 58. Unlike the regular Soxhlet extractor, the high-pressure Soxhlet extractor is placed inside a stainless steel chamber. The neck of the extraction component is not tightly fitted to the condenser so that the pressure inside and outside the extractor is equalized, and high pressure can be applied. The solvent in the flask is heated and evaporated, as in the regular Soxhlet extractor and is then condensed through a condenser to extract the tar sand sample in a thimble such that the excess solvent overflowed back to the flask. Carbon dioxide can be used as a solvent in this system if the recovering of the light extract is desired.

One advantage of the Soxhlet extractor is that only a relatively small amount of tar sand can be processed at a time. Additionally, in the high-pressure Soxhlet extractor, the amount of solvent used, as well as the operating temperature and pressure can be accurately controlled. An alternate apparatus for tar sand bitumen extraction using a solvent such as n-butane or pentane is shown in Figure 59. With this apparatus tar sand is first charged

273
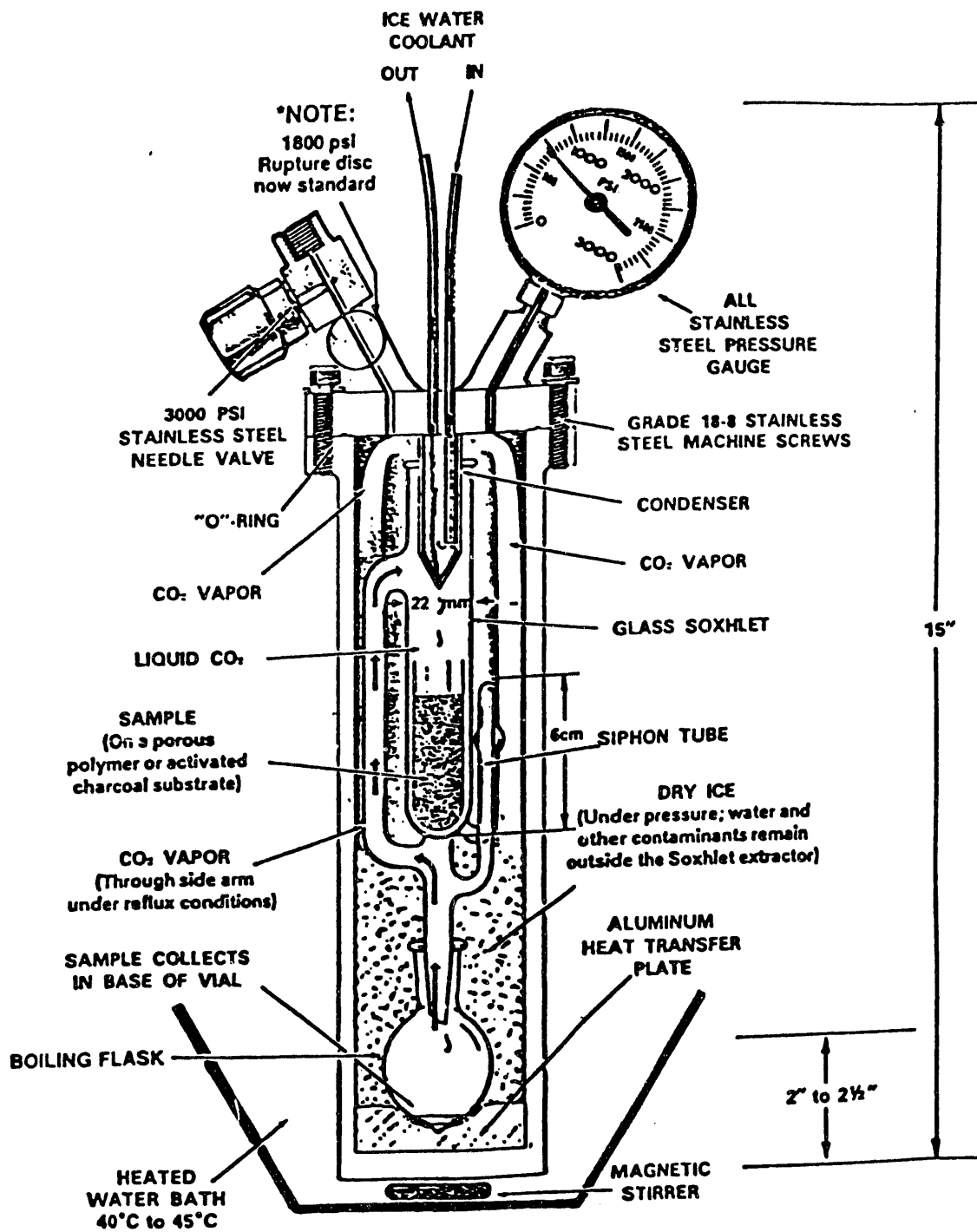
Figure 58   High Pressure Soxlett Extractor
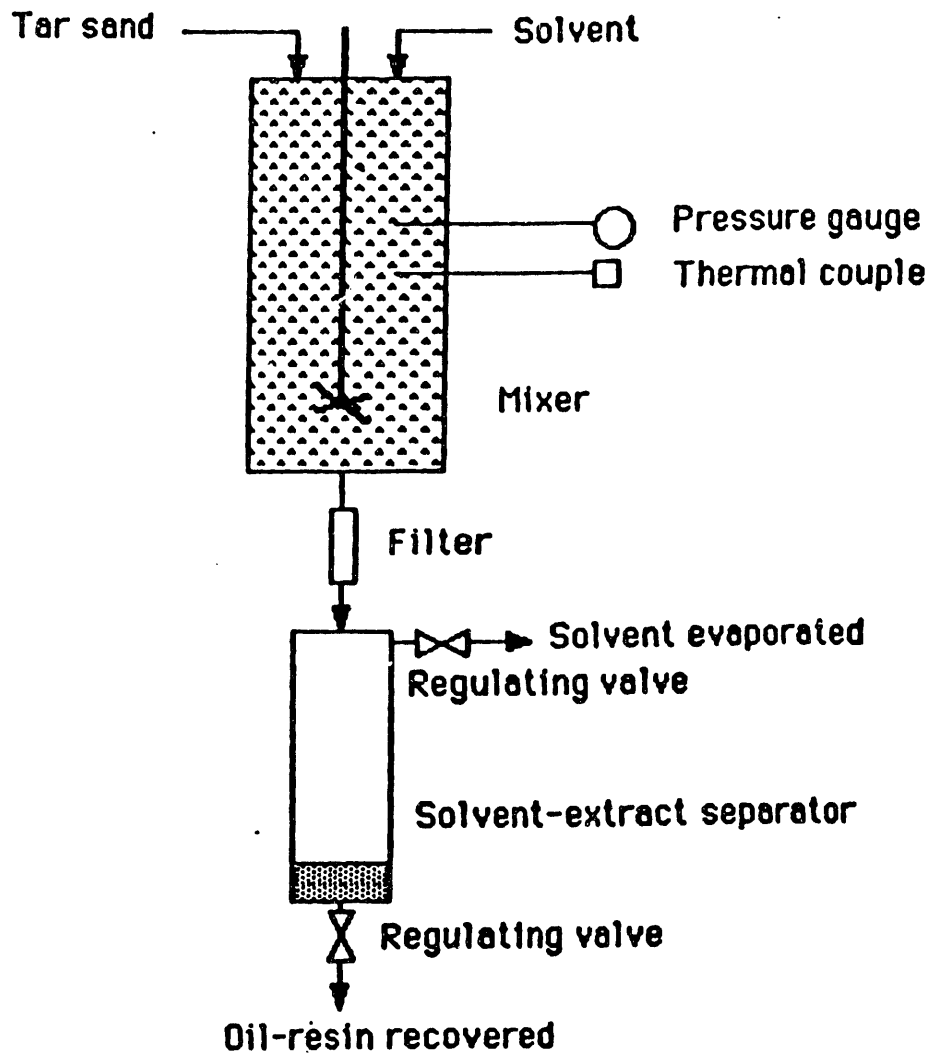
Figure 59   Apparatus for Tar Sand Solvent Extraction

into the mixer, then the solvent from the cylinder container is charged into the mixer. The solvent is kept in a liquid phase in the mixer by maintaining a solvent pressure greater than the saturation pressure at the extraction temperature. After the extraction is completed, the extract and solvent mixture are drained to a separator where the solvent is evaporated through release of the separator pressure. If desired, supercritical solvent extraction may be conducted by using a temperature-controlled furnace outside the mixer where the solvent is heated above its critical temperature and pressure.

The advantage of using n-butane or pentane as an extractant is that a higher quality of extract can be obtained, and that the extractant can be easily separated from the mixture by reducing the pressure. The disadvantage of this method is that there is a smaller amount of extract available. The selection of solvent depends on what extract is desired. For a high-quality oil extract, butane or propane may be used for a maximum oil-resin recovery, n-pentane is suitable; and for a total extraction of bitumen, carbon disulfide, toluene, or cyclopentane will be preferred. In pilot plant operations, the safety of the solvent (i.e., explosion and health hazard) during operation must be considered as well as the economic evaluation. The combination of several solvents may be a preferred choice. The recovery and recycle of the solvent need not be considered in the initial laboratory scale experimental program; however, in the later stages of the process development studies continuous operation should be

investigated.

A laboratory apparatus for the study of solvent (such as pentane or hexane) separation from the solvent-extract mixture at solvent supercritical conditions is shown in Figure 60. The solvent-extract mixture is pumped into the separator where the temperature and pressure are maintained above critical temperature and pressure of the solvent. If the solvent is n-pentane, the separator operating temperature could be 200°C and the pressure could be 500 psi. A back pressure relief valve is set to equal the operating pressure. Continuous feed of solvent-extract causes the pressure of the supercritical solvent to increase, and excess supercritical solvent is withdrawn through the back pressure relief valve and recovered in a condenser. The amount of extract (oil resin) in the separator is indicated by a flow indicator on the high-pressure side and can be withdrawn through two regulating valves.

Research Objectives

The research objectives for the solvent extraction subproject are as follows:

1. The fraction of bitumen extracted and the time required in relation to the amount of solvent used (solvent/bitumen ratio).

    The influence of mixing (stirring speed) should also be examined for extraction studies in an agitated mixer.

2. The characterization of bitumen, extract, and residue.

    The properties of bitumen, extract (deasphalted oil), and

277

Recovered solvent

Solvent-extract
container

Condenser

Pump

Back pressure relief valve

Pressure gauge
Thermal couple
Furnace
Copper

Supercritical
Solvent-extract
separator

High pressure
side flow indicator

Regulating valves

Oil-resin recovered
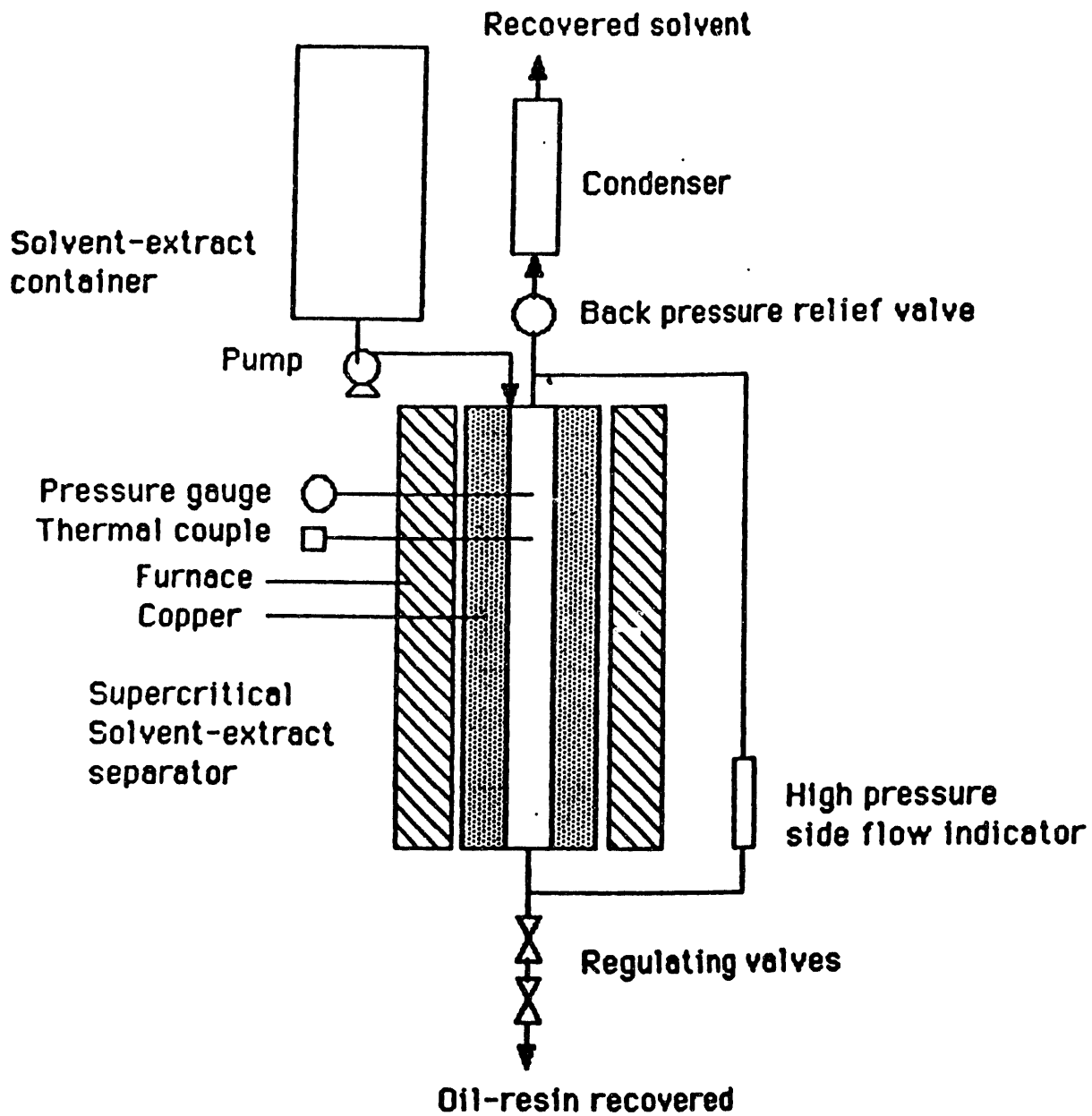
**Figure 60   Apparatus for Supercritical Solvent-Extract
Separation**

residue (asphaltene) of Athabasca tar sand are listed in Table 47[137]. The deasphalted oil has a lower metal content and can be upgraded by refinery processing such as hydrotreating, which may not be suitable and economical for the whole bitumen.

3. The viscosity behavior of the solvent-extract mixture as a function of solvent/bitumen ratio.

The viscosity of the n-pentane-extract mixture as related to the pentane-bitumen ratio is presented in Figure 61[141]. A sharp increase in the viscosity occurs at a pentane-bitumen ratio of approximately one. This suggests that a solvent extraction process would require a pentane/bitumen ratio at least equal to one; below this ratio, the viscosity of the pentane-extract increases rapidly and makes solid-liquid separation difficult. Above a ratio of one, there is little reduction in viscosity. In order to determine the optimal solvent-bitumen ratio, in addition to the influence on viscosity, the number of contacting stages as a function of solvent-bitumen ratio is also required. An analysis of this problem has been studied and is presented in Figure 62[148]. A pentane/bitumen ratio of one will require about ten theoretical contacting stages. An increase in pentane/bitumen ratio reduces contacting stages significantly. At sufficiently high solvent ratio, only one contacting stage is needed; in this case, all extractable constituents are extracted and the solvent is not above its saturated condition. Based on the preceding information, a solvent/bitumen ratio of two to 10 was used in a paraffinic solvent extraction process[149].

Table 47

Properties of the Bitumen, Pentane Deasphalted Oil, and Asphaltene for Athabasca Tar Sands

	Bitumen	Deasphalted Oil	Asphaltene
Specific gravity	1.02	1.01	1.06
C, %	82.9	83.15	81.90
H, %	10.7	11.10	9.10
S, %	4.8	4.50	6.00
N, %	0.4	0.25	1.00
O, %	1.20	1.00	2.00
V, ppm	290	65	1190
Ni, ppm	90	21	1190
H/C atomic ratio	1.55	1.60	1.33
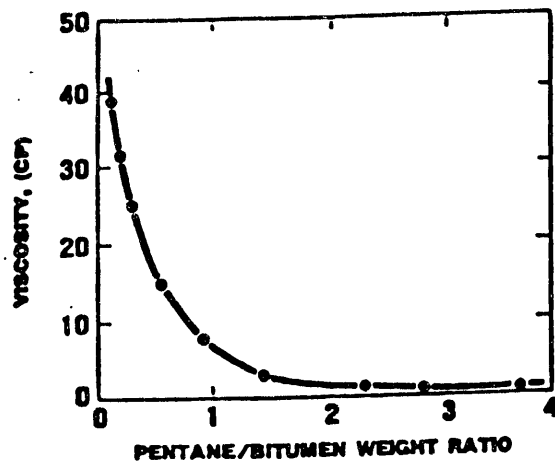
Figure 61 Viscosity behavior of pentane/bitumen mixtures
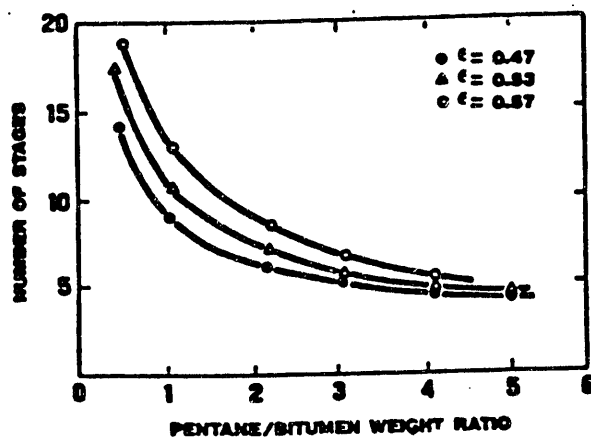
Figure 62   Number of required contacting stages as a function of the pentane/bitumen ratio.

4. Determination of the parameters and mechanisms in the solvent extraction at ambient or elevated temperatures using an agitated mixer.

The efficiency of solvent extraction of bitumen from tar sand could be studied in batch stirred vessels. Solvent type, stirred speed, and contact time have been identified as important parameters[150]. A theoretical analysis of the extraction process provides a basis by which the various parameters can be assessed in terms of relative overall mass transfer coefficients. For simplicity, the analysis assumes that the tar sand aggregates are essentially spherical, and during the extraction process, the aggregates retain their shape but diminish in size as the bitumen is removed. The rate of dissolution of a single aggregate during extraction is considered first, and the analysis is then extended to a distribution of aggregate sizes. The mass transfer coefficient, k, is used to describe the transport of bitumen from the surface of the aggregates to the bulk solution. The mass transfer coefficient is defined such that

$$-dN_B/4 \; \rho \; R^2 \; dt = k \; \varepsilon_1 \; (C_s - C) \tag{56}$$

and

$$dN_B = \varepsilon_2 \; C_s \; dV = \varepsilon_2 \; C_s \; 4 \; \rho \; R^2 \; dR \tag{57}$$

where N_B is the amount of bitumen in the aggregate, g:

   C is the concentration of bitumen in the solution, g/cm^3 solution)

   C_s is the concentration of bitumen, g/cm^3 (bitumen);

   R is the radius of aggregate at time t, cm;

ε_1 is the fraction of the exposed aggregate surface which is bitumen; and

ε_2 is the volume fraction of bitumen in the aggregate.

Substitution of Equation 57 into Equation 56 gives

$$-\varepsilon_2 \; C_s \; dR/dt = k \; \varepsilon_1 \; (C_s - C) \qquad (58)$$

The mass transfer coefficient for solute transport from solid particles, has been shown to be particle size dependent[151]. The relationship was expressed as:

$$k = k_r \; R^n \qquad (59)$$

where k_r is a radial independent coefficient, and n is a constant in the range of 0.07 ~ 0.15. The undetermined constant will continue to be n, since it is not clear if the same range of n is valid for the tar sand extraction. If the solvent/bitumen ratio is high, then $C \ll C_s$. Thus, the term $(C_s - C)$ in Equation 58 can be approximately by C_s. Equation 58 can be integrated to give

$$R = \{R_o^{\;1-n} - (1-n) \; k \; (\varepsilon_1/\varepsilon_2) \; t\}^{\;1/(1-n)} \qquad (60)$$

where R_o is the initial radius of the aggregate. It can be shown from an over all mass balance that the concentration of bitumen in the solvent phase is given by

$$C = (4/3) \; \pi \; (N/V) \; [R_o^{\;3} - R^3] \; C_s \varepsilon_2^{\;2} \qquad (61)$$

283

This can be rewritten as

$$C_{max} - C = (4/3) \pi (N/V) R^3 C_s \mathcal{E}_2 \tag{62}$$

where

$$C_{max} = (4/3) \pi (N/V) R_o^3 C_s \mathcal{E}_2, \text{ and} \tag{63}$$

C_{max} is the maximum concentration after extraction is
completed, g/cm^3;

N is the number of aggregates of radius R at 5 - 0; and

V is the volume of solvent, cm^3.

Equations 60 and 62 can be combined to give the variation of
concentration with respect to time for constant radius (R_o)
aggregates:

$$C_{max} - C = (4/3) \pi (N/V) C_s \mathcal{E}_2 \{R_o^{1-n} - (1-n) k (\mathcal{E}_1/\mathcal{E}_2)t\}^{3/(1-n)} \tag{64}$$

The variation of concentration with time for a distribution of
particle size is somewhat complex. However, the relative ratio of
the two mass transfer coefficients is simple. It can be shown[150]
that

$$\frac{k_B}{k_A} = \frac{\phi_A C_{max,A} V_A}{\phi_B C_{max,B} V_B} \tag{65}$$

where
$$\phi = \int (1-\eta) \, dt \tag{66}$$

and
$$\eta = C/C_{max} \tag{67}$$

represents the extent of extraction and can be easily measured by taking samples of solution during the process of extraction. The spectrophotometric method of analysis was used to measure the extract concentration[142,150]. Hence, ϕ can be evaluated from the profile of η versus t. If the initial distribution of aggregates in the sample are the same for two solvents, this could be approximated by the mixing of a relatively narrow range of tar sand aggregates in which $(k_B/k_A)_1$ is equal to $(k_B/k_A)_2$. Thus, equation 65 provides a convenient basis from which to compare the ability of solvents to dissolve bitumen.

The previous analysis has been restricted to dilute solutions since the analytical solutions were obtained under the assumption that $C \ll C_s$. For concentrated solution where $(C_s - C)$ in Equation 58 cannot be approximated by C_s, the analytical solutions are not available since the equations are non-linear.

The relative mass transfer coefficients of various solvents with respect to kerosene[150] according to Equation 65 are presented in Table 48. The ratios give the relative solvency power. The data indicate that toluene and benzene are capable of dissolving bitumen more than three times faster than kerosene. A weak correlation was also found between the relative mass transfer coefficient and the solvent aromaticity; however, aromatic compounds tend to be better solvents for bitumen. A weak correlation was also found between the relative mass transfer coefficient and the average solvent boiling temperature. A solvent with low boiling point solvents tend to have small, mobile

Table 48

**Relative Mass Transfer Coefficient of Solvents with
Respect to Kerosene at a Stirrer Speed of 300 rpm**

Solvent	k_l / k_{kero}
toluene	3.52
benzene	3.30
Gulfsol 2329	2.63
Gulfsol 3139	1.08
kerosene	1.00

molecules which can diffuse more readily though the bitumen, thereby speeding up the mass transfer process. It was found that the relative mass transfer coefficient is a linear function of the stirring rate, and approaches zero at a stirring rate of about 95 rpm. This stirring rate corresponds approximately to the stirring rate at which solid particles precipitate in the vessel. The 95 rpm cut-off indicates that a minimum stirrer speed must be exceeded before the extraction of bitumen will proceed at a reasonable rate.

The effect of agitation rates with various solvents has been quantified by following the rate of the change of the relative mass transfer coefficients with respect to stirrer speed[150], S, which is presented in Table 49. The reason for the greater enhancement with strong solvents compared to weak solvents was explained as follows: the diffusion of the solvent into the bitumen is envisaged as producing a region of reduced viscosity at the surface of the particle. For strong solvents, which have high diffusivities in bitumen, this region of reduced viscosity is deeper than for weak solvents. With shear, the outer layer of the particle (which has the lowest viscosity) will be steadily stripped away. The rate of removal will depend not only on the level of shear but also on the rate at which the solvent can diffuse into the bitumen to deepen the low viscosity layer. Hence, it is expected that the solvency power of a strong solvent (which has a high diffusivity in bitumen) will be greatly assisted by high rates of shear, whereas a poor solvent will be assisted to a lesser extent[150].

Table 49

Rate of Change of Relative Mass Transfer Coefficients with Stirring Speed, S, Normalized with Respect to Kerosene at S = 300 rpm

Solvent	$\partial(k_l / k_{kero})/\partial S$
toluene	0.017
benzene	0.016
Gulfsol 2329	0.012
Gulfsol 3139	0.005
kerosene	0.005

The strong dependence of mass transfer coefficient on stirrer speed is contrary to observations in conventional solid-liquid mass transfer situations. This indicates that the viscosity reduction and shear strip-off mechanism discussed above are quite unlike the mechanism which controls the conventional solid-liquid mass transfer operations[150].

In addition to the tar sand bitumen (in aggregates) extraction, the solvent extraction process can be applied to pure bitumen without the mineral matrix. Since the surface area (i.e., the cross-sectional area of the vessel, A) for mass transfer is constant, the analysis is simplified as

$$V \, dC/dt = k \, A \, (C_s - C) \tag{68}$$

Equation 69 can be rearranged to the form for dilute solution

$$k = (V/AC_s) \, dC/dt \tag{69}$$

The ratio of mass transfer coefficients then becomes

$$\frac{k_A}{k_B} = \frac{(dC/dt)_A}{(dc/dt)_B} \tag{70}$$

Once again, there are weak correlations between relative mass transfer coefficients, boiling temperature, and aromaticity of solvents. A weak correlation was also found between the relative mass transfer coefficient and the solvent Hildebrand solubility parameter. Solvents with a large solubility parameter tend to have larger mass transfer coefficients.

289

A linear correlation is found between the relative mass transfer coefficient and the stirrer speed. Similar to the tar sand aggregates case, a minimum speed of agitation which is common to all solvents must be exceeded so that the extraction will proceed at a reasonable rate. Above this minimum rate, the mass transfer coefficient increases linearly with stirrer speed[150].

In addition to the solvent boiling point and the Hildebrand solubility parameter, the physical and chemical properties which correlated with the degree of bitumen extraction were hydrogen bonding, dipole moment, and solvent strength[152].

5.   Study the mechanism of bitumen dissolution with solvents at ambient or elevated temperatures using the spinning disc technique.

The spinning disc technique for examining mass transfer and dissolution phenomena in electrochemistry[153] has been applied to solvent extraction of bitumen using paraffinic solvents[142,154]. The experimental technique consisted of rotating a bitumen-coated disc immersed in a solvent at a constant speed. A circular glass disc 2.54 cm in diameter was used[142,154]. The advantage of using the circular disc is that the mass transfer coefficient is the same at all points on the surface. The analytical solution for the mass transfer coefficient, k, (solvent to bitumen layer) was given as[153]

$$k = 0.62 D^{2/3} v^{-1/6} \omega^{1/2}$$

$$(71)$$

where D is the binary diffusion coefficient, ν is the kinematic viscosity of solvent, and ω is the rotational speed of the disc. The diffusive molar flux of solvent into bitumen layer is then

$$j = k \ C_b \qquad \qquad (72)$$

where C_b is the bulk molar concentration of solvent outside bitumen layer. If equal-molar countercurrent diffusion is assumed, Equation 72 gives the molar flux of deasphalted oil diffusing from the bitumen layer into the solvent phase. Equation 71 applies only to the laminar flow region; that is, $Re < 10^5$ where $Re = \omega d/\chi$ and d is the diameter of the disc[151].

The concentration of bitumen in the solution was measured using a Beckman DB-G spectrophotometer. Details of this analytical technique are given by Funk and Gomez[155]. The experimental results for the extraction of Athabasca tar sand with n-pentane at 25°C are shown in Figure 63[142]. It was observed that the bitumen dissolution was independent of the rotational speed in the range studied. Thus, equation 71, indicates that the principal resistance to dissolution resides in the bitumen layer and not in the transport across the solvent-bitumen interface. This resistance within the bitumen layer is large enough to require about 10 minutes for all the deasphalted oil to diffuse out of the bitumen layer[142]. On the contrary, aromatic solvents rapidly dissolve all the bitumen, which suggests that little resistance exists in the bitumen layer and the principal resistance is the mass transport at the solvent-bitumen interface.

The figure shows a plot of BITUMEN CONCENTRATION, PPM (y-axis, 0 to 2000) versus TIME, MINUTES (x-axis, 0 to 8). Labels inside plot: T = 25°C, n-PENTANE. Legend: • W = 0 RPM, ○ W = 7 RPM, ▲ W = 15 RPM.
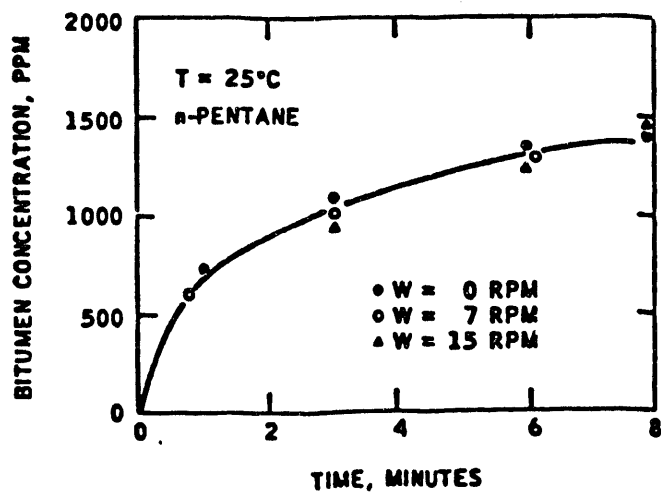
Figure 63   Spinning Disc Experiments for Tar Sand Bitumen Dissolution in Pentane

Thus, unlike n-pentane, aromatic solvents give a dissolution rate which is dependent on the rotational speed of the disc[142,150].

To obtain the binary diffusion coefficient, D, and effective diffusion coefficient, D_{AB}, deasphalted oil was allowed to diffuse through the sponge-like network of insoluble asphaltenes. D_{AB} was calculated from the experimental data modeled using Fick's second law. Considering the deasphalted oil concentration in the bitumen layer and assuming equal-molar countercurrent diffusion, Fick's second law gives

$$\partial C/\partial t = D_{AB}\partial^2 C/\partial x^2$$

(73)

The following initial value and boundary condition were used

$$\text{at } t = 0, \; C = C_o;$$

(74)

at $x = \pm 1$ (boundary of bitumen layer and bulk solution),

$$C=0;$$

(75)

where C is the concentration of deasphalted oil in the bitumen layer and C_0 is the initial value. The solutions of equations 18 through 20 were given by Crank[156] as:

$$\frac{M_t}{M_\infty} = 1-\sum_{n=0}^{\infty}\frac{8}{(2n+1)^2\pi^2}\exp-D_{AB}(2n+1)^2\pi^2 t/L^2$$

(76)

where M_t/M_∞ is the fraction of deasphalted oil which has been leached out in time t and L is the thickness of the bitumen layer (neglect the existence of the disc by using a thick one). Equation 76 can be fit to experimental data to obtain D_{AB}; or, more simply, D_{AB} can be calculated by from

$$D_{AB} = 0.049/(t/L^2) \quad at \; M_t/M_\infty = 0.5 \tag{77}$$

Experimental data which fit the model outlined in Equations 73 through 77 usually show a linear plot of M_t/M_∞ versus $t^{1/2}$ over a considerable time range[142]

The effective diffusion coefficients determined from Equation 77 are reasonably consistent with those found for the diffusion of liquids through porous membranes which are often expressed as

$$D_{AB} = (\varepsilon/\tau^2)D \tag{78}$$

where ε is the voidage, and τ is the tortuosity (determined to be 2.5 in the pentane-bitumen system[142]). Thus, the binary diffusion coefficient D can be related to the effective diffusion coefficient D_{AB}, and the mass transfer coefficient k can be estimated.

The remaining insoluble asphaltene on the surface of the disc was examined by SEM photomicrographs. The results show that the asphaltenes form a porous network. The pore size is about one micron for the pentane insoluble asphaltenes, whereas the pore size is smaller for paraffinic solvents with higher carbon numbers[142]. A thorough investigation of the solubility of Athabasca bitumen has been reported[157]. Insoluble organic material (precipitate) was separated from bitumen by a standardized procedure which involved

dissolution of the bitumen in an equal volume of benzene and subsequent dilution of the solution with 40 volumes of the specified solvent or solvent blend. The amount of precipitates were corrected with two types of solubility parameters[157,158]. Hidebrand related the non-polar solvent power, expressed as a solubility parameter, δ, to their internal pressure, i.e., the ratio between the surface tension, γ, and the cubic root of the molar volume V:

$$\delta_1 = \gamma V^{-1/3} \tag{79}$$

and accordingly concluded that the miscibility of non-polar liquids is governed by the difference in their internal pressures. The second type of solubility parameter of non-polar solvents was related to the energy vaporization, ΔE^V, and the molar volume:

$$\delta_2 = (\Delta E^V/V)^{1/2} = [\Delta H^V - RT)/V]^{1/2} \tag{80}$$

where ΔH^V is the heat of vaporization, T is the temperature, and R is the universal gas constant. The precipitate and solubility parameter for various types of solvents are given in Table 50[157]. The amount of precipitate was correlated with the solvent types as shown in Figure 64[15]. It has been observed that solvent power (i.e., the ability of the solvent to dissolve bitumen) increases with an increase in number of carbon atoms in solvent, especially for C3 to C6. It also has been observed that for the same number of carbon atoms, the solvent power increases in the following

Table 50

Yields of Precipitate Using Various Solvents

Solvent	Solubility Parameter, δ		Precipitate (wt % bitumen, mmf)
	$\gamma V^{-1/3}$ (dyn mol$^{1/3}$ cm^{-2})	$[(\Delta H^V - RT)/V]^{1/2}$ (cal$^{1/2}$ mol$^{1/2}$ cm$^{-3/2}$)†	
normal hydrocarbons			
pentane	3.2	7.0	16.9
hexane	3.5	7.3	13.5
heptane	3.8	7.5	11.4
octane	3.9	7.6	9.8
nonane	4.0	7.7	9.4
decane	4.1	7.7	9.0
2-methyl hydrocarbons			
isopentane	3.1	6.8	17.6
isohexane	3.4	7.1	15.3
isoheptane	3.7	7.2	12.8
'iso'-octane	3.8	7.4	11.5
isononane	3.9	7.5	10.0
isodecane	3.9	7.6	9.8
terminal olefins			
pentene	3.4	7.1	16.2
hexene	3.6	7.3	13.0
heptene	3.8	7.5	10.9
octene	4.0	7.6	9.0
nonene	4.1	7.7	8.6
decene	4.1	7.8	8.5
cycloparaffins			
cyclopentane	5.0	8.2	1.0
methylcyclopentane	4.6	7.9	1.4
ethylcyclopentane	4.6	9.0	1.9
cyclohexane	5.3	8.2	0.7
methylcyclohexane	4.7	7.9	1.0
ethylcyclohexane	4.9	8.1	1.4
decalin	5.5	8.6	0
aromatics			
benzene	6.5	9.2	0
toluene	6.0	8.9	0
o-xylene	6.1	9.0	0
m-xylene	5.8	8.8	0
p-xylene	5.7	8.8	0

Table 50, con't

ethylbenzene		5.9	8.8	0
n-propylbenzene		5.6	8.7	0
isopropylbenzene		5.4	8.6	0
n-butylbenzene		5.4	8.6	0
isobutylbenzene		5.6	8.4	0
s-butylbenzene		5.5	8.5	0
t-butylbenzene		5.6	8.5	0
tetralin		6.9	9.5	0
nonylbenzene		4.8	8.2	0.3
decylbenzene		4.7	8.3	0.4
miscellaneous hydrocarbons				
2,2,4-trimethylpentane				
(iso-octane)		3.4	6.9	15.8
neopentane		2.4	6.2	21.5
neohexane		3.2	6.7	17.9
cyclohexane		6.0	8.5	0
other solvents				
pyridine		8.6	10.6	0
nitrobenzene		9.3	10.8	0
methylene dichloride		7.1	9.8	0
chloroform		6.3	9.2	0
carbon tetrachloride		5.8	8.6	0
blend				
benzene n-pentane				
(mol)	(mol)			
0.14	2.09	3.4	7.2	14.9
0.28	1.99	3.6	7.3	12.9
0.56	1.78	4.0	7.5	7.9
0.67	1.67	4.2	7.6	5.7
0.78	1.58	4.3	7.7	3.8
0.84	1.54	4.4	7.8	1.9
0.90	1.50	4.5	7.8	2.3
1.01	1.41	4.6	7.9	1.3
1.12	1.32	4.7	8.0	0.9

*1 dyn mol$^{1/3}$ cm^{-1} = 0.1 N mol$^{1/3}$ mm^{-2} ($\approx$10^5 J mol$^{1/3}$ m^{-3})

†1 cal$^{1/2}$ mol$^{1/2}$ cm$^{-3/2}$ = 2040 J$^{1/2}$ mol$^{1/2}$ m$^{-3/2}$
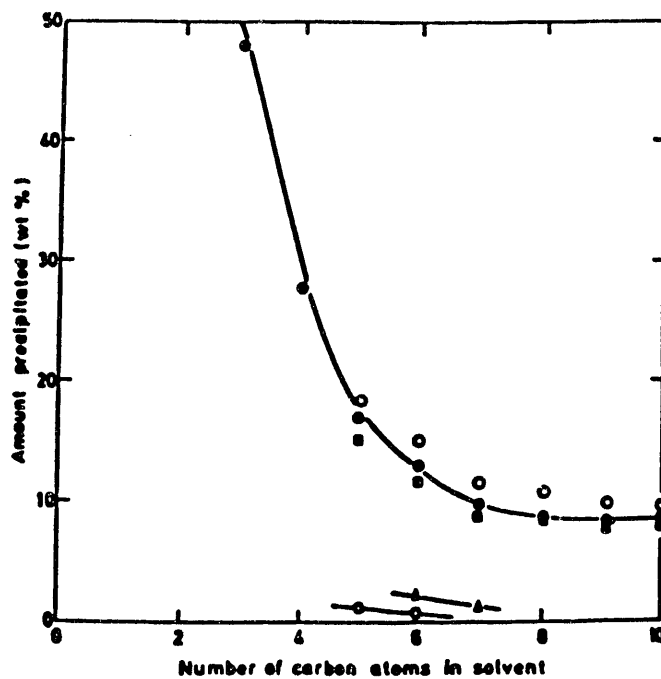
Figure 64   Relation of amount precipitated to carbon atoms
in non-aromatic solvents
•n-paraffins,   ▫ cycloparaffins,
○2-methylparaffins   ▲ methylcycloparaffins
'terminal olefins,

298

order: 2-methyl paraffin <n-paraffin < terminal olefin. Cycloparaffins have a remarkable solvent power in that almost all of the bitumen can be dissolved, and the aromatic solvents completely dissolve the bitumen. The bitumen solubility can be controlled by mixing pentane with benzene in a variety of proportions as indicated in Table 50.

The amount of precipitate was correlated with the solubility parameters, as illustrated in Figure 65. A high solubility parameter indicates greater solvent power. More precipitate was noted at elevated temperatures (up to 70°C). This was presumed to be due to the decrease of both the heat of vaporization and the surface tension with increasing temperature i.e., the solubility parameters decreased[157].

It was indicated that a prime requirement for a solvent to dissolve an oil or bitumen is an ability to penetrate the asphaltene micelle. The process of dissolution involves diffusion of solvent towards the nucleus, with the components held by the weaker forces dissolving first[157]. This solvent diffusion mechanism was also reported by other researchers[142,150,154] as discussed before. The energy supplied to overcome the association forces the micelle is supplied by the solution of the solvent system. Paraffinic systems have the least amount of solution energy because of a tendency toward parallel self-association, while aromatics have greater dispersion forces and, hence, higher solution energy. Thus, the solubility parameter is a measure of the energy of solution which may be used to overcome the forces of the micelle[157].
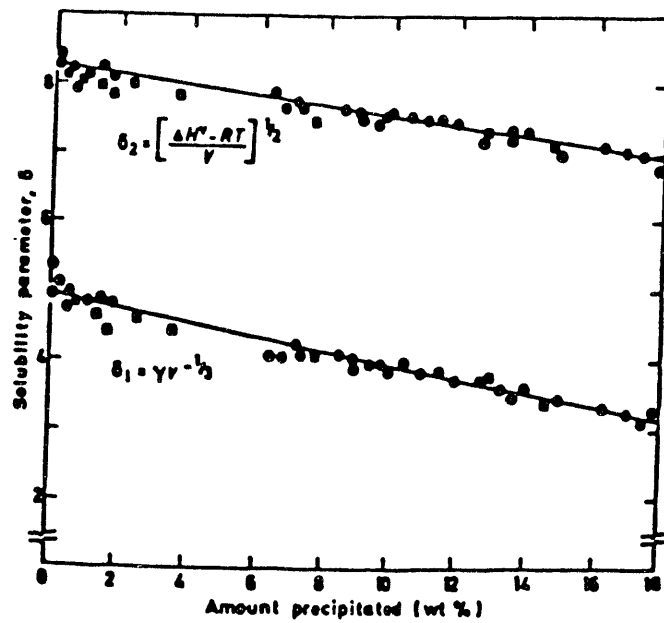
Figure 65   Relation of Amount Precipitated to Solubility
                 Parameters δ_1 and δ_2
                 •pure solvents   ■solvent blends

300

Design and Specification of the Solvent Extraction Reactor System

Two supercritical fluid extraction process development units were considered for purchase after completion of a review of the requirements for the successful laboratory scale investigation of supercritical fluid extraction. The primary requirement of the experimental apparatus was the ability to transfer the supercritical extract phase from the extractor/reactor to the separator at supercritical conditions. The first apparatus considered for purchase was a Marc Sim Supercritical Fluid Extraction Process Development Unit (SFE PDU), Model PDU-10. Unfortunately, despite the apparent technical quality of the apparatus, economics ($180,000.00/Price Quote dated November 1, 1989), dictated that the search for an alternative SFE reactor-separator system continue.

Summary and Conclusions

The system selected for purchase appeared to meet the technical experimental specifications as well as the economic constraints. The SFE reactor/separator purchased was a Model 08U-1 SFE Process development unit manufactured by Autoclave Engineers, Inc. The purchase order was placed in November 1989 and the apparatus was delivered in March of 1990. Total delivered and installed cost of the system was approximately $27,000.00.

Future Activities

Preliminary testing of the apparatus was initiated in May of 1990 using carbon dioxide on the extraction fluid and a light paraffinic, Uinta Basin crude oil as the hydrocarbon phase. The

initial experiments will also include a bitumen-derived hydrocarbon fluid and a native bitumen to assist in developing the handling and operating procedures.

Catalytic Upgrading of Bitumen
and Bitumen-Derived Liquids

Principal Investigator: F.V. Hanson

Fixed Bed Hydrotreating and Hydrocracking

Graduate Student: D.C. Longstaff

Introduction

Liquid hydrocarbon fuels based on petroleum will continue to be a major source of energy for the United States in the coming years despite the decline in domestic production and reserves. Fortunately, there are significant hydrocarbon resources such as tar sands which could be used to produce alternative fuels. Some of these deposits can be economically recovered through hot water extraction or steam flooding particularly with the evolution of horizontal drilling and production technology. The native bitumens all possess two key characteristics: high distillation end points and high organic heteroatom concentrations.

Once recovered the bitumen can be converted to asphalt for use in highway construction with a minimum of processing, or the bitumen can be upgraded to produce diesel, aviation turbine, and gasoline boiling range transportation fuels and kerosene and heating fuels. Since bitumen consists principally of high boiling range compounds it must be upgraded by thermal or catalytic cracking processes to produce the lower boiling range hydrocarbons. Thermal cracking is less expensive than hydrocracking but the principal by-product is a solid coke which cannot be reprocessed or

economically burned due to its high heteroatom content. In
addition to boiling range reduction the heteroatom concentration
must be reduced via hydrotreating.

Bitumen upgrading involving hydrocracking circumvents the
problems associated with coke formation because a necessary step in
the preparation of bitumen for hydrocracking is the hydrotreatment
of the bitumen to remove nitrogen and sulfur. Nitrogen must be
removed from the hydrocracking feed stacks primarily because basic
nitrogen compounds will poison the acidic function of a hydro-
cracking catalyst. Nitrogen and sulfur are removed as ammonia and
hydrogen sulfide, respectively, which are then easily removed from
the product streams.

Research Objectives

The Canadian bitumens which are currently being converted to
transportation fuels are high in sulfur, containing about five
percent. However, Uinta basin bitumens are unique in that they
were deposited in a fresh water environment, consequently they
contain an order of magnitude less sulfur (˜0.5wt%). However, they
contain about twice as much nitrogen as the Athabasca bitumen.

This subproject was undertaken to determine the kinetic
parameters and process operating conditions necessary for the
hydrotreating of Uinta basin bitumens. The bitumen from the
Whiterocks tar sand deposit was the focus of the initial studies.

A high pressure, high temperature reactor system was
constructed which will be used to determine the process variables
necessary to effect the HDN (hydrodenitrogenation) of bitumen. It

is assumed that a level of process severity necessary to hydrodenitrogenate Uinta basin bitumen will be in excess of what is required to hydrodesulfurize the same bitumen. This assumption will be supported or refuted in further studies.

Catalysts and Operating Conditions

Process conditions for hydrotreating vary depending on the amount of sulfur and nitrogen and the chemical nature of the heteroatom compounds. For example, mercaptal sulfur is easier to remove than sulfur present in dibenzothiophenic type molecules. Hydrotreating pressures range from 100 psi up to 3000 psi[159] and hydrotreating temperatures vary between about 315-425°C[159,160] depending on the desired operating severity and catalyst activity.

A pressure of 2000 psig[160] may be sufficient to hydrotreat Uinta Basin bitumens, however, the hydrotreater has been designed to operate at pressures up to 3000 psig if required. Over the lifetime of the catalyst the process temperature will need to be periodically increased to supplant lost catalytic activity due to catalyst poisoning. Hydrotreating catalysts are most often poisoned by coke and metals (nickel and vanadium). However, mineral fines and arsenic can also poison catalysts when present in the feedstock[161].

Hydrotreating catalysts usually consist of promoted molybdenum or tungsten sulfides supported on alumina. Cobalt or nickel are most frequently employed as promoters. Rhodium or ruthenium have been shown to be more active at promoting HDS and HDN than cobalt or nickel[162] but their use is prohibitive due to their higher cost.

When silica-alumina is substituted for the less acidic alumina support initial catalyst activity is increased by 60-80 percent for the HDN of quinoline and by 20 percent for the HDN of indole. The increased activity is due to the effect of support acidity on the intermediate ring opening steps in the HDN of quinoline and indole[163]. However, metal sulfides supported on silica alumina are probably more susceptible to poisoning by basic nitrogen compounds because of their strong acidity.

The catalysts that are currently employed for HDN were developed primarily to catalyze HDS[164] and provide a starting point for the development of strategies for bitumen upgrading. A very efficient shale oil hydrodenitrogenation catalyst has been developed which contains cobalt, molybdenum and chromium oxides supported on alumina or on acidic supports[164]. The chromium reduces catalyst HSN activity, but was required to impart high temperature thermal stability.

Reactor System

A reactor system in which hydrotreating and hydrocracking catalyst evaluation and process variable studies can be conducted with bitumens and bitumen-derived hydrocarbon liquids is under construction. Modifications in the design have been made to process viscous feedstocks and to operate the reactor in upflow or downflow modes.

Commercial hydrotreating is generally operated in a downflow mode. This is difficult to reproduce on a laboratory scale due to the much lower superficial mass velocities in laboratory size

reactors. Low superficial mass velocities result in poor liquid-solid contact and a lower apparent catalyst activity. Laboratory scale upflow hydrotreating more closely approximates commercial hydrotreating conditions through improved liquid distribution[165-167].

Satisfactory solid-liquid contact can be obtained in a downflow mode by diluting the catalyst with sand and by placing glass wool plugs periodically in the reactor to redistribute the liquid phase[168].

Three schematics of the reactor system are provided in Figures 66 through 68. The various valving and tubing arrangements that permit upflow and downflow operation of the reactor are illustrated in Figure 66.

The reactor furnace is a three zone furnace with three independently controlled heating zones. The central heating zone is twelve inches long and will be employed to heat the catalyst bed. The other two zones are each six inches long and are located above and below the central zone. These zones will be used to balance the heat loss such that the central zone can be operated nearly isothermally. Thermocouples placed outside and inside the reactor tube will be used for monitoring and control when isothermal operation is desired. A 316 stainless steel tube has been purchased for fabrication of the reactor and has one inch inside diameter.

The design of the recycle compressor loop to supply hydrogen to the reactor at high pressure is shown in Figure 67. Since high pressure hydrogen is a requirement for HDN a compressor is required

to boost the regulated pressure from the cylinder. A recycle loop between the compressor outlet and inlet circumvents the need to control the compressor flow rate. Specifications of the Whitey Laboratory compressor state that the operation of the compressor with an inlet pressure less than 50 psi will result in compressor damage. For this reason a pressure switch has been installed at the compressor inlet to turn off the compressor if the inlet pressure drops below 200 psi.

The product recovery train in which vapor and liquid are separated and collected at atmospheric pressure is presented in Figure 68. Two vapor-liquid separators are employed. A high pressure vapor-liquid separator to separate the liquid and gas and a low pressure vapor-liquid separator to weather the liquid and volatiles in a safe manner. A BPRV (Back Pressure Regulating Valve) mounted in the gas stream exiting the high pressure vapor-liquid separator will control the reactor pressure.

Liquid level controllers will be installed that will open valves when the liquid level reaches a certain level. The liquid level controllers allow operation of the reactor system for long periods of time with a minimum of supervision. Each vapor-liquid separator is provided with an additional valve which will by pass the valve controlled by the liquid level controller when needed.
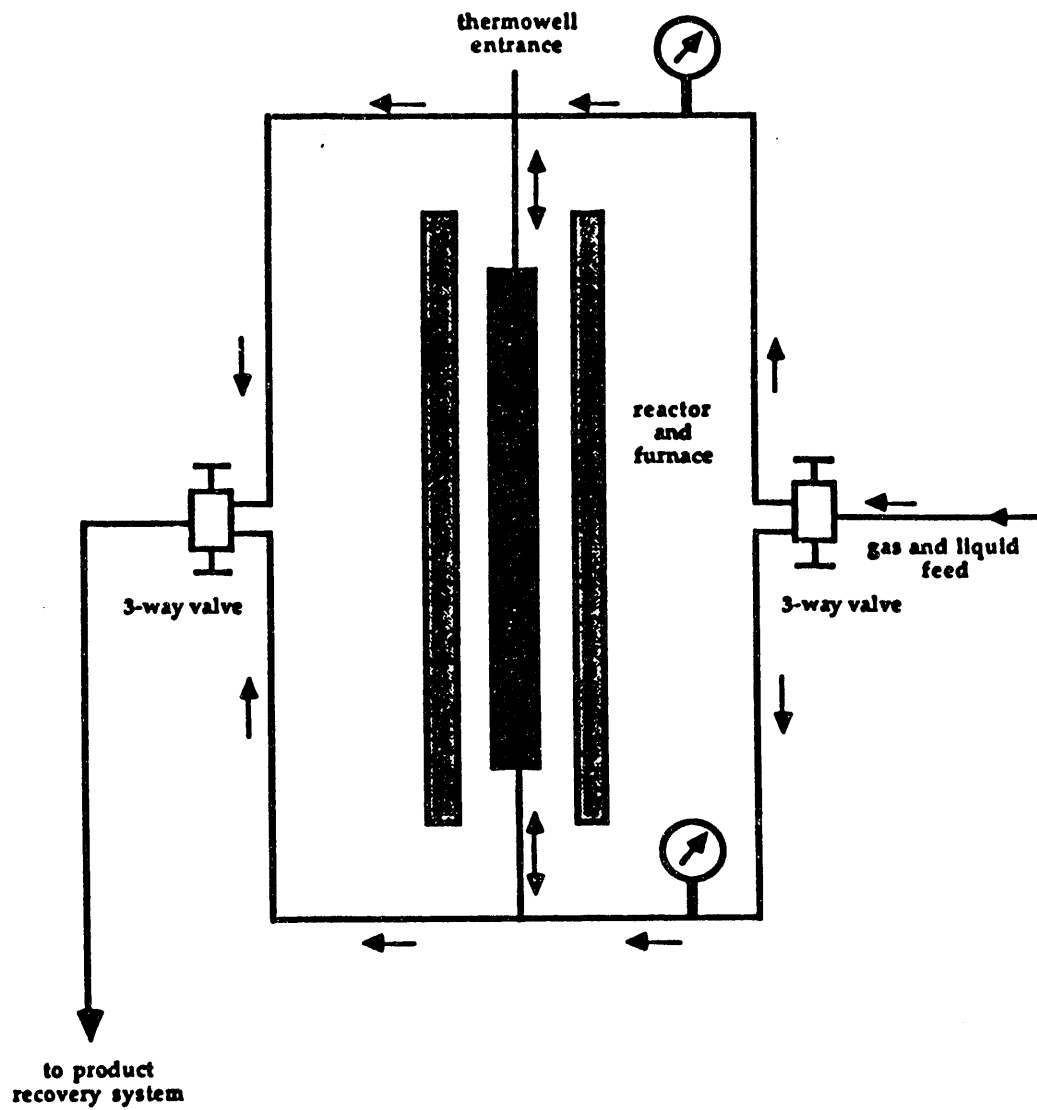
Upflow/downflow Reactor System

Figure 66. Upflow/Downflow Reactor System

309
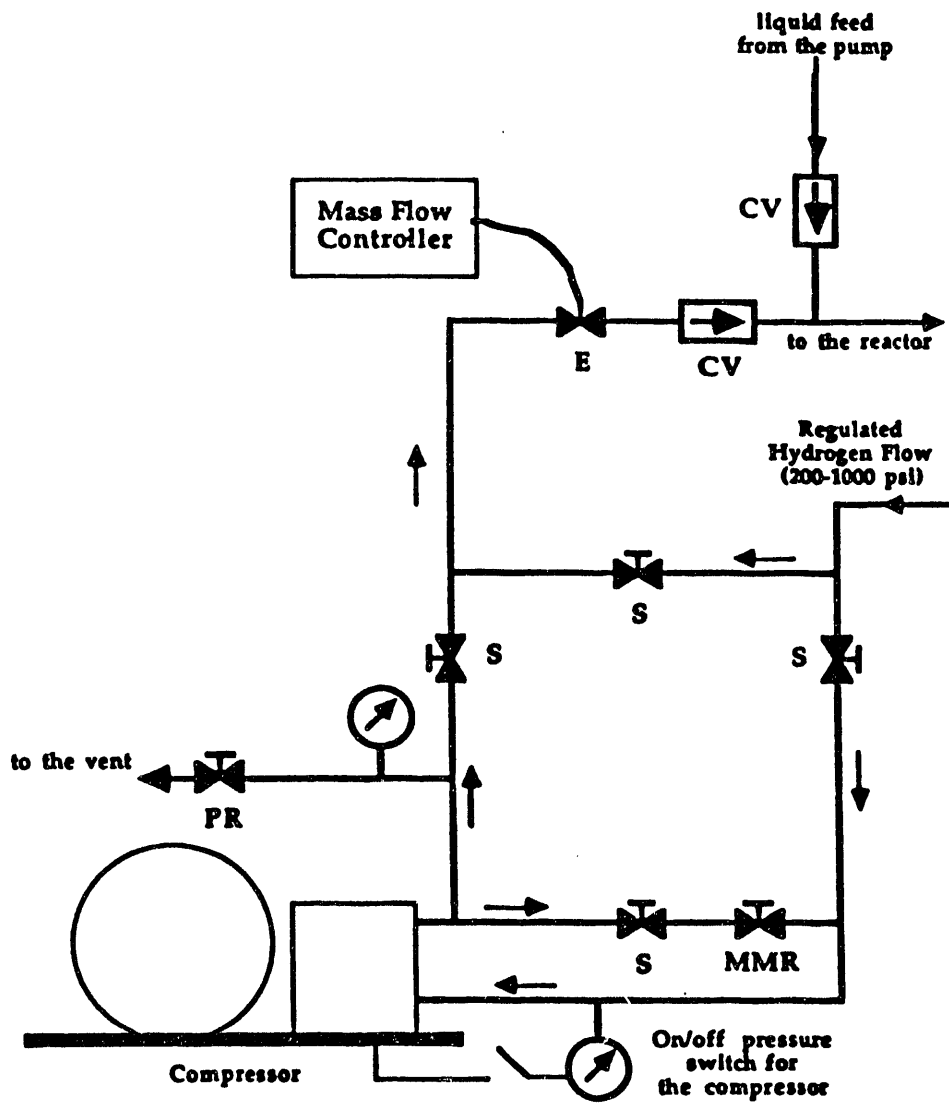
Gas Feed Control and Supply System

**Figure 67 Gas Feed Control and Supply System**

310
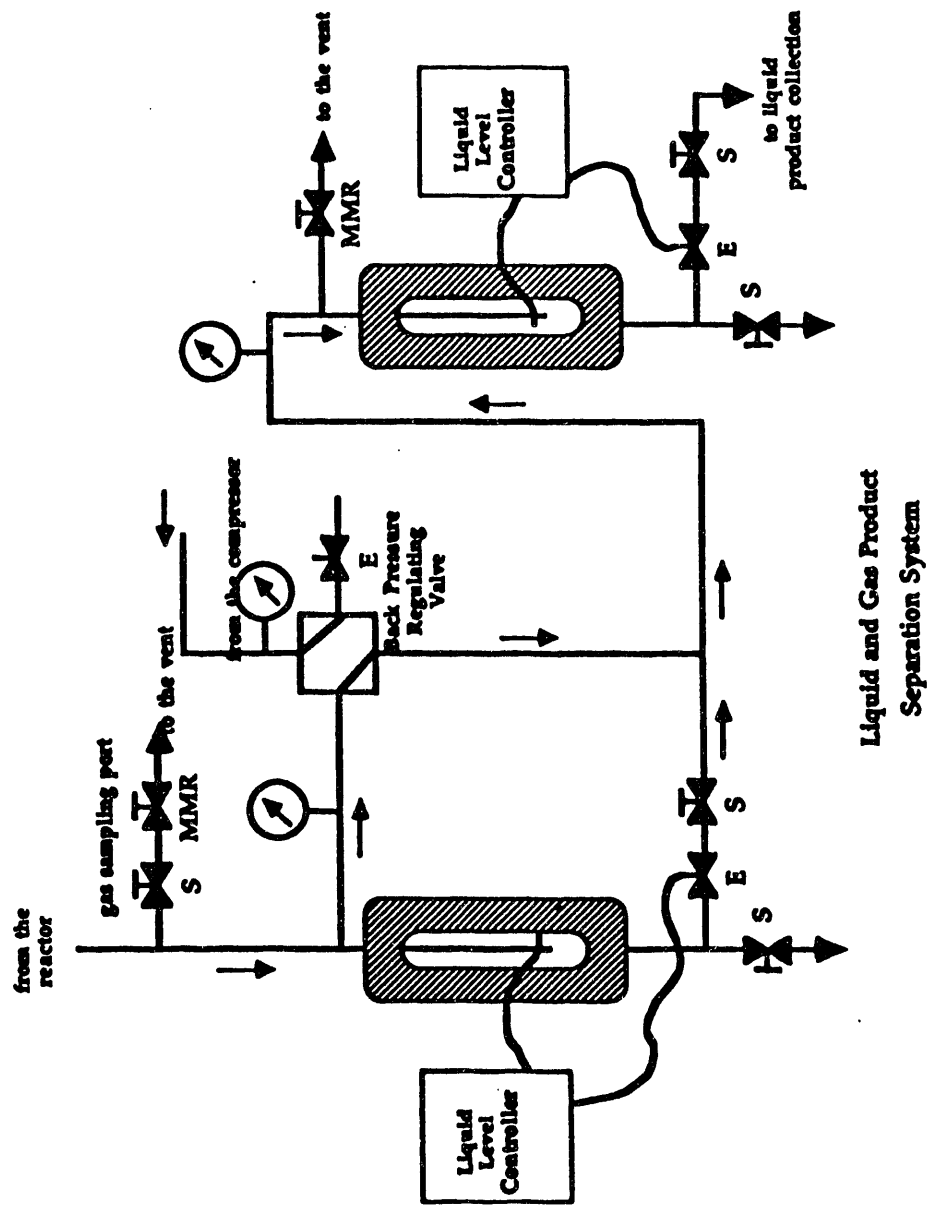
Figure 68   Liquid and Gas Product Separation System

311

Sometimes it is necessary to sample gas shortly after it exists the reactor, a series of two valves will be connected near the entrance of the high pressure vapor-liquid separator to throttle high pressure product gas to atmospheric pressure for sampling.

The liquid feed system consists of a Durco U-pump which will be used to transfer the liquid feed from the feed reservoir to the reactor. This pump was chosen due to the ease of heat tracing the externally mounted check valves and plunger pumping mechanism. The maximum flow rate for this pump is over 1200 cc/h. Which is about ten times the feed rate at the mean design LHSV. Lower rated pumps have smaller inlets and there was concern about pumping a highly viscous material such as bitumen through these systems.

A smaller high performance liquid chromatography Eldex brand pump will also be connected for introducing sulfur containing compounds to the feed for catalyst sulfiding or for pumping lower viscosity liquids in hydrocracking studies.

The reactor system tubing will be heat traced and insulated to avoid problems arising due to the high viscosity of bitumen. Special heat traced burets will be employed to insure that bitumen feed will flow readily into the pump. It is assumed that feed burets, pump, process tubing and vapor-liquid separators will need to be heated to 150 C., for the bitumen to flow readily.

Feedstock Preparation

It is expected that 30-100 cm^3 of bitumen will be consumed for each hour of operation. Some experiments will be conducted for days to study catalyst deactivation. Consequently relatively large

312

amount of bitumen will be consumed. Solvent extraction of tar sand from the northwest of the Whiterocks formation with toluene is currently being performed to produce the required quantity of bitumen. About 35 liters of bitumen have been prepared to date. Solutions of toluene and bitumen produced from the Soxhlet extraction of tar sand have been heated under a vacuum to remove the majority of the toluene. The remainder of the toluene will then be removed by batch distillation in a still.

Bitumen produced by solvent extraction differs from bitumen produced by the hot water extraction process in that it has a lower fines content and contains no kerosene or diesel diluents. If large quantities of bitumen from the hot water extraction process becomes available they will be studied. The initial process variable studies will be conducted with a bitumen-derived liquid produced by fluidized bed pyrolysis of the Whiterocks tar sand ore.

Future Activities

The design and preparation of the reactor system will be completed during the 1990-1991 contract period. The design and operating procedures have not been finalized and will continue to evolve as the preliminary, shake-down experiments dictate.

The initial process variable study will use a bitumen-derived hydrocarbon liquid produced during pyrolysis of the Whiterocks tar sand in a large diameter fluidized bed. The native bitumen from the Whiterocks tar sand deposit will be hydrotreated in a subsequent series of experiments.

Ebullieted Bed Hydrotreating and Hydrocracking

Graduate Student: D. Deshpande

Introduction

The native bitumens of the Uinta Basin are a very viscous, high distillation end-point hydrocarbon resource which have high heteroatom concentrations. Integration of this resource into a transportation fuels refinery will require hydrotreating to remove nitrogen and sulfur followed by either hydrocracking or catalytic cracking to reduce the boiling range. The heavy nature of these bitumens make efficient contacting of the feedstock, catalyst and hydrogen in the hydrotreating step difficult to achieve. The design or specification of the reactor in which to accomplish the hydrotreating step must also take into account the following factors:

1. Reduction of the nitrogen content to levels below 100 ppm and preferably to below 10-25ppm in the hydrotreater will be accompanied by the generation of a large amount of thermal energy in the catalyst beds due to the global heat of reaction. This would require large quantities of recycle quench gas to maintain temperature control in a conventional, fixed bed hydrotreater.

2. The high concentration of polynuclear aromatics and asphaltenes in the native bitumens may cause excessive coking/fouling of the catalyst in a conventional hydrotreater especially at the high temperature which

314

will be required to hydrotreat these bitumens. Suppression of coke formation by increasing the hydrogen partial pressure in the reactor may also be limited in conventional, fixed bed hydrotreaters.

3. The high concentration of asphaltenes and the high Conradson carbon residues of the native bitumens coupled with residual sand fines from the extraction process could lead to fouling of the upper catalyst beds in a conventional fixed bed, hydrotreater and to the eventual plugging of the reactor.

These considerations, among others led to a review and evaluation of the ebullieted bed reactor as an alternative to the fixed-bed reactor for the hydrotreating of the native bitumens from the Uinta Basin. This review led to a consideration and review of the H-Oil process which had been developed for the upgrading of coal-derived liquids and residual petroleum fractions.

The essential features of the H-oil process are outlined in the following:

1. Since the reactor is maintained in a thoroughly ebullieted condition with the catalyst particles circulating throughout the liquid phase efficient contacting between the liquid feed, hydrogen and catalyst is achieved.

2. The recycle product stream serves to carry away the heat of the exothermic reaction thereby maintaining a near isothermal condition in the reactor. The cooling by the

315

recycle stream is very effective, eliminating the need for an elaborate quench system for reactor temperature control.

3. The coke formation reaction is suppressed due to better reactor temperature control and the high hydrogen partial pressure in the reactor. This combination permits the H-Oil process to be operated at a lower hydrogen partial pressure.

4. The rapid poisoning of the catalyst due to organo-metalic compounds and nitrogen can be avoided by employing a two stage reactor where the organo-metallic compounds and nitrogen are removed in the first stage by using a catalyst with high a metal loading.

5. Since the catalyst is in a state of continuous motion, fine particles (like sand), asphaltenes or carbon cannot plug the catalyst bed.

6. In the ebullieted state, the catalyst behaves much like a gas solid fluidized bed and can be made to flow into or out of the reactor. Catalyst can thus be added or withdrawn, while the unit is in operation, to maintain the catalyst activity constant at a desired level without shutting the unit down for catalyst regeneration or replacement.

7. An inherent advantage of an ebullieted bed reactor is the lack of catalyst carry over in the products. Thus an entrained catalyst-liquid product separator is not needed.

316

8. Since the ebullieted reactor contains a continuous liquid phase, with a low pressure drop, the velocity of the vapor phase flow relative to liquid is much higher than in the case of a downflow fixed bed reactor. Consequently, the middle distillates and light gas oils are removed from the reactor as rapidly as they are formed, tending to concentrate the heavy gas oils and resid boiling range fractions in the reactor thereby increasing the effective residence time of these fractions.

9. The low pressure drop associated with the ebullieted bed system permits the use of smaller catalyst sizes than is practical in a fixed bed system. These smaller size catalysts are more effective for the conversion of high molecular weight species than the usual 1/8 inch catalyst particles.

Furthermore, City Services has used the H-oil process to upgrade the bitumen obtained from Athabasca tar sands. The analysis of the feed and products from pilot plant studies with the Athabasca bitumen are presented in Table 51. Inspection of the feed properties indicate that the initial upgrading H-Oil process will require cracking for boiling range reduction, sulfur reduction and hydrogenation. Inspection of the products indicate that they were not in a final product state ready for integrations into a refinery product state. The distillate fractions will require further processing to reduce the sulfur and nitrogen contents and

Table 51

H-OIL PROCESSING OF ATHABASCA BITUMEN

Feed Inspections:

Gravity °API.	8.3
Sulfur, weight percent	4.9
Nitrogen, weight percent	0.45
Percent Boiling to 975°F	49.7
Percent Boiling to 975°F	50.3

Product Inspections:

	Wt. %	API	Sulfur Wt. %	Diesel Index
H_2S	2.7	---	---	---
$C_1 - C_3$	3.2	---	---	---
255				
	Vol.%			
C_4	2.5	---	---	---
C_5-380°F	16.0	51.0	1.0	---
380 - 650°F	43.0	28.0	2.0	30
650 - 975°F	26.4	13.0	3.5	13
975°F+	16.0	-9.0	5.7	---
C_4 - EP	103.9	21.2	2.7	---

to saturate olefin. The particular quality of these products were a result of the mild processing conditions employed in the pilot plant. These conditions were employed to suppress hydrogen consumption in the heavy ends which were intended to be burned as fuel and would not need to be of a high quality.

The analyses of bitumens from Uinta Basin tar sands indicate that the weight percent of sulfur is an order of magnitude less than the Canadian bitumens (0.5 weight percent maximum against 4.9 weight percent), however, the nitrogen content is higher (1.1 to 1.3 weight percent against 0.45 weight percent). This implies that if the HDN step in the first stage of the reactor is effective in reducing the nitrogen to a desired level, the products from the H-oil process will also have a low sulfur content.

The use of a fixed bed hydrotreating-hydrocracking process was not considered because of the tendency of fixed beds to plug when processing extra heavy feedstocks and due to the advantages of the ebullieted bed over the fixed bed reactor.

The review and evaluation of the ebullieted bed reactor led to the conclusion that a hydrotreating-hydrocracking process employing a liquid ebullieted, two stage reactor could be effectively used for upgrading the bitumen, derived from Utah tar sands, to a refinery feedstock.

Design Considerations for a Laboratory Scale Ebullieted Bed Reactor

Process research and development for a viable process usually proceeds from the laboratory or bench scale studies to the pilot plant operation to the commercial scale plant. In this instance

319

the process has been reversed: the commercial H-oil plant operation has been reviewed, a bitumen upgrading pilot plant operation has been reviewed and a laboratory scale reactor system concept has been developed. Schematics of the commercial H-oil plant, the upgrading pilot plant and the proposed laboratory scale reactor system are presented in Figure 69 through 71. The major differences in the three schematics are as follows:

Processing/Analysis of Upgraded Product

(i)   Commercial Process: The upgraded product from the second stage of the reactor is subjected to heating and distillation to produce various transportation and heating fuel cuts.

(ii)   Pilot/Laboratory Process: The upgraded product from the second state of the reactor will be separated into gas and liquid phases in a high pressure separator. The separated phases will be subjected to laboratory analyses to determine their properties and compositions.

Performance of Reactor

(i)   Commercial Process: The product from the first stage of the reactor is passed into the second stage of the reactor. Final product from the second stage is then subjected to distillation. thus combined performance of both the reactor stages is reflected on the quality of products.

(ii)   Pilot/Laboratory Process: The reactor system has been
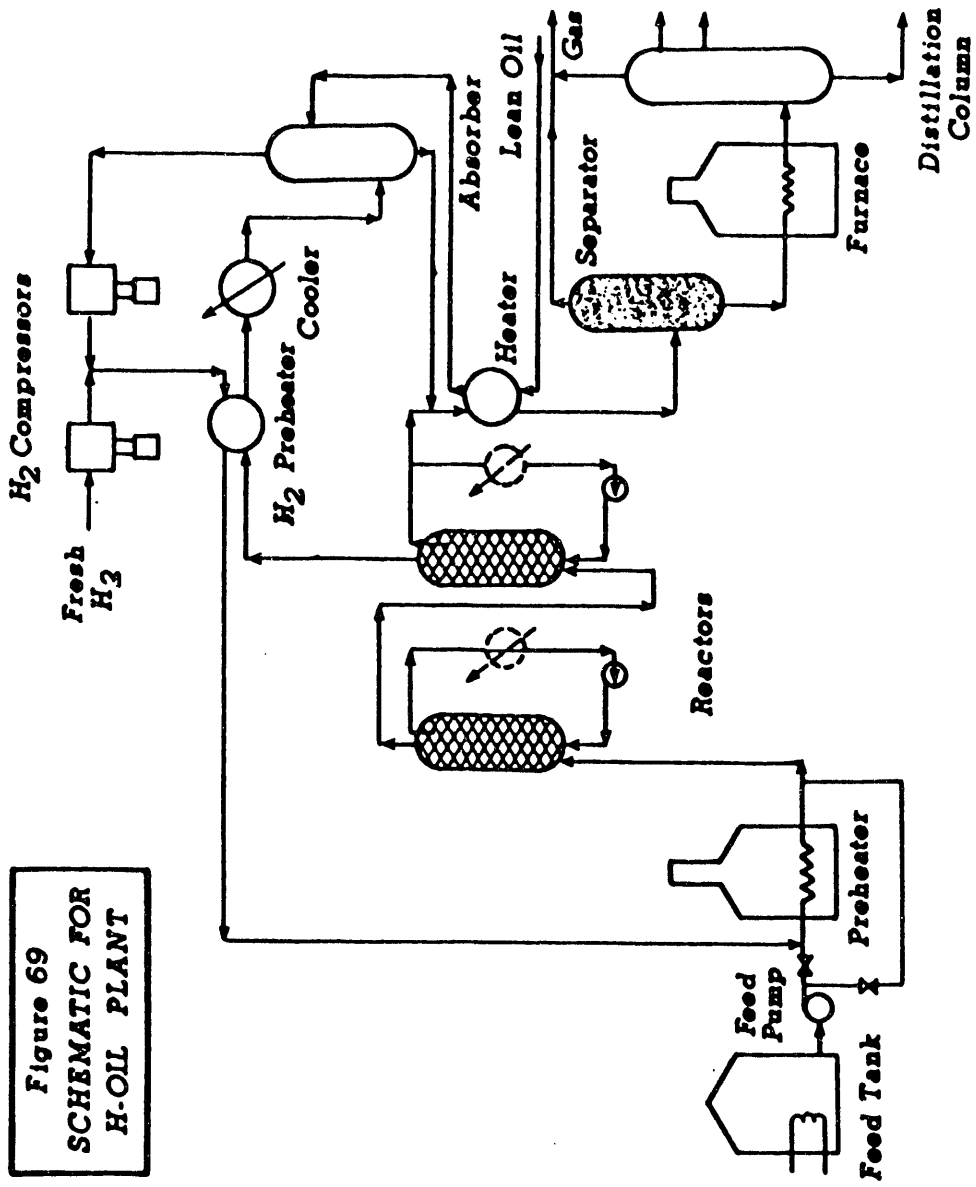
Figure 69
SCHEMATIC FOR
H-OIL PLANT

Figure 69. Schematic for Commercial H-Oil Resid Upgrading Process
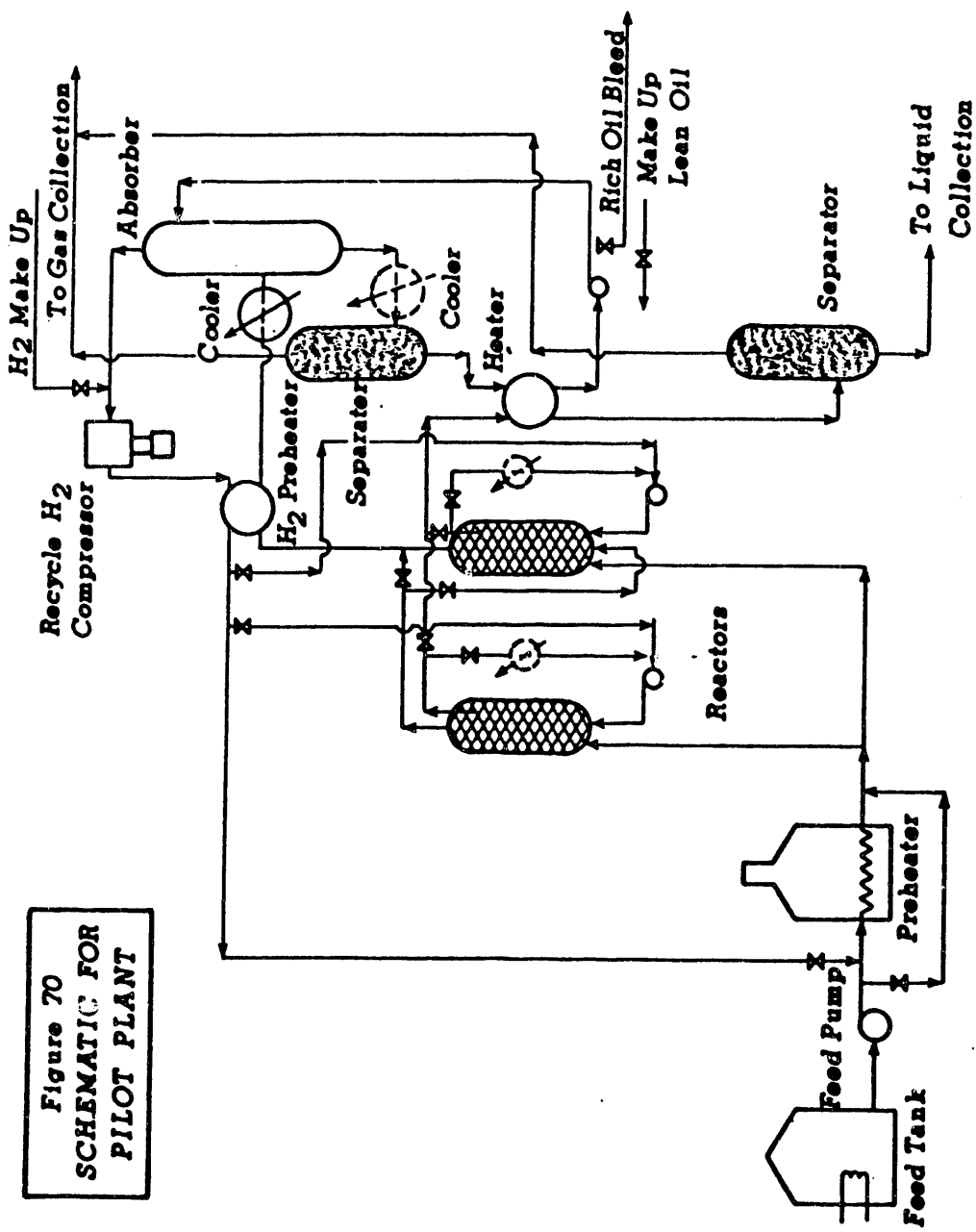
Figure 70. Schematic of an H-Oil Process Pilot Plant

322

Figure 71. Schematic for a Laboratory Scale Ebullieted Bed Reactor

designed to permit by-passing and isolation of the product streams from the individual reactor stages. This will facilitate the evaluation of the performance of individual reactor stages, especially for the HDN, HDS and HDM steps and finally for the hydrocracking step.

Hydrogen Compressor

(i) Commercial Process: Separate compressors have been used for recycle hydrogen and fresh hydrogen.

(ii) Pilot/Laboratory Process: The fresh hydrogen compressor has been deleted. Fresh hydrogen will be fed at the suction part of the recycle hydrogen compressor. Flow rate of fresh hydrogen will be adjusted to keep the pressure of the recycle hydrogen stream at a desired value. This will provide a means to monitor the consumption of fresh hydrogen for hydrocracking and also the efficiency of hydrogen purification in the absorber.

Hydrogen Inlet-to-Bitumen Feed Ratio

(i) Commercial Process: The recycle hydrogen is mixed with the feed upstream of the feed preheater. Thus both the feed and hydrogen get preheated before entering the reactor.

(ii) Pilot/Laboratory Process: The unit will be designed so that the point at which hydrogen and the feed are mixed can be varied:

- upstream of feed preheater

- on suction side of product recycle pump to the reactor.

Since the hydrocracking reactions are highly exothermic, it may be possible to use this heat to heat the hydrogen thereby eliminating the need for preheating the hydrogen in the feed preheater.

Hydrogen Purification System

(i)   Commercial Process: Lean oil is used to absorb the hydrocarbon vapor in the absorber. The resulting rich oil is then mixed with the liquid product from the reactor and is fractionated in the distillation column.

(ii)   Pilot Process: Lean oil will be used to absorb the hydrocarbon vapors, however, it will not be mixed with the liquid products from the reactor. Instead the lean oil, after flashing, will be recycled back to the absorber. Occasional bleeding of rich oil (out of the recirculation circuit) and make up of absorbent by feeding in lean oil will be required. This will also involve incorporation of an extra recirculation pump. Since the rich oil from the hydrogen purification system is not mixed with the product stream, the product stream will be "uncontaminated" and thus the analysis of this stream will give the actual yields and performance of the hydrocracking process.

(iii)   Laboratory Process: The hydrogen purification process has been simplified: The hydrocarbon vapor is absorbed in a column of lean oil through which the gas is bubbled.

325

There is no flashing or recycling of the rich oil, however, rich oil will be occasionally bled off and make-up lean oil will fed to the absorber directly. This system, suitable for the low expected throughput, will be simple and will have the same advantages of the pilot plant recycle system discussed above. However, a separate analysis of the rich oil bleed stream will be necessary for material balances.

Overall Approach to System Design

The critical areas are listed in order of priority. The development of the overall hydrocracking process development unit will proceed in stages.

- reactor stage
- reactor hydrogen separation and purification stage
- product separation and collection stage

Since the reactor is the most important component of the system, the initial effort will be concentrated on designing the reactor system. The review of the H-Oil process technology led to the conclusion that the reactor system should consist of two stages:

- First stage for HDN, HDS and HDM
- Second stage for Hydrocracking

The following steps are proposed for developing the reactor system:

Type of Design Data Required

As a first step, the type of data required to develop the

reactor system must be specified:

(i)   Expected/desired products from hydrotreating/hydro-
        cracking

(ii)   Chemical and physical properties of the feed

(iii)   Hydrodynamic data for the design of the ebullieted bed

(iv)   Mass and heat transfer coefficients for transport between
        variance phases

(v)   Kinetic data for HDN, HDM and hydrocracking reactions

     The above is a very broad classification of the requirements
and each will be discussed in due course. Using the assembled
data, it would be possible to develop a mathematical model of the
process.

Design Data Collection:

(i)   From literature: It is expected that some data,
        especially data in the areas of hydrodynamics, mass
        transfer and heat transfer may exist in the literature.
        A search for such data has been initiated.

(ii)   From laboratory experiments:

        (a) Chemical and physical data for the native bitumen,
            from the Whiterocks tar sand deposit is available.

        (b) Procedure for collecting the kinetic and
            hydrodynamic data.

        -   Collection of the hydrodynamic data may be possible
            by carrying out fluidization experiments on a
            dynamically similar model of the ebullieted bed.
            Thus a "cold" fluidized bed could be used to

327

simulate conditions in the ebullieted bed.

- The combined effect of reaction kinetics, hydrodynamics, mass transfer and heat transfer could be studied in a laboratory scale model as suggested in section 3 above (please refer to Figure 71).

- The data collected from the above steps can then be analyzed and compared with the predictions of the mathematical model for the reactor. It would be possible to use the mathematical model for process scale-up leading to the design of a pilot plant.

Mechanical Features of the Reactor

Following mechanical features of the rector will have to be specified before the laboratory model is constructed.

(i)   method of ebullieting the catalyst bed (sparger, jet mixer, etc.)

(ii)   withdrawal techniques for the liquid and the gas products and the recirculation stream

(iii)   control system for the central of pressure, temperature and space velocity

(iv)   Method of monitoring the ebullieted bed density at various in the reactor

Other features of the overall system which will have to be specified before setting up the laboratory reactor system:

(i)   method of preheating/heating the feed

(ii)   laboratory scale recycle hydrogen purification/pumping

system (including flow monitoring)

(iii)   product liquid and product gas separation system

(iv)   product liquid and product gas collection system

A similituted analysis for the laboratory reactor design has been initiated. This analysis will enable the scale-down and design of the laboratory-scale reactor.

Future Activities

A cold flow model of the reactor will be designed and constructed. The objective will be to develop an understanding of the hydrodynamics of three-phase ebullieted bed containing hydrotreating catalyst pellets.

Bitumen Upgrading

Co-Principal Investigator: J. W. Bunger
Graduate Students: J. Pu
                             S. Jeong

PROCESS SIMULATION AND CONCEPTUAL DESIGN OF A COMMERCIAL HYDROPYROLYSIS UNIT

Process Simulation and Design

The field of computer-aided process engineering and process design has emerged as an important tool in recent years. Computer-based models of process plants are used routinely as aids in process development, process scale-up, and plant design and operation. The term flowsheeting[169] has been coined to describe "the use of computer aids to perform steady-state heat and mass balance sizing and costing calculations for a chemical process." The general field has been reviewed elsewhere.[170-175] These reviews discuss features of the simulators that have been documented in the open literature, including structure, module algorithms, data base and computation efficiency.

Commercially available software systems such as ASPEN PLUS,[176] CONCEPT,[177] DESIGN II,[178] FLOWPACK II,[179] FLOWTRAN,[180] and PROCESS[181] are widely used, and many companies also use their own proprietary in-house computer programs.

The purpose of this study is to develop a representative simulation model, of hydropyrolysis, to produce synthetic crude from tar sand bitumens which incorporate economics and to demonstrate the utility of this model for optimization.

330

Hydropyrolysis Process

Hydropyrolysis is a thermal hydrocracking process which has been under development at the University of Utah for more than a decade following the pioneering work of Oblad and co-workers.[182-188] A schematic of the bench-scale hydropyrolysis process unit is presented in Figure 72. Feedstock is pumped to system pressure and heated to 350-400°C. Make-up hydrogen, both a reactant and a heat transfer medium, is mixed with the hydrogen-rich recycle gas stream, compressed to the system pressure, and heated to about 600°C. The preheated feedstock is introduced to the reaction zone through a spray nozzle to provide good contact between the vapor and the atomized liquid. The product stream was separated into light products, heavy products, and gases. The heavy products are either recycled to the inlet of reactor or collected. Gas products consist of the reaction products and unreacted excess hydrogen. A portion of these are vented to maintain system pressure and prevent buildup of hydrocarbon gases in the recycle stream. The remainder of the gases are recycled and combined with fresh make-up hydrogen to maintain reactor hydrogen partial pressure. In the reactor, the hydrogen partial pressure is reduced by consumption due to the chemical reaction, by transport out of the reactor as dissolved hydrogen in the liquid product, and by the formation of light hydrocarbons, which dilute the remaining hydrogen.

331
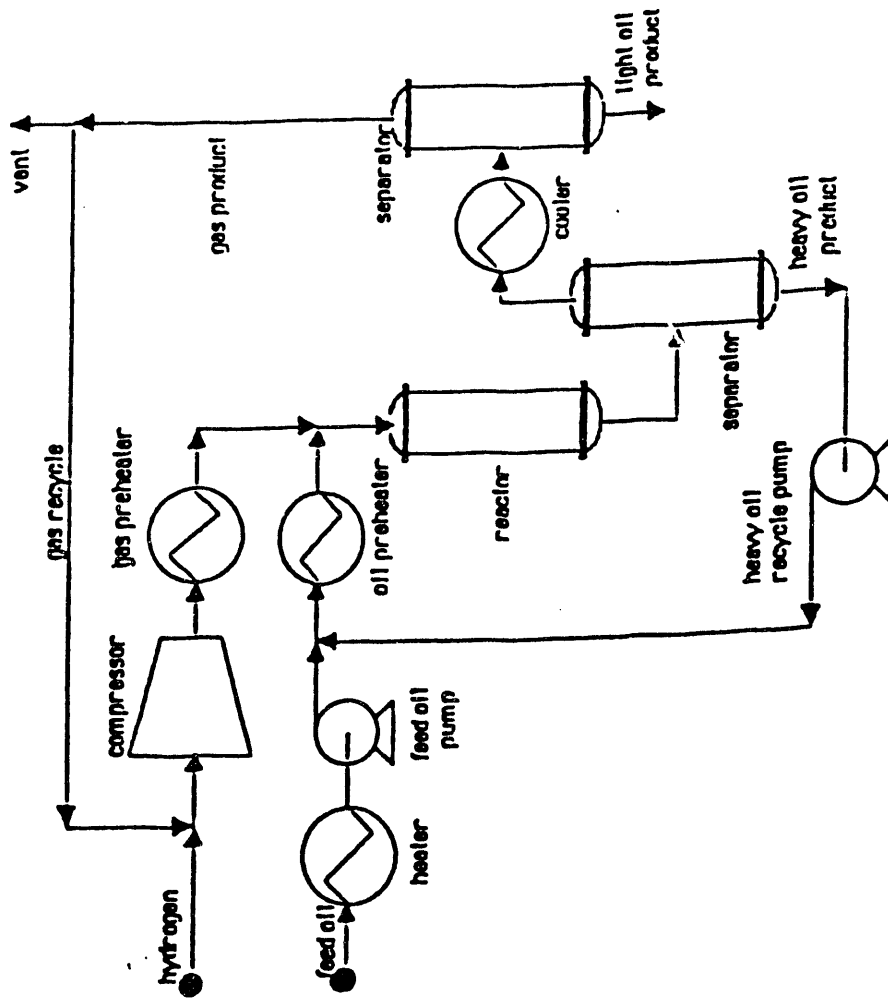
Figure 72 A Schematic of the Bench-Scale Hydropyrolysis Process

Simulation Approach

The plant should be simulated so that the simulation model can then be used to optimize the plant operation. This means identifying the set of independent process variables which will maximize (or minimize) a predetermined objective function such as cost of production, profit, or conversion.

Simulation Flow Diagram and Unit Computations

The hydropyrolysis process, Figure 72, was modeled using PROCESS simulator[181], a product of Simulation Science, Inc. The simulation flow diagram is presented in Figure 73. The upper character string in the rectangles, is the unit identifier specified by the user. The lower character string is the name of the unit operation in PROCESS simulator. It is composed of 15 unit computations connected by 16 information streams. In general, the information flow diagram resembles the process flow diagram in Figure 72, where process equipment items are connected by process streams. With the exception of the reactor section, the process was modeled using standard PROCESS unit operations. A brief description of these unit computations is presented Table 52. The user-added subroutine,[189] for the reactor model was written for a lumped kinetic model. This subroutine calculated the pseudo-component distribution at the reaction conditions for an isothermal plug-flow reactor, and stored the results in the output stream. Data, such as reaction conditions, residence time, reactor volume, and the component profile along the reactor length,

333
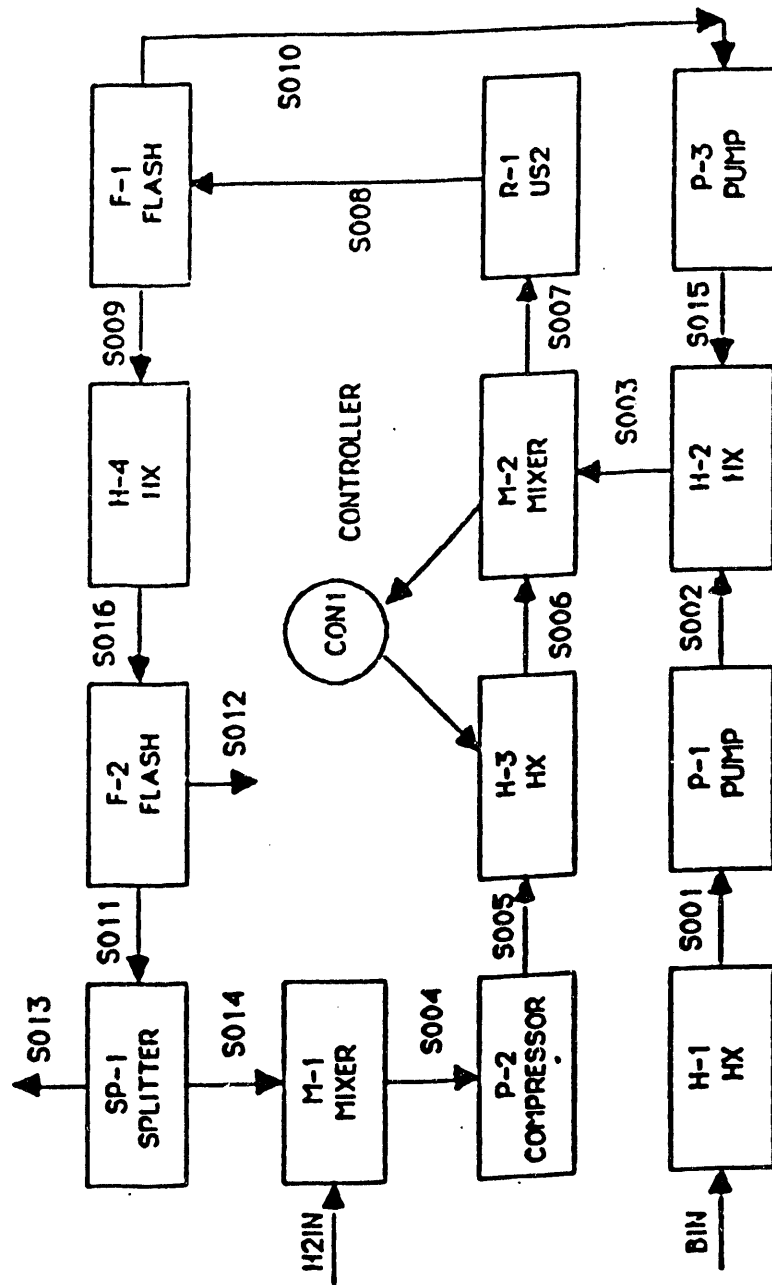
Figure 73 Simulation Flow Diagram of the Bench Scale Hydropyrolysis Process

334

Table 52

Process Unit Computations Used in Hydropyrolysis Simulation Model

Name	Item	Function
M-1	Mixer	Mixing of makeup hydrogen and recycle gas stream; outlet temperature is decided by adiabatic flash and the pressure is the same as the lowest pressure among inlet streams.
P-2	Compressor	The compressor simulates a single stage isotropic compression. Outlet conditions and power requirements can be calculated using a polytropic efficiency.
H-3	Gas Preheater	Outlet temperature is adjusted according to the reaction temperature.
H-1	Liquid Heater	Preheating of feed oil to 100°C.
P-1	Pump	Feed oil pump. The energy required is added to the feed enthalpy to compute the outlet temperature.
H-2	Liquid Heater	Feed oil and recycled oil are mixed and heated to 350-400°C.
M-2	Mixer	Mixing of heated gas and oil stream into the reactor.
CON1	Controller	Feedback controller; outlet temperature of H-3 is adjusted by CON1 to approach a specified temperature of reactor inlet.
F-1	Flash	Isothermal flash to separate into recycle liquid and vapor stream.
H-4	Cooler	Set the outlet temperature for F-2.
F-2	Flash	Isothermal flash to separate into liquid product and recycle gas stream.
SP-1	Splitter	Adjust the purge rate to maintain the system pressure and prevent hydrocarbon gases buildup.
CON2	Controller	Feedback controller; makeup hydrogen flow rate is adjusted to give a fixed percentage of hydrogen concentration in gas stream.

are transferred to an output subroutine and intermediate and final results are printed out. The data provided by the user for the model are passed through keyword vectors, IPARM and RPARM, as follows:

IPARM(1)	number of steps in solving the rate equations;
IPARM(2)	number of tubes in the reactor;
IPARM(3)	a flag indicator to show the sources of residence time;
IPARM(3)=0	if residence time is calculated by program;
IPARM(3)=1	if residence time is provided by user;
RPARM(1)	diameter of tube (inch);
RPARM(2)	length of tube (feet); and;
RPARM(3)	residence time (sec) if IPARM(3)=1.

An analysis of the degrees of freedom was conducted for each of the processing steps and for the entire system. The more important fixed design variables are listed in Table 53; the free design variables considered in the study are given in Table 54.

Simulation Procedure

The main functions performed by the PROCESS executive in conjunction with the user subroutine in this application were:

1. Retrieve input data for a particular case from an input file. These data include the name and number of each unit computation, the identifying number of each stream of information either entering or leaving a unit computation; values of initialized variables and physical properties used in the calculation; criteria for establishing acceptable convergence of recycle

336

Table 53

Partial List of Fixed Design Variables for Hydropyrolysis Reactors System

Item	Value
Fresh bitumen feed rate/feed temperature/feed pressure	5.3 lb/hr/20°C /14.7 psia
Makeup hydrogen temperature/pressure	20°C /1814.7 psia
Recycle gas pressure drop	40 lb/psia
Liquid pump efficiency and recycle compressor polytropic efficiency	0.80 psia
Preheater pressure drop	0 psia
Flash pressure drop/purge drum pressure drop	20 psia
Exchanger pressure drop	0 psia

Table 54

List of Free Design Variables for Hydropyrolysis Reactor System

Variable	Constraint
Hydrogen weight fraction in recycle gas	≥ 0.70
Reactor inlet temperature	--
Residence time	--
Gas preheater inlet temperature	--
Flash temperature	--

337

calculations; and the order of calculation of the unit computations corresponding to the connections of the process units in the input file.

2. Direct the simulation calculations by calling the unit computations and storing the computation results, and testing for the convergence of processes involving recycle. The following procedures (2a-2d) are specified for a user-added subroutine:

2a. Calculate the rate constants from the reaction conditions, the total weight flow rate, the volumetric flow rate of the feedstream, the volume of reactor, and the residence time if IPARM(3) has been set equal to zero.

2b. Determine the stepsize from the residence time, the number of steps and solve the rate equations.

2c. Check the mass balance. The calculation of rate equations does not give hydrogen consumption due to the assumption of zero-order reaction with respect to hydrogen. Series cracking reactions for $C_{50}H_{102}$, $C_{23}H_{48}$, and $C_{13}H_{25}$ in the presence of hydrogen are assumed to calculate hydrogen consumption based on the reaction scheme published previously. These three components are selected as representative of the residual; gas oil, and middle distillate fractions, respectively, based on molecular weight and normal boiling point analyses. Afterwards, the mass balance can be checked by a unidimensional search subroutine, ZERO, in TEAPACK.[190]

2d. Calculate the molal flow rates, store the results in the output stream, and transfer data to an output subroutine for printout.

338

3. Print the final results for each case.

4. Repeat the calculation procedure for parametric case studies.

Verification and Utilization of the Process Model

Results from the PROCESS simulation for hydropyrolysis may be compared with experimental results[191] which were obtained in the two liter per hour semibatch bench-scale unit at the University of Utah. The comparison as presented in Figure 74 indicated that the model reasonably predicts the product yield of 25% AAD despite several different flow patterns and different nozzle configurations. TS-IIC bitumen was used in most of the runs. The discrepancy between these comparisons can be explained by the fact that it was very difficult to achieve the steady-state operations and to separate the products in the equilibrium state, due to the equipment limitations and the nature of thermal cracking. The comparison would be more conclusive if the experimental results had been obtained under true steady-state conditions.

In order to determine the optimum hydropyrolysis conditions several different cases were simulated. A plant size of 10,000 bbl/day was selected due to the equipment size limitation on the PROCESS simulator for economic calculations. These case studies are based on the configuration of the bench-scale unit, the reaction temperature varied from 460 to 585°C, and the residence time varied from 12 to 40 seconds (total 24 cases). The concentration of middle distillate was assumed to attain a maximum at a specific temperature, above which a decline in concentration

occurred. This observation suggested that there may be an optimum condition which promises the most cost-effective operation. Also, it is anticipated that the selectivity at temperatures above and below the optimum temperature are not desirable because of low middle distillate and high gas production, respectively.

The amount of hydrogen in the purge gas stream was the same for all cases studied. For example, at two extreme conditions, 1) the shortest residence time and the lowest temperature, 12 seconds and 460°C, and 2) the longest residence time and the highest temperature, 40 seconds and 585°C, the hydrogen vent rates were 398 and 385 lb/hr, respectively. Thus, the difference in the cost of vented hydrogen was negligible for the cases studied. In addition, the other costs except for the utilities and fuel gas are nearly the same in all cases. A plot of operating cost per unit of middle distillate produced as a function of reaction temperature at four different residence times is presented in Figure 75. The preferred operating conditions appear to be lower reaction temperature (about 510°C) and longer residence time (40 seconds). However, it is noted that the optimum process conditions should be sought through the optimization of the process with the heat-exchanger network because the optimum process conditions always involve an economic tradeoff between the costs.

Optimization

In process design optimization it is essential to have a model which accurately describes the way in which the economic valuation of a process varies as the operating conditions change. Since the

340
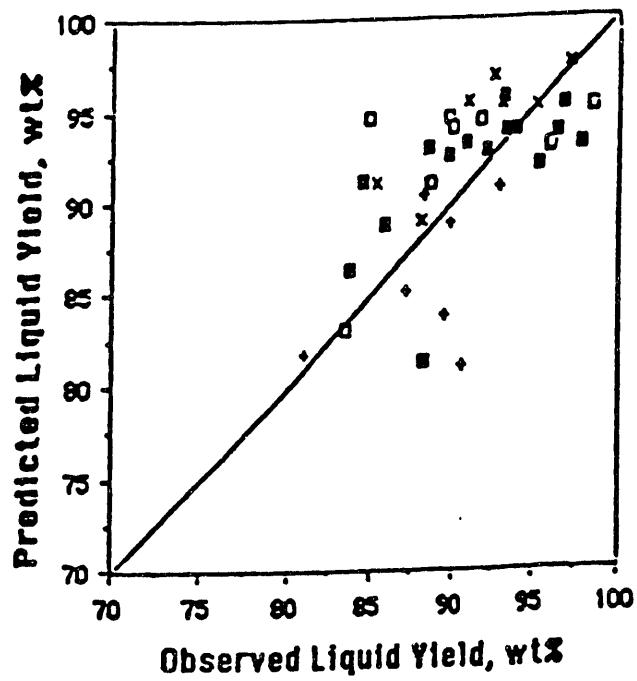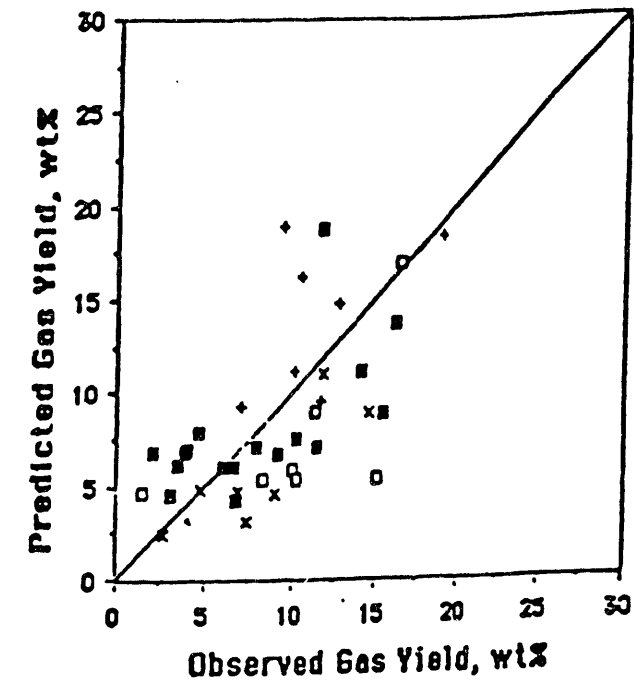
Figure 74 Parity Plot of Predicted Yields vs. Measured Yield of Gas
and Liquid Product of Hydropyrolysis of Tar Sand Bitumen
Flow Pattern and nozzle configuration used in the
experiments:□ - counter-current flow mode, 3-orifice
nozzle; + - cocurrent flow mode, 1-hole nozzle; ▪ -
countercurrent flow mode, spray nozzle; and x - cocurrent
flow mode;spray nozzle

341

profit and investment of a process are determined from a model made up of numerous interacting parts, all the process variables must normally be considered simultaneously in order to find the most desirable combination of variables. Also, it is noted that at the conceptual design stage, the focus should be directed toward the best flow-sheet alternatives, rather than rigorous design calculations. If the conceptual designs appear to be sufficiently profitable then rigorous design and optimization calculations are justified and should be performed to develop a final design.

Conceptual Design for Scale-Up of the Hydropyrolysis Process

Several modifications to the bench-scale unit configuration Figure 72 were required for conceptual design of the scaled-up hydropyrolysis process: incorporation of purge gas hydrogen recovery, modification of the heat exchanger network and inclusion of a multistage compressor. Gas separation via membrane technology was used as the hydrogen recovery process. The alternatives considered included oil scrubbing, pressure swing adsorption (PSA), and cryogenic separation. PRISM separator systems developed by Monsanto[192] were selected because it has been successfully applied for selective separation of gases on an industrial scale for many years. PRISM separators, utilizing a patented hollow fiber membrane,[192] have found worldwide acceptance and are currently being used for recovering hydrogen from a variety of plant off-gases or purge streams. The following values have been used for the hydrogen recovery system: \$1.06 x 10^6 for the base investment
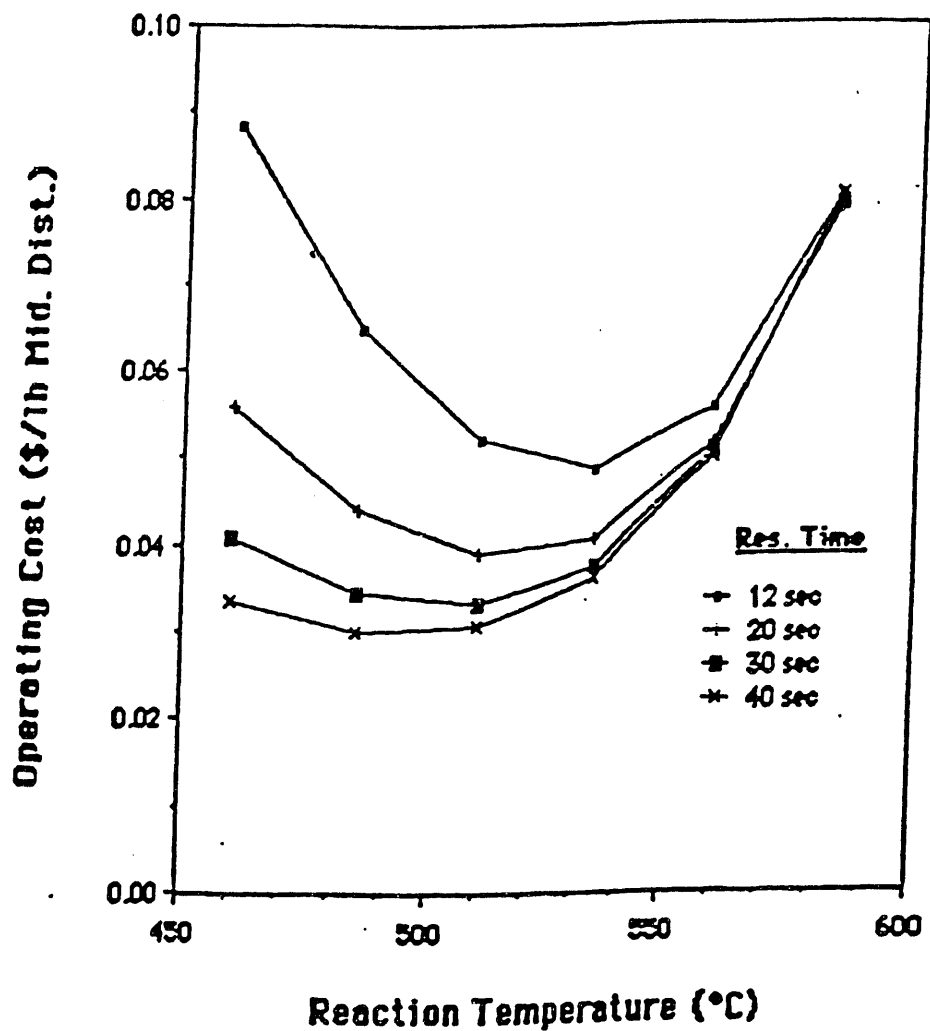
Figure 75 Effect of Reaction Condition on Operating Cost of a 10,000 bbl/day Hypothetic Hydropyrolysis Plant Residence time (sec): •-12; + - 20; ■ - 30; x -40

cost;[193] $0.05/Mscf for hydrogen recovery cost;[194] 95% for recovery rate;[195] 150°C and 500 psig for inlet temperature and outlet pressure, respectively.[196]

A conceptual design with a simple heat exchange scheme added to the bench-scale unit configuration is considered in the base case as shown in Figure 76. In this case, the inlet streams to the reactor, the H_2-rich gas, and mixed the liquid stream of feed and heavy recycle product can be heated by the outlet stream of the reactor. It is noted that the problem of designing a heat exchanger network cannot be decoupled from the design of the remainder of the process. The interaction between the optimization of the process flows and the heat exchanger network has recently been discussed.[197,198] Here it was suggested that the optimum profit from the simultaneous approach was much higher than the sequential case. Hence, the Problem Table Analysis[198] and the pinch design method are used to generate three HEN (Heat Exchanger Network) alternatives for this optimization study. More alternatives exist, but these are adequate to illustrate the behavior of the process. These three alternatives with similar energy recovery duties are presented in Figures 77,78, and 79. Pinch technology allows determination of the temperature point (the pinch) that divides the temperature scale in a process into two parts. Heat from external sources must be supplied to the process at temperatures above the pinch, and must be taken from the system by cooling media at temperatures below the pinch. The pinch design method is simple and straightforward. It is used to generate low cost solutions to
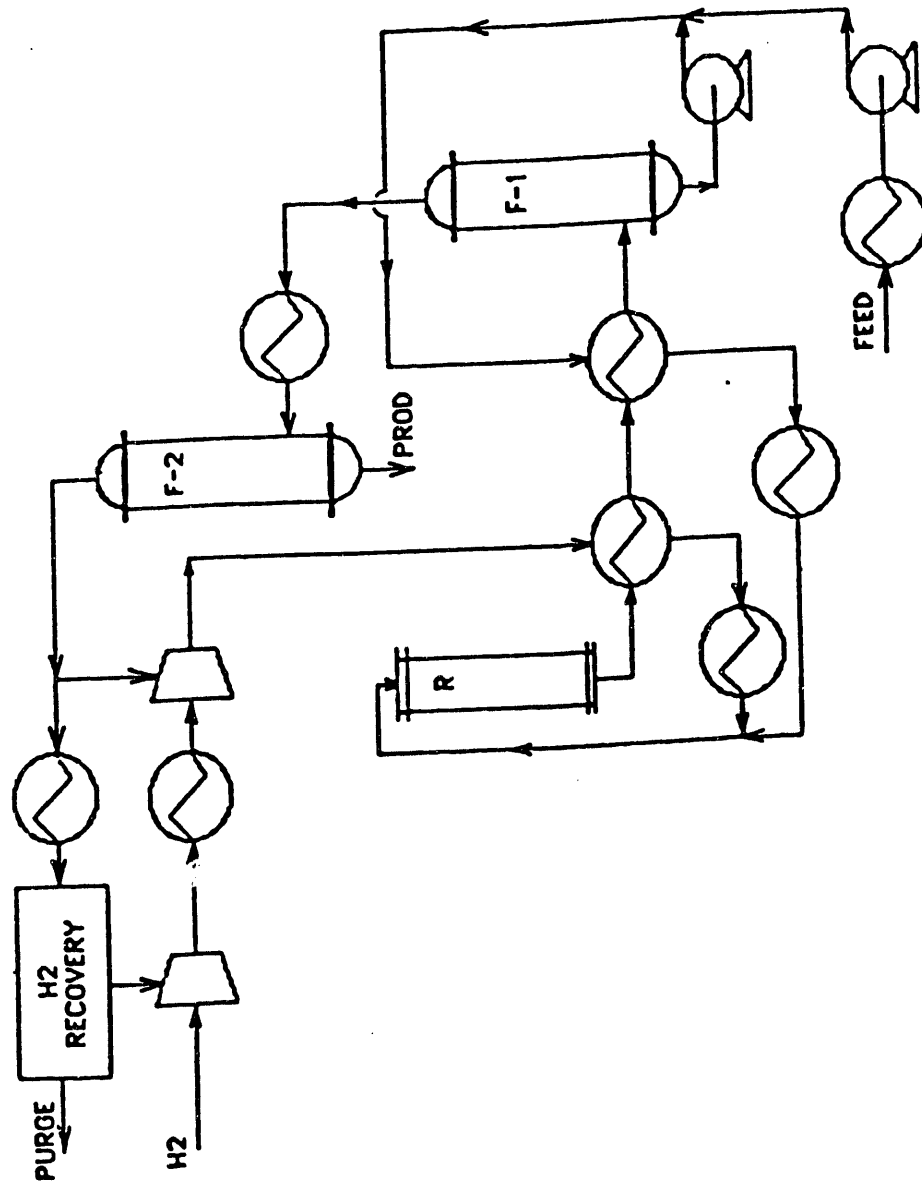
Figure 76 A conceptual Design of Hydropyrolysis Process – Base Case

HEN problems with a high degree of certainty by producing minimum utility designs with as few units as is compatible with minimum utility usage.

Alternative I (Figure 77) has the most complicated HEN. Basically, the heat in the effluent streams for the reactor (R) and the first flash column (F-1) are used to drive the remaining unit operations. Several control schemes are used to meet the temperature requirements. In fact, the economics will be dependent upon the differential between the savings due to waste energy utilization and the investment in the energy integration system. The flowsheets for the base case and the three alternatives are not presented here, but pretty much resemble their process flow diagrams: 20 unit computations and 29 information streams for the base case; 24 and 37, respectively, for Alternative I; 22 and 33, respectively, for Alternative II; and 22 and 30, respectively, for Alternative III.

Economic Evaluation of Hydropyrolysis Process Alternatives
Economic Evaluations

In order to compare flow-sheet alternatives, it is necessary to estimate the optimum design conditions for each alternative. A larger number of alternatives can be conveniently explored by using simpler calculations than those used for final designs. The optimum heat exchanger network and operating conditions are not guaranteed with this case study approach; however, a better understanding of the importance of energy integration and of the

346
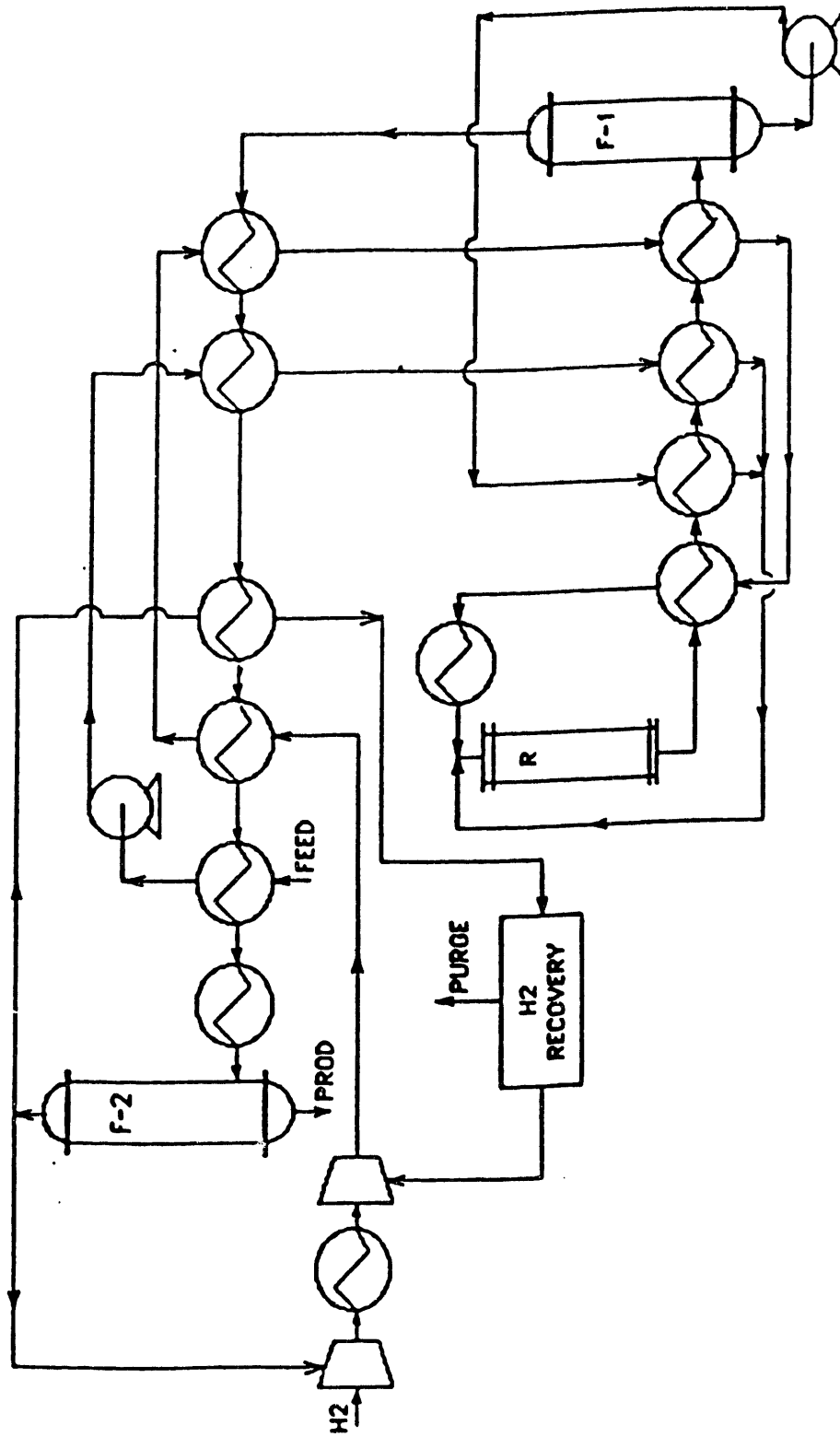
Figure 77   A Conceptual Design of Hydropyrolysis Process – Alternative I

347
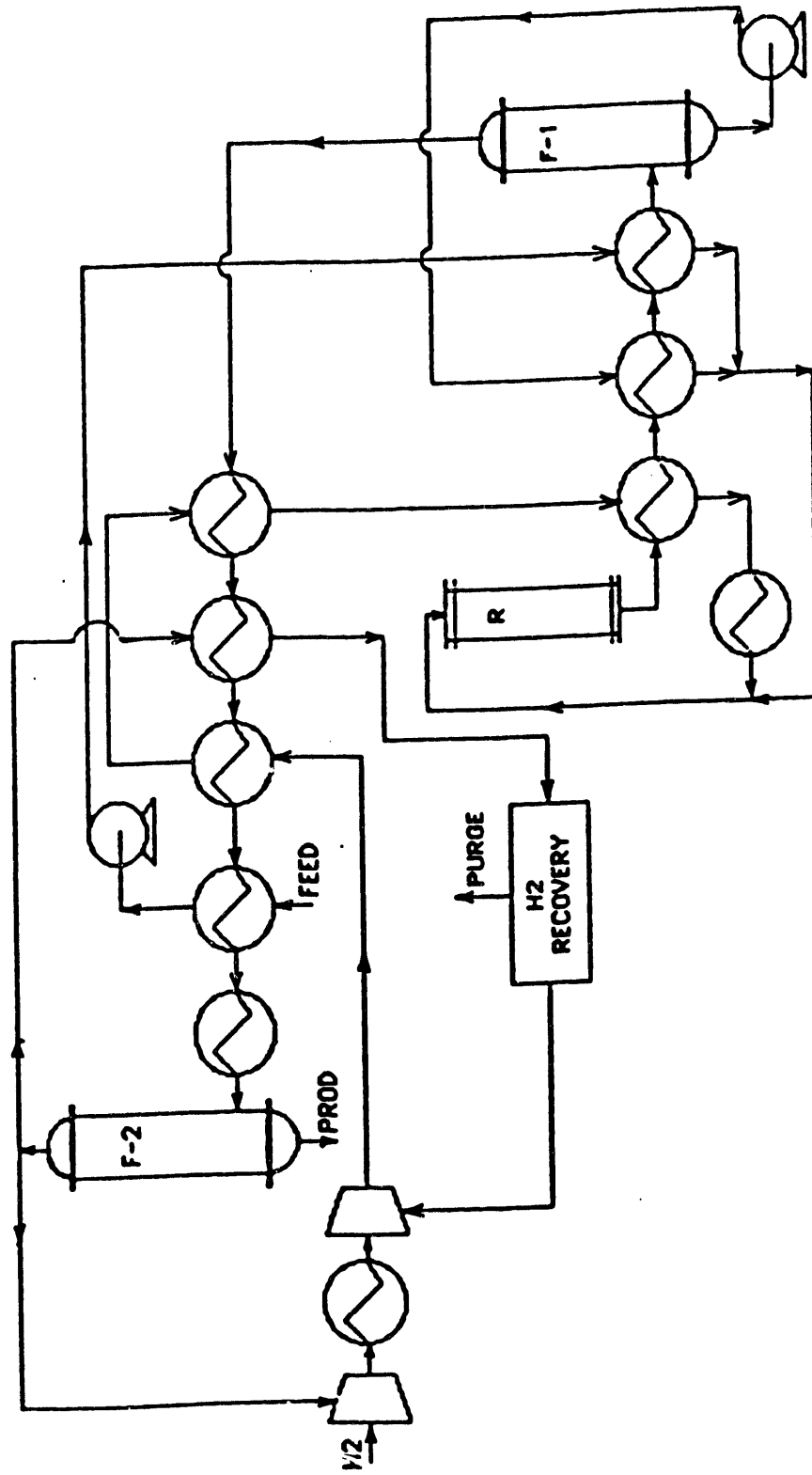
Figure 78 A Conceptual Design of Hydropyrolysis Process - Alternative II
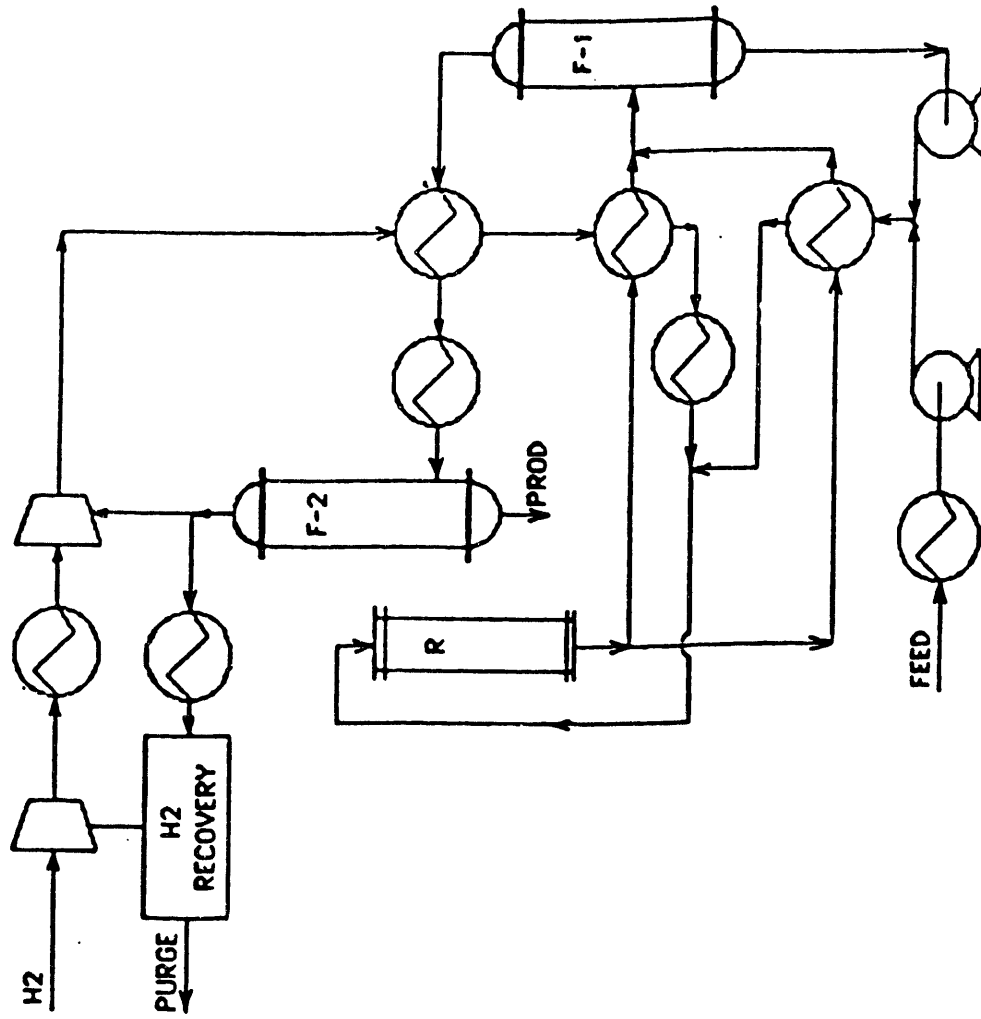
Figure 79 A Conceptual Design of Hydropyrolysis Process - Alternative III

process behavior can be obtained.

In approaching the process optimization from a design standpoint, equipment size and process operability are no longer severely constrained and the investment becomes an important economic parameter. Thus the problem can be formulated in terms of the return on investment (ROI), as the objective function in optimizing the hydropyrolysis process. The optimization can be stated as follows: maximize ROI = $f(x_1, x_2, ...)$ where the x_i are the independent variables of the process. The ROI from the simulation model includes the effect of changing investment, operating cost and revenues for the entire hydropyrolysis plant. The ROI is believed to be a sensitive measure of improvements in the economics and is good enough to make judgements regarding the economic evaluation of the conceptual process designs. No time scale was used in the economic analysis, so discounting was not possible.

Since cost estimates are the driving force for any design study, a factored estimate[201] is used to screen the alternatives. The cost factors[199] used in this study are summarized in Table 55. The equipment cost correlations in PROCESS simulator are used conjunction with the economic factors listed in Table 55. The calculation routines for ROI are programmed into the PROCESS input file for Alternative II. This routine can be found elsewhere.[200]

Optimization Results and Discussion

A plant size of 10,000 bbl/day (500,000 TPY) is hypothesized for determining the best flow-sheet alternatives for simulation and

Table 55

List of Cost Factors Used in Economics Evaluation

Item	Cost/Factor	Remarks
Economic Factors		
Inflation	1.110	
Material - SS316	2.1	
- CS	1.0	
Installation	2.42	
Economic Indexes[197]		
Heat Exchanger and Tanks	368.0	Costs of PROCESS
Pipe, Valves, and Fitting	458.1	are based on 1984.
Pumps and Compressors	473.1	
Base Cost of Equipments		PROCESS built-in
Reactor	2.85×10^5	data are used for
H_2 recovery	1.06×10^6	other equipments
H_2 recovery cost	$0.05/mscf	
Cost of fuel gas	$3.5/MMBtu	
Price - H_2	$0.48/lb	Variable
- Bitumen	$15/bbl	
- Liquid product	$35/bbl	
Operation - days/yr	330	
- operators/shift	3	
- shifts/day	3	
- salary	$20.0/hr-man	

optimization. A base case, based on the bench-scale unit operation, was developed. The reaction conditions chose were 535°C and 20 second residence time which are upper limits predicted from the kinetic model and simulation results. Other conditions can be investigated through a case study and/or sensitivity study once the program has been developed. After all recycle and control calculations attain convergence, the economic calculations are performed to determine operating cost and profitability. The results from the base case analysis are preserved for comparison to the results for the alternatives at base-case conditions.

The investment and operating cost summaries are listed in Tables 56 and 57, respectively. The most significant items are the heat exchangers, compressors, and raw materials; therefore, it is expected that minimization of costs will involve a complex interaction between these variables. Also, the cost of hydrogen amounts to 15-20% of the raw materials cost. Before attempting to optimize the process, several case studies were conducted to investigate the sensitivity of the ROI to hydrogen cost and split ratio. The results are presented in Figure 80. As can be seen, the ROI is more sensitive to changes in the split ratio (purge rate) because the split ratio alters both the investment and operating costs.

The assessment of possible improvements has been determined by simulating and optimizing the total process flows and target temperatures for the process and heat-exchanger network alternatives in Figures 77, 78 and 79. The simulation results shown in

352

Table 56

Investment Summary

Unit: 10^7	Base Case	Alternative I	II	III
a. ISBL	2.95	3.15	2.99	2.58
(relative % on base case)	(100)	(106.8)	(101.1)	(87.4)
- Heat exchangers (% ISBL)	(52.3)	(67.1)	(60.0)	(52.2)
- Compressors (% ISBL)	(28.3)	(16.2)	(19.5)	(25.9)
b. OSBL	1.16	1.11	1.07	0.96
	(100)	(95.6)	(92.0)	(83.0)
c. Direct plant cost	4.11	4.26	4.06	3.54
	(100)	(103.6)	(98.5)	(86.1)
d. Indirect plant cost	0.83	0.79	0.76	0.69
	(100)	(95.6)	(92.0)	(83.0)
e. Fixed capital investment	5.68	5.82	5.54	4.87
f. Working capital investment	1.00	1.03	0.98	0.86
g. Total investment	6.69	6.84	6.52	5.73
	(100)	(102.3)	(97.4)	(85.6)

353

Table 57

Operating Cost Summary

Unit: 10^7/yr	Base Case	Alternative		
		I	II	III
a. Direct Production Cost	8.01	7.49	7.49	7.48
(relative % on Base case)	(100)	(93.5)	(93.5)	(93.4)
- raw material cost (% of a.)	(72.5)	(77.2)	(80.2)	(79.3)
- utilities (% of a.)	(7.6)	(12.1)	(10.1)	(11.5)
b. Total fixed charges	0.74	0.75	0.72	0.63
c. Plant overhead	0.37	0.38	0.37	0.33
d. Manufacturing cost	9.12	8.63	8.58	8.44
	(100.0)	(94.6)	(94.0)	(92.5)
e. SARE	2.48	2.36	2.34	2.28
f. Total product cost	11.60	10.99	11.90	10.72
	(100.0)	(94.7)	(94.1)	(92.4)
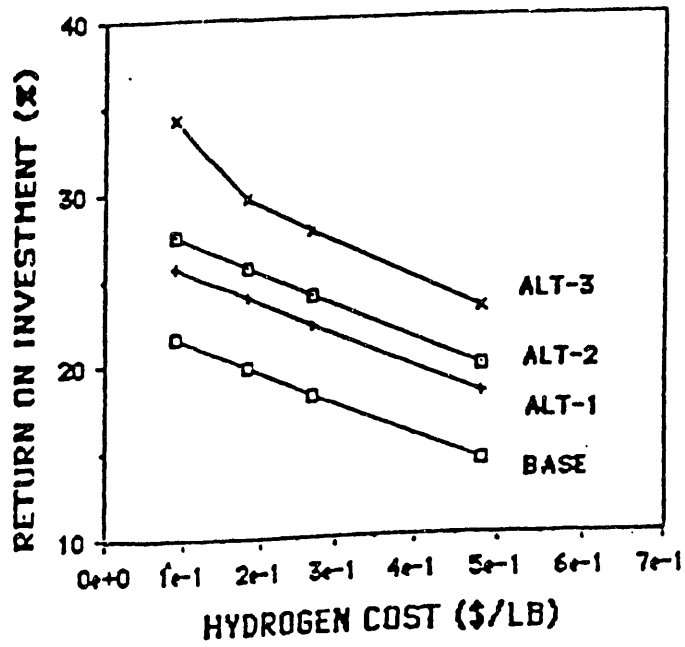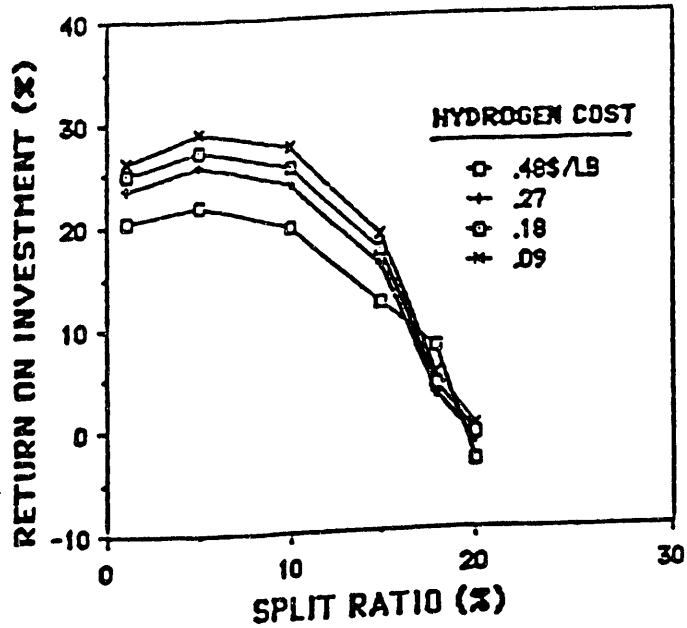
Figure 80 Sensitivity Studies of HEN Alternatives (a) Sensitivity studies of H_2 cost on after tax ROI; 10% of split ratio; and (b) Sensitivity studies of split ratio on after tax ROI for alternative 2

rows a1-a5 of Table 58 list the utility costs and the ROI for the base case and HEN alternatives with the base case design conditions (using the typical assumption of a minimum approach temperature of 20 K, of H_2 cost of \$0.48/lb, and of split ratio of 10%). As can be seen, the installation of various HEN alternatives gives 30-50% energy savings (rows a1 and a2) and 30-60% improvements on the ROI (rows a3 and a4). Also, a 20-30% increase of thermal efficiency can be obtained (row a5) in proportion to energy savings. The thermal efficiency was calculated by a lost-work analysis and was defined as:[202]

$$\text{Efficiency} = \frac{\text{Quantitative Value of Desired Result}}{\text{Qauntitative Value of Inputs Used to Produce that Result}} \tag{81}$$

The lost work is defined by

$$dLW = T_o dS_{irr}$$

The reversible work for a continuous, steady-state, flow process is given by

$$\dot{W}_{rev} = \Sigma \dot{W}_e + \dot{LW} = \Sigma_j B_j + \Sigma_j (1 - T_0/T) \dot{Q}_j \tag{83}$$

where LW is lost work; T_o is of the temperature surrounding; S_{irr} is irreversible entropy production; W_{rev} is the reversible work of the process; W_e is the external work production; B is the availability function $(H - T_o S)$ where H and S include enthalpy of formation and

Table 58

Comparison of ROI and Utility Savings of HEN Alternatives

	Base Case	Alternative I	Alternative II	Alternative III
a1. Utility cost for alternatives with base case design values, $10⁻³/lb product	13.18	7.56	7.17	8.91
a2. Energy savings from new HEN, %		43	46	32
a3. ROI for alternatives with base case design values, %	14.24	18.25	19.82	23.04
a4. Improvement from new HEN, %		28	39	62
a5. Thermodynamic Efficiency, %	31.0	38.3	25.1	24.1
b1. Optimization Results				
ΔT_{min}, K		132	115	99
No. of heat exchangers		12	10	8
split ratio		0.02	0.03	0.12
b2. Utility cost for optimized alternatives, $10⁻³/lb product		8.58	6.96	8.59
b3. Energy savings from optimization and new HEN, %			35	33
b4. ROI for optimized alternatives, %		21.94	28.77	24.81
b5. Improvement from optimization and new HEN, %		54	102	74
b6. Thermodynamic efficiency, %		33.9	44.0	10.7

357

entropy of formation, respectively, in order to handle chemical reaction; Q is heat; and superscript dot means the time rate of change.

The analysis of Alternative I gave the highest thermal efficiency, but the ROI was the lowest among the alternatives because of the high costs associated with energy management; that is, the investment is too high to offset with the utility savings. The results for the optimized alternatives are listed in rows b1-b6 of Table 58. The utility savings at the optimized design conditions for HEN alternatives are not much improved. For Alternative I, the energy savings were lower because of the coupling of the process flow and energy integration optimization. However, the ROI for optimized Alternative I improved nearly twice due to the savings in raw materials and investment. This provides an incentive to optimize both the flows and the energy integration. In fact, all the optimized alternatives show profitability improvements in the range from 54% to 102%. The optimized Alternative II, gave the highest ROI improvement and utility savings by optimizing the process flow and the approach temperature at the pinch. It also gave the highest thermal efficiency, 44%.

The minimum approach temperature of the HEN and the split ratio of the recycle compressor are the key design variables for the hydropyrolysis process, and there are no rules of thumb available to fix these values. Also, hydrogen costs have an impact on process profitability.

The results of this study indicate that a simultaneous

358

optimization is very useful for selecting the best flowsheet alternative, using it as the basis for the development of a detailed heat recovery network structure, and obtaining an estimate of the optimum design conditions.

Conclusions on Simulation and Economic Optimization

A representative hydropyrolysis simulation model has been developed using a commercially available flowsheet program, PROCESS. The user-added subroutine for a kinetic reactor model has been written and the results were successfully correlated with experimental data. The process simulation provides information on the physical and thermodynamic properties, flow rates, component fractions, etc., in each stream and for all unit operations. A sensitivity and case study of this process simulation model will provide a better understanding of the process.

The process model based on the configuration of a bench-scale unit was further improved by adding heat exchanger networks by pinch technology and hydrogen recovery system (gas membrane) technology to provide three alternatives for a conceptual design of a scaled-up hydropyrolysis process.

An ROI profitability calculation routine has been added to a flowsheet program to provide an objective function for the optimization of these alternatives.

The results of simulation and optimization of these alternatives have shown that great improvements in energy savings, thermal efficiency, and profitability are attained. Therefore, the integrated process model developed in this study can be utilized in

several ways: to predict the optimum operating condition of the process, to compare the economic viability and technical tradeoffs of differing design for hydropyrolysis, and to investigate possibilities for the operation debottlenecking and retrofitting designs, etc.

Design of the Tandem Hydropyrolysis-Hydrotreating Unit

Purpose of Design

Hydropyrolysis is a process in which high molecular weight products are cracked to lower molecular weight products without the formation of coke. Operated at optimized conditions, hydropyrolysis does not consume substantial hydrogen nor does it remove significant quantities of heteroatoms. If the process is operated at higher severity to remove heteroatoms an increased yield of gas and higher hydrogen consumption results which is less economic. Therefore, the hydropyrolysis liquid product must be catalytically hydroprocessed for removal of heteroatoms. Catalytic hydroprocessing is made considerably easier because of the improved volatility and reduced molecular weight of the hydropyrolysis products.

The concept of passing the hydropyrolysis products directly over a catalyst bed has been studied by the University of Utah for several years. The advantages are that the hydrocarbons and hydrogen are already at reaction temperatures and simultaneous two-stage processing (HP-HT) may result in a highly energy efficient heavy oil conversion process.

The difficulties encountered in the design of a tandem HP/HT

360

unit derive from two factors: the hydrogen-to-oil ratio in the hydropyrolysis unit is approximately five times that which is normally practiced in hydrotreater units and the contact times for hydrotreating are much longer than those for hydropyrolysis, minutes versus seconds. If the total product stream from the hydropyrolysis unit were to be added to a hydrotreating unit and each unit were to be operated under their normally optimized condition, the hydrotreating unit would be an unreasonably large size in relationship to the hydropyrolysis unit. Therefore, the design of the HP/HT unit becomes a non-trivial task and promises to result in an HT unit operating at gas-to-oil ratios and contact times far removed from conventional practice.

Configuration of HP/HT Considered

Several schemes were compared to determine the configuration of HP/HT. Block flow diagrams were constructed and simulations of the mass and heat balances were performed.

The output stream of the hydropyrolysis process simulation described in the prior section is labeled S008. The most straight forward configuration is shown by Case A in Figure 81. In this configuration the hydropyrolysis stream is cooled just enough to allow phase disengagement in the flash drum, with the underflow being recycled to the hydropyrolysic unit and the vapor phase being passed directly to the hydrotreator unit at an appropriate temperature. Hydrotreated products are then cooled to ambient temperatures where liquid products are removed. Stream S014 and gas are recycled through a hydrogen separator (not shown) and the

361
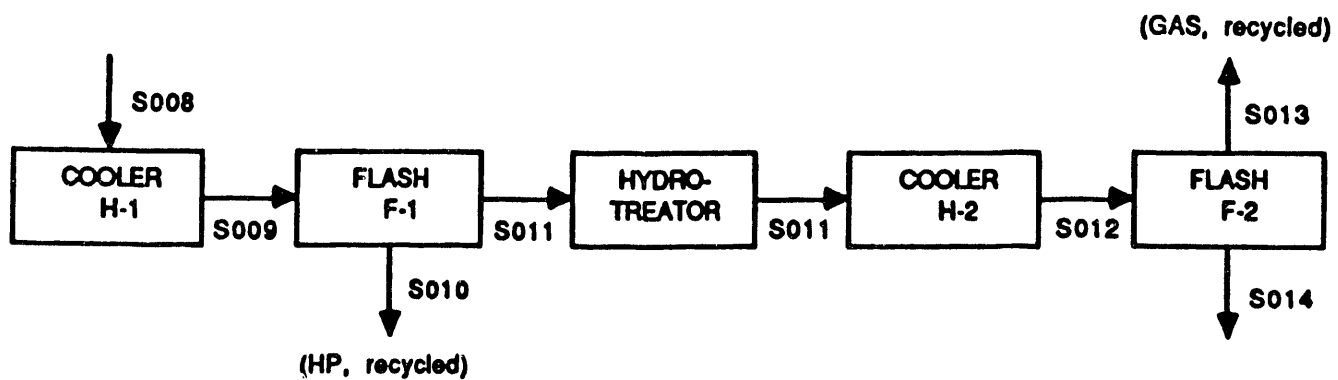
Figure 81   Simulation Flow Diagram of Case A
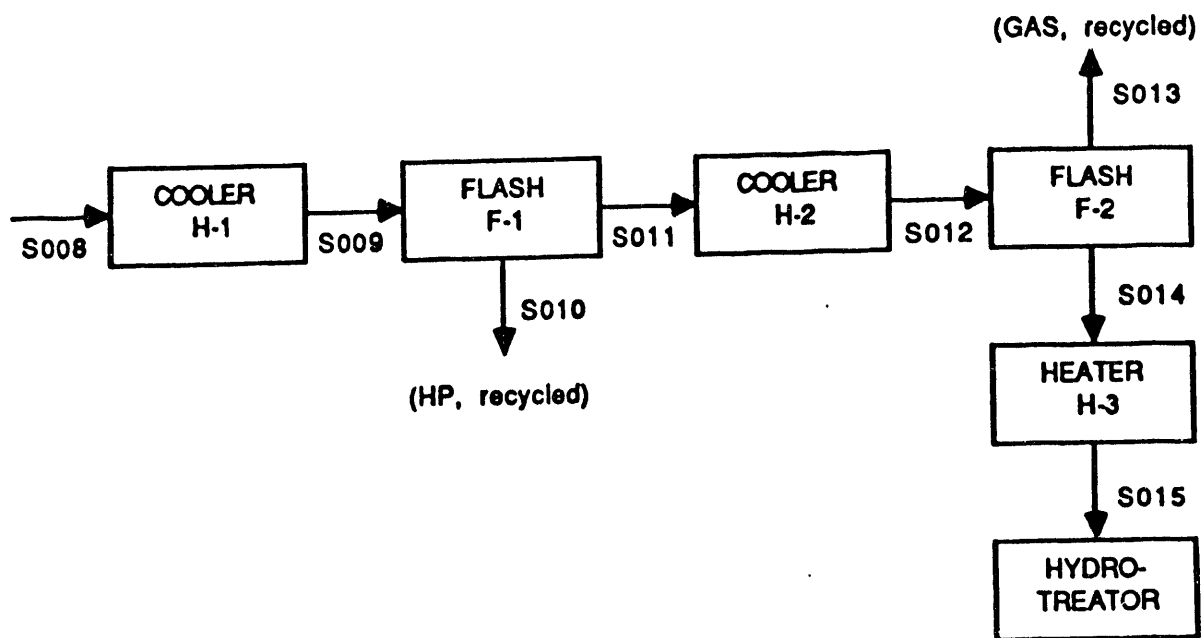
Figure 82 Simulation Flow Diagram of Case B

hydrogen is recycled to the inlet of the hydropyrolysis unit.

Case B, Figure 82, shows a second stage cooler and flash drum combination to liquify the primary products and allow the majority of the hydrogen to be removed. The condensed products are then re-heated and processed through the hydrotreator. Stream S012 has been cooled to 81^0 C. and S014 is heated to 380^0 C. In practice, these heating and cooling requirements may effectively be coupled in a feed-effluent heat exchanger to improve the energy efficiency.

Case C shown in Figure 83 is a variation of Case B in which the product stream undergoes a staged cooling and two hydrotreaters are used, one for a heavy product and one for a lighter product. Splitting the product in this fashion is practiced by Syncrude (Canada) in which the heavy coker distillate is independently processed from the light distillate ends. Stream 1-V is cooled to 217^0 C and contains the gas oil fraction. Stream 3-L is cooled to 81^0 C and is the middle distillate fraction.

Comparison of Cases A, B, and C.

The input Stream S008 is the outlet stream of the HP reactor and is at 535^0 C and 1800 psig. The flow rate of Stream S008 in the process development unit is 18.64 pounds per hour of which 5.3 pounds is bitumen and bitumen products.

If commercially practiced hydrotreated conditions are to be achieved, the hydrotreated feed stream must be at 380^0 C, 2200 psig and H2/oil ratio of 2500 scf/bbl. The reactor size must be such that a contact time of 1.25 hours is achieved. This contact time
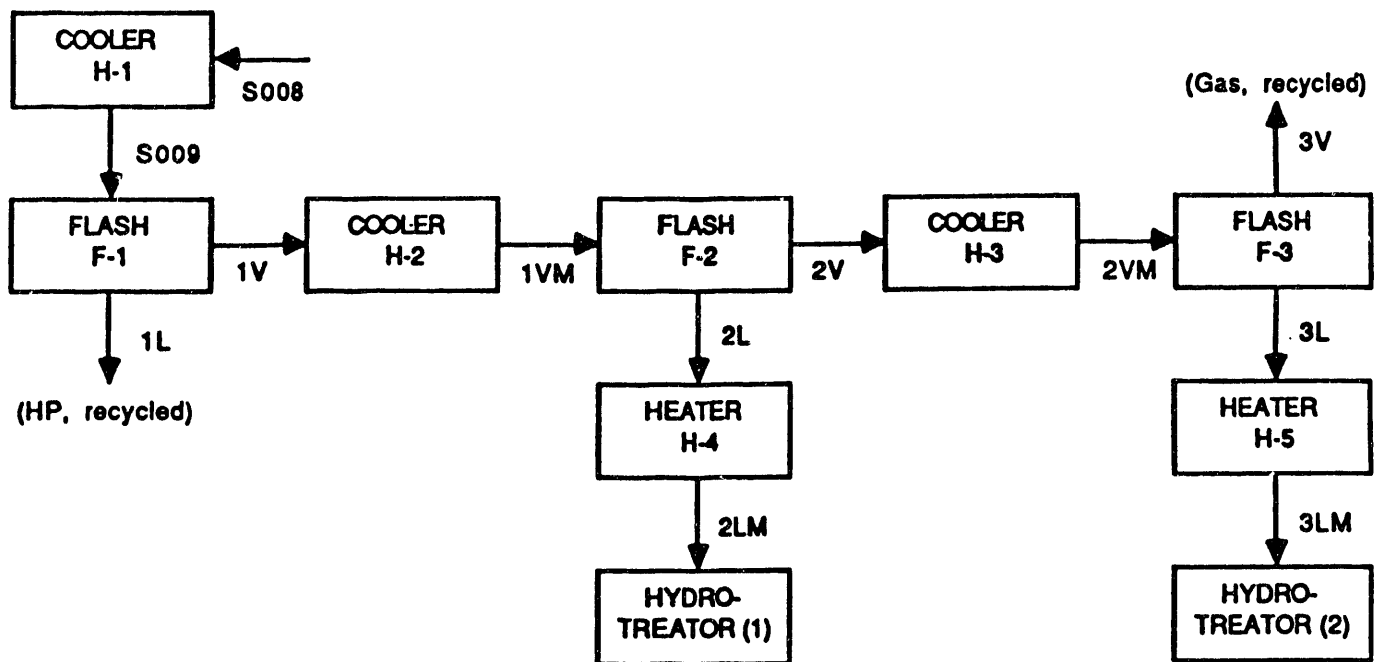
Figure 83   Simulation Flow Diagram of Case C

can be corrected for the actual pressure by multiplying the ratio of the desired pressure to the actual pressure times the 1.25 hours. This calculation makes the reasonable assumption that conversion for a given contact time is a first order linear function of hydrogen pressure. The volume of the HT reactor may be calculated by multiplying the volumetric flow rate and reactor conditions of the vapor phase times the contact time calculated as above.

A summary of the results for the three cases using heat and mass balances calculated from the process simulator are presented in Table 59. The results indicate that the number of heaters and coolers increases from two in Case A to five for Case C. However, the total amount of heat removed from the system does not vary significantly between the three cases. The main differences between cases are the number of operating units required. The primary difference between the three cases is the total volume of the hydrotreater reactors. The volume of the reactor in Case A is 28 times as large as the reactor systems in Cases B and C. Because the hydrotreater reactor is a high pressure vessel the investment cost increases exponentially with volume. Case A is clearly not practical.

The selection between Case B or Case C at the experimental level is based on the relative complications of construction and operation in relationship to the data required. Case C may well turn out to be the preferred configuration for a commercial operation because the re-heating requirements are reduced and we

366

Table 59

Comparison of Three HP/HT Cases

Case	A	B	C
No. of Heaters	0	1	2
No. of Coolers	2	2	3
Heat added (MM Btu/hr)	-	0.00163	0.00140
Heat removed (MM Btu/hr)	0.02632	0.2633	0.02611
Net Heat* (MM Btu/hr)	0.02632	0.02470	0.02471
No. of HT Reactor	1	1	2
Volume of HT reaction (ft^3)	41.90	1.497	0.4791(1) 1.0240(2)
No. of flash drums	2	2	3

*Positive value mean heat is removed from the system.

can anticipate that overall reaction rates and hydrogen utilization will be better in the split system than in the combined broad range feed. However, construction and operation of a system of this complexity at the laboratory scale becomes a formidable problem.

The requirement for independent hydrogen control in the hydrotreator requires an individual compressor and recycle stream. While this may appear cumbersome at the laboratory scale it is not a significant problem at the commercial scale in that multiple compressors will be required.

It will be sufficient at this stage of development to demonstrate the feasibility of the tandem HP/HT unit and to learn of the important coupling and operability parameters, therefore, we have decided to use Case B as the model for development of the laboratory HP/HT unit.

A schematic of the tandem HP/HT unit proposed for construction is presented in Figure 84. Note that a dual HP reactor system will be installed to allow for cycling of the HP reactors between on line and burnout and thereby affording longer term continuous runs. The recycle compressor has been ordered and will be installed in the unit during the next phase of the program.

Summary and Conclusions

Process data from hydropyrolysis was reduced to a mathematical model. The reaction model was then used for the reactor block of a process simulation model. Process simulation was performed to optimize the heat exchange network for a conceptual commercial design. An economic trade-off exists between maximizing the heat

368
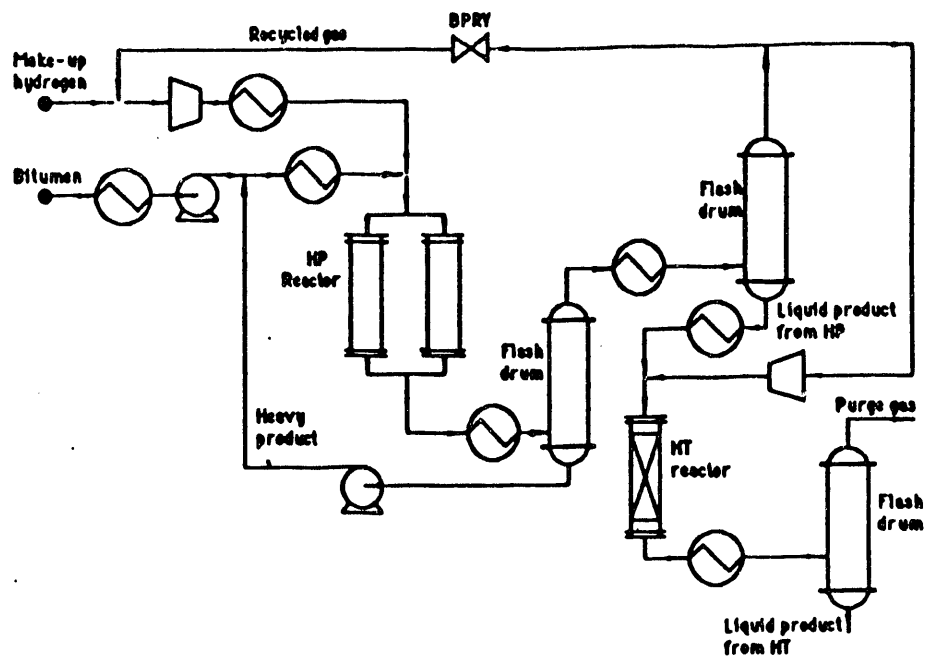
Figure 84   The Scheme of Tandem Unit of HP and HT

utilization and minimizing the equipment costs.

The optimized HEN was used in the process configuration to optimize the H_2 split ratio. Results showed that 5-10% of the recycle stream should be sent to the hydrogen recovery unit. Optimum reactor conditions depend strongly on the feedstock/product value assumptions. results suggest an economic optimum of about 500°C, 20 sec residence time and 1800 psig H_2 pressure. At these conditions process yields are 2% gas, 60% distillate and 38% residue. The residue is recycled for further conversion. One of the primary cost factors, hydrogen make-up, is minimized at low conversion per pass.

Future Activities

The optimum results projected from the process simulation should be confirmed experimentally. Experiments will be run to establish the basis for a hydropyrolysis/hydrotreater tandem unit. Exploratory work will be conducted on direct catalytic upgrading as an alternative to hydropyrolysis. A design basis will be developed for comparison of process options.

REFERENCES

1. Schumacher, MM. (Ed.) 1982. <u>Heavy Oils and Tar Sands Recovery and Upgrading</u>, Noyes Data Corp., Park Ridge, IL.

2. Funk, E.W., 1986. Thermodynamic Analysis of Separation Process for Athabasca Tar Sands, Energy Sources, 8, (2-3), 177-190.

3. Bowman, C.W., 1967. Molecular and Interfacial Properties of Athabasca Tar Sands, Seventh World Petroleum Congress, Mexico City, Proceedings, 3, 583-604.

4. Miller, J.D. and Misra, M., 1982. Hot Water Process Development for Utah Tar Sands, Can. J. Chem. Eng., 46, 479-481.

5. Hall, E.S., and Tollefson, E.L., 1982. Stabilization and Destabilization of Mineral Fines-Bitumen-Water Dispersions in Tailings from Oil Sand Extraction Plant that use Hot Water Process, Can. J.Chem. Eng., 60, 812-821.

6. Hupka, J., Oblad, A.G., and Miller, J.D., 1987. Diluent-Assisted Hot-Water Processing of Tar Sands, AOSTRA J. Res., 3, 95-102.

7. Hupka, J., Miller, J.D. and Cortes, A.B., 1983. Importance of Bitumen Viscosity in the Hot Water Processing of Domestic Tar Sands, Mining Eng., 33, 1635-1641.

8. Stachurski, J., and Michalek, M., 1985. The Zeta Potential of Emulsion Droplets of the Aliphatic Hydrocarbons in Aqueous Solutions, Colloids Surf., 15, 255-259.

9. Kitahara, A., and Watanabe, A., 1985. Electrical Phenomena at Interfaces, Marcel Dekker, New York, NY.

10. Schramm, L.L., and Smith, R.G., 1987. Two Classes of Anionic Surfactants and their Significance in Hot Water Processing of Oil Sands, Can. J. Chem. Eng., 65, 799-811.

11. Chan, M., Sharma, M.M., and Yen, T.F., 1982. Generation of Surface Active Acids in Crude Oil for Caustic Flooding Enhanced Oil Recovery, Ind. Eng. Chem. Process. Des.

12. Schramm, L.L., Russell, G.S., and Stone, J.A., 1984. The Influence of Natural Surfactant Concentration on the Hot Water Process for Recovering Bitumen from the Athabasca Oil Sands, AOSTRA J. Res., 1(1) 5-13.

13. Takamura, K., 1985. Physico-chemical Characterization of Athabasca Oil Sand and its Significance of Bitumen Recovery, AOSTRA J. Res., 2(1) 1-10.

14. Babchin, A.J., Chow, R.S., and Sawatzky, R.P., 1989. Electrokinetic Measurements by Electroacoustical Methods, Adv. Coloids Interface Sci., 30, 111-151.

15. Misra, M., Aguilar, R., and Miller, J.D., 1981. Surface Chemistry Features in the Hot Water Processing of Utah Tar Sand, Sci. Technol., 16(10) 1523-1544.

16. Srinivasan, N.S., Spitzer, J.J., and Hepler, L.G., 1982. Electrophoretic Properties of Oil Sands Tailings and Constituent Clays in Aqueous Suspensions, J.Can. Petrol. Tech., 21(4) 25-30.

17. Kotlyar, L.S., Sparks, B.D., and Kodama, H.., 1984. Some Chemical and Mineralogical Properties of Fine Solids Derived from Oil Sands, AOSTRA J.Res., 1(2) 99-106.

18. Hupka, J., and Miller, J.D., 1982. Modified Hot Water Processing of Domestic Tar Sands, SME-AIME Annual Meeting, Dallas, Texas, Feb. 14-18, preprint No. 82-85. Dev., 21, 580-58.

19. Leja, J., and Bowman, C.W., 1968. Application of Thermodynamics to the Athabasca Tar Sand, Can.J.Chem. Eng., 46, 479-481.

20. Protoczny, Z.M., Vargha,-Butler, E.I., Zubovits, T.K., and Neuman, A.W., 1984, Surface Tension of Bitumen. I. Temperature Dependence. II. Solvent and Fractionation Effects, AOSTRA J.Res., 1(2) 107-120.

21. Burchfield, T.E., and Hepler, L.G., 1979. Some Chemical and Physical Properties of Tailings Water from Oil Sands Extraction Plants, Fuel, 58, 745-747.

22. Vorndran, L.D.L., Serres, A.J., Donnelly,R.G., Moore, R.G. and Bennion, D.W., 1980. Bitumen Separation for Experimental Use, Can. J. Chem. Eng., 58, 580-587.

23. Dealy, J.M., 1979. Rehological Properties of Oil Sand Bitumens, Can. J. Chem. Eng., 57, 677-683.

24. Netzel, D.A., and Turner, T.F., A Correlation of United States Bitumen Viscosities with NMR Spectroscopic Parameters - Progress Report, Topical Report for U.S. Department of Energy, Contract No.: DE-AC21-86MC11076, Western Research Institute, Laramie, WY, June 1989.

25. Wallace, D., and Henry, D., 1987. A Correlation for Correcting the Viscosity of Solvent-Extracted Bitumen to a Solvent-Free Basis, AOSTRA J. Res., 3, 239-247.

26. Gy, P.M. 1979. Sampling of Particulate Materials, Theory and Practice, Elsevier, New York, p. 431-22.

27. Christensen, R.J., Lindberg, W.R., and Dorrence, S.M., 1984. Viscous Characteristics of Utah Tar Sand Bitumen, Fuel, 63, 1312-1317.

28. Yang, Y.J., Bukka, K., and Miller, J.D., 1989. Selection and Evaluation of Diluents in the Modified Hot Water Process, Energy Processing/Canada, 82(1), 14-21.

29. Church, J.M., and Shinnar, R., 1961. Stabilizing Liquid-Liquid Dispersions by Agitation, Ind. Eng. Chem., 53, 479.

30. Bednarski, S., Graphical and Analytical Interpretation of Investigation Results of the Flow Rate in Hydrocyclones with Variable Process and design Parameters, 2nd International Conference on Hydrocyclones, Bath. England, 19-21 September 1984. Proc. 297-322.

31. Cheng D. C-H., Viscosity-Concentration equations and Flow Curves for Suspensions, Chem. Ind., 17 May 1980, 403-406.

32. Rutgers, I.R., Relative Viscosity and concentration, Rheological Acta, 2(4), 305-353 (1962).

33. Goto, H., and Kuno, H., Flow of Suspensions Containing Particles of Two Different Sizes through a Capillary Tube; Rheol, J. 26(4), 387-398, (1982).

34. Thitkulchai, C.T. and Austin, L.G., Rheology of Concentrated Slurries of Particles of Natural Size Distribution Produced by Grinding; Powder Technology, 56, 293-299, (1988).

35. Chong, J.S., Christiansen, E.B., and Baer, A.D., Flow of Viscous Fluid Through a Circular Aperture; J. Applied Polymer Sci. 15,369-379, (1971).

36. Okuma, O., Mae, K., and Yanai,S-I., Viscosity of Brown Coal-Solvent Slurry; Fuel Processing Technology, 22, 73-86, (1989).

37. Deng, C.R., Nio, T., Sanada, Y., and Chila, T., Relationship Between Swelling of Coal Particles and Apparent viscosity of Slurry During Coal Liquefaction for Akabira Coal/Creosote Oil Slurry System; Fuel, 68, (1989)

38. Frith, W.J., Mewis, J., Rheology of Concentrated Suspensions: Experimental Investigations; Powder Technology, $\underline{51}$, 27-34, (1987).

39. Overend, I.J., Horsley, R.R., Jones, R.L., and Vinycomb, R.K., A New Method for the Measurement of Rheological Properties of Settling Slurries; Proc. IX International Congress on Rheology, Mexico, 583-590, (1984).

40. Schramm, L., The Influence of Suspension Viscosity on bitumen Rise Velocity and Potential Recovery in the Hot Water Flotation Process for Oil Sands; J. Can. Petrol Technol. $\underline{38}$(3), 73-80, (1989).

41. Miller, J.D. and Hupka, J., Bitumen recovery from tar sands, U.S. Pat. 4470899, Sept. 11, 1984.

42. Crickmore, P.J., Schutte, R. and Cleaver, J.A.S., The yield-grade relationship in the extraction of bitumen from oil sands, AOSTRA J. Res., $\underline{5}$, 195-201 (1989).

43. Sanford, E.C., Interrelationship between oil sand fine solids, process aids, mechanical energy and oil sand age after mining, Can. J. Chem. Eng., $\underline{61}$, 554-566 (1983).

44. Lissant, K.J., 1983. Demulsification: Industrial Applications, Surfact. Sci. Ser., $\underline{13}$: 114.

45. U.S. Patents, No.: 2,038,479 (1932); 2,364,118 (1939); 4,049,535 (1977); 4,056,451 (1977); 4,226,690 (1980); 4,419,-200 (1983).

46. Li, N.N., 1966. Separating Hydrocarbons with Liquid Membranes, U.S. Patent 3,410,794; March 14.

47. Hsu, E.C., and Li, N. N., 1985. Membrane Recovery in Liquid Membrane Separation Processes, Sep. Sci. Technol., $\underline{20}$(2-3):115.

48. Kowalski, W., and Noworyta, A., 1986. Elektrostatyczna separacja emulsji, Zesz. Nauk. Polit. Poznanskiej, $\underline{17}$:89.

49. Schlosser, S., and Kossaczky, E., 1986. Breaking of W/O Emulsions in Electric Field, Prace Nauk. Inz. Chem. Urzadz. Ciepl. Pol. Wroclawskiej, Ser. Konf., $\underline{46}$(8):189.

50. Goto, M., Irie, J., Kondo, K., and Nakashio, F., 1989. Electrical Demulsification of W/O Emulsion by Continuous Tubular Coalescer, J. Chem. Engng. Japan, $\underline{22}$(4):401.

51. Fujinawa, K., Morishita, M., Hozawa, M., Imaishi, N., and Ino, H., 1984. Demulsification of W/O Emulsion by Use of High Voltage of A.C. Fields, ibid, $\underline{17}$(6):632.

52. Hano, T., Ohtake, T., and Takagi, K., 1988. Demulsification Kinetics of W/O Emulsion in an A.C. Electric Field, ibid, $\underline{21}$(4):345.

53. Yamaguchi, M., Sugaya, H., and Katayama, T., 1989. Liquid-Liquid Extraction Characteristics of a Spray Column with a D.C. Electric Field, ibid, $\underline{22}$(1):25.

54. Bailes, P.J. and Stitt, E.H., 1987. Column Liquid Contacting with Vigorous Agitation Balanced by Electrostatic Coalescence. Part I: Intensified Coalescence-Redispersion, Chem. Engng, Res. Des., $\underline{65}$(6):514.

55. Stenzel, R.W., and Eberz, W.F., 1960. The Role of Electrostatic Precipitation in the Resolution of Industrial Emulsions. Presented before the Division of Petroleum Chemistry American Chemical Society, New York Meeting, September 11-16, p. 121.

56. Brown, A.H., and Hanson, C., 1965. Effect of Oscillating Electric Fields on Coalescence in Liquid-Liquid Systems, Trans. Faraday Soc., $\underline{61}$:1754.

57. Ziolkowski, Z., 1980. Ekstrakcja cieczy w przemysle chemicznym. WNT, Warszawa, p.120.

58. Brown, A.H., and Hanson, C., 1968. The Effect of Oscillating Electric Fields on the Coalescence of Liquid Drops, Chem, Engng Sci., $\underline{23}$:841.

59. Bailes, P.J., and Larkai, S.K.L., 1981. Trans. I. Chem. E., $\underline{59}$:229.

60. Idem., 1983. The Application of Electric Fields to Phase Separation in a Solvent Extraction System, WICHE Symp. Ser, $\underline{238}$(80):170.

61. Idem., 1985. Polarization Effects in Liquid Phase Separation by Pulsed Electric Fields, I. Chem. E. Symp. Ser., (94):235.

62. Zhong, Y., Siya, L., Yaochuan, Y., and Xuelun, Z., 1987. An Investigation into the Breaking-down of Water-in-Oil Type Emulsions by Means of Pulsed Voltage, Desalination, $\underline{62}$:323.

63. Zhaolin, F., Xiangde, W., Xingtai, Z., Qiongjia, F., Zhenfang, L., Pingyu, H., and Xiujuan, Z., 1987. A New High Voltage Electrostatic Coalescer EC-1 Used for Industrial Application in Liquid Membrane Separation. Presented at Second International Conference on Separation Technology, Schloss Elmau, Germany, April 26-May 1.

64. Zhaolin, F., Xiangde, W., and Xiujuan, Z., 1988. High Voltage Modulating Pulse Electrostatic Power and Its Application in Electrostatic Demulsification. Presented at First International Conference on Recovery Technology, Beijing, P.R. China, October.

65. Degener, W., Hauertmann, H.B., and Schugerl, K., 1988. Effects of Medium Composition and Electric Field Properties on Emulsion Splitting. Presented at ISEC'88, Moscow, July 18-24, Conference Papers, 2:164.

66. Panczenkow, T.M., and Cabek, L.K., 1969. Emulsion Behavior in External Electric Field (Russ.), Chimia, Moscow.

67. Joos, F.M., and Snaddon, R.W.L., 1985. On the Frequency Dependence of Electrically Enhanced Emulsion Separation, Chem. Eng. Res. Des., 63:305.

68. Matusiak, R., 1976. Teoria pola elektromagnetycznego, WNT, Warszawa, p.58.

69. Bailes, P.J., and Larkai, S.K.L., 1984. Influence of Phase Ratio on Electrostatic Coalescence of Water-in-Oil Dispersions, Chem. Eng. Res. Des., 62(1):33.

70. Robinson, R.N., 1987. Chemical Engineering Reference Manual, Professional Publications, Belmont, CA. 5-3.

71. Kunii, D., and Levenspiel, O., 1969. "Fluidization Engineering", John Wiley & Sons, New York, NY.

72. Smart, L.M. 1984. Thermal Processing of Utah Tar Sands, M.S. Thesis, University of Utah.

73. Bunger, J.W., 1979. Processing Utah Tar Sands, Ph.D. Dissertation, University of Utah, Salt Lake City.

74. Grace, J.R., 1984. "Generalized Models for Isothermal Fluidized-Bed Reactors," Recent Advances in Engineering Analysis of Chemically Reacting Systems, L.K. Doraiswami, ed., Wiley Eastern, New Delhi Chapter 13.

75. Grace, J.R. and H.I. DeLasa 1978. "Reaction Near the Grid in Fluidized Beds," AIChE J. 24 (2) 364.

76. Stubington, J.F., D. Barrett and G. Lowry. 1984. "Bubble Size Measurements and Correlation in a Fluidized Bed at High Temperatures, "Chem. Eng. Res. Des. 62, May, 173.

77. Geldart, D., 1973. "Types of Gas Fluidization, " Powder Technol., 7 285.

78. Darton, R.C., R.D. LaNauze, J.F. Davidson, and D. Harrison. 1977. "Bubble Growth Due to Coalescence in Fluidized Beds," Trans. I. Chem. E., 55, 274.

79. Venkateson, V.N., 1979. Fluid bed thermal recovery of synthetic crude from bituminous sands of Utah. Ph.D. Dissertation. University of Utah, Salt Lake City, Utah.

80. Wang, J., (1983). The production of hydrocarbon liquids from a bitumen-impregnated sandstone in a fluidized bed pyrolysis reactor. MS thesis. University of Utah. Salt Lake City, Utah.

81. Dorius, J.C., 1985. The pyrolysis of bitumen-impregnated sandstone from the PR Spring (Utah) deposit in a fluidized bed. Ph.D. Dissertation. University of Utah, Salt Lake City, Utah.

82. Shun, D.W. 1990. The fluidized bed pyrolysis of bitumen-impregnated sandstone from the Circle Cliffs (Utah) deposit. Ph.D. Dissertation. University of Utah. Salt Lake City, Utah.

83. Geldart, D., (1990). "Estimation of Basic particle Properties for Use in Fluid-Particle Process Calculations," Powder Technol., 60, 1-13.

84. Grewal, N.S. and Gupta, A. (1989). "Total and Gas Convective Heat Transfer from a Vertical Tube to a Mixed Particle Gas-Solid Fluidized Bed," Powder Technol., 57, 27-38.

85. Bin, A.K. (1986). "Minimum Fluidization Velocity at Elevated Temperatures and Pressures," Can. J. Chem. Eng., 64, 854-857.

86. Couderc, J.P. (1985). "Incipient Fluidization and Particulate Systems," in Davidson, J.F., Clift, R. and Harrison, D. (eds), Fluidization, 2nd ed., Academic Press, London, Ch. 1

87. Hong, S.C., Jo, B.R., Doh, S. and Choi, C.S. (1990). "Determination of Minimum Fluidization Velocity by the Statistical Analysis of Pressure Fluctuations in a Gas-Solid Fluidized Bed," Powder Technol., 60, 215-221.

88. Leva, M. (1959). Fluidization, McGraw-Hill book Co., New York.

89. Geldart, D. (1972). "The Effect of Particle Size and Size Distribution on the Behavior of Gas-Fluidized Beds, "Powder Technol., 6, 201-215.

90. Hanson, F.V. and Oblad, A.G. (1988). "The Fluidized Bed Pyrolysis of Bitumen-Impregnated Sandstone from the Tar Sand Deposits of Utah". The Fourth UNITAT/UNDP Proceedings, Volume 5, paper No. 155, p. 421-438.

91. Hartman, M. and Svoboda, K. (1986). "Predicting the Effect of Operating Temperature on the Minimum Fluidization Velocity," Ind. Eng. Chem. Process Des. Dev., 25, 649-654.

92. Lucas, A., Arnaldos, J., Casal. J. and Puigjaner, L. (1986). Improved Equation for the Calculation of Minimum Fluidization Velocity, "Ind. Eng. Chem. Process Des. Dev., 25, 426-429.

93. Mathur, A., Saxena, S.C., Zhang, Z.F., (1986). "Hydrodynamic Characteristics of Gas-Fluidized Beds Over a Broad Temperature Range." Powder Technol, 47, 247-256.

94. Nakamura, M., Hamada, T., Toyama, S., Fouda, A.E. and Capes, C.E. (1985). "An Experimental Investigation of Minimum Fluidization Velocity at Elevated Temperatures and Pressures." Can. J. Chem. Eng., 63, 8-13.

95. Thonglimp, V., Hiquily, N. and LaGuerie, C. (1984). Vitese Minimal de Fluidisation et Expansion des Couches Fluidises par un Gaz, " Powder Technol., 38, 233-253.

96. Wen, C.Y., Chitester, D.C., Kornosky, R.M. and Keairns, D.L. (1985). "A Generalized Methodology for Estimating Minimum Fluidization Velocity at Elevated Pressure and Temperature," AIChE J., 3, 1086-1092.

97. Jayakar, K.M. (1979). Thermal Recovery of Oil from Tar Sands, Ph.D. Dissertation, University of Utah.

98. Sung, S. (1988). The Fluidized Bed Pyrolysis of Bitumen-Impregnated Sandstone in a Large Diameter Reactor, M.S. Thesis, University of Utah.

99. Wen, C.Y. and Yu, Y.H. (1966). "A Generalized Method for Predicting the Minimum Fluidization Velocity," AIChE J., 12, 610-612.

100. Reid, R.C., Prausnitz, J.M. and Poling , B.E. (1987). The Properties of Gases and Liquids, 4th ed., McGraw-Hill Book Company, New York, Ch. 9.

101. White, F.M. (1988). Heat and Transfer, Addison Welsley, New York.

102. Bourgeois. P. and Grenier, P. (1968). "The Ratio of Terminal Velocity to Minimum Fluidizing Velocity for Special Particles, Can. J. Chem. Eng., 46, 325-328.

103. Richardson, J.F. and M.A. Da St. Jeronimo, (1979) Chem. Eng. Sci., 34, 1419

104. Saxena, S.C. and Vogel, G.S. (1977). "The Measurement of Incipient Fluidisation Velocities in a Bed of Coarse Dolomite at Temperature and Pressure," Trans. Instn. Chem. Engrs., 55, 184-189.

105. Babu, S.P. Sha, B. and Talwalker, A. (1978). "Fluidization Correlations for Coal Gasification Materials - Minimum Fluidization Velocity and Bed Expansion Ratio," AIChe Symp. Ser., 74(176), 176-186.

106. Thonglimp, V., Hiquily, N., and LaGuerie, C. (1984). "Vitesse Minimal de Fluidisation et Expansion des Couches de Melauges de Particules Dolides Fluidises par un Gaz," Powder Technol. 39, 223-239.

107. Grace, J.F. (1982). "Fluidized-Bed Hydrodynamics," in Hetsroni, G. (ed.), Handbook of Multiphases Systems, Hemisphere, New York, Ch. 8, p. 6.

108. Zeng, Z.X., Yamazaki, R. and Jimbo, G. (1985). "Minimum Fluidizing Velocity of Large Particles at Elevated Temperatures," Kagaku Kogaku Ronsunshu, 11 115-117.

109. Chitester, D.C., Kornosky, R.M, Fan, L.S. and Danko, J.P. (1984). "Characteristics of Fluidization at High Pressure," Chem. Eng. Sci., 39(2), 253-261.

110. Geldart, D. (March 26, 1990). Personal Communication.

111. Botterill, J.S.M., Teoman, Y, and Yuregir, K.R. (1982). "The Effect of Operating Temperature on the Velocity of Minimum Fluidization, Bed Voidage and General Behavior." Powder Technol, 31, 101-110.

112. Goroshko, V.D., Rozenbaum, R.B. and Todes, O.M. 91958). "Approximate Hydraulic Relationships for Suspended Beds and Hindered Fall," Izvestiya Vuzov, Neft. Gaz, 1, 125-131.

113. Botterill, J.S.M., Teoman, Y and Yuregir, K.R. (1982). "Comments on 'Minimum Fluidization Velocity at High Temperatures'," Ind. Eng. Chem. Process Des. Dev., 21-784-785.

114. Pattipati, R.R. and C.Y. Wen, (1981). Ind. Eng. Chem. Process Eds. Dev., 20, 705.

115. Macek, A. and Amin, N.D. (1988). "Solids Dispersion Coefficients in High Temperature Fluidized Beds" AIChe Symposium Series, 262(84), 22-35.

116. Yan, Z., Yao, J.Z., Wang, W.L., Liu, S.J. and Kwauk, M. (1984). "Concurrent Shallow Multistate Fluid-Bed Reactor," in D. Kunii and R. Toei (eds.), Fluidization, Engineering Foundation, New York, pp. 607-614.

117. Pattipati, R.R. and Wen, C.Y. (1982). "Response to Comments on 'Minimum Fluidization Velocity at High Temperatures'" Ind. Eng. Chem. Process Des. Dev., 21, 785-786.

118. Mori, S. and Wen, C.Y. (1975). "Estimation of Bubble Diameter in Gaseous Fluidized Beds," AIChE J., 21, 109-115.

119. Knowlton, F., and I. Hissan. 1978. "L valves characterized for solids flow." Hydrocarbon Processing, 57, 149-156.

120. Zenz, F.A. 1986. "Maintaining dense-phase standpipe downflow." Power Technology, 47, 105-113.

121. Brink, Jr., J.A., W.F. Burggrabe, L.E. Greenwell. 1966. "Mist Removal from Compressed Gases," Chem. Eng. Prog., 62 (4), 60.

122. Rendall, J.S., 1979. "Solvent Extraction Process" U.S. Patent Number 4,160, 718 (July 10, 1979).

123. Rendall, J.S., 1984. "Method and Apparatus for Solvent Extraction," U.S. Patent Number 4,424, 112 (January 3, 1984).

124. Rendall, J.S., 1989. "Hot Water Bitumen Extraction Process," U.S. Patent Number 4, 875, 998 (October 24, 1989).

125. Hanson, F.V., Miller, J.D. and Oblad, A.G., 1982 "Process for Obtaining Products from Tar Sand" U.S. Patent Number 4,337,143.

126. Hanson, F.V., Miller, J.D. and Oblad, A.G., 1983. "Process for Recovering Products from Tar Sands U.S. Patent Number. 4,409,090.

127. Cha, S., Longstaff, D.C., Hanson, F.V., and Oblad A.G., "Process for Recovering Products from Tar Sands", Proc. 1990 Eastern Oil Shale Conference, to be published in Fuels.

128 Cheremisinoff, M.P., and Cheremisinoff, P.N. 1984. "Hydrodynamics of Gas-Solids Fluidization," Gulf Publishing Company, Houston, Texas.

129. Geldart D. 1986. "Gas Fluidization Technology, John Wiley and Sons, New York.

130. Zenz, F.A. and Othmer, D.F. 1960. Fluidization and Fluid-Particle Systems, Reinhold, New York.

131. Zhang, J. and Yang, G. 1986. "Determination of the Optimum Velocity for Dilute Phase Transport of Coarse Particles in Large Tubes" in "Circulating Fluidized Bed Technology", Basu, P. ed., Pergamon Press, New York.

132. Wen, C.Y. and Galli, A.F. 1971. "Dilute Phase System" in "Fluidization" Harrison, D. ed, Academic Press, New York.

133. Lin, L.C. 1988. The Kinetics of the Pyrolysis of Tar Sands and of the Combustion of Coked Sands, Ph.D. Dissertation, University of Utah, Salt Lake City, Utah.

134. McCabe, W.L. and Smith J.C., 1985. Unit Operations of Chemical Engineering, 4th ed. McGraw-Hill Co., New York.

135. Sandy, C.W., Daubert, T.E., and Jones J.H. 1970. "Vertical Dense-Phase Gas-Solid Transport," in "Fluidization Fundamental and Application," Littman H. etc. eds., vol. 66.

136. Hikita, T. Ikeda, M. and Asano, H. 1984. "Upward Transportation of Particles in Dense Phase," in "Proceedings of the Fourth International Conference on Fluidization," Kunii, D., Toei, R. eds., Engineering Foundation, New York.

137. Camp, F.W. 1974. The Tar Sands of Alberta, Canada, 2nd Ed., Cameron Engineering, Inc., Denver, Colorado.

138. McDermott, J. 1972. Liquid Fuels from Oil Shale and Tar Sands, Noyes Data Corp., Park Ridge, New Jersey.

139. Ranney, M.W., 1982. Oil Shale and Tar Sand Technology, Recent Developments, Noyes Data Corp., Park Ridge, New Jersey.

140. Gearhart, J. A. and Garwin, Leo, 1976. "ROSE Process Improves Resid Feed," Reprint, Hydrocarbon Processing.

141. Funk, E.W., Pirkle, J.C., and May, W.G. 1984. "Processing Approach for the Solvent Extraction of Athabasca Tar Sand,: Energy Process, 4(1), 12.

142. Funk, E.W., 1979. "Behavior of Tar Sand Bitumen with Paraffinic Solvents and its Application to Separation for Athabasca Tar Sands," Can. J. Chem. eng. 57, 333.

143. Speight, J.G., and Moschopedis, S.E. 1981. "The Influence of Crude Oil Composition on the Nature of the Upgrading Process: Athabasca Bitumen," in The Future of Heavy Crude Oils and Tar Sands, Meyer, R.F., and Steele, C.T., eds., McGraw-Hill Book Company, New York.

144. Weast, R.C., ed., 1982. CRC Handbook of Chemistry and Physics, 63rd., CRC Press, Inc., Boca Raton, Florida.

145. Williams, D.F., and Martin, T.G., 1978. "Extraction of Oil Shales and Tar Sands," U.S. Patent 4,108,760.

146. Nelson, S. and Corbet, R.W., "Kerr-McGee's ROSE Process Expands on Proven Extraction Technology," presented at the Third International UNITAR Conference on Heavy Crude and Tar Sands.

147. Operating Manual, J.& W. High Pressure Soxhlet Extractor.

148. Pirkle, J.C., Levy, C.W., Funk, E.W., and May, W.G., 1979. "Computer Design of Multistage Sedimentation Operation for Separation of Asphaltenes, Sand and Bitumen in Tar Sands," Proceedings of Summer Computer Simulation Conference, Toronto, Canada, 213.

149. Irai, C.A., Funk, E.W., Gomez, E., and Espino, R.L. 1977. "Tar Sands Extraction," U.S. Patent 4,036,732 assigned to Exxon Research and Engineering Company (1977).

150. Cormack, D.E., Kenchington, J.M. Phillips, C.R. and Leblanc, P.J., 1977. "Parameters and Mechanisms in the Solvent Extraction of Mined Athabasca Oil Sand," Can. J. Chem. Eng. 55, 572.

151. Nienow, A.W., 1975. "Agitated Vessel Particle-Liquid Mass Transfer: A Comparison Between theories and Data," Chem. Eng. J., 9, 153.

152. McGinnis, E.L., and Wen, C.S., "Effects of Solvent Properties on Tar Sand Extraction," a paper presented at the Tenth Symposium of the Rocky Mountain Fuel Society, February 22, 1985.

153. Levich, V.G., 1962. Physicochemical Hydrodynamics, Prentice-Hall, Englewood Cliffs, New Jersey.

154. Funk, E.W. 1978. "Behavior of Athabasca Tar Sand Bitumen with a Paraffinic Solvents," Am. Chem. Soc. Div. Fuel, 23(4), 81.

155. Funk, E.W. and Gomez, E. 1977. "Determination of Vanadiumin Athabasca Bitumen and Other Heavy Hydrocarbons by Visible Spectometry, "Anal.Chem. 49, 972.

156. Crank, J., 1975. The Mathematics of Diffusion, "Oxford University Press, 2nd Ed.

157. Mitchell, D.L. and Speight, J.G. 1973. "The Solubility of Asphaltenes in Hydrocarbon Solvents," Fuel, 52, 149.

158. Hidebrand, J.H, Prausnitz, J.M. and Scott, R.L. 1970. Regular Solutions, Van Nostrand-Reinhold Co., New York.

159. Gary, J.H., Handwerk, G.E., 1984. "Petroleum Refining: Technology and Economics", Marcel Dekker, Inc., New York.

160. Soutar, P.S., McColgan, E.G., Merrill, W.H., Parsons Derived from Athabasca Bitumen, "Mines Branch Technical Bulletin TB-179.

161. Stiegel, G.J., Krisnamurthy, S., Sha, Y.T., 1983. "Catalytic Hydroprocessing of Synthetic Fuels," Rev. Chem. Eng., 1,4 357-401.

162. Hirschon, A.S., Laine, R.M., Wilson, R.B., 1987. "Enhanced Catalysts for Hydrodenitrogenation of Coal Liquids," Amer. Chem. Soc., Div. Fuel Chem. 268-270.

163. Aboul-Gheit, A.K., "Effect of Support Acidity on the Intermediate Steps in Hydrodenitrogenation of Quinoline and Indole", Amer. Chem. Soc., Div. Fuel Chem.

164. Ho, Teh, C., 1988. "Hydrodenitrogenation Catalysis,", Catal. Rev. -Sci. Eng., 30 1, 117-160.

165. De Wind, M., Plantenga, F.L., Heinerman, J.J.L., and Homan Free, H.W., 1988. "Upflow versus Downflow Testing of Hydrotreating Catalysts, Appl. Catal. 43, 239-252.

166. Gierman, H., 1988. "Design of Laboratory Hydrotreating Reactors Scaling Down of Trickle-flow Reactors," Appl. Catal. 43, 277-286.

167. Carruthers, J.D. and DiCamillo, D.J., 1988. "Pilot Plant Testing of Hydrotreating Catalysts: Influence of Catalyst Condition Bed Loading and Dilution," Appl. Catal. 43, 253-276.

168. Gierman, H., 1988. "Design of Laboratory Hydrotreating Reactors: Scaling Down of Trickle Bed Reactors," Appl. Catal., 43, 277-286.

169. Hangos, K.M., and Toth, J., 1988. "Maximum Likelihood Estimation of Reaction Rate Constants, "Computers and Chemical Engineering, 12 p. 135-139.

170. Westerberg, A.W., Hutchison, H.P., Motard, R.L., and Winter, P., 1979. "Process Flowsheeting," Cambridge University, Cambridge, England.

171. Evans, L.B., Joseph, B., and Seider, W.D., 1977. "System Structure for Process Simulation," AIChE J., p. 658-666.

172. Motard, R.L., Shacham, M., and Rosen, E.M., 1975. "Steady State Chemical Process Simulation," AIChE J., 21. p. 417-436.

173. Rosen, E.M., 1980. "Steady State chemical Process Simulation: A State-of-the-Art Review," in "Computer Applications to Chemical Engineering - Process Design and Simulation;" Squires, R.G., and Reklaitis, G.V., Eds.; ACS Symp. Ser.: 124, p. 3-36.

174. Husain, A., 1986. "Chemical Process Simulation,' Halsted, New Delhi, India.

175. Evans, L.B. 1987. "Computer-Aided Design (CAD): Advances in Process Flowsheeting Systems," in "Recent Developments in Chemical Process and Plant Design;" Liu, Y.A., McGee, J.A., Jr., and Epperly, W.R., Eds.: John Wiley & Sons, p. 261-287.

176. Aspen Technology, Inc., "ASPEN PLUS Introductory Manual," Aspen Technology, Cambridge, MA.

177. Winter, P., CONCEPT: Interactive Process Flowsheeting," in "Computer-Aided Process and Plant Design," Leesley, M.E., Ed.; Gulf Publishing, Houston, Texas, p. 512-535.

178. ChemShare Corporation, 1985. "DESIGN II USER'S GUIDE," Chemshare, Houston, Texas.

179. Perris, F.A., 1982. FLOWPACK II: A Third-Generation Flowsheeting System," in "Computer-Aided Process and Plant Design;" Leesley, M.E., Ed.; Gulf Publishing, Houston, Texas. p. 609-689.

180. Seader, J.D., Seider, W.D., and Pauls, A.C., 1977. "FLOWTRAN Simulation--An Introduction," CACHE, Cambridge, Mass.

181. Simulation Sciences, Inc., 1987. "PROCESS Input Manual, "Simulation Sciences, Fullerton, CA.

182. Ramakrishnan, R., 1978. "Hydropyrolysis of Coal Derived and Related Model Compounds," Ph.D. Dissertation, University of Utah, Salt Lake City, Utah.

183. Ramakrishnan, R., J. Shabtai and A. G. Oblad. 1978. "Hydropyrolysis of Model Compounds," Preprints, Div. of Pet. Chem.

184. Oblad, A.G. and J. Shabtai. 1981. "Hydropyrolysis of Tar Sand Bitumen and Heavy Petroleum Oils, U.S. Pat. No. 4298487.

185. Bunger, J.W., Cogswell, D.E., Wood, R.E., and Oblad, A.G., 1981. "Hydropyrolysis: The Potential for Primary Upgrading of Tar Sand Bitumen," in "Oil Shale, Tar Sand and Related Materials,"; Stauffer, H.C., Ed.; ACS Symp. Ser.: 163, p. 369-380.

186. Bunger, J.W. and Cogswell, D.E., 1981. "Characteristics of Tar Sand Bitumen Asphaltenes as Studied by Conversion of Bitumen by Hydropyrolysis," in Chem. Series: 195: p. 219-236.

187. Oblad, A.G., Bunger, J.W., Hanson, F.V., Miller, J.D. and Seader, J.D. 1982-1984. "Recovery and Hydropyrolysis of Oil from Utah's Tar Sands," Final Report, U.S. Department of Energy, Contract #DE-AS-20-82LC10942.

188. McColgan, E.C. and Parsons, B.I. 1972. "The Hydrocracking of Residual Oils and Tars, Part 2: The Catalytic Hydrocracking of Athabasca Bitumen," Mines Branch Report R-253, Department of Energy, Mines and Resources, Ottawa, Canada.

189. Simulation Sciences, Inc., 1988. "PROCESS Simulation Program--User Added Subroutines, "Simulation Sciences, Fullerton, CA.

190. Johnson, R.L., 1982. "TEAPACK Users' Manual--Mathematical Subroutines for Numerical Methods," John Wiley and Sons, New York.

191. Tsai, C.H. 1987. "Reaction Kinetics and Mechanisms of Hydropyrolysis Processing of Tar Sand Bitumen and Related Materials, M.S. Thesis, University of Utah, Salt Lake City, Utah.

192. Ballinger, W.A., MacLean, D.L. and Narayan, R.S., 1982. "Application of PRISM® separators in Oil Refining and Production," presented in AIChE National Meeting, Anaheim, CA.

193. Spillman, R.W., 1989. "Economics of Gas Separation Membranes," Chemical Engineering Process, 85, No. 1. p. 41-70.

194. 1988 Gas Process Handbook, Hydrocarbon Processing, 67, NO. 4, p 62.

195. Fritzsche, A.K., 1988. "Gas Separation by Poly Sulfone Hollow Fiber Membranes," Polymer News 13, No. 9, p. 266-274.

196. Ballinger, W.A., Long, S.P., and Metzger, T.R. 1984. "Optimizing Hydrocracker Hydrogen," Chemical Engineering Progress, 80, No. 5, p. 51-57.

197. Papoulias, S.A. and Grosmann, I.E., 1983. "A Structural Optimization Approach in Process Synthesis - Total Processing System," Computers and Chemical Engineering, 7, NO. 6, p. 723-734.

198. Duran, M.A. and Grossmann, I.E. 1986. "Simultaneous Optimization and Heat Integration of Chemical Processes, "AIChE J. 32, p. 123-138.

199. Linnhoff, B., and Hindmarsh, E., 1983. "The Pinch Design Method for Heat Exchanger Networks," Chem. Eng. Sci., 38, No. 5, p. 745-763.

200. Peters, M.S. and Timmerhaus, K.D., 1980. "Plant Design and Economics for Chemical Engineers, McGraw-Hill, N.Y.

201. Chemical Engineering, 1989. "Cost Indexes End 1988. April, 1989. p. 202.

202. deNevers, N., 1982. "The Second Way to use the Second Law," CHEMTECH, 5, p. 306-317.

Appendix A
Lithology of Core Number 1
WHITEROCKS TAR SAND DEPOSIT
UINTAH COUNTY, UTAH

Table A-1
Lithology of Core Number 1
Whiterocks Tar Sand Deposit

INTERVAL (feet)	SATURATION							LITHOLOGY & STRUCTURES
	B	S	W	M	R	HR	VR	
11.0-11.3					R			100% sandstone, even silt banding averaging 12 deg.
11.3								fracture- 75 deg., open and oozing tar, Soft sand contact
11.3-11.5					R			typical sandstone lithology
11.5								fracture- 60 deg., sealed with silt
11.5-11.9					R			typical sandstone lithology
11.9								fracture- 65 deg., closed
11.9-13.7					R			typical sandstone lithology, even silt banding
13.7-15.2					R			typical sandstone lithology, contorted silt banding
15.2-16-0					R			typical sandstone lithology, erratic slit banding
16.0-17.3					R			typical sandstone lithology, contorted silt banding
17.3-18.4					R			typical sandstone lithology, erratic silt banding and occasional spots
18.4-1808					R			typical sandstone lithology, contorted silt banding
18.8-19.0					R			typical sandstone lithology, contorted silt banding
19.0					R			fracture- 58 deg., sealed with tar
19.9-19.9					R			typical sandstone lithology
19.9								fracture- 72 deg., sealed with tar

INTERVAL	SATURATION							LITHOLOGY & STRUCTURES
(feet)	B	S	W	M	R	HR	VR	
19.9-20.3					R			typical sandstone lithology
20.3								silt permeability barrier
20.3-20.4					R			typical sandstone lithology
20.4								fracture- 75 deg., open and oozing
20.4-21.0					R			typical sandstone lithology, contorted silt banding
21.0-21.1					R			typical sandstone lithology, contorted silt banding
21.1.-22.9					R			typical sandstone lithology, fragmented silt banding
22.9-23.3					R			typical sandstone lithology, contorted silt banding
23.3								fracture- 63 deg., sealed with silt
23.3-24.6					R			typical sandstone lithology
24.6								fracture- 70 deg., sealed with silt
24.7-24.9					R			typical sandstone lithology
24.9								fracture- 70 deg., sealed with silt
24.9-27.5					R			typical sandstone lithology, even silt banding
26.4-26.9				M--R				typical sandstone lithology, even silt banding
26.9								fracture- 60 deg., sealed with silt
26.9-27.5					R			typical sandstone lithology, even silt banding
27.5-29.4					R			typical sandstone lithology, fragmented silt banding
29.4								fracture- 65 deg., sealed with silt

INTERVAL	SATURATION							LITHOLOGY & STRUCTURES
(feet)	B	S	W	M	R	HR	VR	
29.4-31.0				M--R				typical sandstone lithology, fragmented silt banding
31.9-33.0				M--R				typical sandstone lithology, highly braided silt banding
32.2-32.4								silt permeability barrier
33.0-33.4				M--R				typical sandstone lithology, even silt banding and occasional spots
33.4								fracture- 65 deg., firm filling with blebs <u>hard tar</u>
33.4-33.8				M--R				typical sandstone lithology
33.8								fracture- 75 deg., sealed with silt
33.8-36.5				M--R				typical sandstone lithology
34.5-34.7								fracture zone- average 65 deg., sealed with silt
36.5-36.9				M--R				typical sandstone lithology, even silt banding
36.9-38.9				M				typical sandstone lithology, even silt banding
38.9-41.2					R			typical sandstone lithology, 5% spots
41.2								wood block
41.2-45.0					R			typical sandstone lithology, 5% spots
45.0-46.5				M--R				typical sandstone lithology, 5% spots
46.5-47.0	B							silt permeability barrier, very dense silt, very erratic lenses of <u>weak saturation</u>
47.0-47.3		S						very dense silt, 50% of rock containing erratic lenses of <u>weak saturation</u>

390

INTERNAL	SATURATION							LITHOLOGY & STRUCTURES
(feet)	B	S	W	M	R	HR	VR	
47.3-49.2				M--R				typical sandstone lithology, occasional spots
49.2								fracture- 59 deg., sealed with silt
49.2-50.4				M--R				typical sandstone lithology
50.4-51.0					R			typical sandstone lithology, 2-5% spots
51.0								wood block
51.0-52.0					R			typical sandstone lithology
52.0-52.1								silt permeability barrier-highly braided silt lenses
52.1-54.0					R			typical sandstone lithology, 1-5% spots
54.0-56.0				M--R				typical sandstone lithology, occasional spots
56.0-59.4					R			typical sandstone lithology, Eoccasional silt banding
59.4-60.9					R			silt banding at 85 deg.
60.9								fracture- 70 deg., sealed with silt
60.9								wood block
60.9-61.7				M				typical sandstone lithology, occasional silt banding
61.9-69.4					R			typical sandstone lithology, minor silt banding and spots
69.4-71.0					R			typical sandstone lithology, minor spots
71.0								wood block
71.0-72.2					R			typical sandstone lithology
72.2-72.3								silt permeability barrier
72.3-79.0					R			typical sandstone lithology, minor silt banding

INTERVAL (feet)	SATURATION							LITHOLOGY & STRUCTURES
	B	S	W	M	R	HR	VR	
70.9-81.0					R			typical sandstone lithology, minor silt banding and spots
81.0								wood block
81.0-88.6					R			typical sandstone lithology, minor silt banding and spots
88.6-90.1					R			typical sandstone lithology, silt banding grading from approx. 5% on top to 20% on bottom
90.1-91.0				M--R				typical sandstone lithology, minor spots and 20% silt banding
91.0								wood block
91.0-92.4				M				typical sandstone lithology, minor spots and 20% silt banding
92.4-94.4				M--R				typical sandstone lithology, occasional spots and 20% silt banding
94.4-98.2					R			typical sandstone lithology, occasional spots and 20% silt banding
111.0								wood block
111.0-114.6						HR		typical sandstone lithology, 2% silt banding
114.5-117.1				M				typical sandstone lithology, occasional spots and 5% silt banding
117.1-119.1				M				typical sandstone lithology 5% spots and 20% silt banding
119.1-121.1				M--R				typical sandstone lithology, 5% spots and 20% silt banding, several thin streaks of bleeding
121.1								wood block
121.1-123.0				M--R				typical sandstone lithology, 2% spots and 10% silt banding, several thin streaks of bleeding

INTERVAL (feet)	SATURATION							LITHOLOGY & STRUCTURES
	B	S	W	M	R	HR	VR	
123.0-125.0					R			typical sandstone lithology, minor spots and 10% silt banding, midway down think streak of <u>bleeding</u>
125.0-126.9					M--R			typical sandstone lithology, increasing
126.9-128.8			W					increased silting, 1% spots and 20% silt banding
128.8-131.1	S							very silty sandstone, 1% spots and 25% silt banding
131.1								wood block
131.1-132.3	S							very silty sandstone
132.3-132.9								fracture zone- approx. 7 inches of length missing
132.9-134.3	B							typical siltstone lithology
134.3-135.0		S						typical siltstone lithology
135.0-136.0	B							typical siltstone lithology
136.0-135.5		S						typical siltstone lithology
135.5-136.7	B							typical siltstone lithology
136.7-138.8	B							typical siltstone lithology
138.8								wood block
138.8-141.1	B							typical siltstone lithology
141.1								wood block
141.1-141.3	B							typical siltstone lithology
141.3-145.2		S						typical siltstone lithology
145.2-146.2		S--W						typical siltstone lithology
146.2-146.4			W					typical siltstone lithology
145.4-148.2							VR	typical sandstone lithology soft sand (tar cementing), <u>oozing tar</u>

INTERVAL	SATURATION							LITHOLOGY & STRUCTURES
(feet)	B	S	W	M	R	HR	VR	
148.2-150.0							HR--VR	typical sandstone lithology,
150.0-151.1							HR	typical sandstone lithology, very little silt banding visible
151.1								wood block
151.1-155.8							HR	typical sandstone lithology, very little silt banding visible, bleeding evident top 2 inches
155.8-161.5							VR	typical sandstone lithology, slight indication of silt banding, soft sand (tar cementing), oozing and bleeding tar
161.5								wood block
161.5-165.7							VR	typical sandstone lithology, slight indication of silt banding, soft sand (tar cementing), oozing and bleeding tar
165.7-169.6							VR	typical sandstone lithology soft sand (tar cementing), bleeding tar
169.6-170.2							HR--VR	typical sandstone lithology, soft sand (tar cementing), bleeding tar
170.2								fracture- 30 deg., sealed with silt
170.2-174.0					R			typical sandstone lithology, soft sand (poor cementing)
171.1								wood block
171.1-171.7					R			typical sandstone lithology
171.7								fracture- 65. deg., open and bleeding
174.0-175.2					M--R			typical sandstone lithology, 5% silt banding

INTERVAL	SATURATION							LITHOLOGY & STRUCTURES
(feet)	B	S	W	M	R	HR	VR	
175.2-175.9				M--R				typical sandstone lithology, 25% silt banding
175.9								fracture- 45 deg., sealed with silt
175.9-179.4					R			typical sandstone lithology, bleeding below fracture contact, grading from no silt banding on top to 2% silt banding on bottom
179.4-181.1							VR	typical sandstone lithology, oozing tar
181.1								wood block
181.1-184.9						HR		typical sandstone lithology, soft sand (tar cementing)
184.9-188.6						HR		typical sandstone lithology
188.6-188.9							VR	typical sandstone lithology, crumbly sand (tar cementing)
188.9-190.8						HR		typical sandstone lithology, 5% silt banding
190.8-191.1					R			typical sandstone lithology, 5% silt banding
191.1								wood block
191.1-192.3				M				typical sandstone lithology, rapidly grading downward to 25% silt banding
192.7-195.0		S--W						typical siltstone lithology
195.0-195.1		S						typical siltstone lithology
195.1-195.6							VR	typical sandstone lithology, oozing tar
195.6-196.3					R			typical sandstone lithology, 5% silt banding
196.3-200.7				M				silty sandstone lithology
200.7-201.1			W--M					very silty sandstone lithology

INTERVAL (feet)	B	S	W	M	R	HR	VR	LITHOLOGY & STRUCTURES
201.1								wood block
201.1-201.5			W--M					very silty sandstone lithology
201.5-201.7				M				typical sandstone lithology, 5% silt banding
201.7								silt permeability barrier- 23 deg.
201.7-204.1					R			typical sandstone lithology no banding evident
204.1-205.0					R			typical sandstone lithology, no banding evident
205.0-205.2	B							split permeability barrier
205.2-207.0					R			typical sandstone lithology, no banding evident
207.0-208.9					R---HR			typical sandstone lithology
211.1								wood block
211.1-213.8					R			typical sandstone lithology
213.8-215.8					R---HR			typical sandstone lithology, several bleeding zones
215.8-221.1							VR	typical sandstone lithology, top 2 inches is bleeding
221.1								wood block
221.1-221.5							VR	typical sandstone lithology, completely bleeding
221.5-223.5						HR		typical sandstone lithology
223.8-223.8						HR		typical sandstone lithology
223.8-224.3							VR	typical sandstone lithology, bleeding tar
224.3-224.9					R			typical sandstone lithology
224.9-225.5				M				very silty sandstone lithology, highly braided

INTERVAL (feet)	SATURATION							LITHOLOGY & STRUCTURES
	B	S	W	M	R	HR	VR	
225.5-226.3	B							typical sandstone lithology, bleeding tar, 10% braided silt
230.1-231.0						R--HR		typical sandstone lithology
231.0								wood block
231.0-233.1						R--HR		typical sandstone lithology
233.1-235.7					R			typical sandstone lithology, 5% braided silt banding
235.7-235.8								silt permeability barrier
235.8-236.5							VR	typical sandstone lithology, oozing tar, soft sand
236.5-238.4						HR-VR		typical sandstone lithology, 5% braided silt banding, bleeding zones
238.4-240.8					R			typical sandstone lithology, 5% braided silt banding
240.8								wood block
240.8-242.7							VR	typical sandstone lithology
242.7-244.7						HR-VR		typical sandstone lithology, bleeding zones, no banding
244.7-247.1						HR		typical sandstone lithology, no banding
247.1								fracture- 35 deg. open and oozing
247.1-247.5	B-S							typical siltstone lithology
247.5-248.5	S--W							typical siltstone lithology
248.5								fracture- 50 deg. open and oozing
248.5-250.1			W					typical siltstone lithology
250.1								wood block

- NOTES -

Core Box Identification

Box No.	Depth		Box No.	Depth
1	11 – 21		14	136.7 – 146.2
2	21 – 31		15	146.2 – 155.8
3	31 – 41		16	155.8 – 165.7
4	41.2 – 50.4		17	165.7 – 175.2
5	50.4 – 59.4		18	175.2 – 184.9
6	59.4 – 69.4		19	184.9 – 195.0
7	69.4 – 79.0		20	195.0 – 204.1
8	79.0 – 88.6		21	204.1 – 213.8
9	88.6 – 98.2		22	213.8 – 223.5
10	98.2 – 107.7		23	223.5 – 233.1
11	107.7 – 117.1		24	223.1 – 242.7
12	117.1 – 126.9		25	242.7 – 250.7
13	126.9 – 136.7			

Saturation Grades

Code	Name	
B	Barren	No Visible evidence of tar saturation.
S	Slight	Pore spaces not filled with tar but rock matrix stained gray to brown.
W	Weak	Pore spaces incompletely filled and rock light gray
M	Moderate	Pore spaces completely filled with tar sand rock dull black. Sand grains and original cementing visible.
R		Rich Pore spaces completely filled with tar and rock glistening black. Sand grains visible.
HR	Highly Rich	Pore spaces completely filled with tar, rock tacky and spotty zones of bleeding tar. Original cementing partly replaced by tar.
VR	Very Rich	Pore spaces completely files with tar, bleeding and/or oozing zones, and rock tacky. Original cementing is replaced by tar, with rock being plastic or soft when fresh.

Appendix B

Lithology of Core Number 2

WHITEROCKS TAR SAND DEPOSIT

UINTAH COUNTY, UTAH

Table A-2
Lithology of Core Number 2
Whiterocks Tar Sand Deposit

INTERVAL (feet)	SATURATION							LITHOLOGY & STRUCTURES
	B	S	W	M	R	HR	VR	
80.0-80.8	B							typical sandstone lighology
80.8-81.2	B							permeability barrier
81.2-81.8	B							typical sandstone lithology
81.8-82.0	B							silty zone, highly calcareous, limonitic staining; possibily weathered zone
82.0-84.0	B							typical sandstone lithology
84.0-84.2	B							alareous zone
84.2-90.0	B							typical sandstone lithology
90.0-94.0	B							typical sandstone lithology
94.0-94.1	B							highly calcareous zone, limonitic staining
94.1-100.0	B							typical sandstone lithology
100.0-102.5	B							typical sandstone lithology
102.5-102.6								highly calcareous zone, limmonitic staining
102.6-103.5	B							typical sandstone lithology
103.5-103.6	B							highly calcareous zone, limonitic staining
103.6-104.2	B							typical sandstone lithology
104.2-104.3								highly calcareous zone, limonitic staining
104.3-105.0	B							typical sandstone lithology
105.0-112.8		S						typical sandstone lithology
112.8-114.0			W					typical sandstone lithology
114.0-115.9		S--W						typical sandstone lithology

400

INTERVAL	SATURATION							LITHOLOGY & STRUCTURES
(feet)	B	S	W	M	R	HR	VR	
115.9								wood block
115.9-119.8		S						typical sandstone lithology
119.8-120.4		S--W						typical sandstone lithology
120.4								wood block
120.4-122-5		S--W						typical sandstone lithology
122-5-123.9			W					typical sandstone lithology 75-80 deg. bedding
123.95-124.0								highly calcareous zone, limonitic straining
124.0-129.6				M				typical sandstone lithology
129.6-130.9				M				typical sandstone lithology
130.9								wood block
130.9-134.4				M				typical sandstone lithology
134.4-134-9			W					typical sandstone lithology
134.9								angular unconformity:70deg. bedding above and 80 deg. bedding below
134.9-137.0			W					typical sandstone lithology
137.0-139.0				M				typical sandstone lithology
139.0-140-4					R			typical sandstone lithology
140.4								wood block
140.4-145-4.					R			typical sandstone lithology ocasional thin split banding 30-40 deg.dips.
145.4-148-7 lithology,				M				typical sandstone 70 deg. bedding
148.7-150.4 lithology,				M				typical sandstone 69 deg, bedding
150.4								wood block

INTERVAL	SATURATION							LITHOLOGY & STRUCTURES
(feet)	B	S	W	M	R	HR	VR	
150.4-151.8				M				typical sandstone lithology
151.8-153.2					R			typical sandstone lithology
153.2-154.7					R			typical sandstone lithology numerous thin slit banding at 30 deg. dips
154.71-58.3					R			typical sandstone lithology 70 deg. bedding
158.3-160.4					R			typical sandstone lithology 70 deg. bedding
160.4								wood block
160.4-167-9					R			typical sandstone lithology occasional slit banding
167.9-169.1					R			typical sandstone lithology 70 deg. bedding
169.1								wood block
169.1-174.3 lithology,					R			typical sandstone numerous silt banding at 30 deg. dips
174.3-179.8 lithology					R			typicaaal sandstone
179.8					R			wood block
179.8-180-9 lithology,					R			typical sandstone 70 deg. bedding
189.9182-9					R			typical sandstone lithology 80 deg. bedding
182.9-186.7					R			typical sandstone lithology 60 deg. bedding, numerous silt banding at 30 deg. dips
186.7-189.8					R			typical sandstone lithology 60 deg. bedding
189.9								wood block

INTERVAL	SATURATION							LITHOLOGY & STRUCTURES
(feet)	B	S	W	M	R	HR	VR	
189.8-195.3					R			typical sandstone lithology 60 deg. bedding
195.3								wood block
195.3-196.1					R			typical sandstone lithology 60 deg. bedding
196.1								wood block
196.1-199.2					R			typical sandstone lithology 70 deg. bedding
199.2-199.3								braided premeability barrier 30 deg. dip
199.3-204.0					R			typical sandstone lithology 70 deg. bedding
204.0								wood block
204.0-206.0					R			typical sandstone lithology 70 deg. bedding
206.0-211.1					R			typical sandstone lithology 70 deg. bedding
211.1-214.9					R			typical sandstone lithology 65 deg. bedding
21.40								wood block
214.0-216-2					R			typical sandstone lithology 65 deg. bedding
216.2-221.7					R			typical sandstone lithology 60 deg. bedding
211.7-222.3		S						typical sandstone lithology calareous cement
222.3-223.0					R			typical sandstone lithology 60 deg. bedding
223.0-223.8		S						typical sandstone lithology calcareous cement
223.8-224.1					R			typical sandstone lithology 60 deg. bedding

INTERVAL	SATURATION							LITHOLOGY & STRUCTURES
(feet)	B	S	W	M	R	HR	VR	
224.1								wood block
224.1-224.5					R			typical sandstone lithology 60 deg. bedding
224.5-224.8		S						typical sandstone lithology calcareous cement
224.8-230-2					R			typical sandstone lithology 60 deg. bedding
230.2-233.6	B--S							typical sandstone lithology calcareous cement
233.6-223.7								fracture, tar sealed, 20 deg. dip
223.7-234.1				M				typical sandstone lithology
234.1-234.2					R			typical sandstone lithology
234.2								wood block
234.2-239.5					R			typical sandstone lithology
239.5-241.7	B							typical sandstone lithology calcareous cement
241.7-244.1		S--W						typical sandstone lithology calcareous cement
244.1								wood block
244.1-245.5		S--W						typical sandstone lithology calcareous cement
245.5-247.5	B							typical sandstone lithology calcareous cement, 65 deg. bedding
247.5-249.5		S						typical sandstone lithology calcareous cement
249.5-251.5			W					typical sandstone lithology calcareous cement, 65 deg.
251.5-253.5			W--M					typical sandstone lithology calcareous cement

INTERVAL	SATURATION							LITHOLOGY & STRUCTURES
(feet)	B	S	W	M	R	HR	VR	
253.5-254.3				M				typical sandstone lithology calcareous cement
254.3								wood block
254.3-261.4				M				typical sandstone lithology calcareous cement
261-4-263.4			W--M					typical sandstone lithology calcareous cement
263.4-264.3			W					typical sandstone lithology calcareous cement
264.3								wood block
264.3-274.6			W					typical sandstone lithology calcareous cement, 68 deg.
274.6								wood block
274.6-275.1			W					typical sandstone lithology
275.1-276.2			W					typical sandstone lithology calcareous cement
276.2-281.4				M--R				typical sandstone lithology occasional braided silt stringers
281.4-284.6			W					typical sandstone lithology calcareous cement
284.6			W--M					typical sandstone lithology 65 deg. bedding, calcareous cement
292.2-294.8					R			typical sandstone lithology
294.8								wood block
294.8-298.2					R			typical sandstone lithology
298.2-300.3						HR		typical sandstone lithology
300.3-304.6					R			typical sandstone lithology
304.6								wood block

INTERVAL (feet)	SATURATION							LITHOLOGY & STRUCTURES
	B	S	W	M	R	HR	VR	
304.6-310.0					R			typical sandstone lithology
310.0-311.7					R--HR			typical sandstone lithology
311.7-314.6					R			typical sandstone lithology
314.6								wood block
314.6-319.5				M--R				typical sandstone lithologt 70 deg. bedding, calcareous cement
319.5-323.5			W--M					typical sandstone lithology
323.5-324.7				M				typical sandstone lithology
324.7								wood block
324.7-325.4				M				typical sandstone lithology
325.4-329.3				M--R				typical sandstone lithology
329.3-331.3				M				typical sandstone lithology
331.3-333.4			W					typical sandstone lithology
333.4-334.8		S						typical sandstone lithology contorted bedding
334.8								wood block
334.8-335.2		S						typical sandstone lithology 80 deg. bedding
335.2-337.1		S						typical sandstone lithology calcareous cement
337.1-341.0		S						typical sandstone lithology
341.0-342.4		S						typical sandstone lithology calcareous cement
342.4-345.0						HR		typical sandstone lithology
345.0								wood block
345.0-351.3						HR		typical sandstone lithology

INTERVAL	SATURATION							LITHOLOGY & STRUCTURES
(feet)	B	S	W	M	R	HR	VR	
351.3-352.0				M				typical sandstone lithology 70 deg. bedding
352.0-352.7	B							typical sandstone lithology calcareous cement
352.7-354.7			W--M					typical sandstone lithology 75 deg. bedding, calcareous cement
354.7-355.0				M				typical sandstone lithology
355.0								wood block
355.0-360.4					R			typical sandstone lithology 75 deg. bedding
360.4-362.2				M				typical sandstone lithology
362.2-364.1				M---R				typical sandstone lithology
364.1-365.0					R			typical sandstone lithology
365.0								wood block
365.0-366.0					R			typical sandstone lithology
366.0-367.9						HR		typical sandstone lithology
367.9-369.9				M---R				typical sandstone lithology
369.9-371.6			W--M					typical sandstone lithology 60 deg. bedding
371.6-371.7								premeability barrier
371.7-373.8						HR		typical sandstone lithology
373.8-375.9					R			typical sandstone lithology
375.0								wood block
375.0-375.6					R			typical sandstone lithology
375.6-377.6						HR		typical sandstone lithology
377.6-379.6					R			typical sandstone lithology

INTERVAL (feet)	SATURATION							LITHOLOGY & STRUCTURES
	B	S	W	M	R	HR	VR	
379.6-383.5				M---R				typical sandstone lithology
383.5-385.0					R			typical sandstone lithology
385.0								wood block
385.0-385.5					R			typical sandstone lithology
385.5-391.2						HR		typical sandstone lithology
391.2-393-2					R			typical sandstone lithology
393.2-395.0			W--M					typical sandstone lithology
395.0								wood block
395.0-397.0			W					typical sandstone lithology
397.0-400.8			W--M					typical sandstone lithology 70 deg. bedding
400.8-405.0			W					typical sandstone lithology
405.0								wood block
405.0-410.2			W					typical sandstone lithology
410.2-412.1			W					typical sandstone lithology bedding contorted to wavy
412.1-414.0			W					typical sandstone lithology bedding wavy
414.0-415.0			W--M					typical sandstone lithology 65 deg. bedding
415.0								wood block
415.0-417.3				M				typical sandstone lithology
417.3-419.3			W--M					typical sandstone lithology bedding 65 to 70 deg.
419.3-420				M				typical sandstone lithology
420.0-421.6				M---R				typical sandstone lithology 60 deg. bedding

INTERVAL	SATURATION							LITHOLOGY & STRUCTURES
(feet)	B	S	W	M	R	HR	VR	
421.6-422.6			W--M					typical sandstone lithology 60 deg. bedding
422.6								fracture, sealed, 15 deg.
422.6-422.7			W--M					typical sandstone lithology 85 deg. bedding
422.7								fracture, sealed, 30 deg.
422.7-423.8			W--M					typical sandstone lithology bedding 80 deg.
423.8-425.0			W--M					typical sandstone lithology bedding 70 deg.

Core Box Identification

Box No.	Depth	Box No.	Depth
1	80.0 – 90.0	19	255.5 – 265.4
2	90.0 – 100	20	265.4 – 275.1
3	100.0 – 100.0	21	275.1 – 284.6
4	110.0 – 119.8	22	284.6 – 294.4
5	119.5 – 129.6	23	294.4 – 304.1
6	129.6 – 139.0	24	304.1 – 313.7
7	139.0 – 148.7	25	313.7 – 323.5
8	148.7 – 158.3	26	323.5 – 333.4
9	158.3 – 167.9	27	333.4 – 343.2
10	167.9 – 177.1	28	343.2 – 352.7
11	177.1 – 186.7	29	352.7 – 362.2
12	186.7 – 196.1	30	362.2 – 371.8
13	196.1 – 206.0	31	371.8 – 381.6
14	206.0 – 216.2	32	381.6 – 391.2
15	216.2 – 225.7	33	391.2 – 400.8
16	225.7 – 235.6	34	400.8 – 410.2
17	235.6 – 245.5	35	410.2 – 420.0
18	245.5 – 255.5	36	420.0 – 425.0

Saturation Grades

Code	Name	Description
B	Barren	No visible evidence of tar saturation.
S	Slight	Pore spaces not filled with tar but rock matrix stained gray to brown.
W	Weak	Pore spaces incompletely filled and rock light gray.
M	Moderate	Pore spaces completely filles wtih tar and rock dull black. Sand grains and original cementing visible.
R	Rich	Pore spaces completely filled with tar and rock glistening black. Sand grains visible.
HR	Highly Rich	Pore spaces completely filled with tar, rock tacky and spotty zones of bleeding tar. Original cementing partly replaced by tar.
VR	Very Rich	Pore spaces completely filled with tar, bleeding and/or oozing zones, and rock tacky. Orignial cementing is replaced by tar, with rock being plastic or soft when fresh.

Listing of the FORTRAN coding
for the Simulation Algorithm Program

```
      Program main
      implicit none
      Integer NElem,i,Istate,IWork(27),NEq(2),count,MaxCou,nPart,NumPar,
     +lrw,liw
      Parameter (NElem = 500,NumPar=10)
      Character*1 tab
      data tab /'09'x/
      logical test, LCon
      Double Precision CBTemp, AirVis,dpMean,RhoS,PreOut,MWAir,RGas,
     +Gravit,Arch,Epsmf,PhiS,Remf,umf,dBubEq,zzzzvl,EpsBub,Lmf,NTO,
     +L,HTRat,delX,dHP,Pi,CCOb0,CO2b0,
     +z,dz,A0,COd,O2d,dpTOT,EpsBed,
     +PO,RTol,Atol(7),Val(7),RWork(134),dval(7),u0,OldL,
     +Pressu,uCalc,CCOb,CCOd,
     +RhoGas,CO2b,CO2d,tol,FT,kp,CH2OO,xPhiB,yH2OO,scale,xGas,
     +dbMax,fcc,RhoC,delta,tau(1:NumPar),dpi(1:NumPar),wpart(1:NumPar),
     +dpEl,ArdMax,ret,hold(1:2),vtStar,MFlux,ResTim,tank,
     +v1(0:NElem),v2(0:Nelem),v3(0:nElem),xi(1:NumPar),xdbar,O2Conv

C The following are used in the bounded Wegstein algorithm in finding the bed
C height L.
      double precision q,s,eff,effold,ell,ellold

      Parameter (Pi=3.14159265358979)

      External Deriv, JDum, Init, F, Cd

      common /param1/ EpsBed,dBubEq,CCOb,CCOd,CO2b,CO2d,EpsBub,Pressu,
     +uCalc
      common /param2/ NTO,HTrat,PreOut,dPTot,CBTemp,A0,RhoS,dbMax
      common /param3/ umf,FT,O2d,COd,CH2OO,u0,kp,dpMean,PhiS,epsmf,xPhiB
     +,Lmf
      Common /param4/ fcc,RhoC,wpart,dpi,npart,ResTim
      common /param5/ xi, tank
      common/termin/hold,ardMax


      Call Getdp (dpMean)
      Call Init (RhoS,MwAir,RGas,EpsMf,PhiS,PreOut,Gravit,DelX,dhp,
     +tol,A0,MaxCou,CBTemp,xPhiB,yH2OO,xGas,fcc,RhoC,MFlux,ResTim)
      AirVis = 2.4169d-7 * CBTemp ** 0.76
      RhoGas = PreOut * MWAir / RGas / CBTemp
      Arch = Gravit * dpMean **3 * RhoS * RhoGas / AirVis ** 2
      Call MinFlu (Arch,EpsMf,PhiS,Remf)
      umf = Remf * AirVis / dpMean / RhoGas
      u0 = umf * xGas
      Lmf = ResTim * MFlux * (1d0 - fcc) / (1d0 - epsmf) / RhoS
      Call ElutDp (u0,dpEl,airVis,RhoGas,RhoS,Gravit)
      dBubEq = 0.044129
      zzzzvl = (u0-umf) / 0.711 / sqrt (gravit * dBubEq)
      EpsBed = (zzzzvl + epsmf) / (1. + zzzzvl)
      EpsBub = (EpsBed - epsmf) / (1. - epsmf )
      L = Lmf / (1. - EpsBub)
      dz = L / DBLE (nElem)
```

411

```
          dpTot = Lmf * (1. - Epsmf) * RhoS * Gravit
          HTRat = Pi / sqrt(3.d0) * (dHP / delX) **2

C Find a dbMax.  It will be given by the minimum of two correlations:
C The first based on the terminal velocity of a particle of size 2.7 * dpMean
C and the second based on the geometry of the system.

          ArdMax=Gravit * (2.7*dpMean) **3 * RhoS * RhoGas / AirVis ** 2
C
C The following call to secant computes the terminal Reynolds number for a particle
C of size d = 2.7 * dpMean
C
          Call secant (Cd,.2,2.,1d-5,Ret,50)
          vtStar = Ret * AirVis / RhoGas / (2.7*dpMean)
          dbMax = min (sqrt(3D0)*delX - 2 * dHP, (vtStar/0.711)**2 / Gravit)
C
C FT gives the ratio of carbon monoxide production to carbon dioxide production by
C the heterogeneous coke oxidation reaction.
C
          FT = 2.5d3  * exp (-6.24 d3/CBTemp)
          kp = 0.8596 * exp (-1.796d4/CBTemp)
          P0 = PreOut + dpTot
          NT0 = u0 * P0 / CBTemp / RGas / (1.-HTRat)
          CCOb0 = 0D0
          CO2b0 = P0 * 0.2095 / RGas / CBTemp
          CH2O0 = yH2O0 * P0 / Rgas / CBTemp

C The following call to secant finds delta, the uniform thickness of coke
C on the particles.

          call secant (f,1.3d-6,2.d-6,1.d-7,delta,200)

          write (6,1005) dpMean,CBTemp,Arch,umf,u0,dpEl,Epsmf,Lmf,PreOut

          scale = 1.d-6
          RTol      = 1.d-2 * scale
          ATol (1) = 1.d-10* scale
          Atol (2) = 1.d-9 * scale
          Atol (3) = 1.d+4 * scale
          Atol (4) = 1.d-2 * scale
          Atol (5) = 1.d-4 * scale
          do 99 i = 5,10
             RWork (i) = 0.
             IWork (i) = 0
 99       continue
          IWork (5) = 0          !No print Out on method switch
          IWork (6) = 1000

C Neq (1) is the number of 1st order ODEs being solved by LSODA

          Neq(1) = 5
          lrw = max(20+16*neq(1),22+9*Neq(1)+Neq(1)**2)
          liw = 20 + Neq(1)

          tank = 0d0
          do 130 i = 1, nPart
             tau(i) = 8d1
             xi(i) = 1d0 - exp (-tau(i)/ResTim)
             tank = tank + wPart(i) * xi(i) / dpi(i)
 130      continue

C The following loop will determine the correct L
          count = 1
          LCon = .false.
```

412

```
1100 continue

      write (6,1004) count,L

      O2d = CO2b0
      COd = CCOb0

      Val (1) = u0 * CCOb0
      Val (2) = u0 * CO2b0
      Val (3) = 0.        !integral of dpdz
      Val (4) = 0.        !integral of epsBub
      Val (5) = 0.        !integral of nbe + nde

C  v1, v2, and v3 are arrays which hold the integrated values of Val (1),
C  Val (2), and Val (3) through the height of the bed.

      v1(0) = val (1)
      v2(0) = val (2)
      v3(0) = val (3)

      Istate = 1

      z = 0D0
      NEq (2) = 1

      do 100 i = 1, NElem
        Call LSODA (Deriv,Neq,Val,z,z+dz,2,RTol,ATol,1,Istate,1,RWork,
     +         lrw,IWork,liw,JDum,2)
        If (IState.lt.0) then
          write (6,1001)  istate,z
          stop 'Stop: LSODA Error'
        endif
        V1(i) = val (1)
        V2(i) = val (2)
        V3(i) = val (3)
100      continue

      count = count + 1
      OldL = L
      ellOld = ell
      effOld = eff
      ell = L
      L = Lmf + Val(4)
      eff = L

C  Now we'll apply the bounded Wegstein successive substitution method if enough
C  iterates have been computed.

      if ((.not.LCon).and.(count.ge.3)) then
        s = (eff-effOld) / (ell - ellOld)
        q = s / (s - 1.)
        if (q.gt. 0d0) q =  0d0
        if (q.lt.-5d0) q = -5d0
        L = q * ell + (1.- q) * eff
      endif
      dz = L / dble (nElem)
      EpsBub = Val(4) / L
      if (abs (L-OldL) .gt. tol * L) then
        if (count .gt. MaxCou) then
          write (6,1002) count,L
          stop 'Stop: L not converged'
        endif
        LCon = .false.
        goto 1100
```

413

```
          endif

C  We've now computed the approximate bed height (subject to small changes due
C  to changes in xi)

          LCon = .true.

C  Now we'll compute tau, the time for complete coke combustion.

          Call FindTa (delta, Val(5), Tau)

C  Recompute the xi's and check for convergence.  Subroutine GetXi will check
C  for convergence and return the conclusion through Test.

          Call GetXi (test,tau,tol)
          if (.not.test) goto 1100

C  Now we know the gas concentration profiles, the bed height, hydrodynamic
C  parameters, and the particle "activities".  Print Out these data.

          z = 0.
          write (6,1003)
          Neq(2) = -1
          do 110 i = 0,Nelem, (nElem/50)
             val(1) = v1(i)
             val(2) = v2(i)
             val(3) = v3(i)
             call deriv (Neq,z,val,dval)
             write (6,1006) z,CO2b,CO2d,CCOb,CCOd,uCalc,Pressu,dBubEq,EpsBed
     +               ,EpsBub
             z = z + dz * dble (nelem/50)
 110      continue

          EpsBub = Val(4) / L
          EpsBed = Epsmf + EpsBub * (1d0 - Epsmf)
          O2Conv = (CO2b0*u0-CO2b*uCalc)/(CO2b0*u0)
          write (6,1007) L, EpsBed, EpsBub, Val(3), O2Conv
          do 150 i = 1, nPart
             write (6,1008) dpi(i)*1d6, tau(i), xi(i)
 150      continue
C
C  Finally, based on the above computations, we can determine the net exit coke
C  conversion, xdbar.
C
          call CConv (Tau,nPart,ResTim,xi,delta,RhoC,dpi,wPart,xdbar,phiS)
          write (6,1009) ResTim, xdbar* 1d2


 1001 format (1x,'Error in LSODA integration: IState = ',i3,/' At z ='
     +,g11.3)
 1002 format (1x,'The iterations for L have failed to converge in ',i3,
     +' iterations'/' L = ',g11.5)
 1003 format (20x,40(1h*)/20x,15(1h*),'Bed Profile',14(1h*)/20x,40(1h*)/
     +2x,'Bed      CO2bub    CO2den    CCObub    CCOden    u',7x,'P',5x,
     +'Bubble eps  eps'/1x,'Height',4('  kg mol/ '),15x,'Diameter',5x,
     +'Bub'/1x,' (m)   ',4('  m ** 3  '),' (m/s)    (Pa)      (m)  ',
     +2(' (-) ')//)
 1004 format (1x,'At iteration number ',i3,'  L =',g14.7)
 1005 format(20x,40(1h*)/' Fluidized Bed Model of Tar-Sands Extraction:'
     +,' Preliminary Computations'//
     +' Average Particle Diameter (m) = ',e10.3/
     +' Combustion Temperature (K) = ',f6.1/
     +' Characteristic Archimedes Number (-) = ',g10.3/
     +' Superficial Gas Velocity at minimum fluidization (m/s) = ',f7.4/
```

```
      +' Superficial Entering Gas Velocity (m/s) = ',f7.4/
      +' Particle size with above terminal velocity (m) = ',e10.3/
      +' Void Fraction at minimum fluidization (-) = ',f5.3/
      +' Bed Height at minimum fluidization (m) = ',g11.3/
      +' Exit Pressure from Bed (Pa) = ',e11.4)
 1006 format (1x,f6.3,4e10.3,f6.2,e10.3,f6.3,2f5.2)
 1007 format (//1x,'The total bed height (m) = ',g11.5/
      +1x,'The Average Void Fraction in the Bed (-) = ',f8.6/
      +1x,'The Average Bubble Volume Fraction (-) = ',f10.8/
      +1x,'The Total Pressure Drop Through the Bed (Pa) = ',e11.4/
      +1x,'The Oxygen Conversion = ',f8.4//
      +1x,'Particle Size     Tau      xi'
      +/2x,' (microns)       (sec)     (-)')
 1008 format (4x,f6.1,7x,f6.1,3x,f5.3)
 1009 format (/1x,'With the mean Particle Residence time = ',f7.1,
      +' seconds'/1x,'The mean coke conversion = 'f6.1,' %')
       end




       Subroutine Init (RhoS,MwAir,RGas,EpsMf,PhiS,PreOut,Gravit,DelX,dhp
      +,tol,A0,MaxCou,CBTemp,xPhiB,yH2OO,xGas,fcc,RhoC,MFlux,ResTim)
       implicit None
       double Precision RhoS,MWAir,RGas,Epsmf,PhiS,PreOut,Gravit,DelX,dhp
      +,tol,A0,CBTemp,yH2OO,xPhiB,xGas,fcc,RhoC,MFlux,ResTim
       integer MaxCou
       open (unit=5,file='main.dat',ReadOnly,status='old')
       read (5,*) RhoS
       read (5,*) MwAir
       read (5,*) Rgas
       read (5,*) EpsMf
       read (5,*) PhiS
       read (5,*) PreOut
       read (5,*) Gravit
       read (5,*) DelX
       read (5,*) dHP
       read (5,*) Tol
       read (5,*) A0
       read (5,*) MaxCou
       read (5,*) CBTemp
       read (5,*) xPhiB
       read (5,*) yH2OO
       read (5,*) xGas
       read (5,*) fcc
       read (5,*) RhoC
       read (5,*) MFlux
       read (5,*) ResTim
       close (unit=5,status = 'keep')
       Call Notice (RhoS,EpsMf,PhiS,PreOut,DelX,dhp,
      +A0,CBTemp,xPhiB,yH2OO,xGas,fcc,RhoC,MFlux,ResTim)
       end




       Subroutine Notice (RhoS,EpsMf,PhiS,PreOut,DelX,dhp,
      +A0,CBTemp,xPhiB,yH2OO,xGas,fcc,RhoC,MFlux,ResTim)

C  This routine will find any parameters which are not equal to their base case
C  values and print them out.

       implicit none
       double Precision RhoS,EpsMf,PhiS,PreOut,DelX,dhp,
      +A0,CBTemp,xPhiB,yH2OO,xGas,fcc,RhoC,MFlux,ResTim,
      +BRhoS,BEpsMf,BPhiS,BPreOu,BDelX,Bdhp,BA0,BCBTem,
```

415

```fortran
+BxPhiB,ByH2OO,BxGas,Bfcc,BRhoC,BMFlux,BResTi
 logical base
 data BRhoS,BEpsMf,BPhiS,  BPreOu,  BDelX,  Bdhp, BA0, BCBTem
+    /2600., 0.46, 0.8,  8.916d4,  0.0549, 0.019, 1.d-4,848./
+BxPhiB, ByH2OO, BxGas, Bfcc,  BRhoC, BMFlux, BResTi
+/0.005, 0.008,  19d0, 0.01961, 900., 0.137,  4000d0/

 base = .true.
 if (abs(Rhos-BRhoS).gt.1d-5*abs(RhoS)) then
    write (6,1000) 'RhoS', RhoS
    Base = .false.
 endif
 if (abs(Epsmf-BEpsmf).gt.1d-5*abs(Epsmf)) then
    write (6,1000) 'Epsmf', Epsmf
    Base = .false.
 endif
 if (abs(PhiS-BPhiS).gt.1d-5*abs(PhiS)) then
    write (6,1000) 'PhiS', PhiS
    Base = .false.
 endif
 if (abs(PreOut-BPreOu).gt.1d-5*abs(PreOut)) then
    write (6,1000) 'PreOut', PreOut
    Base = .false.
 endif
 if (abs(Delx-BDelx).gt.1d-5*abs(Delx)) then
    write (6,1000) 'Delx', Delx
    Base = .false.
 endif
 if (abs(dhp-Bdhp).gt.1d-5*abs(dhp)) then
    write (6,1000) 'dhp', dhp
    Base = .false.
 endif
 if (abs(A0-BA0).gt.1d-5*abs(A0)) then
    write (6,1000) 'A0', A0
    Base = .false.
 endif
 if (abs(CBTemp-BCBTem).gt.1d-5*abs(CBTemp)) then
    write (6,1000) 'CBTemp', CBTemp
    Base = .false.
 endif
 if (abs(xPhiB-BxPhiB).gt.1d-5*abs(xPhiB)) then
    write (6,1000) 'xPhiB', xPhiB
    Base = .false.
 endif
 if (abs(yH2OO-ByH2OO).gt.1d-5*abs(yH2OO)) then
    write (6,1000) 'yH2OO', yH2OO
    Base = .false.
 endif
 if (abs(xGas-BxGas).gt.1d-5*abs(xGas)) then
    write (6,1000) 'xGas', xGas
    Base = .false.
 endif
 if (abs(fcc-Bfcc).gt.1d-5*abs(fcc)) then
    write (6,1000) 'fcc', fcc
    Base = .false.
 endif
 if (abs(RhoC-BRhoC).gt.1d-5*abs(RhoC)) then
    write (6,1000) 'RhoC', RhoC
    Base = .false.
 endif
 if (abs(MFlux-BMFlux).gt.1d-5*abs(MFlux)) then
    write (6,1000) 'MFlux', MFlux
    Base = .false.
 endif
```

416

```
      if (abs(ResTim-BResTi).gt.1d-5*abs(ResTim)) then
         write (6,1000) 'ResTim', ResTim
         Base = .false.
      endif
      If (Base) write (6,1001)
 1000 format (1x,a6,' = ',g12.4)
 1001 format (1x,'All Parameters are Base-Case Values')
      end



      Subroutine GetXi (test,tau,tol)
      implicit none
      logical test
      integer NumPar, nPart, i
      parameter (NumPar=10)
      double precision tau (NumPar), ResTim, xi(NumPar), xii, err, tol,
     +hold(2), w(NumPar), dp(NumPar), tank
      common /param4/ hold, w, dp, nPart, ResTim
      common /param5/ xi, tank

C  This subroutine will recompute the xi's and check for convergence

      err = 0d0
      tank = 0d0
      do 100 i = 1, nPart
         xii = 1d0 - exp (-Tau(i)/ResTim)
         err = err + abs (xii - xi(i)) / xii
         xi(i) = xii
         tank = tank + w(i) * xii / dp(i)
  100 continue
      test = (err.lt.tol)
      end



      Subroutine FindTa (delta,Integ,Tau)

C  This Subroutine will find the values of Tau, the residence time required for
C  complete combustion of the coke on a particle in the combustion bed.

      implicit none
      integer NumPar,nPart,i
      parameter (numPar=10)
      double precision delta,hold(8), xPhiB,Lmf,Integ, Tau(NumPar), emf,
     +fcc,RhoC,w(NumPar), dp(NumPar), xi(NumPar), MC, tank, CO, phiS, pi
      common /param3/ hold,PhiS,emf,xphib,lmf
      common /param4/ fcc,RhoC,w,dp,npart
      common /param5/ xi, tank
      data pi, MC /3.14159265358979,12.01/
      do 100 i = 1,nPart
         CO = Rhoc * Pi * delta * Phis**3 / MC / 3d0 * (3d0* dp(i)**2 +
     +           6d0 * dp(i) * delta + 4d0 * delta**2)
         Tau(i) = 6d0 * lmf * CO * (1d0 - emf) * tank / (pi * phiS**3 *
     +           dp(i)**2 * Integ)
  100 continue
      end



      Subroutine CConv (Tau,nPart,ResTim,xi,delta,RhoC,d,w,xdbar,PhiS)

C  This subroutine will find the mean coke conversion of the combustion bed
C  assuming CSTR modelling of the particle exit age distribution.

      implicit none
      integer nPart,i
```

417

```fortran
      double precision Tau(nPart), theta, ResTim, Num, Den, onemxb, xi
     +(nPart), C0, pi, delta, RhoC, MC, d(nPart), w(nPart), xdbar, phiS
      data pi, MC /3.14159265358979,12.01/
      num = 0d0
      den = 0d0
      do 100 i = 1, nPart
         theta = Tau(i) / ResTim
         onemxb = xi(i) + ((Theta + 1d0) * exp (-theta) - 1d0) / theta
         C0 = pi * delta * RhoC / 3d0 / MC * (3d0 * d(i)**2 + 6d0 * d(i)
     +            * delta + 4d0 * delta**2) * phiS **3
         num = num + C0 * onemxb * w(i) / d(i)**3
         den = den + C0 *     w(i) / d(i)**3
100   continue
      xcbar = 1d0 - num / den
      end




      Subroutine GetDp (dp)

C  This subroutine opens the correct data file for the particle size data,
C  the weight fractions, and then compute the harmonic mass mean average.

      implicit none
      integer n,i,NumPar
      Parameter (NumPar = 10)
      double precision x(1:NumPar), d(1:NumPar), dp, dum, hold(1:2)
      common /param4/ hold, x, d, n
      open (unit=7,file='particle.dat',ReadOnly,Status='old')
      read (7,*) n
      do 2 i = 1,n
         read (7,*) x(i)
2     continue
      do 3 i = 1,n
         read (7,*) d(i)
3     continue
      close (unit=7,status='keep')
      dum = 0.
      do 1 i = 1,n
         dum = dum + x(i) / d(i)
1     continue
      dp = 1/dum
      end




      Subroutine MinFlu (Ar,emf,Phis,Remf)
      implicit none

c  This routine uses the modified Ergun equation to predict Remf for LOW
C  Re.  This won't be valid in the event that Remf > 2.

      double precision Ar, emf, phis, remf
      remf = Ar * Phis **2 * emf **3 / 144.9 / (1.-emf)
      if (Remf.gt.2.) then
         write (6,1000) Ar, Remf
         stop 'Stop: Bad Remf'
      endif
1000  format (1x,'Subroutine MinFlu Predicts Remf too high'/
     +' Ar = ',g12.5/' Remf predicted = ',g12.5)
      end




      Subroutine MTCoef (kqO2,kqCO, db, emf, T, P, u, umf)
```

```
C  This subroutine will determine the mass transfer coefficients as given by
C  Grace (1984).

      implicit none
      double precision kqO2, kqCO, db, emf,T, P, u, umf, zz, ub, g, ID,
     +x, diff, pi
      data pi, g/3.14159265358979, 9.807/
      ID (x) = 0.78755 - 0.20382 * x + 4.8823e-2 * x **2
     +         - 6.4097e-3 * x **3      + 4.3165e-4 * x **4
     +         - 1.1672e-5 * x **5

      ub = u - umf + 0.711 * sqrt (g * db)
      zz = 4. * emf * ub / pi / db
      x = T / 104.8
      if ((x.lt.2.6).or.(x.gt.10)) write (6,100) x
      diff = 2.1059e-4 * T * sqrt(T) / p / ID (x)
      kqO2 = umf / 3. + sqrt (diff * zz)
      x = T / 103.4
      if ((x.lt.2.6).or.(x.gt.10)) write (6,100) x
      diff = 2.0727e-4 * T * sqrt(T) / p / ID (x)
      kqCO = umf / 3. + sqrt (diff * zz)
  100 format (1x,'**Warning from Subroutine MTCoef**'/' x = ',g10.3
     +/' which is out of proper range for diffusivity computation')
      end




      Subroutine Rates (nbe,nbo,nde,ndo,EpsBub, CCOden, CCObub,
     +   CO2den, CO2bub, P, u, T)
      implicit none

C  This routine will compute the rates of molar reaction n.
C  nbe- molar rate of heterogeneous Carbon combustion in the bubble phase.
C  nbo- molar rate of homogeneous CO oxidation in the bubble phase.
C  nde- molar rate of heterogeneous Carbon combustion in the dense phase.
C  ndo- molar rate of homogeneous CO oxidation in the dense phase.

      integer NumPar,i,nPart
      parameter (NumPar = 10)
      double precision nbe,nbo,nde,ndo,EpsBub,CCOden,CCObub,CO2den,
     +CO2bub,P,u,T,yO2b,yO2d,RGas,yCOb,yCOd,yH2O,CH2OO,u0,Apb,Apd,
     +Phib,PhiD,PhiS,dp,kp,MC, hold(1:4), emf, xPhiB, xi(1:NumPar),
     +tank

      data RGas, MC/8314.34,12.01/

      common /Param3/ Hold,CH2OO,u0,kp,dp,PhiS,emf,xPhiB
      common /Param5/ xi, tank

      yO2b = CO2bub * RGas * T / P
      yO2d = CO2den * RGas * T / P
      yCOb = CCObub * RGas * T / P
      yCOd = CCOden * RGas * T / P
      yH2O = CH2OO * u0 * Rgas * T/ P / u
      phiD = (1. - EpsBub) * (1. - Emf)
      PhiB = xPhiB * EpsBub
      nbo = 42.02 * exp (-8052/T) * yO2b ** 0.3 * yCOb * sqrt (yH2O) *
     + (P/T) ** 1.8
      ndo = 42.02 * exp (-8052/T) * yO2d ** 0.3 * yCOd * sqrt (yH2O) *
     + (P/T) ** 1.8
      Apb = 6d0 * PhiB / (Phis * EpsBub) * tank
      Apd = 6d0 * Phid / (Phis * (1d0 - EpsBub)) * tank
      nbe = kp * Apb / MC * P * yO2b
```

419

```
      nde = kp * Apd / MC * P * yO2d
      end




      Subroutine Dense (CCOb, CO2b, CCOd, CO2d, EpsB, P, T, u, db)

C  This Subroutine will Compute the dense phase concentrations from the known
C  bubble phase concentrations computed in subroutine Deriv.  They will be found
C  by a 2-dimensional application of the Newton - Raphson method to the dense-
C  phase mass-balance equations. Initial Guesses will be the last computed
C  values COd and O2d stored in common block Param3

      implicit none
      integer i,MaxIt,NumPar, nPart
      parameter (NumPar = 10)
      double precision CCOb, CO2b, CCOd, CO2d, epsB, P, T, u, db, O2d,
     +COd, CH2OO, u0, yH2O, RGas, BGam, MC, kp, Apd, dp, Phis, Phid,
     +LGam, FT, umf, d1, d2, x1, x2, x3, F, G, FX, FY, GX, GY, Jac,
     +dx, dy, tol, emf, kqO2, kqCO, PhiB, xPhiB, xi(1:NumPar), tank

      data RGas, MC, tol/8314.34, 12.01, 1.d-7/,MaxIt/500/

      common /Param3/ umf,FT,O2d,COd,CH2OO,u0,kp,dp,PhiS,emf,xPhiB
      common /param5/ xi, tank

      PhiD = (1. - EpsB) * (1. - emf)
      yH2O = CH2OO * u0 * Rgas * T / u / P
      BGam = 42.02 * exp (-8052./T) * sqrt (yH2O) * (P/T) ** 1.8
      Apd = 6d0 * phiD/ (PhiS * (1d0 - epsB)) * tank
      LGam = kp / MC * APd * RGas * T
      Call MTCoef (KqO2, kqCO, db, emf, T, P, u, umf)
      d1 = kqCO * 6./ db * epsB / (1. - epsB)
      d2 = kqO2 * 6./ db * epsB / (1. - epsB)
      x1 = lgam * FT / (FT + 1.)
      x2 = BGam * (RGas * T / P) ** 1.3
      x3 = lgam * (1.+ FT/2.)/(1.+ FT)
      CCOd = COd
      CO2d = O2d
      if  (CCOb.lt.0.0) CCOd = 0.0
      if  (CO2b.lt.0.0) CO2d = 0.0
      if ((CCOb.lt.0.0).or.(CO2b.lt.0.0)) return

C  In these calculations, F and G represent the mass balances for dense phase CO
C  and O2, respectively, and X and Y represent CCOd and CO2d, respectively. Fx,
C  Fy,Gx, and Gy are partial derivatives.

      do 100 i = 1,MaxIt
         F = CCOb - CCOd + (x1 * CO2d - x2 * CO2d ** 0.3 * CCOd) / d1
         G = CO2b - CO2d - (x3 * CO2d + x2/2.* CO2d**0.3 * CCOd) / d2
         Fx =-1. - x2 * CO2d ** 0.3 / d1
         Fy = (x3 - 0.3 * x2 * CO2d ** -0.7 * CCOd) / d1
         Gx =  -x2/2. * CO2d ** 0.3 / d2
         Gy = -1. - (x3 + 0.15 * x2 * CO2d ** -0.7 * CCOd) / d2
         Jac = Fx * Gy - Fy * Gx
         if (abs(Jac).lt. 1.d-19) then
            write (6,1001) Jac
            stop 'Stop: error in subroutine dense'
         endif
         dx = (-F * Gy + G * Fy) / Jac
         dy = (-G * Fx + F * Gx) / Jac
         CCOd = CCOd + dx
         if (CCOd.lt.0) CCOd = 0d0
         CO2d = CO2d + dy
```

```
          if (CO2d.lt.0) CO2d = 0d0
          if ((abs(dx).le.tol*CCod).and.(abs(dy).le.tol*CO2d).and.
     +            (abs(F) + abs (G) .lt.tol)) then
            if (CCOd.gt.0.0) COd = CCOd
            if (CO2d.gt.0.0) O2d = CO2d
            return
          endif
 100    continue
        write (6,1000) MaxIt
        stop 'Stop: Newton not converged'
 1000   format (1x,'Newton didn''t converge in ',i4,' iterations in'
     +,' Subroutine Dense')
 1001   format (1x,'In subroutine dense Jac= ',e15.5/' This is too small')
        end




          Subroutine Deriv (N,z,val,dval)

C   This routine will be called by LSODA to evaluate the derivatives for the
C   variables which are being integrated.  There are currently 5 such variables.
C   The contents of val contain the current values of these, and dval is the
C   derivatives of these with respect to z, bed height.
C   val (1)   -   u * CCObub
C   val (2)   -   u * CO2bub
C   val (3)   -   IdelP, the integral of pressure drop through the bed, delP.
C   val (4)   -   IepsB, the integral of bed bubble volume fraction, epsBub.
C   val (5)   -   The integral of (nbe + nde)

        Implicit none
        integer N (2)
        Double Precision z, Val(1), dval(1), P,POut,dPTot, NTO, u,RGas,
     +CBTemp, dBubEq, grav, eps, emf, EpsBub, dpdz, RhoS, HTRat, Psi,
     +CCObub, CO2Bub, CO2Den, CCODen, kqO2, kqCO, ndo, nde,
     +nbo, nbe, FT, umf, A0, hold (1:7), dbMax

        common /Param1/ Eps,dBubEq,CCObub,CCOden,CO2bub,CO2den,EpsBub,P,u
        common /Param2/ NTO,HTRat,POut,dPTot,CBTemp,A0,RhoS,dbMax
        common /Param3/ umf,FT,hold,emf

        data RGas,Grav/ 8314.34,9.807/

        Psi = Val(1) / NTO / (1.-HTRat)
        P = Pout + dPTot - val (3)
        CCOBub = P * Psi / Rgas / CBTemp / (1. + psi / 2.)
        u = NTO / (P / RGas / CBTemp - CCOBub / 2d0) * (1d0 - HTRat)
        dBubEq = 0.43 * (u-umf)**0.4 * (z + 4 * sqrt (A0))**0.8 /grav**0.2
        if (dBubEq.GT.dbMax) dBubEq = dbMax
        Eps = 1. - (1.-emf)/(1.+ (u-umf)/(0.711*sqrt(grav * dbubEq)))
        EpsBub = (eps - emf) / (1. - emf)
        dpdz = (1. - eps) * rhos * grav
        CO2Bub = Val(2) / u
        Call Dense (CCOBub, CO2Bub, CCODen, CO2Den, EpsBub, P,
     +            CBTemp, u, dBubEq)
        If (N(2).eq.1) then
          Call MtCoef (kqO2, kqCO, dBubEq, emf, CBTemp, P, u, umf)
          Call Rates (nbe, nbo, nde, ndo, EpsBub, CCODen, CCOBub, CO2Den,
     +            CO2Bub, P, u, CBTemp)
          dval(1) = kqCO * 6./ dBubEq * EpsBub *(CCOden - CCOBub) + nbe
     +            * FT / (1.+ FT) * EpsBub - nbo * EpsBub
          dval(2) = kqO2 * 6./ dBubEq * EpsBub * (CO2den - CO2Bub) - nbe
     +            * (1.+ FT/2.) / (1.+FT) *EpsBub - nbo / 2.* EpsBub
          dVal(3) = dpdz
          dval(4) = EpsBub
```

```fortran
            dval(5) = nbe + nde
          endif
          end


          SUBROUTINE SECANT (F,XX1,XX2,EPS,X,NMAX)
          IMPLICIT NONE
          INTEGER I,NMAX
          double precision X1,X2,XX1,XX2,F,EPS,X,FX,FX1,FX2
          X1=XX1
          X2=XX2
          FX1= F(X1)
          FX2= F(X2)
          DO 97 I=1,NMAX
                  X=(X1*FX2-X2*FX1)/(FX2-FX1)
                  FX=F(X)
                  IF ((ABS(FX).LT.EPS).and.(ABS(FX-FX1).LT.SQRT(EPS)).and.
     +                    (ABS(X-X1).LT.EPS*x)) RETURN
                  X2=X1
                  FX2=FX1
                  X1=X
                  FX1=FX
97        CONTINUE
          write (6,101)
101       FORMAT (1X,'SECANT FAILS TO CONVERGE')
          STOP 'Secant Fails'
          END


          SUBROUTINE SECNT (F,XX1,XX2,EPS,X,NMAX)
          IMPLICIT NONE
          INTEGER I,NMAX
          double precision X1,X2,XX1,XX2,F,EPS,X,FX,FX1,FX2
          X1=XX1
          X2=XX2
          FX1= F(X1)
          FX2= F(X2)
          DO 97 I=1,NMAX
                  X=(X1*FX2-X2*FX1)/(FX2-FX1)
                  FX=F(X)
                  IF ((ABS(FX).LT.EPS).and.(ABS(FX-FX1).LT.SQRT(EPS)).and.
     +                    (ABS(X-X1).LT.EPS*x)) RETURN
                  X2=X1
                  FX2=FX1
                  X1=X
                  FX1=FX
97        CONTINUE
          write (6,101)
101       FORMAT (1X,'SECANT FAILS TO CONVERGE')
          STOP 'Secant Fails'
          END


      Double Precision Function F (delta)

C  This Routine is called by secant while solving for delta, the uniform thick-
C  ness of the layer of coke initially on the sand particles when entering the
C  combustion bed.

      implicit none
      integer n,i,NumPar
      Parameter (NumPar=10)
      double precision w(1:NumPar), d(1:NumPar), delta, fcc, RhoS,
     +RhoC, dum, x,hold(1:6), hold1(1:8), PhiS
      Common /Param4/ fcc,RhoC,w,d,n
      Common /Param2/ hold, RhoS
```

```
      Common /Param3/ holdl, PhiS

      dum = 0.
      do 50 i = 1,n
         x = delta / d(i)
         dum = dum + w(i) * (3.* x + 6.* x ** 2 + 4.* x ** 3)
50    continue
      f = dum - fcc * RhoS / 2. / (1.-fcc) / RhoC
      end



      Subroutine ElutDp (u,dpTerm,mu,RhoG,RhoS,g)

C  Compute Particle diameter with terminal reynolds num = u

      implicit none
      double precision ar,rhog,rhos,g,mu,u,dpTerm,reddp,arddp3
      common/termin/ Reddp,Arddp3,ar
      external ddd
      Reddp = u * RhoG / mu
      arddp3 = g * rhoG * (RhoS - RhoG) / mu ** 2
      call Secnt (ddd,40d-6,70d-6,0.0001,dpTerm,100)
      end



      Double Precision function ddd (dp)

C  Compute Ret - u

      implicit none
      external cd
      double precision dp,ar,reddp,arddp3,ret,reg
      common/termin/ reddp,arddp3,ar
      ar=dp**3 * arddp3
      Reg = reddp * dp
      call secant (Cd,.2,2.,1.d-5,Ret,50)
      ddd = Ret - reg
      end



      double precision Function Cd (Re)

C  Ret =~ ar / 18x

      implicit none
      double precision re,x,hold(1:2),ar
      common/termin/hold,ar
      if (re.lt.0.01) then
         x=1.
      else if (re.lt.20.) then
         x = 1. + 0.1315 * re ** (0.82 - 0.05 * log10 (re))
      else if (re.lt.260.) then
         x= 1. + 0.1935 * re ** 0.6305
      else
         write (6,1001) Re,Ar
         stop'stop:Terminal Velocity out of Range'
      endif
      Cd = re - ar/(18.*x)
      return
1001  format (' Re = ',f10.2/' Ar = ', e10.3/
     +' Re is too big for the correlations of Cd: execution Killed')
      end
```

APPENDIX D

UNIVERSITY OF UTAH TAR SANDS BIBLIOGRAPHY

<u>Theses and Dissertations</u>

Sepulveda, J.E. 1977. <u>Hot Water Separation of Bitumen from Utah Tar Sands.</u> M.S. thesis. University of Utah, Salt Lake City, Utah.

Weeks, J.K. Jr. 1977. <u>Fluidized-bed processing of Utah tar sands</u>. M.S. thesis. University of Utah, Salt Lake City, Utah.

Bunger, J.W. 1979. <u>Processing Utah tar sand bitumen</u>. Ph.D. dissertation. University of Utah, Salt Lake City, Utah.

Jayakar, K.M. 1979. <u>The thermal recovery of oil from tar sand Ph.D. dissertation</u>. University of Utah, Salt Lake City, Utah.

Venkatesan, V.N. 1979. <u>Fluidized-bed thermal recovery of synthetic crude from bituminous sands of Utah</u>. Ph.D. dissertation. University of Utah, Salt Lake City, Utah.

Hanks, K.C. 1979. <u>Chemistry of oil production from tar saund</u>. M.S. thesis. University of Utah, Salt Lake City, Utah.

Misra, M. 1981. <u>Physical separation of bitumen from Utah tar sands</u>. Ph.D. dissertation. University of Utah, Salt Lake City, Utah.

Smith, R. 1981. <u>Asphalt Ridge tar sands—flotation behavior and process design.</u> M.S. thesis. University of Utah, Salt Lake City, Utah.

Aguilar, R. 1981. <u>Physical separation of bitumen from Utah tar sands</u>. M.S. thesis. University of Utah, Salt Lake City, Utah.

Brechtel, C.E. 1981. <u>Hydrotreating Utah tar sand products</u>. M.S. thesis. University of Utah, Salt Lake City, Utah.

Umoh, R.A. 1981. <u>Steam cracking of Utah tar sand bitumen in a Kellogg millisecond furnace</u>. M.S. thesis. University of Utah, Salt Lake City, Utah.

Bezama, R.J. 1983. <u>An energy efficient method for thermal processing of Utah tar sands</u>. Ph.D. dissertation. University of Utah, Salt Lake City, Utah.

Wang, J. 1983. <u>The production of hydrocarbon liquids from a bitumen-impregnated sandstone in a fluidized bed pyrolysis reactor</u>. M.S. thesis. University of Utah, Salt Lake City, Utah.

424

Wang, C.J. 1984. The solubility of carbon dioxide in tar sand bitumens. M.S. thesis. University of Utah, Salt Lake City, Utah.

Smart, L.M. 1984. Thermal processing of tar sands. M.S. thesis. University of Utah, Salt Lake City, Utah.

Dorius, J.C. 1985. The pyrolysis of bitumen impregnated sandstone from the P.R. Spring (Utah) deposit in a fluidized bed. Ph.D. dissertation. University of Utah, Salt Lake City, Utah

Tsai, C.H. 1987. Reaction kinetics and mechanisms of hydropyrolysis processing of tar sand Bitumen and related materials. M.S. Thesis, University of Utah, Salt Lake City, Utah.

Lin, L.C. 1988. The kinetics of the pyrolysis of tar sand and of the combustion of coked sands. Ph.D. dissertation, University of Utah, Salt Lake City, Utah.

Sung, S.H. 1988. The fluidized bed pyrolysis of bitumen-impregnated sandstone in a large diameter reactor. M.S. Thesis University of Utah, Salt Lake City, Utah.

Coronella, C.J. 1989. Modelling a Coupled Fluidized-Bed Reactor for Extraction of Bitumen from Tar Sands. M.S. Thesis. University of Utah, Salt Lake City, Utah.

Ryu, H. 1989. Kinetic Modelling Applied to Hydrocarbon Process Design and Engineering: I Hydropyrolysis of Heavy Oils, II: Acetylene from Calcium Carbide, Ph.D. dissertation, University of Utah, Salt Lake City, Utah.

Shun, D. 1990. Fluidized Bed Pyrolysis of The Bitumen-Impregnated Sandstone from the Circle Cliff Deposit. Ph.D. dissertation University of Utah, Salt Lake City, Utah.

Cogswell, D. 1990. Effect of H_2S on the Hydropyrolysis of Tetralin. M.S. Thesis, University of Utah, Salt Lake City, Utah.

Final Reports

Oblad, A.G., Bunger, J.W., Miller, J.D., Seader, J.D. 1977. Recovery of oil from Utah's tar sands. Final Report. Grant ASR74-21867, Natl. Sci. Found. RANN Program

Oblad, A.G., Bunger, J.W., Hanson, F.V., Miller, J.D., Seader, J.D. 1979. Recovery of oil from Utah's tar sands. Final Report, 1977-79. US Dept. Energy (DOE) Contract #ET77-S-03-1762. 140 pp.

Bunger, J.W., Wells, H.M. 1980. Economic evaluation of tar sand resources located in the state of Utah. Phase I. <u>Final Report</u>. Utah Eng. Exp. Stn., Sept. 2. 211 pp.

Wells, H.M., Bunger, J.W., Jensen, G.F. 1984. Economic evaluation of oil shale and tar sands located in the state of Utah. <u>Final Report</u>. Utah Eng. Exp. Stn. 5 volumes, May

Oblad, A.G., Bunger, J.W., Hanson, F.V., Miller, J.D., Seader, J.D. 1984. Recovery of oil from Utah's tar sands. <u>Final Report</u>. DOE Contract #DE-AS20-80LC10332, May

Oblad, A.G., Bunger, J.W., Hanson, F.V., Miller, J.D., Seader, J.D. 1984. Recovery and hydropyrolysis of oil from Utah's tar sands. <u>Final Report</u>. DOE Contract #DE-AS20-82LC10942, Dec.

Oblad, A.G., Bunger, J.W., Hanson, F.V., Miller, J.D., Seader, J.D. 1985. Recovery and upgrading of oil from Utah tar sands. <u>First Annual Report</u>. DOE Contract #DE-FG20-84LC11057, Sept.

Oblad, A.G., Bunger, J.W., Hanson, F.V., Miller, J.D., Seader, J.D. 1986. Recovery and upgrading of oil from Utah tar sands. <u>Second Annual Report</u>. DOE Contract #DE-FG20-84LC11057, Sept.

Oblad, A.G., Bunger, J.W., Hanson, F.V., Miller, J.D., Seader, J.D. 1987. Recovery and upgrading of oil from Utah tar sands. <u>Final Technical Report</u>. DOE Contract #DE-FG20-84LC11057, Jan.

Oblad, A.G., Hanson, F.V. 1988. Production of bitumen-derived hydrocarbon liquids from Utah's tar sands. <u>Final Technical Report</u>. DOE Contract # DE-FG21-87MC11090, Sept.

Oblad, A.G., Bunger, J.W., Hanson, F.V., Miller, J.D., Seader, J.D., 1989, The Extraction of Bitumen from Western Tar Sands, <u>Final Technical Report</u>. DOE Contract # DE-FG21-88MC25046.

Patents

Miller, J.D., Sepulveda, J.E. Oct. 17, 1978. Separation of bitumen from dry tar sands. <u>U.S. Patent 4,120,776</u>.

Seader, J.D., Jayakar, K.M. July 10, 1979. Process and apparatus to produce synthetic crude oil from tar sands. <u>U.S. Patent 4,160,720</u>.

Oblad, A.G., Shabtai, J.S. Nov. 3, 1981. Hydropyrolysis of tar sand bitumens and heavy petroleum oils. <u>U.S. Patent 4,298,487</u>.

Hanson, F.V., Miller, J.D., Oblad, A.G. June 29, 1982. Process for obtaining products from tar sands. <u>U.S. Patent 4,337,143</u>.

426

Hanson, F.V., Miller, J.D., Oblad, A.G. Oct. 11, 1983. Process for recovering products from tar sand. U.S. Patent 4,409,090.

Miller, J.D., Hupka, J. Sept. 11, 1984. Bitumen recovery from tar sands. U.S. Patent 4,470,899.

Miller, J.D., Misra, M. Dec. 4, 1984. Process for separating high viscosity bitumen from tar sands. U.S. Patent 4,486,294.

Publications

1976

Bunger, J.W., Mori, S., Oblad, A.G. 1976. Processing of tar sand bitumens. Part I. Thermal cracking of Utah and Athabasca tar sand bitumens. Preprints, Div. Fuel Chem., ACS, 21(6):147.

Oblad, A.G., Seader, J.D., Miller, J.D., Bunger, J.W. 1976. Recovery of bitumen from oil-impregnated sandstone deposits of Utah. Oil Shale and Tar Sands, AIChE Symp. Ser. 72, No. 155, p.69.

Sepulveda, J.E., Miller, J.D., Oblad, A.G. 1976. Hot water extraction of bitumen from Utah tar sands. I. Symp. on Oil Shale, Tar Sands and Related Materials—Production and Utilization of Synfuels, Preprints, Div. Fuel Chem., ACS 21(6):110.

1977

Bunger, J.W. 1977. Development of Utah tar sands—A status report, Mines and Mineral Rep. No. 5, 1-10, Oct.

Bunger, J.W. 1977. Techniques of analysis of tar sand bitumens. Preprints, Div. Pet. Chem., ACS 22(2):716-26.

1978

Sepulveda, J.E., Miller, J.D. 1978. Separation of bitumen from Utah tar sands by a hot water digestion-flotation technique. Min. Eng. 30(9):1311 (also published in Trans SME/AIME, Sept. 1978).

Sepulveda, J.E., Miller, J.D., Oblad, A.G. 1978. Hot water extraction of bitumen from Utah tar sands III. Min. Eng. 30:1311.

Bunger, J.W., Cogswell, D.E., Oblad, A.G. 1978. Influence of chemical factors on primary processing of Utah tar sand bitumen. Preprints, Div. Fuel Chem., ACS 23(4):98-109.

Bunger, J.W., Cogswell, D.E., Oblad, A.G. 1977. Thermal processing of a Utah tar sand bitumen. Proc. Canada-Venezuela Oil Sand Symp.-77. Edmonton, Alberta, Canada; The oil sands of Canada-Venezuela-1977, ed. D.A. Redford, A.G. Winestock. 1978. CIM Special 17:178-82. 1979

Bunger, J.W., Cogswell, D.E., Oblad, A.G. 1979. Catalytic cracking of Asphalt Ridge bitumen. Refining of Synthetic Crude Oils, ACS Adv. Chem., Ser. 179, 67.

Venkatesan, V.N., Hanson, F.V., Oblad, A.G. 1979. The thermal recovery of synthetic crude from the bituminous sands of the Sunnyside (Utah) deposit, Proc. First Int. Conf. on the Future of Heavy Crude and Tar Sands. Edmonton, Alberta, Canada, June 4-12.

1980

Hanson, F.V., Miller, J.D., Oblad, A.G. 1980. A combined hot water-thermal pyrolysis strategy for the production of bitumen-derived liquids. 15th Intersoc. Energy Conversion Conf. Seattle, Wash. Aug.

1981

Bunger, J.W., Cogswell, D.E. 1981. Characteristics of tar sand bitumen asphaltenes as studied by conversion of bitumen by hydropyrolysis. Chemistry of Asphaltenes, ACS Adv. Chem. Ser., ed. J.W. Bunger, N.C. Li. No. 195, pp. 219-36. ACS, Washington, D.C.

Miller, J.D., Misra, M. 1981. Hot water process development for Utah tar sands. Present at the 90th Natl. AIChE Meet. Houston, Tex. Apr. 5-8.

Smith, R.J., Miller, J.D. 1981. Flotation behavior digested Asphalt Ridge tar sands, Mining Eng. 33(12):1724.

Misra, M., Miller, J.D. 1981. Surface chemistry features in the hot water processing of Utah tar sands. Presented at the Symp on Separation Sci. and Technol., Gatlinburg, Tenn. May 5-8; Separation Sci. Technol. 16(10):1523-44.

Bunger, J.W., Cogswell, D.E., Oblad, A.G. 1981. Hydropyrolysis—potential for primary upgrading. Oil Shale, Tar Sands and Related Material, ed. H. Stauffer. ACS Symp. Ser., No. 163: pp. 369-80.

1982

Venkatesan, V.N., Hanson, F.V., Oblad, A.G. 1982. A fluidized bed-thermal process for the recovery of a bitumen-derived liquid from the bitumen-impregnated sandstone deposits of Utah. AIChE, Symp. Ser. 216, 78:42-55.

Hupka, J., Miller, J.D., Aguilar, R., Cortex, A. 1982. Modified hot water processing of domestic tar sands. AIME Ann. Meet., Dallas, Tex., Feb. 14-18, 1982. Preprint No. 82-85. Submitted for publication.

Miller, J.D., Misra, M. 1982. Hot water process development for Utah tar sands. Fuel Proc. Tech. 6:27-59.

Miller, J.D., Misra, M. 1982. Concentration of Utah tar sands by an ambient flotation process, Int. J. Miner. Proc. 9:269-87.

1983

Wang, J., Hanson, F.V., Oblad, A.G. 1983. The fluidized bed pyrolysis of the bitumen-impregnated sandstone from the Whiterocks (Utah) deposit, Preprint AIChE Symp. Adv. Tar Sand Technol. Denver, Colo., Aug.

Hupka, J., Miller, J.D., Oblad, A.G. 1983. Hot water processing of U.S. tar sands—hot water recycle and tailing disposal, 4th Int. Conf. for Protection of the Environment. Toulouse, France, Sept. 20-23.

Hupka, J., Miller, J.D., Cortes, A. 1983. The importance of bitumen viscosity in the hot water processing of domestic tar sands. SME/AIME, Mining Eng. 35(12):1635-41, Dec.

1984

Hatfield, K.E., Oblad, A.G. 1984. Pilot plant program for upgrading of heavy oils by hydropyrolysis. Proc. of the Second Int. Conf. Heavy Crude and Tar Sand. Caracas, Venezuela, Feb. 7-17, UNITAR 1175-79.

Bunger, J.W. 1984. Upgrading Utah tar sand bitumen to syncrude. Proc. WRI-DOE Tar Sand Symp. Vail, Colo., June 26-29.

Dorius, J.C., Hanson, F.V., Oblad, A.G. 1984. The pyrolysis of the bitumen-impregnated sandstcne from the P.R. Spring (Utah) deposit in a fluidized-bed, Proc. WRI-DOE Tar Sand Symp., Vail, Colo., June 26-29.

Smart, L., Seader, J.D. 1984. Thermal recovery of bitumen. Proc. WRI-DOE Tar Sand Symp., Vail, Colo., June 26-29.

1985

Bunger, J.W., Oblad, A.G. 1985. Upgrading of bitumen by hydropyrolysis—a process for low coke and high syncrude yields. Proc. Third Int. Conf. on Heavy Crude and Tar Sands, UNITAR/UNDP Inf. Centr. New York City, Los Angeles, Calif. pp. 1717-26, July 22-31.

429

Bunger, J.W. 1985. Reactions of hydrogen during hydropyrolysis processing of heavy crudes. Preprints, Div. Pet. Chem., Am. Chem. Soc. 30 (4):658-63.

Bunger, J.W. 1985. Inhibition of coke formation in hydropyrolysis of residual oils. Preprints, Div. Pet. Chem., Am. Chem. Soc. 30 (3):549-54.

1986

Bunger, J.W., Tsai, C.H., Russell, C.P. 1986. Competing reactions during hydropyrolysis upgrading of tar sand bitumen and residual materials. Proc. WRI/DOE Tar Sand Symp., ed. J.D. Westhoff, L.C. Marchant. Jackson, Wyo., July 7-10.

Seader, J.D., Bezama, R.J., Charavarty, T. 1986. Design and economic evaluation of an energy-integrated thermal process for recovery of oil from tar sands. Proc. WRI/DOE Tar Sand Symp., ed. J.D. Westhoff, L.C. Marchant. Jackson, Wyo., July 7-10.

Lin, L.C., Hanson, F.V., Oblad, A.G. 1986. A preliminary mathematical model of the pyrolysis of bitumen-impregnated sandstone in a fluidized bed. Proc. WRI/DOE Tar Sand Symp., ed. J.D. Westhoff, L.C. Marchant. Jackson, Wyo., July 7-10.

1987

Hupka, J., Miller, J.D., Oblad, A.G. 1987. Diluent-assisted hot water processing of tar sands, AOSTRA J. Res. 3,95-102.

Lin, L.C., Hanson, F.V., Oblad, A.G., Westhoff, J.D. 1987. The pyrolysis of bitumen-impregnated sandstone in short-contact time reactors. I. Cyclone Reactor. Fuel Proc. Tech. 16, 173-190.

Oblad, A.G., Bunger, J.W., Hanson, F.V., Miller, J.D., Ritzma, H.R., and Seader, J.D. 1987. Tar sand research and development at the University of Utah. Ann. Rev. Energy. 12:283-356.

1988

Hanson, F.V., Oblad A.G. 1988. The fluidized bed pyrolysis of bitumen-impregnated sandstone from the tar sand deposits of Utah. Proceedings UNITAR/UNDP International Conference on Heavy Crude and Tar Sands, Vol. 5. Extraction, Upgrading, Transportation .Paper No. 155 421-438. Edmonton, Alberta, Canada.

1989

Lin, L.C., Hanson, F.V., Oblad, A.G. 1989. Mathematical Model of the Pyrolysis of Bitumen-Impregnated Sandstone Particles. I. Diffusion Dominant Transport Regime. Fuel Proc. Tech. 22, 41-63.

Yang, Y.J., Bukka, K., Miller, J.D. 1989. Selection and Evaluation of diluents in the modified hot water process, Energy Processing, Canada, 82(1), 14-21.

<u>1990</u>

Deo, M.D., Fletcher, J.V., Shun, D.W., Hanson, F.V., Oblad, A.G., Modeling of the pyrolysis of tar sand in fluidized bed reactors. <u>Proc. 1990 Eastern Oil Shale Symposium</u>, 105-119.

Cha, S., Longstaff, D.C., Hanson, F.V. and Oblad, A.G. 1990. Pyrolysis of Bitumen Impregnated Sandstones: A comparison of Fluidized - Bed and Rotary Kiln Reactors, <u>Proc. 1990 Eastern Oil Shale Symposium</u>, 136-145.

Lin, L.C., Deo, M.D., Hanson, F.V., and Oblad, A.G. 1990. Kinetics of Tar Sands Pyrolysis Using a Distribution of Activation Energy Model. AIChE J. <u>36</u>, 1585-1588.

Hupka, J., Drelich, J., Miller, J.D., White, R.R., Hanson, F.V., and Oblad, A.G., 1990. Impact of Water Recycle on Water-Based Processing of Whiterocks Tar Sand. <u>Proc. 1990 Eastern Oil Shale</u>, 39-44.

Seader, J.D. and Coronella, C.J. 1990. An advanced Energy-Efficient Coupled Fluidized-Bed System for Recovering Bitumen From Tar Sand. <u>Proc. 1990 Eastern Oil Shale Symposium</u>, 120-129.

Hupka, J. and Miller, J.D., 1990. "Modest-Temperature Water-Based Bitumen Recovery from Tar Sand." <u>Proc. 1990 Eastern Oil Shale Symposium</u>, 130-135.

DATE
FILMED
6 / 2 / 92